

Investigating the relationship between BRAF status and melanoma response to anti-angiogenic therapy

Submission for the degree of Doctor of Philosophy (DPhil) in

Oncology

Lina Guo

St Hilda's College



University of Oxford

Department of Oncology

Contents

Abstract

Acknowledgements

List of Figures

List of Tables

Abbreviations

Chapter 1: Introduction 17

1.1 Malignant Melanoma 17

1.1.1 Epidemiology 17

1.1.2 Risk Factors 17

1.1.3 Classification of Malignant Cutaneous Melanoma 18

1.1.4 Molecular Changes in Malignant Melanoma 20

1.1.5 Melanoma Therapeutics 29

1.2 Angiogenesis in melanoma 34

1.2.1 Blood Vessel Formation 35

1.2.2 Molecular Mechanisms of Vessel Branching 38

1.2.3 Important Players Involved in Angiogenesis 39

1.2.4 Antiangiogenic Therapy 50

1.3 Project objectives 58

Chapter 2: Materials and Methods 60

2.1 Cell lines and cell culture 60

2.2 Cell-based assays 62

2.2.1 Viability assay 62

2.2.2 3D Spheroid assay 62

2.2.3 Wound healing assay 63

2.2.4 Determining cell population doubling time 63

2.3 Protein analysis 63

2.3.1 Western blotting 63

2.3.2 VEGF enzyme-linked immunosorbent assay (ELISA) 65

2.3.3 Flow cytometry 67

2.4 Generating a BRAF WT/V600E Isogenic model using retroviral system 67

2.4.1 Preparation of plasmids 67

2.4.2 Site-directed mutagenesis 68
2.4.3 Preparation of plasmids for DNA sequencing 70
2.4.4 Polyethylenimine transfection 70
2.4.5 Retroviral infection 71
2.5 Generating a *BRAF* WT/V600E Isogenic model using CRISPR-Cas9 system 71
2.5.1 Fluorescence *In Situ* Hybridisation (FISH) 71
2.5.2 Lipofectamine® 2000 transfection 73
2.5.3 Cell sorting for GFP-positive cells 74
2.5.4 Genetic analysis for the CRISPR clones 74
2.6 RNA analysis 77
2.6.1 RNA extraction 77
2.6.2 Reverse transcription (RT) 77
2.6.3 Quantitative real-time PCR (qRT-PCR) 78
2.6.4 Human HT12v4.0 Illumina microarray analysis 78
2.6.5 Sample preparation for RNA Sequencing from fresh frozen patient tumours 80
2.6.6 Primer design 81
2.7 Analysis of gene expression 82
2.7.1 Melanoma cell line panel from Ludwig Institute for Cancer Research Melbourne 82
2.7.2 Illumina microarray analysis of gene expression in isogenic melanoma clones 83
2.7.3 RNA-seq on fresh frozen melanoma samples 84
2.8 *In vivo* studies 84
2.8.1 Quantifying human VEGF and mouse VEGF levels in blood samples 85
2.8.2 Immunohistochemistry 86

Chapter 3: VEGF expression and characterisation of bevacizumab response in melanoma cell lines. 88
3.1 Investigation of the hypothesis that the inhibition of autocrine VEGF signalling suppresses growth in *BRAF* mutant melanomas 88
3.2 Results 89
3.2.1 Detection of expression of VEGF signalling proteins and testing for the effects of bevacizumab on the signalling in melanoma cell lines 89
3.2.2 Testing for direct effects of bevacizumab on two-dimensional (2D) growth of melanoma cells 94
3.2.3 Testing for direct effects of bevacizumab on three-dimensional (3D) growth of melanoma cells 98
3.2.4 Testing for direct effects of bevacizumab in cell migration of melanoma cell lines 100
3.3 VEGF expression in melanoma cell line panel 103
3.4 VEGF expression in newly established LM-MEL melanoma cell lines 106

3.5 Discussion 110

Chapter 4: Generating an isogenic WT/V600E melanoma cell line model and identifying differentially expressed genes between *BRAF* WT and V600E melanomas 112

4.1 Introduction 112

4.2 Retroviral expression of pBabe-Puro-*BRAF*-V600E in *BRAF* WT cell lines 114

4.3 Generating an isogenic WT/V600E model using CRISPR/Cas9 system 117

4.3.1 Pre-transfection screening for suitable host cell lines 117

4.3.2 Transfection and selection for positive clones 119

4.4 Validating the isogenic BRAF WT/V600E CRISPR model 123

4.4.1 *BRAF* expression in the CRISPR clones 123

4.4.2 Sensitivity of the *BRAF* V600E clones to BRAF inhibitor PLX4720 126

4.4.3 2D and 3D growth of CRISPR clones 131

4.5 Differential gene expression between BRAF WT and V600E melanomas 133

4.5.1 Human HT12v4.0 Illumina array analysis on the CRISPR *BRAF* WT/V600E isogenic model 133

4.5.2 RNA sequencing analysis of 12 fresh frozen melanoma patient tumour samples 139

4.5.3 Differential gene expression analysis between *BRAF* WT and mutant LM-MELANOMA cell lines 143

4.5.4 Validating the differentially expressed genes between *BRAF* WT and V600E melanoma cells 145

4.6 Discussion 150

Chapter 5: Testing effect of the introduced *BRAF* V600E mutation to anti-angiogenic therapy *in vitro* and *in vivo* 155

5.1 Introduction 155

5.2 Effects of inhibiting VEGF on growth of *BRAF* V600E clones 156

5.3 VEGF expression in CRISPR *BRAF* V600E and WT clones 159

5.4 Testing response of isogenic *BRAF* WT/V600E xenografts to anti-angiogenic therapy *in vivo* 162

5.4.1 Growth of isogenic *BRAF* WT and V600E melanoma clones as xenografts treated with bevacizumab 162

5.4.2 Immunohistochemical analysis of WT3 vs. F10 xenografts without bevacizumab treatment 165

5.4.3 Immunohistochemical analysis of WT7 vs. 3F2 xenografts treated with bevacizumab 167

5.4.4 Serum VEGF protein in mice bearing BRAF WT or V600E xenografts 172

5.5 Discussion 173

Chapter 6: Conclusions and Future Directions 178

Bibliography 187

Abstract

A large phase 3 trial (AVAST-M) assessing bevacizumab as adjuvant therapy for melanoma has shown that patients with BRAF V600E melanomas had improved disease-free interval compared to the wild-type (WT) BRAF population, suggesting a differential sensitivity of BRAF V600E to Bevacizumab. Bevacizumab is a monoclonal antibody that inhibits VEGF, targeting angiogenesis and other endothelial cell functions. The aim of this project was to investigate two hypotheses: 1) Bevacizumab differentially targets autocrine VEGF-VEGF receptor (VEGFR) signalling on BRAF V600E vs WT tumour cells; 2) Inhibitory effects of bevacizumab in BRAF V600E melanoma are mediated indirectly via effects on angiogenesis or other components of the tumour microenvironment. Initially, VEGFRs were detected in melanoma cell lines, and secreted and intracellular VEGF levels were significantly higher in BRAF V600E cell lines, but this difference was not seen in newly-derived LM cell lines from Ludwig Institute Melbourne. To remove BRAF-unrelated variation between cell lines, isogenic BRAF WT/V600E clones were generated by CRISPR/Cas9 genome editing in BRAF WT CHL-1 cells. The introduced mutant allele was shown to mediate increased MEK-ERK pathway activation and sensitivity to mutant BRAF inhibitor PLX4720. There was no difference between BRAF WT and V600E clones in 2D growth, however, the V600E clones increased in size more rapidly in 3D growth compared to WT, indicating a more aggressive phenotype. In the cell line panel and isogenic clones, bevacizumab did not inhibit 2D or 3D growth or migration (scratch assays), suggesting that direct anti-melanoma effects are unlikely. However, VEGF ELISA showed that secreted and intracellular VEGF levels were significantly higher in isogenic BRAF V600E clones, suggesting that BRAF V600E upregulated VEGF. *In vivo,* xenografts grown from BRAF V600E isogenic cells were more

vascular with less hypoxia and necrosis than BRAF WT tumours. Furthermore, bevacizumab significantly reduced tumour size and prolonged survival in nude mice bearing BRAF V600E xenografts, but not in the WT group. Immunohistochemical analysis showed that bevacizumab induced significantly more hypoxia and reduced the vascularity of BRAF V600E but not WT tumours. There was an increase in mouse serum VEGF levels in mice bearing BRAF V600E xenografts treated with bevacizumab, suggesting a possible compensatory up-regulation of murine VEGF upon human VEGF inhibition. To identify differentially expressed genes that may contribute to the sensitivity of BRAF V600E melanomas to anti-angiogenic therapy, microarray analysis on the isogenic clones was combined with four datasets including RNA-seq on RNA extracted from frozen patient tumours, tumour samples from the AVAST-M trial, publicly-available data on gene expression in the LM melanoma cell line panel, and patient-derived melanomas from TCGA. Out of the genes validated, ROR2 was shown to upregulate VEGF in BRAF V600E clones, indicating a possible mechanism for the link between BRAF V600E mutation and VEGF upregulation. In summary, this project generated an isogenic BRAFWT/V600E melanoma model and showed that the introduced V600E mutation led to increased 3D growth, VEGF upregulation, and increased tumour vascularity and bevacizumab sensitivity *in vivo*, paralleling results of the AVAST-M trial. Transcriptional analysis identified candidate genes upregulated by BRAF V600E that may mediate increased dependence on tumour angiogenesis.

Acknowledgements

I would first like to thank my supervisors, Dr Valentine Macaulay and Professor Mark Middleton, for their support, advice and guidance throughout my DPhil. I would like to thank Dr Esther Bridges, for her help with the in vivo experiments, Dr Francesca Buffa and Dr Ruud Van Stiphout, for their help with the tumour array data analysis, and Dr Nick Coupe, for his clinical advice and collaboration on this project. I would also like to thank all members of the IGF group for their advice and support during my time in Oxford.

Dedication

To my mother,
who taught me love, courage and the power of resilience.

献给我的母亲
她教会了我爱，勇气，以及坚韧的力量。

List of Figures

Figure 1-1: MAPK and PI3K pathways and relevant therapeutic strategies..... 32

Figure 1-2: Common methods of blood vessel formation in tumours..... 37

Figure 1-3: Steps of vessel branching in angiogenesis..... 39

Figure 1-4: Disease-free interval for patients with determined BRAF status in the interim analysis of AVAST-M study. 57

Figure 1-5: Overall survival for patients in the observation arm, and overall survival for BRAF mutant patients treated with bevacizumab in the AVAST-M trial. 58

Figure 3-1: Expression of VEGF signalling proteins and effects of bevacizumab on cell signalling in melanoma cell lines. 93

Figure 3-2: effects of inhibiting VEGF signalling by bevacizumab in 2D growth in melanoma cell lines..... 96

Figure 3-3: effects of inhibiting VEGF signalling with cediranib (AZD2127) in 2D growth in melanoma cell lines in normoxia..... 97

Figure 3-4: Effects bevacizumab on 3D spheroid growth of melanoma cell lines..... 99

Figure 3-5: Effect of bevacizumab on cell migration in melanoma cell lines.....102

Figure 3-6: Secreted and intracellular VEGF levels of melanoma cell lines.....105

Figure 3-7: Secreted and intracellular VEGF levels of LM cell lines. 108

Figure 3-8: Levels of RNA expression of VEGF in LM cell lines. 109

Figure 4-1: Retroviral expression of WT and V600E *BRAF* in *BRAF* WT cell line. 116

Figure 4-2: Copy number of *BRAF* gene and transfection efficiency for different *BRAF* WT cell lines were determined. 119

Figure 4-3: CRISPR plasmid design and targeting and screening strategy. 121

Figure 4-4: Selection and genetic confirmation of *BRAF* V600E positive clones. 122

Figure 4-5: Expression of *BRAF* mRNA and BRAF protein in WT and knocked in V600E CRISPR clones.....125
Figure 4-6: Response of *BRAF* WT and V600E clones to BRAFi (PLX4720) in the MAPK pathway and in 2D growth. 129
Figure 4-7: Testing response of *BRAF* WT or V600E clones to BRAFi (PLX4720) in 3D growth.....130
Figure 4-8: 2D and 3D growth comparison between the *BRAF* WT and V600E cell clones. 132
Figure 4-9: Technical and sample QC metrics and the hierarchical clustering. 135
Figure 4-10: Expression heatmap of top 50 differentially expressed genes between *BRAF* WT and V600E melanoma cells. 137
Figure 4-11: Quality control for the tumour samples and extracted RNA.....141
Figure 4-12: a Venn diagram of the significantly differentially expressed genes between *BRAF* WT and V600E melanomas in three data sets.....146
Figure 4-13: ROR2 is upregulated in *BRAF* V600E mutant melanoma cells and influences cell growth and VEGF secretion. 149
Figure 5-1: VEGFR expression in *BRAF* WT and V600E clones.....157
Figure 5-2: the effects of VEGF inhibition on the growth of clones. 158
Figure 5-3: RNA expression of HIF1α and VEGF in the CRISPR cell clones. 160
Figure 5-4: Human VEGF ELISA in CRISPR clones. 161
Figure 5-5: Tumour growth response to bevacizumab and survival of CD1 nude mice bearing *BRAF* WT (WT7) and V600E (3F2) xenografts.....164
Figure 5-6: Immunohistochemical analysis of WT3 (*BRAF* WT) and F10 (*BRAF* V600E) xenografts.....166
Figure 5-7: CA9 expression in WT7 (*BRAF* WT) and 3F2 (*BRAF* V600E) xenografts.....169

Figure 5-8: Number of blood vessels and percentage of necrosis in WT7 (*BRAF* WT) and 3F2 (*BRAF* V600E) xenografts. 170
Figure 5-9: Proliferation quantified by Ki67 staining in WT7 (*BRAF* WT) and 3F2 (*BRAF* V600E) xenografts. 171
Figure 5-10: Mouse VEGF concentrations in mice bearing *BRAF* WT and V600E xenografts. 172

List of Tables

Table 2-1: Culture conditions and genetic mutations of cell lines. 61

Table 2-2: Primary antibodies for western blotting..... 65

Table 2-3: Setup of the sample reaction for QuikChange site-directed mutagenesis. 68

Table 2-4: Cycling parameters for Quikchange site-directed mutagenesis..... 69

Table 2-5: Cycling parameters for DNA release. 75

Table 3-1: tumour origins or the 9 LM melanoma cell lines. 91

Table 4-1: Copy number of BRAF gene in cell lines. 118

Table 4-2: Top 50 differentially expressed genes ranked by t value. 136

Table 4-3: Significantly differentially expressed genes that are related to the angiogenesis pathway from PANTHER analysis. 138

Table 4-4: Significantly differentially expressed genes that are related to the VEGF pathway from PANTHER analysis. 138

Table 4-5: fresh frozen patient melanomas for RNA sequencing. 142

Table 4-6: Significantly differentially expressed genes between *BRAF* WT and V600E primary skin melanomas.....142

Table 4-7: Significantly differentially expressed genes between *BRAF* WT and V600E melanoma lymph node metastases. 142

Table 4-8: Top 50 probes sorted on average ranking (AvgRank) for differential expression between *BRAF* WT versus mutant melanoma cell lines. P-values are reported for all three methods LIMMA, SAMR and RP. 144

Abbreviations

5-(3-methyl-1-triazeno)imidazole-4-carboxamide (MTIC)
Angiopoietin (Ang)
Angiopoietin (ANG-2)
Arrest-defective-1 (ARD-1)
Basic fibroblast growth factor (bFGF)
B-cell leukaemia/lymphoma 2 (BCL-2)
Bicinchoninic Acid (BCA)
Bone-marrow-derived cells (BMDCs)
Bovine serum albumin (BSA)
Cancer Cell Line Encyclopedia (CCLE)
Cancer-associated fibroblasts (CAFs)
Carbonic Anhydrase 9 (CA9)
Cisplatin, Vindesine and Dacarbazine (CVD)
Clustered Regularly Interspaced Short Palindromic Repeats (CRISPR)
Complementary DNA (cDNA)
Cyclin-dependent kinase inhibitor 2A (CDNK2A)
Cyclin-dependent kinases (CDK)
Cytotoxic T-lymphocyte-associated antigen 4 (CTLA4)
Dacarbazine (DTIC)
Deoxyribonucleic acid (DNA)
Dimethyl sulfoxide (DMSO)
empty vector (EV)
Endothelial progenitor cells (EPCs)
Enzyme-linked immunosorbent assay (ELISA)
Epidermal growth factor (EGF)
Extracellular matrix (ECM)
Extracellular regulated kinases (ERK)
Fibroblast growth factors (FGFs)
Flow Cytometry (FACS)
Fluorescence *In Situ* Hybridisation (FISH)
Foetal calf serum (FCS)
Food and Drug Administration (FDA)

G protein subunit alpha 11 (GNA11)
Glucose transporters (GLUTs)
Green fluorescent protein (GFP)
Guanine nucleotide-binding protein G subunit alpha (GNAQ)
Hematoxylin and Eosin (H & E)
Human Umbilical Vein Endothelial Cells (HUVECs)
Hypoxia response elements (HERs)
Interleukin-8 (IL-8)
Intratumoural microvessel density (MVD)
Loss-of-Function (LoF)
Luria Broth (LB)
MAP kinase interacting kinase (MNK)
Matrix metalloproteinases (MMPs)
Metalloproteinases (TIMPs)
Metallothionein-2 (MT2A)
Microphthalmia-associated transcription factor (MITF)
Mitogen-activated protein kinase (MAPK)
Mitogen-activated protein kinase kinase 1 (MEK1)
Mouse double minute 2 homolog (MDM2)
Neuroblastoma RAS viral oncogene homolog (NRAS)
Neurofibromin 1 (NF1)
Neuropilin (NRP)
Non-small-cell lung cancer (NSCLC)
Osteopontin (OPN)
Overall survival (OS)
Oxford Gene Technology (OGT)
Oxygen-dependent degradation domain (ODDD)
Papillary thyroid cancer (PTC)
Phosphatase and tensin homolog (PTEN)
Phosphate-buffered saline (PBS)
Phosphatidylinositol 3-kinase/protein kinase B (PI3K/AKT)
Phosphatidylinositol-3,4,5-triphosphate (PIP_3)
Phosphorylation of mitogen-activated protein kinase kinases (MAPKKs)
PiggyBac (PB)
Placental growth factor (PIGF)

Platelet-derived growth factor (PDGF)
Polymerase chain reaction (PCR)
Programmed cell-death protein 1 (PD1)
Progression-Free Survival (PFS)
Prolyl-4-hydroxylases (PHDs)
von Hippel-Lindau protein (pVHL)
Quality control (QC)
Quantitative real-time PCR (qRT-PCR)
Radiation necrosis (RN)
Radioimmunoprecipitation assay buffer (RIPA buffer)
RAS-guanosine diphosphate (RAS-GDP)
RAS-guanosine triphosphate (RAS-GTP)
Receptor tyrosine kinase (RTK)
Receptor Tyrosine Kinase Like Orphan Receptor 2 (ROR2)
Reverse transcription (RT)
Ribonucleic acid (RNA)
RNA Integrity Number (RIN)
RNA sequencing (RNA-seq)
Room temperature (RT)
Signal transducer and activation of transcription 3 (STAT3)
S100 Calcium Binding Protein A4 (S100A4)
Saline Sodium Citrate (SSC)
Telomerase reverse transcriptase (TERT)
Telomerase RNA component (TERC)
The Cancer Genome Atlas (TCGA)
Three-dimensional (3D)
Transcription factor Hypoxia Inducible Factor 1 (HIF-1)
Transforming growth factor-1 (TGF-1)
Transforming growth factor-α (TGF-α)
Tris-acetate-EDTA (TAE)
Tris-buffered saline with Tween (TBS-T)
Tumour necrosis factor-α (TNF-α)
Tumour-associated macrophages (TAMs)
Two-dimensional (2D)
Ultraviolet (UV)

Vascular endothelial (VE)

Vascular endothelial growth factor (VEGF)

von Hippel-Lindau tumour suppressor protein (pVHL)

v-Raf murine sarcoma viral oncogene homolog B1 (BRAF)

Wellcome Trust Centre for Human Genetics (WTCHG)

Wild type (WT)

Chapter 1: Introduction

1.1 Malignant Melanoma

1.1.1 Epidemiology

Melanoma is a common and aggressive malignant tumour of melanocytes, the pigment producing cells of the skin. Although melanocytes are mainly found in the basal epidermis, populations can be found in other parts of the body, including the hair follicles, the eye, the inner ear, meninges, and mucosal surfaces (Tas et al., 2011). Work presented in this thesis focuses on the most common form, cutaneous melanoma.

The incidence of melanoma skin cancers has been increasing over the past decades, with 132,000 new cases globally each year ('WHO | Skin cancers', 2017). Melanoma accounts for only 1% of skin cancer cases but results in most deaths (PDQ Adult Treatment Editorial Board, 2018). In the UK, there were around 15,400 newly diagnosed melanomas in 2014, making it the fifth most common cancer type. In the last ten years, the incidence of melanoma skin cancer has increased by almost a half (45%), with more increase in males (56%) than in females (35%) (Cancer Research UK | Skin cancer statistics, 2018). Melanoma is a young person's disease, being the most common cancer in young adults aged 25 to 29 years and the second most common cancer in those aged 15 to 29 years (Parsons et al., 2015).

1.1.2 Risk Factors

With increased incidence of melanoma, especially in young adults, there has been a great interest and appreciation in risk factors for the disease. Major risk factors can be intrinsic (genetic and phenotype) or extrinsic (environmental or exposure), including sun exposure,

multiple nevi and family history (Rastrelli et al., 2014). Although intrinsic risk factors such as fair skin and family history are not modifiable, patients identified with increased intrinsic risk can adjust their behaviours and exposures to extrinsic risk factors such as Ultraviolet (UV) and chemical exposure (Rigel, 2010).

1.1.2.1 UV Radiation

Studies have shown that the exposure to UV radiation is a major risk factor for melanoma development: blistering sunburn during childhood or adolescence more than doubles the risk in later life (Weinstock et al., 1989). Epidemiological studies have shown that fair skinned individuals living at lower latitudes have increased incidence rates, indicating the association of sun exposure with malignant transformation of cutaneous melanocytes (Moan et al., 2008). deoxyribonucleic acid (DNA) mutation rate in cutaneous melanomas is higher than most other forms of solid cancer, demonstrating the high potency of UV mutagenic effects (Hodis et al., 2012). Individuals with history of familial melanoma have a high sensitivity to UV radiation, and are likely to develop melanoma at a younger age (Aitken et al., 1996; Soufir et al., 1998).

1.1.2.2 Melanocytic Nevi

Melanocytic nevi are benign lesions that present as dark pigmented spots on the skin. Nevi can be congenital or acquired later in life. Multiple atypical acquired nevi are a potential risk factor for malignant melanoma, and changes in shape, colour, or texture can be a strong diagnostic feature for melanoma development (Rhodes et al., 1987). Although the indication of changing nevi helps early detection in melanoma, not all changing nevi lead to melanoma (Batistatou et al., 2007).

1.1.3 Classification of Malignant Cutaneous Melanoma

Melanoma is produced by the transformation of a melanocyte into a malignant cell, progressing into a primary tumour. Over time, the primary tumour begins to thicken and invade the lower levels of the dermis to develop a vertical growth phase, increasing the likelihood of metastasis (Heasley et al., 1996). Historically, in relation to clinical and histological features, the descriptive terms for cellular subtypes of malignant cutaneous melanoma, first described by Dr Wallace Clark, are the following (Rastrelli et al., 2014):

- Superficial Spreading.
- Nodular.
- Lentigo maligna.
- Acral Lentiginous.
- Desmoplastic.

However, the terms used in this cellular classification do not have independent prognostic or therapeutic significance in clinical practice (Viros et al., 2008). In recent years, mutually exclusive oncogenic mutations in melanomas have been identified, promoting a new molecular classification of melanoma. With this molecular classification, biologically distinct subsets of cutaneous melanoma share a common oncogenic mechanism, behave clinically in a similar fashion and respond similarly to different treatments (Scolyer et al., 2011).

In 2015, The Cancer Genome Atlas (TCGA) Network performed the largest integrative analysis of cutaneous melanoma, characterised 333 tumour samples from 331 patients, and established four major genomic subtypes, with molecular analysis at DNA, ribonucleic acid (RNA), and protein levels (Akbani et al., 2015). These four major genomic subtypes identified in this study are:

- v-Raf murine sarcoma viral oncogene homolog B1 (*BRAF*) mutant (52%)

- Neuroblastoma RAS viral oncogene homolog (*NRAS*) mutant (28%)
- Neurofibromin 1 (*NF1*) mutant (14%)
- Triple (*BRAF, NRAS* and *NF1*) wild-type (WT) (14.5%)

As some oncogenic mutations such as *BRAF* have already been successfully exploited as therapeutic targets, this genomic classification may suggest new drug targets and clinical trial design, and could influence clinical decision-making for targeted therapies. More details on molecular changes associated with malignant melanoma are discussed in the next section.

1.1.4 Molecular Changes in Malignant Melanoma

Technological advances in recent years have enabled better understanding of the molecular pathogenesis of a wide variety of diseases including melanoma, and the importance of oncogenic *BRAF* mutation was recognised in 2002 (Davies et al., 2002). Curtin and colleagues in 2005 published their hallmark genome-wide study of 126 melanomas, showing distinct sets of genetic alterations, their associations with the anatomical site of the primary tumour, and different relationships to ultraviolet light (Curtin et al., 2005). Over the past decade, it has become clear that subsets of melanoma can be further defined by recurrent 'driver' mutations in multiple oncogenes, including *BRAF, NRAS, KIT* proto-oncogene receptor tyrosine kinase, G protein subunit alpha 11 (GNA11), guanine nucleotide-binding protein G subunit alpha (GNAQ), and mitogen-activated protein kinase kinase 1 (MEK1) (Curtin et al., 2005; Hodis et al., 2012). Aberrant activation of the mitogen-activated protein kinase (MAPK) pathway is present in over 80% of primary melanomas, and mutations implicated in this pathway are mutually exclusive in different subtypes. Cutaneous melanomas harbour 52% *BRAF*, 28% *NRAS*, and up to 14% *NF1* mutations, while mutations in mucosal melanomas show a different pattern: 11% *BRAF*, 5% *NRAS*, and 21% *KIT* (Akbani et al., 2015; Hayward et al., 2017). Differing significantly from cutaneous melanomas, more

than 80% of uveal melanomas have a constitutively active somatic mutation in *GNAQ* or *GNA11* (Van Raamsdonk et al., 2009, 2010). For cutaneous melanomas, other mutations that may have potential therapeutic relevance include cyclin-dependent kinase inhibitor 2A (*CDNK2A*) deletions, microphthalmia-associated transcription factor (*MITF*) amplification, and phosphatase and tensin homolog (*PTEN*) disruption leading to phosphatidylinositol 3-kinase/protein kinase B (PI3K/AKT) activation (Hodis et al., 2012; Akbani et al., 2015). Since oncogenic *NRAS* also induces the PI3K cascade, the molecular changes associated with MAPK and PI3K pathways are the most prevalent, occurring in more than 90% of cutaneous melanomas (Akbani et al., 2015).

1.1.4.1 MAPK and PI3K Pathways

The MAPK signalling pathway promotes cell proliferation, differentiation, cell survival and transformation (Sullivan and Flaherty, 2013). This pathway contains the most frequently observed recurrent mutations in cutaneous melanoma (figure 1-1). In normal cells, the MAPK pathway is only activated when ligand binds to receptor tyrosine kinases or cytokine receptors. Stimulation of receptors activates the GTPase RAS, which in turn, recruits RAF to the plasma membrane and induces activation of RAF, by homo- or hetero- dimerization as well as phosphorylation (Niault and Baccarini, 2010). Activated RAF then leads to phosphorylation of mitogen-activated protein kinase kinases (MAPKKs), MEK1 and MEK2 thereafter. Phosphorylated MEK phosphorylates and activates extracellular regulated kinases (ERK) 1/2, also known as mitogen-activated protein kinase (MAPK). ERK is an effector serine/threonine kinase that can then phosphorylate targets such as transcription factors, as well as bind directly to DNA sequences, as a transcriptional inducer or repressor (Plotnikov et al., 2011). MAPK signalling is constitutively activated in almost all melanomas (Hayward et al., 2017).

BRAF

ARAF, BRAF, and CRAF are a family of three protein-serine/threonine kinases that participate in the RAS-RAF-MEK-ERK signal transduction cascade (Leicht et al., 2007). As a proto-oncogene, *BRAF* is a dominant genetic target in the MAPK signalling pathway. Although BRAF mutations are observed in many cancer types, they occur most frequently in melanomas, with more than 50% of cutaneous melanomas carrying a somatic *BRAF* mutation (Davies et al., 2002; Akbani et al., 2015; Hayward et al., 2017). In non-malignant cells, BRAF is activated by homo- or heterodimerisation with another RAF kinase in response to upstream signals, however, mutations in *BRAF* enable it to act as a self-sufficient and constitutively activated monomer, leading to uncontrolled proliferation, promoting cell survival and tumour development (Tsai et al., 2008).

The most common *BRAF* mutation in melanoma (90% of all variants) is a missense mutation, with a valine to glutamic acid substitution at codon 600 (V600E), constitutively activating the kinase domain of the protein (Wellbrock et al., 2004). The other *BRAF* mutations found in exon 15 are V600K, V600R, and K601, with V600K being the second most common (Akbani et al., 2015). Rarely, melanomas harbour other *BRAF* mutations such as G469E and D594G, which produce low kinase activity of BRAF, but can activate MAPK signalling through CRAF. Melanomas with these rare low activity *BRAF* mutations are more dependent on CRAF for survival (Smalley et al., 2009).

NRAS

RAS is another important oncogene that is frequently mutated in tumours. Mutations that increase RAS activity can also promote uncontrolled cell proliferation and tumour growth (Ji et al., 2012). Compared to other tumour types, *RAS* mutations are relatively less prevalent in cutaneous melanomas, occurring in fewer than 30% of all cases. Although mutations have been found in all three *RAS* family members (N-, K- and H-RAS), *NRAS* mutation is the most

common in melanoma, involving changes in glycine 12 (G12R/D/A), glycine 13 (G13R/D), and glutamine 61 (Q61R/K/L/H), sustaining NRAS in its active, GTP-bound conformation (Muñoz-Couselo et al., 2017). Although oncogenic mutations are usually not stand-alone in melanoma, major *NRAS* and *BRAF* mutations have been found to be mutually exclusive, suggesting that either is sufficient for constitutive activation of the MAPK pathway. Only in rare cases non-V600E *BRAF* mutations with low kinase activities are found to be co-occurring with mutant *NRAS* (Akbani et al., 2015). Both *BRAF* and *NRAS* mutations are associated with poorer clinical prognosis (Houben et al., 2004). While BRAF mutations are involved in MAPK signalling pathway only, mutant NRAS can activate both the MAPK and PI3K pathways (Fedorenko et al., 2013).

NF1

The tumour suppressor gene *NF1* is the third most frequently mutated gene in melanoma, occurring in 10 to 15% of all cutaneous melanomas. The majority of *NF1* mutations are loss-of-function (LoF) events and these melanomas have the highest number of mutations (Akbani et al., 2015; Hayward et al., 2017). The NF1 protein is a GTPase-activating protein that downregulates RAS activity by converting the active RAS-guanosine triphosphate (RAS-GTP) to the inactive RAS-guanosine diphosphate (RAS-GDP) (Kiuru and Busam, 2017). LoF mutation of *NF1* occurs in much higher rate in non-hotspot *BRAF/NRAS* melanomas (25~38% in non-hotspot compared to 2% in *BRAF* or *NRAS* hotspot mutated melanomas), suggesting that NF1 alternatively promotes RAS and its downstream signalling via MAPK and PI3K pathways (Hodis et al., 2012; Maertens et al., 2013; Akbani et al., 2015).

MEK1 and MEK2

The serine-threonine kinases MEK1 and MEK2 (also known as MAP2K1 and MAP2K2) are downstream substrates of RAF in the MAPK signalling pathway. Phosphorylated MEK activates its effector ERK by phosphorylation, leading to proliferation and cell survival. *MEK1* and *MEK2* mutations are found in 6 to 8% of all melanomas (Nikolaev et al., 2012; Akbani et al., 2015). Some of these mutations are gain-of-function mutations, resulting in constitutive ERK phosphorylation that can mediate resistance to both BRAF and MEK inhibitors (Emery et al., 2009; Nikolaev et al., 2012). Most of the *MEK* mutations reported involve C>T and G>A nucleotide changes, signatures of UV-induced damage, indicating the association between these mutations with exposure to sun radiation (Nikolaev et al., 2012).

PI3K-AKT/PTEN

The phosphatidylinositol-3 kinases (PI3K), signalling pathway plays an important role in cell proliferation and survival, with increased activation of the serine/threonine kinase AKT (also known at protein kinase B). AKT is a major mediator of cell survival through activation of targets such as the mammalian target of rapamycin (mTOR), and inhibition of proapoptotic factors such as BAD and procaspase-9 (Manning and Cantley, 2007). Similarly to the MAPK pathway, mutations in key proteins such as the PI3K subunit PIK3CA and AKT1 can cause constitutive activation of the PI3K-AKT pathway, leading to advantageous gain of cell functions. However, such mutations involving PI3K subunits are rare in melanomas, with fewer than 3% identified (Curtin et al., 2005; Omholt et al., 2006). There are other ways to achieve hyper-activation of PI3K/AKT pathways, including constitutive activation of NRAS and inactivation of phosphatase and tension homolog (PTEN) (figure 1-1).

PTEN is a tumour suppressor gene encoding a lipid and protein phosphatase that negatively regulates the PI3K pathway, inhibiting the activation of AKT by lowering the levels of

phosphatidylinositol-3,4,5-triphosphate (PIP_3) (Carracedo and Pandolfi, 2008). Loss of function in PTEN results in disruption of this negative regulation of AKT and cell survival. The genetic alterations in *PTEN*, scattered along the length of the gene, include point missense mutations, insertions, splice site mutations, and deletions (Eng, 2003). While genetic alterations in *PTEN* have been found in 20 to 30% of melanoma cell lines, they are less common (10 to 20%) in clinical melanoma biopsies (Tsao et al., 1998; Celebi et al., 2000; Reifenberger et al., 2000; Pollock et al., 2002;). The majority of the alterations result in premature termination with transcripts or functional inactivation of the protein (Salmena et al., 2008).

There is frequent co-occurrence of *PTEN* mutations and deletions with *BRAF* mutations observed in melanomas, suggesting a cooperation of BRAF and PTEN in tumorigenesis (Tsao et al., 2012). This theory is supported by a study using genetically engineered mice, in which melanomas could only be developed in mice harbouring *BRAF* V600E with *PTEN* inactivation, but not without (Dankort et al., 2009). The Cancer Genome Atlas (TCGA) Network has found a higher frequency of amplifications and overexpressions of AKT3 in *RAS*, *NF1*, and Triple (*BRAF, NRAS* and *NF1*)-WT melanomas, indicating an alternative mechanism to activate PI3K pathway in these tumours (Akbani et al., 2015).

KIT

The *KIT* gene encodes a receptor tyrosine kinase (RTK) that is involved in melanoma proliferation and survival through both the MAPK and PI3K signalling pathways (Garrido and Bastian, 2010). *KIT* mutations and amplifications are found in 2 to 8% of all melanomas, and are the most common genetic alterations in acral (10 to 20%) and mucosal (15 to 20%) melanomas (Curtin et al., 2006; Torres-Cabala et al., 2009; Hayward et al., 2017). The most

frequently observed *KIT* mutations are L576P in exon 11 and K642E in exon 13, both are activating mutations that can constitutively stimulate MAPK and PI3K/AKT signalling (Kitayama et al., 1995; Willmore-Payne et al., 2005). *KIT* mutations tend to be mutually exclusive with hotspot *BRAF* and *NRAS* mutations, and are associated with poorer clinical outcomes in acral and mucosal melanomas (Willmore-Payne et al., 2005; Curtin et al., 2005; Garrido and Bastian, 2010; Hayward et al., 2017).

1.1.4.2 RB and p53 pathways

Cyclin-dependent kinase inhibitor 2A (*CDKN2A*) is a tumour suppressor gene that has been implicated in melanoma development through regulation of both the retinoblastoma (RB) and TP53 pathways. *CDKN2A* locus at chromosome 9p21 encodes two gene products with alternative splicing, *p16INK4A* and *p14ARF*. Mutations in *p16INK4A* inactivate the RB pathway, while mutations in *p14ARF* inactivate the p53 pathway (Knudsen and Wang, 2010).

p16INK4A/CDK4

The p16INK4A protein is a cell cycle regulator in the RB pathway that binds cyclin-dependent kinases 4 and 6 (CDK4/6). During normal cell cycle progression, the RB tumour suppressor is phosphorylated by mammalian G1 cyclin-CDK complexes, releasing E2F transcription factors and activating genes responsible for S-phase progression. By binding to CDK4/6, p16INK4A inhibits the phosphorylation of RB, regulating G1-S cell cycle transition (Sheppard and McArthur, 2013). Loss of p16INK4A facilitates RB phosphorylation and subsequent cell cycle progression, leading to increased cell proliferation. Loss of p16INK4A occurs in approximately 70 to 80% of all melanomas, most commonly via gene deletion and mutation, but also via promoter methylation (Akbani et al., 2015; Hayward et al., 2017). Alternatively, the RB pathway is dysregulated in melanoma by activating mutations or amplifications in *CDK4*, found in 5% of melanomas (Hodis et al., 2012; Hayward et al., 2017). Mutations in

CDK4 mostly occur at conserved arginine residue R24, located at the inhibitory site of *p16INK4A,* leading to constitutive activation (Rane et al., 2002). Both *p16INK4A* and *CDK4* have been identified as high-risk genes in familial melanomas. However, studies have shown that while 25–40% of familial melanomas have an inactivating *p16INKA* mutation on 9p21 (Kamb et al., 1994; Holland et al., 1995; Liu et al., 1999), only a few families have been identified with a germline mutation in *CDK4* (Goldstein et al., 2000; Molven et al., 2005).

p14ARF/p53

The p53 protein is activated by cell stress or DNA damage and induces an array of responses including cell cycle arrest and apoptosis (Vousden and Lu, 2002). While mutations in *p53* are found in 10 to 20% of melanomas, the p53 pathway is more often inactivated due to loss of function in p14ARF (Hodis et al., 2012; Akbani et al., 2015). p14ARF regulates p53 activity by binding to the mouse double minute 2 homolog (MDM2), an ubiquitin ligase that targets p53 for proteasomal degradation (Bates et al., 1998). Loss of function mutations in p14ARF permit the activity of MDM2, leading to loss of p53 function, deregulation of cell cycle control and genomic instability. Although less common, amplification of *MDM2* has been observed in melanoma, mostly in triple WT tumours (Akbani et al., 2015; Hayward et al., 2017).

1.1.4.3 MITF

Melanogenesis-associated transcription factor (MITF) is the master lineage regulator for melanocyte development and survival. MITF regulates differentiation, proliferation, migration and senescence in melanoma cells, by activating the expression of a range of genes (Hoek et al., 2008; Widmer et al., 2012). MITF can regulate expression of genes involved in cell cycle progression, such as cell cycle kinase CDK2 (Du et al., 2004), CDK inhibitors p16INK4A (Loercher et al., 2005) and p21 (Carreira et al., 2005), and targets anti-apoptotic proteins

such as B-cell leukaemia/lymphoma 2 (BCL-2) (McGill et al., 2002) and its related protein A1 (BCL-2A1) (Haq et al., 2013) to promote cell proliferation and survival. The most common genetic alteration of *MITF* is amplification, which occurs in 15-20% of melanomas (Garraway et al., 2005; Hayward et al., 2017). *MITF* amplification is more prevalent in metastatic disease and correlates with decreased overall patient survival (Garraway et al., 2005). MITF has been shown to be a driver oncogene in melanoma progression, however, its role in suppression of invasion and metastasis has also been recognised (Thurber et al., 2011; Cheli et al., 2012; Bell et al., 2014).

A germline missense mutation in codon 318 of *MITF* (E318K) causes a rare type of familial melanoma. This gain-of-function mutation disrupts a sumoylation site on MITF, resulting in altered transcription of some MITF targets and increased melanoma susceptibility. Individuals with this mutation exhibit high nevus counts, darker eye colour, and increased risk of developing melanoma (Bertolotto et al., 2011; Yokoyama et al., 2011).

1.1.4.4 TERT

Telomerase is a ribonucleoprotein polymerase, whose reverse transcriptase activity is present in germ cells and some stem cells, but normally not in somatic cells (Yi et al., 1999). It is capable of reversing the continued shortening of telomeres by adding 5'-TTAGGG-3' tandem repeats at the end of the chromosomes (Greider and Blackburn, 1989; Lingner and Cech, 1996). The two main components in telomerase are the telomerase reverse transcriptase (TERT), which is the catalytic subunit, and telomerase RNA component (TERC) that provides a template for telomerase elongation (Yi et al., 1999). The expression of TERT is highly regulated, however, upregulation of TERT expression has been found in many cancer types, including melanoma (Takakura et al., 1999; Horn et al., 2013; Huang et al., 2013). Mutations in the *TERT* promoter, mainly C228T and C250T that could generate

binding motifs for Ets/TCF transcription factors to enhance the expression of TERT, have been found in 40 to 70% of melanomas, with a tendency to co-occur with *BRAF/NRAS* mutations (Horn et al., 2013; Huang et al., 2013; Akbani et al., 2015; Hayward et al., 2017). *BRAF/NRAS* mutant melanoma patients with *TERT* promoter mutations have poor overall survival, compared to non-mutated *TERT* patients. (Griewank et al., 2014; Nagore et al., 2016).

1.1.5 Melanoma Therapeutics

Although the incidence of malignant melanoma has continued to increase in the last decade, survival has significantly improved due to better understanding of the biological processes involved in the pathogenesis and progression of the disease (Mattia et al., 2018).

1.1.5.1 Traditional Therapies

The standard treatment for primary melanomas is surgical excision, with a 5-year survival rate of 95% for thin melanomas, reducing progressively for thicker melanomas, and those that have spread to lymph nodes (Essner, 2003). However, following metastasis, survival rate after surgical excision reduces significantly to less than 25% in the UK (Cancer Research UK | Skin cancer statistics, 2018). Metastatic melanomas can be medically managed by chemotherapeutics, with dacarbazine (DTIC) being the most common chemotherapy drug used. Dacarbazine is an alkylating agent that can be converted in the liver to 5-(3-methyl-1-triazeno)imidazole-4-carboxamide (MTIC), to block DNA replication (Sanada et al., 2004). The response rate to dacarbazine is very limited (15 to 20%), with similar results (10-15%) using the oral analogue temozolomide (Middleton et al., 2000). Other single agent chemotherapies, such as antimicrotubule agents taxane and vindesine, cisplatin and nitrosoureaeas, have failed to expand on the responses achieved with dacarbazine when

used alone (Bhatia et al., 2009). Combination chemotherapy, such as cisplatin, vindesine, and dacarbazine (CVD), and the combination of carboplatin and paclitaxel have not demonstrated an improvement in overall survival for metastatic melanoma patients (Wilson and Schuchter, 2016). However, chemotherapy is very rarely used now, due to developments in other forms of treatment.

1.1.5.2 New Therapeutic Approaches

During the last few years, introduction of new targeted and immunological therapies has shown significant improvement for treating metastatic melanoma especially *BRAF*-mutant melanoma. Melanomas are associated with one of the greatest burdens of somatic genetic alterations of all human tumours, resulting in substantial heterogeneity in disease progression and treatment responses (Hayward et al., 2017). New approaches have emerged in recent years to selectively attack cancer cells. These are targeted therapies based on the genetic profile of the tumour, and immunotherapies utilising the body's immune system (Kudchadkar, 2010; Haanen, 2013). Since 2011, all reported large, randomised, phase III studies of targeted or immunotherapy conducted in patients with advanced-stage disease have met their primary end points. In these trials, seven out of eight agents that are newly Food and Drug Administration (FDA) approved have been associated with an improvement in patient overall survival, compared with results of traditional therapies (Mattia et al., 2018). These agents include small molecule inhibitors of BRAF or MEK, and immunotherapeutic antibodies directed at cytotoxic T-lymphocyte-associated antigen 4 (CTLA4) and programmed cell-death protein 1 (PD1).

1.1.5.2.1 Targeted Therapy

The MAPK signalling pathway is an important mediator of cell proliferation, differentiation and survival in melanoma, as discussed in the earlier section (section 1.1.4.1). In 2002, it was discovered that ~50% of cutaneous melanomas have an activating mutation, *BRAF* V600E (Davies et al., 2002b), which ultimately led to the discoveries and FDA approval of the selective BRAF inhibitor vemurafenib and its successor dabrafenib (Zelboraf, Genentech/Roche, South San Francisco, CA) (Tsai et al., 2008; Rheault et al., 2013). It has been well established that BRAF inhibitor treatment improved overall response rate and survival for patients with *BRAF* V600E or BRAF V600K mutations, although responses are typically brief with a median duration of 6 months (Chapman et al., 2011; Hauschild et al., 2012; Zelboraf, 2014). The MEK inhibitor trametinib also inhibits the MAPK pathway (Abe et al., 2011), and improves survival in *BRAF*-mutated melanoma, as compared with chemotherapy (Flaherty et al., 2012). Trametinib was approved by the FDA in 2013 for *BRAF* V600E or *BRAF* V600K positive unresectable or metastatic patients. Although BRAF inhibitors have shown promising results, acquired resistance does occur, especially in patients harbouring additional mutations that reactivate the MAPK pathway (Nazarian et al., 2010). This has subsequently led to the development of combination therapies using BRAF plus MEK inhibitors (dabrafenib plus trametinib, or vemurafenib plus cobimetinib), which improve patient overall survival, compared to BRAF inhibitor monotherapy (Larkin et al., 2014; Robert et al., 2015a).

Although there are other common mutations identified in melanoma, such as mutations in *NRAS* and its negative regulator NF1 (Akbani et al., 2015; Hayward et al., 2017), these are difficult to target therapeutically due to the heterogeneous effector pathways involved (Vu and Aplin, 2016). Activating mutations in *KIT* have been disproportionally found in acral and mucosal melanomas (Curtin et al., 2006). Results from clinical trials have shown limited

sensitivity of some patients to KIT inhibitors, indicating a possible therapeutic target in the *KIT*-mutant melanoma population (Carvajal et al., 2011; Guo et al., 2011; Hodi et al., 2013).

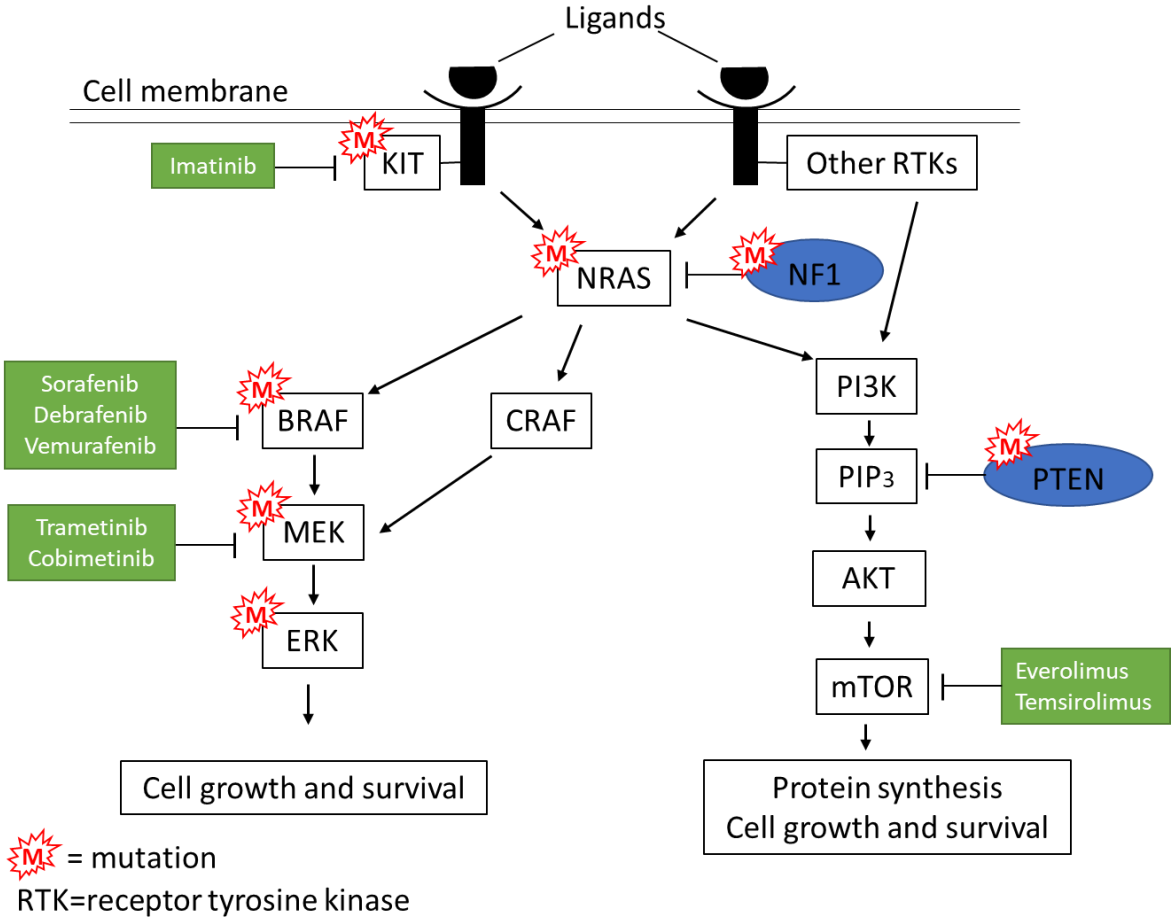


Figure 1-1: MAPK and PI3K pathways and relevant therapeutic strategies.

Binding of ligands to receptor tyrosine kinases (e.g. KIT) activates the downstream MAPK and PI3K signalling pathways, leading to cell growth and survival. Mutations in oncogenes (e.g. NRAS, BRAF and KIT) and tumour suppressors (NF1 and PTEN) frequently occur in melanoma. Inhibition by Imatinib or by different BRAF and MEK inhibitors represents clinically relevant therapeutic strategies.

1.1.5.2.2 **Immunotherapy**

The blockade of immune checkpoints is one of the most promising approaches to activate therapeutic anti-tumour immunity. Immune checkpoints refer to the inhibitory pathways in the immune system that are important for maintaining self-tolerance and suppressing immune responses to minimise normal tissue damage (Mattia et al., 2018). Tumours can dysregulate immune checkpoint proteins as a mechanism of immune resistance, particularly against T cells that are specific for tumour antigens (Pardoll, 2012). The two immune checkpoint inhibitory receptors that have been extensively studies in immunotherapy are cytotoxic T-lymphocyte-associated antigen 4 (CTLA4) and programmed cell death protein 1 (PD1) (Wieder et al., 2016). Monoclonal antibodies have then been developed to block the ligand-receptor interactions at these two immune checkpoints to enhance cell-mediated immunity. This approach was pioneered with the development of the anti-CTLA4 antibodies ipilimumab and tremelimumab, followed by the rapid development of PD1 inhibitors such as nivolumab and pembrolizumab (Callahan et al., 2010; Gong et al., 2018).

CTLA4 was the first immune checkpoint receptor to be targeted clinically. Exclusively expressed on T cells, CTLA4 downmodulates T cell activation by outcompeting co-stimulatory receptor CD28 in binding shared ligands CD80 and CD86 (Azuma et al., 1993; Freeman et al., 1993; Hathcock et al., 1993; Rudd et al., 2009). Two anti-CTLA4 antibodies, ipilimumab and tremelimumab, were developed in parallel, however, only ipilimumab gained FDA approval for melanoma. The evaluation of the efficacy of ipilimumab, as a single agent and in combination with dacarbazine, in phase III clinical trials has demonstrated improved patient overall survival (Hodi et al., 2010; Robert et al., 2011). Studies evaluating the second monoclonal antibody, tremelimumab, showed evidence of tumour regression but no survival

benefit, with more severe immune-related side effects compared to ipilimumab (Ribas, 2010; Ribas et al., 2012;).

The second important immune checkpoint that is targeted in immunotherapy is the PD1 pathway. Unlike CTLA4, which predominantly regulates T cell activation, the major role of receptor PD1 is to maintain T cell tolerance in peripheral tissues and to limit autoimmunity, by predominantly regulating effector T cell activity (Ishida et al., 1992; Freeman et al., 2000; Nishimura et al., 2001; Harris, 2002). The blockade of the interactions between PD1 and its ligands enhances the cytotoxic activity of anti-tumour T cells (Iwai et al., 2002; Hirano et al., 2005; Blank et al., 2006), leading to the development of multiple anti-PD1 monoclonal antibodies. Nivolumab was the first PD1 inhibitor approved by FDA for treatment of patients with advanced and unresponsive melanoma. In the same year pembrolizumab was also approved by the FDA for advanced melanoma patients previously treated with ipilimumab or BRAF inhibitors. Clinical trials have demonstrated efficacy and clinical benefits of both anti-PD1 agents, in the first line setting, as well as in the second line setting after ipilimumab treatment (Ribas et al., 2015; Robert et al., 2015b; Robert et al., 2015c; Weber et al., 2015). Combining PD-1 and CTL4 targeting (nivolumab and ipilimumab) has been shown to achieve response rates of ~60% in patients with metastatic melanoma, however, serious toxicity was reported in some of the patients receiving nivolumab plus ipilimumab (Hodi et al., 2016).

1.2 Angiogenesis in melanoma

Angiogenesis is a dynamic process of the formation of new blood vessels from a pre-existing vasculature (Sherwood et al., 1971). It is a highly regulated phenomenon that normally occurs during embryogenesis, wound healing, and the menstruation cycle. As one of the hallmarks of cancer, angiogenesis is not only essential for tumour growth and progression in the initial

development of the primary lesion, but also pivotal during the establishment of metastases (Hanahan and Weinberg, 2011). To have a constant supply of both oxygen and nutrients to survive, cells need to be within a few hundred micrometres from the nearest blood vessel. For a tumour to grow beyond this size, it must disturb the physiological balance between proangiogenic and antiangiogenic factors, promoting vascular growth by inducing angiogenesis, to meet the demand of cell proliferation (Sherwood et al., 1971). In addition to supplying the oxygen and nutrients, tumour blood vessels remove waste products from tumour tissues and provide a gateway for tumour metastasis (Zetter, PhD, 1998). Pioneering studies led by Folkman in 1971 first suggested the use of angiogenesis inhibition as a new therapeutic strategy for cancer (Sherwood et al., 1971), leading to a shift of research focus towards tumour angiogenesis.

Numerous studies have demonstrated that human melanomas induce angiogenesis, and a correlation has been found between increased angiogenesis, measured by intratumoural microvessel density (MVD), and disease progression and prognosis in those tumours (Srivastava et al., 1988; Fallowfield and Cook, 1991; Kashani-Sabet et al., 2002). During melanomagenesis, the rapid proliferation of tumour cells, especially during the vertical growth phase, increases oxygen and nutrient demands, causing local hypoxia, which then triggers the induction of angiogenesis and vascular remodelling (Carmeliet and Jain, 2011).

1.2.1 Blood Vessel Formation

There are several modes of blood vessel formation identified in tumours (figure 1-2). Sprouting angiogenesis occurs when new vessels are developed from previously existing blood vessels, through the detachment of perivascular cells and activation of endothelial

progenitor cells (Ribatti and Crivellato, 2012). A vascular network could also be assembled by the direct recruitment of bone marrow endothelial progenitor cells (EPCs), within the tumour stroma, that differentiate into endothelial cells to form blood vessels, a process called vasculogenesis (Carmeliet and Jain, 2011). In addition to sprouting angiogenesis and vasculogenesis that are found in normal tissue as well, there are other mechanisms that only exist in tumours. Tumour cells can hijack the blood vessels in surrounding normal tissue along with their invasion through vessel co-option (Donnem et al., 2018). They can also form vessels themselves by acquisition of an endothelial phenotype, a phenomenon known as vascular mimicry (Seftor et al., 2012).

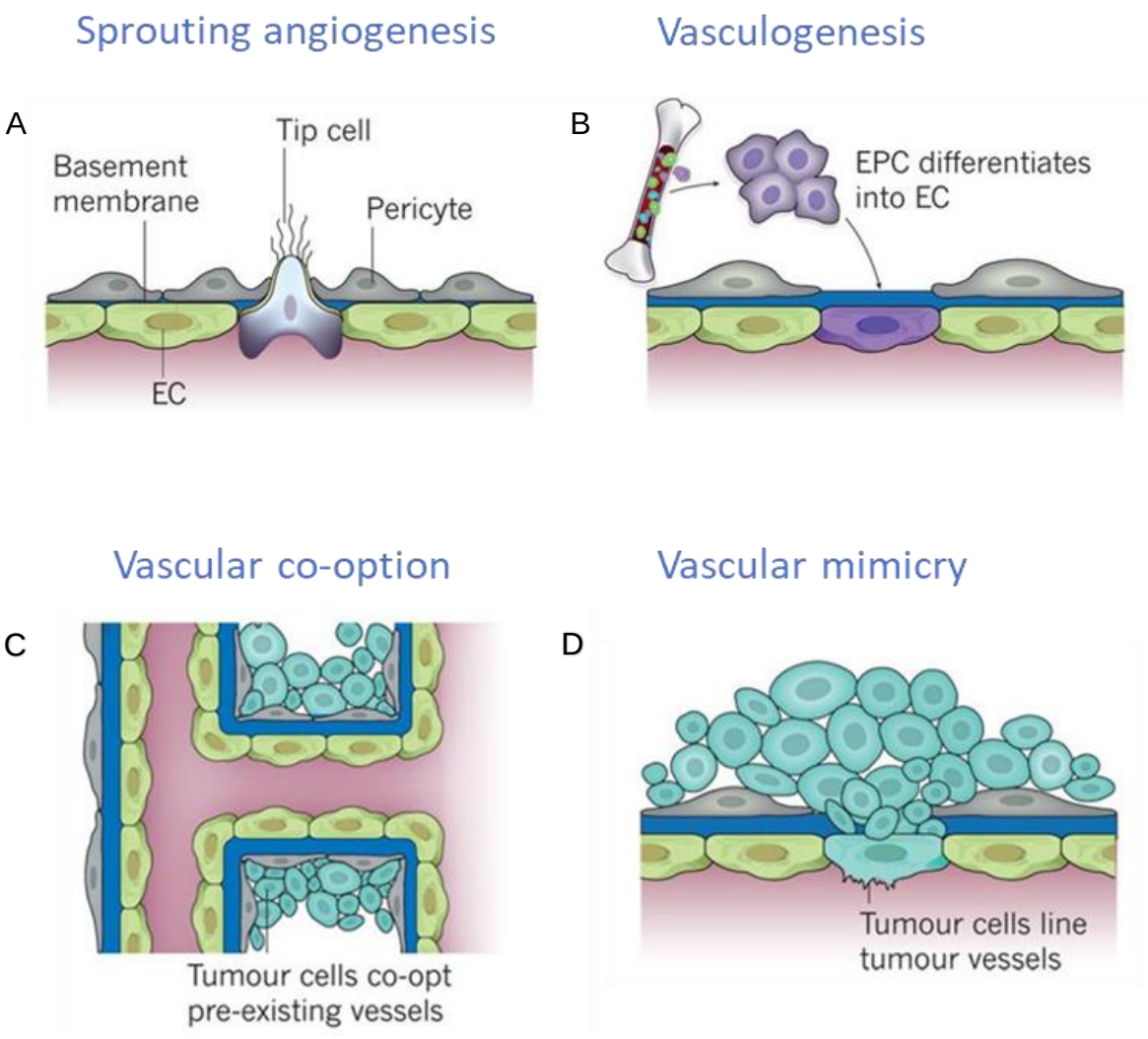


Figure 1-2: Common methods of blood vessel formation in tumours.

A, an endothelial tip cell leads sprouting angiogenesis, followed by pericytes and basement membrane formation. B, a new blood vessel can also be formed by recruitment of bone-marrow-derived and/or vascular-wall-resident endothelial progenitor cells (EPCs) that differentiate into endothelial cells. C, Tumour cells can co-opt pre-existing vessels to obtain oxygen and nutrients. D, tumour cells can acquire a phenotype of endothelial cells and form tumour vessels themselves, a phenomenon known as vascular mimicry. Diagram adapted from Carmeliet and Jain, 2011.

1.2.2 Molecular Mechanisms of Vessel Branching

Quiescent blood vessels are typically formed by a monolayer of endothelial cells with a streamlined surface, interconnected by junctional molecules such as vascular endothelial (VE)-cadherin and claudins, and covered by pericytes to form the basement membrane (Carmeliet and Jain, 2011). Upon receiving an angiogenic signal, such as vascular endothelial growth factor (VEGF), angiopoietin (ANG-2), fibroblast growth factors (FGFs) or chemokines, produced by a hypoxic, inflammatory or tumour cell, pericytes first detach from the vessel wall, and matrix metalloproteinases (MMPs) start the degradation of the basement membrane (Raza et al., 2010). VEGF increases the permeability of the endothelial cell layer, the junctions between these cells are loosened and the vessel dilates (Kevil et al., 1998). This increased permeability causes extravasation of plasma proteins such as fibrinogen and fibronectin to form an extracellular matrix (ECM) scaffold, enabling endothelial cell migration (Halper and Kjaer, 2014). One endothelial cell, known as the tip cell, is then selected to lead the branching. In response to signals such as semaphorins and ephrins, tip cells migrate by adhering to the ECM, mediated by integrins. The surrounding endothelial cells following the tip cell become stalk cells, elongating and forming a lumen (Blanco and Gerhardt, 2013). Pericytes are then recruited to stabilise the basement membrane, leading to vessel maturation. Endothelial cells resume quiescence by transforming into phalanx cells and establishing junctions, after fusion with another vessel (Raza et al., 2010). Figure 1-3 illustrates the steps of blood vessel branching in angiogenesis.

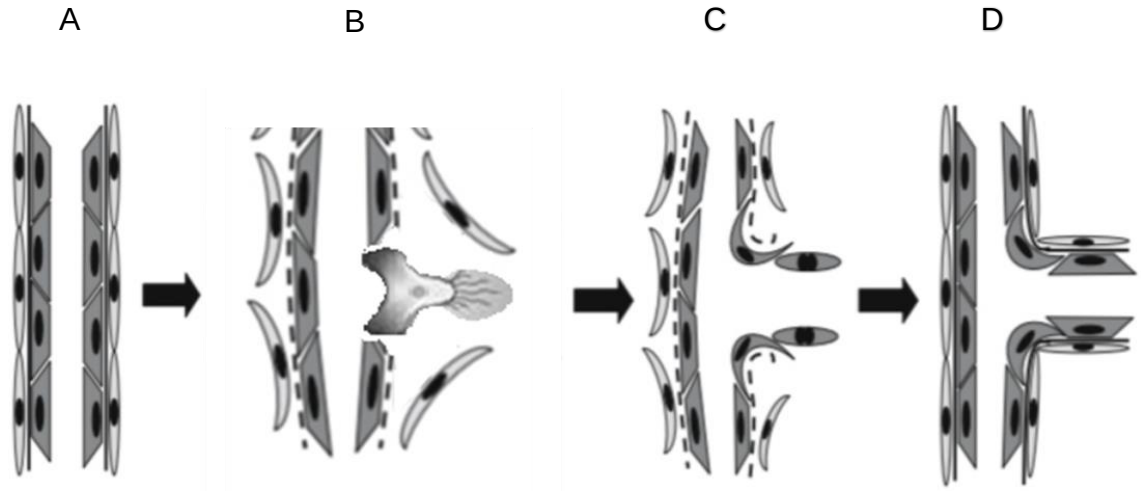


Figure 1-3: Steps of vessel branching in angiogenesis.

A, pre-existing quiescent vessel with endothelial cells (dark grey), pericytes (light grey). B, detachment of pericytes and vasodilation, followed by degradation of the basement membrane. A tip cell is then selected to lead the branching. C, endothelial cells proliferate and migrate to form new vessel, in response to angiogenic signals. D, lumen formation is followed by pericyte attachment and deposition of the basement membrane, leading to vessel maturation. Simplified diagram adapted from Carmeliet and Jain, 2011

1.2.3 Important Players Involved in Angiogenesis

As mentioned earlier, angiogenesis is a complex, multi-step progression regulated by a fine balance of pro and antiangiogenic signals. This balance is disrupted during tumour growth, in favour of proangiogenic signals to activate the 'angiogenic switch'. Tumour hypoxia, caused by increased metabolic activity and oxygen consumption of rapidly proliferating cells, has emerged as one of the primary physiological regulators of the angiogenic switch (Semenza, 2012). The degree of angiogenesis in tumours also depends on the action of various factors produced by different types of cells in the tumour microenvironment, and includes growth factors, chemokines and cytokines such as VEGF, basic fibroblast growth factor (bFGF), interleukin-8 (IL-8), platelet-derived growth factor (PDGF), angiopoietin, integrins, transforming growth factor-α (TGF-α), TGF-β, tumour necrosis factor-α (TNF-α) (Carmeliet and Jain, 2011).

1.2.3.1 HIF

The master regulator of the hypoxic response is the transcription factor Hypoxia Inducible Factor 1 (HIF-1). HIF-1 is a heterodimeric, helix-loop-helix protein that belongs to a transcription factor family, which includes HIF-1α, HIF-2α, HIF-3α, and HIF-1β (Wang et al., 1995). Unlike the oxygen regulated HIF-α subunits, HIF-1β is constitutively expressed and not responsive to oxygen (Semenza, 2012). Of the three HIF-α subunits, HIF-1α is the most ubiquitously expressed, and functions as the master regulator of oxygen homeostasis in many cell types including melanoma (Zbytek et al., 2013).

During normoxia, HIF-1α protein is targeted for proteasomal degradation and ubiquitination involving the actions of prolyl-4-hydroxylases (PHDs) and the von Hippel-Lindau (pVHL) protein. The two proline residues (P^{402}/P^{564}) located in the oxygen-dependent degradation domain (ODDD) of HIF-1α are good substrates for PHDs (Bruick and McKnight, 2001). Another residue lysine (K^{532}) in the ODDD can be acetylated by an acetyl transferase enzyme arrest-defective-1 (ARD-1) (Jeong et al., 2002). Both the hydroxylation of proline residues by PHDs and ARD-1 expression occur only in normoxia. In the presence of co-factors including iron and ascorbate, modified HIF-1*α* subunits with hydroxylated P^{402}/P^{564} and acetylated K^{532} are recognised by pVHL and are targeted for ubiquitination and proteasomal degradation (Maxwell et al., 1999). pVHL is a tumour suppressor and one of the recognised components, together with elongin B and C, of an E3 ubiquitin protein ligase complex (Iwai et al., 1999; Gossage et al., 2015). In response to hypoxia, the degradation ceases, HIF-1α accumulates, binds to HIF-1β (ARNT), and is recruited to hypoxia response elements (HREs) in the promoters of hypoxia inducible genes, resulting in upregulation of many genes including VEGF, the predominant angiogenic factor (Forsythe et al., 1996; Kaelin and Ratcliffe, 2008).

Rapidly growing cancers can outstrip their oxygen supply, so that cells become hypoxic (Hanahan and Weinberg, 2011). The resulting accumulation of HIF-1*α* allows tumour cells to adapt to hypoxic conditions by activating survival pathways. Activated HIF-1 is involved in regulation of over 100 downstream genes that regulate glucose metabolism, cell proliferation, migration and angiogenesis (Powis and Kirkpatrick, 2004). One of the key effects of HIF-1 is to induce transcriptional expression of pro-angiogenic factors including VEGF, stimulating the development of new blood vessels (Carmeliet and Jain, 2011). HIF-1 also promotes overexpression of glucose transporters (GLUTs), enabling tumour cells to shift glucose metabolism from oxidative phosphorylation to the glycolytic pathway to meet their energy needs in low oxygen conditions (Denko, 2008). HIF-1 can promote tumours cells to migrate to more oxygenated tissues by inhibiting expression of E-cadherin and promoting expression of matrix metalloproteinase-2 (MMP-2), thereby increasing the ability of cancer cells to invade and metastasise (Jing et al., 2012).

In addition to the mechanisms of HIF-1α regulation outlined above, growth factor signalling pathways have been reported to be involved in HIF-1α regulation in tumours. Activation of the PI3K pathway, a frequent genetic change in common cancers, can upregulate the translation of HIF-1α protein (Jiang et al., 2001). The downstream effector of PI3K pathway, mTOR, mediates the phosphorylation of the eukaryotic translation initiation factor 4E (elF-4E) binding protein (4E-BP1), inhibiting cap-dependent mRNA translation, leading to enhanced HIF-1α protein translation (Gingras et al., 2001). mTOR also promotes phosphorylation of ribosomal protein S6 via phosphorylating p70 S6 kinase (S6k), inducing protein translation (Gingras et al., 2001). Activation of the MAPK pathway can phosphorylate 4E-BP1, S6K, and MAP kinase interacting kinase (MNK) via its effector ERK, which also upregulates HIF-1α protein translation (Sang et al., 2003). ERK is also involved in transcriptional regulation of

HIF-1α, by phosphorylating the co-activator CBP/p300, leading to increased HIF-1α/p300 complex formation and its transcriptional activation (Sang et al., 2003). Two studies have highlighted the role of mutant BRAF in the MAPK pathway in upregulating HIF-1α and VEGF in melanoma (Kumar et al., 2007; Martin et al., 2012). Kumar et al (2007) reported that both WT and mutant BRAF are involved in regulating HIF-1α expression in melanoma cells. Martin et al (2012) did not compare BRAF WT and mutant melanoma cells but showed that in BRAF mutant cells ERK activity upregulates VEGF, with increased VEGF upregulation when cells are treated with metformin to activate AMP-activated protein kinase (AMPK), which increases ERK activity further via degradation of an ERK phosphatase (Kumar et al., 2007; Martin et al., 2012).

1.2.3.2 VEGF

VEGF Family and Receptors

VEGF is considered one of the most important players in regulating angiogenesis. The VEGF family consists of VEGF-A (also referred to as VEGF), VEGF-B, VEGF-C, VEGF-D, and placental growth factor (PIGF), which mediate their effects through activation of the class III tyrosine kinase receptors VEGFR-1 (Flt-1), VEGFR-2 (KDR), and VEGFR-3 (Flt-4) (Kowanetz and Ferrara, 2006). While VEGF-A, B, and PIGF are mainly angiogenic factors, VEGF-C and D are also important in lymphangiogenesis (Yonemura et al., 2005). The angiogenic response to VEGF is predominantly mediated through the activation of VEGFR-2 on endothelial cells. This activates MAPK and PI3K pathways, leading to integrin-mediated cell adhesion, growth, proliferation, migration, and survival, along with lumen formation and increased vessel dilatation and permeability (Ferrara et al., 2003; Takahashi et al., 1999; Ferrara, 2009). VEGF binds to VEGFR1 with tenfold higher affinity than to VEGFR2, making it a decoy receptor negatively modulating VEGR2 signalling (Fong et al., 1995; Fischer et al.,

2008). Neuropilins (NRP1 and NRP2) are VEGF co-receptors, which enhance the activity of VEGFR-2, but can also signal independently (Ellis, 2006).

VEGF Isoforms

The human VEGFA gene contains eight exons and seven introns. Alternative splicing produces four common isoforms, VEGF121, VEGF165, VEGF189, VEGF206, and other less abundant ones such as VEGF145 and VEGF183, with VEGF165 being the most predominant isoform (Houck et al., 1991). While VEGF121 protein is freely diffusible, VEGF189 and VEGF206 are almost completely bound to ECM (Park et al., 1993). Although VEGF165 is secreted, a significant proportion of it remains bound to the cell surface and ECM. However, this heparin-bound proportion can also be cleaved at the C terminus by plasmin to generate a bioactive diffusible form, and secreted upon stimulation by Ca2+ and protein kinase C (Guzmán-Hernández et al., 2014).

$VEGF_{xxx}b$ family

After identification of the classic VEGF isoforms, it was discovered that exon 8 of the *VEGFA* gene contains two 3' splice sites that can be used to generate two families of isoforms with identical length, but differing C-terminal amino-acid sequences (Bates et al., 2002). Therefore, the *VEGFA* gene is alternatively sliced to form the angiogenic ($VEGF_{xxx}$) and antiangiogenic ($VEGF_{xxx}b$) family of isoforms. The angiogenic form *VEGFxxx* is generated by use of the most proximal sequence in exon 8, resulting from inclusion of exon 8a, whereas the antiangiogenic form *VEGFxxxb* is generated by use of a distal splice site, resulting in splicing out of exon 8a (Bates et al., 2002). *VEGF165b* was the first *VEGFxxxb* isoform identified (Bates et al., 2002), with *VEGF121b, VEGF183b, VEGF145b* (Perrin et al., 2005) and *VEGF189b* (Miller-Kasprzak and Jagodziński, 2008) being discovered subsequently.

The antiangiogenic function of the VEGFxxxb family is carried out by VEGFxxxb homodimers competing with VEGFxxx homodimers for binding to their main receptor VEGFR2, inhibiting cell proliferation and migration (Woolard et al., 2004; Cébe Suarez et al., 2006). VEGF165b inhibits VEGF165-driven angiogenesis in different *in vivo* models, and human melanoma xenografts bearing VEGF165b showed a slower growth in nude mice than VEGF165 alone (Woolard et al., 2004; Cébe Suarez et al., 2006).

Regulation of VEGF signalling

VEGF is produced by various cell types, including tumour cells, macrophages, platelets, keratinocytes, and endothelial cells (Kowanetz and Ferrara, 2006). Several major growth factors, including epidermal growth factor (EGF), FGF, PDGF, TGF-α, TGF-β, keratinocyte growth factor and insulin-like growth factor-1, upregulate VEGF mRNA expression, suggesting that paracrine or autocrine release of such factors cooperates with local hypoxia in regulating VEGF release in the microenvironment (Wang et al., 1999; Miele et al., 2000; Nagineni et al., 2003; Murakami and Simons, 2008; Cascio et al., 2009; Narita et al., 2009). In addition, cytokines such as IL-8, IL-1α, lL-6 and TNF-α induce expression of VEGF (Ryuto et al., 1996; Angelo and Kurzrock, 2007). Some oncogenic mutations in tumours, such as SRC, RAS, MYC, BCR/ABL are also associated with VEGF upregulation (Rak et al., 1995; Baudino et al., 2002; Mayerhofer et al., 2002; Kim et al., 2009).

VEGF/VEGFR autocrine/paracrine signalling

Many tumour types, including melanoma, express VEGF receptors, suggesting potentially functional VEGF/VEGFR signalling which could be autocrine in response to tumour cell-derived VEGF, and/or paracrine in response to stromal cell-derived VEGF, that could promote tumour growth, migration and survival (Straume and Akslen, 2003; Molhoek et al., 2011; Goel and Mercurio, 2013). Studies have shown that VEGF can affect the function of

immune cells via binding to NRP1, regulating tumour growth (Hansen et al., 2012; Yaqoob et al., 2012). Autocrine VEGF signalling has been shown to mediate cell survival in breast carcinoma cells and the inhibition of VEGF expression results in apoptosis (Bachelder et al., 2001). The expression of VEGFR2 is associated with tumour invasion in head and neck carcinomas (Neuchrist et al., 2001). In bladder cancers, VEGF expression correlates with disease stage and muscle invasion, and bladder cancer cell lines show increased invasion in response to VEGF (Xia et al., 2006), demonstrating a possible autocrine loop of VEGF in progression in these tumours. VEGF/VEGFR2 signalling has also been found to increase cell proliferation in gastric cancer (Zhang et al., 2002) and the blockade of such signalling inhibits tumour growth and engraftment in leukaemia (Dias et al., 2001). Adamcic et al showed that inhibiting this autocrine signalling in two melanoma cell lines did not induce direct anti-proliferative effects (Adamcic et al., 2012). In contrast, bevacizumab inhibited growth of uveal melanoma cell lines derived from primary and metastatic uveal melanomas *in vitro* (el Filali et al., 2012; Koch et al., 2014) and reduced hepatic micrometastases from uveal melanoma in an *in vivo* model (Yang et al., 2010).

VEGF expression in melanoma

Melanoma cells produce and secrete VEGF. Multiple studies have demonstrated that VEGF produced by melanoma results in an increase of vascularisation and microvessel permeability of human melanoma xenografts in nude mice (Pötgens et al., 1995; Claffey et al., 1996; Oku et al., 1998). In a clinical study, Ribatti *et al.* have shown that in primary melanomas, strong VEGF-A immunoreactivity in tumour cells increased microvascular density, and increased vessel diameter are correlated to greater thickness of the primary melanoma (Ribatti et al., 2005). Yu *et al.* have demonstrated that in melanoma xenografts, overexpression of VEGF121 and VEGF165 resulted in aggressive tumour growth, whereas melanoma cells

overexpressing VEGF189 remained nontumorigenic and dormant, confirming the tumorigenic effect of the two dominant VEGF isoforms, VEGF121 and 165 (Yu et al., 2002). Increased VEGF expression is associated with the transition from horizontal to vertical growth phase in primary melanoma, and from primary to metastatic melanoma (Erhard et al., 1997; Marcoval et al., 1997; Gorski et al., 2003). Ugurel *et al*. showed that serum levels of VEGF were significantly increased in melanoma patients compared with healthy controls, and increased serum concentrations of VEGF were associated with advanced disease stages and tumour burden (Ugurel et al., 2001). Pelletier *et al*. also reported that blood VEGF levels are significantly increased in patients with melanoma, and the absence of an increase in plasma VEGF levels during follow-up was associated with remission (Pelletier et al., 2005).

1.2.3.3 *BRAF* V600E in regulating VEGF expression

A number of studies have investigated the role of *BRAF* V600E in angiogenesis in different cancers, however, results from these studies are inconsistent. Jo et al found that VEGF expression was significantly higher in *BRAF* V600E papillary thyroid carcinomas (PTC), compared to BRAF WT cancers (Jo et al., 2006). However, a later study led by Durante et al has shown that compared with WT BRAF tumours, VEGF expression was significantly lower in PTCs harbouring *BRAF* V600E mutation, with a decrease in *VEGF* mRNA levels in thyroid cells upon induction of the *BRAF* V600E mutation, and increased expression when *BRAF* V600E was silenced (Durante et al., 2011). A study led by Bottos et al has shown that VEGF was upregulated at the protein level in epithelial cells with knocked-in *BRAF* V600E. However, inhibiting BRAF V600E with PLX4720 did not show significant reduction in VEGF production (Bottos et al., 2012). In melanoma, as outlined above, Martin et al reported that VEGF is upregulated in cells treated with metformin, which activates AMPK and further increases ERK activity (Martin et al., 2012). Kumar et al have reported both WT and mutant

BRAF are involved in regulating HIF-1α expression in melanoma cells (Kumar et al., 2007). These studies indicated that BRAF might upregulate HIF-1α via its downstream effector ERK in the MAPK pathway, which then upregulates *VEGF* at the transcriptional level. ERK is also involved in transcriptional regulation of HIF-1α, by phosphorylating the co-activator CBP/p300, leading to increased HIF-1α/p300 complex formation and its transcriptional activation (Sang et al., 2003). A study led by Niu et al has found that signal transducer and activation of transcription 3 (STAT3) upregulates *VEGF* expression by binding to its promoter (Niu et al., 2002), and STAT3 can be phosphorylated by the activation of MAPK pathway in response to both insulin and osmotic shock (Ceresa et al., 1997), indicating another possible mechanism though which BRAF may regulate VEGF. Additionally, VEGF can be upregulated by increasing protein translation of HIF-1α, via phosphorylation of 4E-BP1, S6K, and MAP kinase interacting kinase (MNK), mediated by ERK (Sang et al., 2003).

1.2.3.4 Other Angiogenic Factors

bFGF

Another important heparin-binding stimulator of melanoma angiogenesis is the basic fibroblast growth factor (bFGF), also known as FGF2 (Shing et al., 1984). bFGF exerts its proangiogenic activity by interacting with various endothelial cell surface receptors, including tyrosine kinase receptor FGFRs and integrins, modulating endothelial cell proliferation, migration, expression of other angiogenic factors such as integrins and cadherin receptor, and intercellular gap-junction formation (Eswarakumar et al., 2005). High levels of bFGF have been found in the ECM, the basement membrane and newly-formed blood vessels in melanoma, especially due to release of EMC-bound bFGF when the EMC is digested by MMPs during new blood vessel formation (Lu et al., 2011; Ornitz and Itoh, 2015). Cross-talk

of bFGF and VEGF may exert a synergistic effect in different angiogenesis models (Pepper et al., 1992; Du et al., 2015).

IL-8

Interleukin-8 (IL-8) expression is found to be overexpressed in primary and metastatic melanomas, but not in benign melanocytic lesions (Singh and Varney, 2000). Several studies have reported that increased circulating level of IL-8 is correlated with disease progression, and poor progression-free and overall survival in melanoma patients (Bar‐Eli, 1999; Birck et al., 1999; Donnini et al., 1999; Helfrich et al., 2009; Kurschat et al., 2007; Ugurel et al., 2001; Westphal et al., 2000). Several reports have demonstrated that IL-8 directly promotes endothelial cell proliferation and migration and regulates angiogenesis (Koch et al., 1992; Li et al., 2003; Melnikova and Bar-Eli, 2006). Liu *et al* have demonstrated that transforming growth factor-1 (TGF-1) enhances expression of IL-8 in human melanoma cells and promotes angiogenesis (Liu et al., 2005).

Angiopoietin

Both Angiopoietin-1 and 2 (Ang-1 and Ang-2) play important roles in angiogenesis (Fagiani and Christofori, 2013). Ang-1 and Ang-2 exert their angiogenic effects by binding to the Tie receptor tyrosine kinase receptors Tie-1 and Tie-2 respectively. Ang-1 stimulates pericyte coverage of blood vessels, leading to stabilisation and maturation of the tumour vasculature; whereas Ang-2, the Ang-1 antagonist, induces the pericytes to become dissociated so that endothelial cells can proliferate and migrate, in response to proangiogenic factors such as VEGF (Huang et al., 2010). Studies have demonstrated that serum Ang-2 levels are associated with disease progression, metastasis and reduced overall survival in melanoma (Helfrich et al., 2009; Nasarre et al., 2009).

Integrins

Integrins are heterodimeric receptors that mediate adhesion of endothelial cells to ECM (Hynes, 2002). Both integrins αvβ3 and αvβ5 have been shown to play important roles in tumour angiogenesis. A number of studies have demonstrated that integrin αvβ3 promotes angiogenesis and endothelial cell survival, and αvβ3 antagonists suppress angiogenesis by inducing endothelial cell apoptosis (Brooks, Clark, et al., 1994; Brooks et al., 1994; Strömblad et al., 1996; Stupack et al., 2001). Studies have shown a correlation between osteopontin (OPN) expression and an aggressive, invasive phenotype in melanoma, possibly mediated by integrin αvβ3, one of the most important osteopontin receptors (Yin et al., 2014). While the angiogenesis induced by bFGF or TNF-α depends on αvβ3, angiogenesis induced by VEGF, and TGF-α is more dependent on αvβ5 (Friedlander et al., 1995). Desch *et al* has found that active Matrix Metalloproteinase-2 (MMP-2) upregulates VEGF at a transcriptional level to promote angiogenesis in melanoma cell via αvβ5/PI3K pathway (Desch et al., 2012).

MMPs and TIMPs

New blood vessel formation in tumours requires remodelling of the ECM, a process that is tightly regulated by Matrix Metalloproteinases (MMPs) and Tissue Inhibitor Metalloproteinases (TIMPs) (Deryugina and Quigley, 2010). Increased expression of MMP-1 and MMP-9 have been correlated to tumour progression and invasion in melanoma (Hofmann et al., 1999; Itoh et al., 1999; Nikkola et al., 2005). Studies have also shown that the membrane type-I metalloproteinase (MT1-MMP) promotes melanoma growth and invasion by activating MMP-2 (Sounni et al., 2002; Iida et al., 2004). MMP-2 has been shown to cleave fibronectin into small fragments to enhance the adhesion and migration of human melanoma cells mediated by αvβ3 integrin (Jiao et al., 2012). As endogenous inhibitors of MMP, TIMPs inhibit melanoma cell growth and invasion. Studies have shown that

overexpression of TIMP-1 and TIMP-3 inhibits tumour growth and invasion, and overexpressed TIMP-2 suppresses both angiogenesis and invasion in melanoma cells (Khokha, 1994; Ahonen et al., 1998; Valente et al., 1998).

1.2.4 Antiangiogenic Therapy

Although angiogenesis is essential for embryogenesis, its role in adulthood is relatively limited and is almost exclusively linked to the menstrual cycle and pathological processes (Carmeliet and Jain, 2011). Angiogenesis is constantly induced in tumour growth and progression to meet the metabolic demands of fast growing tumour cells (Hanahan and Folkman, 1996). This contrast between angiogenesis being pivotal in tumour growth and survival, and the seemingly quiescent nature of normal adult vasculature, suggests an attractive therapeutic target for malignancies by systemically blocking the blood vessel formation in tumours. The work led by Folkman in 1971 first suggested the concept that the vascular network in tumours could be therapeutically targeted, leading to the development of antiangiogenic therapies (Sherwood et al., 1971).

Due to the complexity of tumour angiogenesis, designing an effective targeting approach has been problematic and challenging. Numerous angiogenesis inhibitors have been studied in clinical trials, with some successes in the treatment of metastatic disease in different tumour types, including breast cancer, colorectal cancer, small cell lung cancer and renal cell carcinoma (Carmeliet and Jain, 2000). This has subsequently led to FDA approval of the antiangiogenic therapy bevacizumab for treatment of breast cancer, non-small cell lung cancer, and advanced colorectal cancer (Folkman, 2004). However, FDA approval for breast cancer was later reversed in 2010 due to concerns for safety and lack of improvement in overall survival (OS) in clinical trials (Varella et al., 2017). No antiangiogenic therapy has yet

been approved for the treatment of melanoma, and no study has shown that angiogenesis inhibitors, including multikinase inhibitors, inhibitors of vascular integrins and bevacizumab, provide a significant survival benefit in melanoma patients (Emmett et al., 2011; Jour et al., 2016).

1.2.4.1 Bevacizumab in melanoma

Bevacizumab (Avastin®, ROCHE) is a humanised monoclonal antibody that binds to and neutralises all human VEGFA isoforms, but not murine VEGF, inhibiting VEGF interactions with VEGFR2, but not other VEGF receptors such as NRPs (Ferrara et al., 2005). Bevacizumab has been one of the most frequently investigated antiangiogenic drugs in melanoma, with the majority of studies investigating bevacizumab in advanced metastatic disease.

Bevacizumab was initially evaluated in melanoma in 2007 in a Phase II trial as monotherapy or combined with low dose interferon, IFN-α2b, a cytokine with immunomodulating, antiproliferative and angiogenetic properties (Varker et al., 2007). Patients with metastatic melanoma in this trial were randomised to receive bevacizumab every 2 weeks, with or without low dose IFN-α2b. Prolonged disease stabilisation ranging from 24-146 weeks was observed in 8 patients (25%), although there was no significant improvement in overall survival between bevacizumab monotherapy and combination therapy with IFN-α2b. Combinations with a higher dose of IFN-α2b or dacarbazine have shown improved response rates in later studies (Vihinen et al., 2010; Grignol et al., 2011). In a Phase II trial assessing bevacizumab and high dose IFN-α2b, patients with metastatic melanoma received bevacizumab on day 1 of a 2-week cycle, and IFN-α2b three times weekly. Of 25 patients, 11 required IFN-α2b dose reductions due to toxicity. Objective partial response occurred in

six (24%) patients, with median progression-free survival (PFS) 4.8 months and overall survival (OS) of 17 months (Vihinen et al., 2010; Grignol et al., 2011). In the trial of bevacizumab, dacarbazine and low dose IFN-α2b, there were objective responses in 6/26 patients, with median PFS of 2.3 months and OS 11.5 months (Vihinen et al., 2010).

The BEAM trial was a randomised multi-centre Phase II trial evaluating carboplatin and paclitaxel (CP) with or without bevacizumab (CPB) as first line therapy for metastatic melanoma. In this trial, 240 patients with metastatic melanoma were randomly assigned in a two-to-one ratio to carboplatin plus paclitaxel and bevacizumab or placebo administered once every 3 weeks. Results showed responses in 16.4% and 25.5% of patients on CP and CPB respectively, with a modest but not statistically significant improvement in PFS and OS with the addition of bevacizumab (O'Day et al., 2009; Kim et al., 2012). Similar results were obtained in another Phase II trial combining bevacizumab with paclitaxel/carboplatin in patients with stage IV (metastatic) melanoma (Perez et al., 2009). Of 53 patients, 9 (17%) had partial remission, and 30 (57%) achieved stable disease for at least 8 weeks. Median progression-free survival and median overall survival were 6 months and 12 months, respectively.

The Cancer Therapy Evaluation Programme Trial evaluated the mTOR inhibitor temsirolimus with bevacizumab (Slingluff et al., 2013). In this trial, 17 patients with unresectable stage III or IV melanoma received weekly temsirolimus and bevacizumab every 2 weeks. Of 17 patients, 3 (18%) had partial response (PR), all of whom had BRAF WT melanomas, suggesting this as a promising regimen for this subset of patients who might not have targeted therapies available.

A randomised Phase II trial has compared bevacizumab with temozolomide (TB) or with nab-paclitaxel plus carboplatin, and bevacizumab (ABC) in 93 patients with metastatic melanoma. There was evidence of benefit in the ABC arm, with more prolonged PFS (6.7 vs. 3.8 months) but only minor improvement in OS (13.9 vs. 12.3 months) (Kottschade et al., 2013).

Finally, following evidence that VEGF influences immune regulatory cell function, specifically inhibiting dendritic cell maturation and antigen presentation (Oyama et al., 1998), a Phase I clinical trial assessed the combination of bevacizumab with CTLA-4 checkpoint inhibitor ipilimumab in patients with metastatic melanoma (Hodi et al., 2014). The best response achieved was partial response, in 8/46 (17%) of patients, and the median survival was 25 months. Biopsies obtained during treatment showed evidence of activated vessel endothelium with infiltration of CD8 positive lymphocytes and macrophages (Hodi et al., 2014).

Overall, these results suggested that bevacizumab may have activity when used in combination in patients with metastatic melanoma.

1.2.4.2 Targeting VEGFRs in Melanoma

In addition to VEGF inhibitor bevacizumab, VEGF receptor inhibitors have also been evaluated in clinical studies for patients with metastatic melanoma. A Phase III, randomised, placebo-controlled trial assessed the combination of carboplatin and paclitaxel (CP) alone or with sorafenib, which inhibits VEGF and PDGF receptors and RAF kinases (Hauschild et al., 2009). The trial recruited 270 patients with advanced melanoma, but showed no benefit from addition of sorafenib. Results of this trial showed a median PFS of 17.9 weeks for placebo plus CP arm and 17.4 weeks for the sorafenib plus CP arm, and response rates of 11% and

12% respectively. Another Phase III trial of CP with or without sorafenib for patients with metastatic melanoma recruited 823 patients but also showed disappointing results, with response rates of 20% for CPS and 18% for CP, median PFS of 4.9 months for CPS and 4.2 months for CP, and the same median OS of 11 months on both arms. A small Phase II trial in 32 patients evaluated axitinib, which unlike sorafenib is a potent and selective inhibitor of VEGFR1, 2 and 3, with a response rate of 19%, median response duration of 5.9 months and median overall survival of 6.6 months (Fruehauf et al., 2011).

1.2.4.3 Resistance to Antiangiogenic Therapy

Despite the hope and enthusiasm expressed in earlier studies of antiangiogenic therapy with bevacizumab, progress in the treatment of melanoma has been relatively limited. No study has shown a significant survival benefit using bevacizumab as monotherapy in melanoma. Several hypotheses have been proposed to explain this limited efficiency of antiangiogenic monotherapy, including vascular normalisation, vascular co-option and mimicry, and the presence of compensatory pathways upon treatment with antiangiogenic therapy.

Vascular normalisation

Rakesh Jain in 2001 proposed the hypothesis of 'vascular normalisation', in which blood vessels within the tumour 'normalise' upon receiving antiangiogenic therapy (Jain, 2001). The study showed that tumour vascular networks differ from the homogenous vascular structure in the normal tissue. Tumours contain areas of hypervascularisation as well as hypovascularisation, vessels with variable sizes, low pericyte density, and partly absent basement membrane (Goel et al., 2012a). Antiangiogenic therapy improves the quality of the tumour vascular network during the normalisation window, making chemotherapy/radiation therapy more effective (Goel et al., 2012b). However, this normalisation effect disappears

with prolonged antiangiogenic therapy (Helfrich et al., 2010), which might partially explain the limited responses with bevacizumab monotherapy observed in previous studies.

Vascular co-option and mimicry

In vascular co-option, tumour cells hijack the blood vessels by growing along them, obtaining oxygen and nutrients, compensating for the decreased blood supply caused by antiangiogenic therapy. Vascular co-option has shown to facilitate the melanoma metastases to sustain tumour progression upon inhibition of VEGF (Leenders et al., 2004). Kienast *et al* also demonstrated that melanoma cells grow predominantly in the form of vascular co-option, especially during micrometastasis formation (Kienast et al., 2010). Vascular mimicry, first described by Maniotis *et al* in melanoma, is a phenomenon in which tumour cells acquire an endothelial phenotype and assume endothelial cell functions (Maniotis et al., 1999). This type of neovascularisation reduces the dependency of melanoma cells on angiogenesis, enabling them to escape antiangiogenic therapy (Qiao et al., 2015).

Other compensatory mechanisms

It has been reported that in response to VEGF inhibition, other angiogenic pathways such as the FGF, PIGF and PDGF pathways can be upregulated, suggesting the presence of compensatory mechanisms (Ellis and Hicklin, 2008). Furthermore, the hypoxia caused by vessel regression during antiangiogenic therapy could induce bone marrow stimulation, leading to recruitment of vascular progenitor cells and proangiogenic mon^{oc}ytes. These cells can then differentiate into endothelial cells or proangiogenic tumour-associated macrophages (TAMs), promoting new blood vessel formation in tumours (Bergers and Hanahan, 2008).

1.2.4.4 AVAST-M Trial

Previous studies of antiangiogenic therapy focused on patients with advanced disease. With the limited success presented in these investigations, it has been suggested that it might be more beneficial to target an earlier stage with antiangiogenic therapy, when angiogenesis is likely to be more essential in disease progression (Hanahan and Folkman, 1996). Therefore, AVAST-M trial, a large UK phase III trial, focused on a preventative strategy in high risk melanoma, targeting angiogenesis with adjuvant bevacizumab following surgery (Corrie et al., 2014).

In the AVAST-M trial (Corrie et al., 2014), 1343 patients with stage IIB (primary tumour >2-4 mm ulcerated, or >4 mm non ulcerated, node negative), IIC (ulcerated primary tumour >4 mm, node negative) or III (node positive) melanoma patients were randomised to one year's treatment with bevacizumab (n=671) or observation (n=672). The primary endpoint of the study was overall survival, with secondary end-points relating to disease-free interval, distant metastasis free interval and toxicity. Median follow-up was 25 months for both groups at the time of interim analysis, at which point 286 (21%) of the patients had died, including 140/671 (21%) in the bevacizumab group, and 146/672 (22%) in the observation group. The *BRAF* and *NRAS* mutation status of patient tumours was determined using archival tissue samples, and information was available on *BRAF* status in 645 (48%) patients, with *BRAF* V600 mutation detected in 291 (45%). *NRAS* status was tested in 239 (68%) of 354 patients with *BRAF* WT melanomas, of whom 106 (44%) had a mutation at codon 61. No codon 12 or 13 mutations were detected. At the time of interim analysis, there was no significant difference in OS between the bevacizumab and observation groups (hazard ratio [HR] 0.97, 95% CI 0.78–1.22; p=0.76). However, a longer disease-free interval was observed in patients with *BRAF* V600E melanoma in the bevacizumab group, compared with those in the observation group, whereas no difference was noted between the bevacizumab and observation arms for

patients with *BRAF* WT melanoma (figure 1-4 from Corrie et al., 2014). These results suggested a differential sensitivity of *BRAF* mutant melanomas to antiangiogenic therapy.

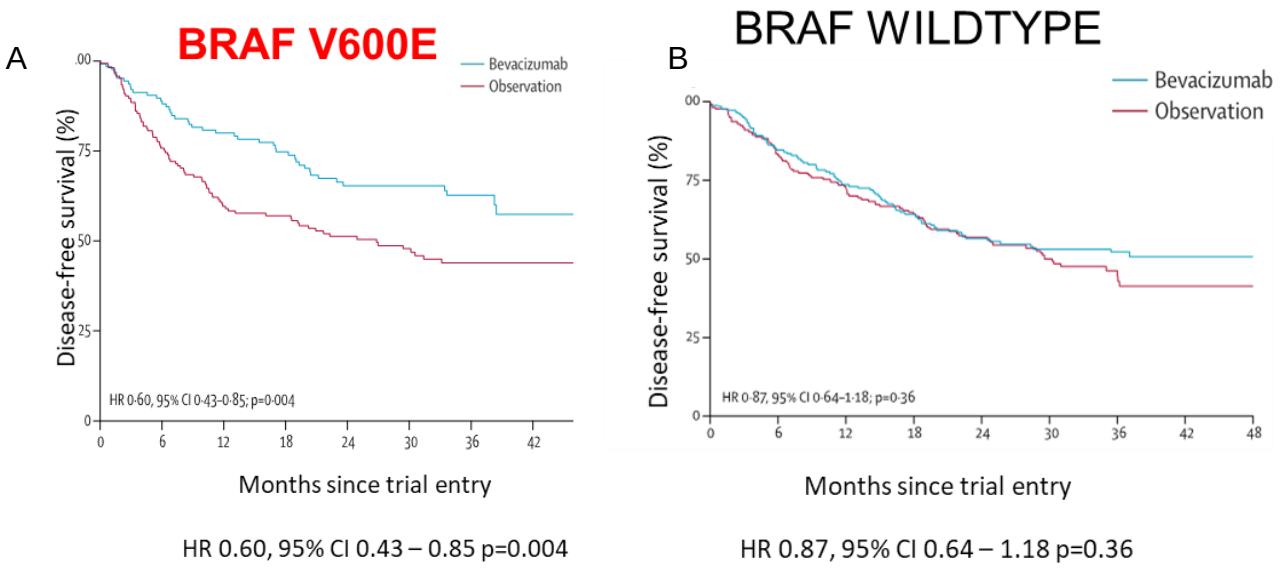


Figure 1-4: Disease-free interval for patients with determined BRAF status in the interim analysis of AVAST-M study.

BRAF status was available for 645 patients in the AVAST-M trial. A, analysis showed that the disease-free interval was prolonged for patients with BRAF V600E mutation, upon receiving adjuvant bevacizumab (A). B, no difference between the bevacizumab group and observation group for BRAF WT patients. Figure adapted from (Corrie et al., 2014).

With 6.4-year median follow-up, an updated analysis of AVAST-M trial was published in 2018 (Corrie et al., 2018). This later report showed that adjuvant bevacizumab after resection of high-risk melanoma improves disease-free interval, but not OS. In this analysis, 515 (38%) patients had died [254 (38%) bevacizumab; 261 (39%) observation], with the OS at 5 years being 64% for both groups. At 5 years, 51% were disease free on bevacizumab versus 45% on observation, and 58% were distant metastasis free on bevacizumab versus 54% on observation. *BRAF* mutant patients had a trend towards poorer OS compared with *BRAF* WT patients (P = 0.06) in the observation arm (Figure 1-5A). A trend towards better OS was still observed in *BRAF* mutant patients with bevacizumab (P = 0.21), compared to the WT group (Figure 1-5B). These results indicate that *BRAF* mutation status may predict for poorer OS in untreated patients, and potential benefit from bevacizumab.

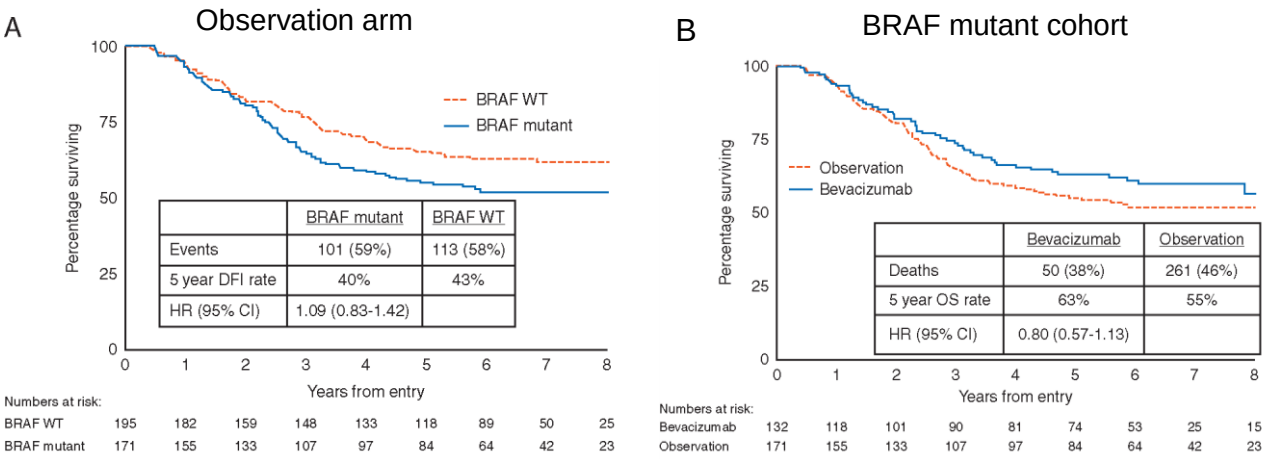


Figure 1-5: Overall survival for patients in the observation arm, and overall survival for BRAF mutant patients treated with bevacizumab in the AVAST-M trial.

A, Overall survival for the observation arm patients showed a trend towards poorer OS in BRAF mutant patients, compared with BRAF WT patients (P = 0.06). B, A trend towards better OS in BRAF mutant patients treated with bevacizumab (P = 0.21). Figure modified from (Corrie et al., 2018).

1.3 Project objectives

The AVAST-M trial assessing bevacizumab as adjuvant therapy for high risk melanoma, showed that patients with BRAF V600E melanomas had improved disease-free interval, while those with wild-type (WT) BRAF melanomas did not benefit (Corrie et al., 2014). Later analysis of AVAST-M trial outcomes will be discussed in later chapters (Corrie et al., 2018). This finding suggested a differential sensitivity of BRAF V600E melanomas to VEGF inhibition. This finding was unexpected. While previous studies have highlighted the role of HIF-1α and VEGF in melanoma angiogenesis (Iervolino et al., 2002; Kumar et al., 2007; Trisciuoglio et al., 2010; Martin et al., 2012; Spinella et al., 2014), no previous studies had specifically compared WT vs. BRAF mutant melanoma cells or patients in terms of angiogenesis or response to antiangiogenic therapy. To investigate the molecular basis for this differential sensitivity, two mechanisms will be evaluated.

The first involves possible autocrine VEGF/VEGFR signalling in melanoma cells, since it has been reported that melanoma cells express VEGF receptors (Molhoek et al., 2011). The second mechanism focuses on the link between BRAF V600E and angiogenesis, with the possible involvement of other mediators in the tumour microenvironment. Therefore, the objectives of this project are to test the following hypotheses:

Hypothesis 1: Inhibition of VEGF by bevacizumab directly suppresses tumour progression via autocrine VEGF/VEGFR signalling in BRAF V600E tumour cells.

Hypothesis 2: The inhibitory effects of bevacizumab in BRAF V600E are mediated indirectly via effects on angiogenesis or other components of the tumour microenvironment.

Chapter 2: Materials and Methods

2.1 Cell lines and cell culture

Melanoma cell lines were cultured in RPMI 1640 or DMEM medium (Gibco®), supplemented with 10% foetal calf serum (FCS, Thermo Fisher), 100 units/ml of penicillin and 0.1 mg/ml streptomycin, and incubated in a humidified atmosphere of 10% CO_2 and 90% air. All LM-Mel cell lines were obtained under Material Transfer Agreement from the Ludwig Institute for Cancer Research Melbourne (Behren et al., 2013). Cell lines CHL1, SKMEL2, HMCB were from American Type Culture Collection, A375, A357M and 501mel from Professor Colin Goding (Ludwig Institute for Cancer Research Oxford), SKMEL28 from Cancer Research UK Cell Services, SKMEL23 from Professor Vincenzo Cerundolo (Weatherall Institute of Molecular Medicine Oxford), genetically modified MDA-MB-231 breast cancer cells MGFP, M121 and M165 from Dr Helen Sheldon (Professor Adrian Harris's Group, University of Oxford) and Phoenix Retrovirus packaging cell line from Dr Judith Cossins (Nuffield Department of Clinical Neurosciences Oxford). HUVEC cells were purchased from Lonza (#2517A) and cultured in EGM™-Plus Growth Medium (Lonza, #CC-3162) at of 10% CO_2. Cell lines were authenticated using the Human cell line authentication services provided by Eurofins Genomics. All cell lines were regularly tested for mycoplasma (MycoAlert kit, Lonza Rockland Inc, Rockland US). When cells were approximately 80% confluent, they were trypsinised (Trypsin-EDTA, Gibco™) and passaged at 1:10 or 1:20 ratio for sub-culturing, before they were discarded after 15 passages. Cells were banked with freezing medium containing 10% dimethyl sulphoxide (DMSO) and 90% FCS. Melanoma cell lines used for this project are listed in Table 2-1.

Table 2-1: Culture conditions and genetic mutations of cell lines.

Cell line	Medium	CO_2 requirement	BRAF	RAS	Other known mutations*
A375	DMEM	10%	V600E	WT	
A375M	DMEM	10%	V600E	WT	
Me	DMEM	10%	V600E	WT	
M14	DMEM	10%	V600E	WT	
501 Mel	DMEM	10%	V600E	WT	CTNNB1
SKMEL 28	DMEM	10%	V600E	WT	EGFR, p53 (Ikediobi et al.,
SKMEL 29	DMEM	10%	V600E	WT	
SKMEL 31	DMEM	10%	V600E	WT	
WM35	DMEM	10%	V600E	WT	
Malme 3M	DMEM	10%	V600E	WT	
Mel 275	DMEM	10%	V600E	WT	
CHL1	DMEM	10%	WT	WT	
CHL1 clones	DMEM	10%	WT	WT	
CHL1-CRISPR clones	DMEM	10%	V600E	WT	
SKMEL 2	DMEM	10%	WT	NRAS	Kit, p53 (Ikediobi et al., 2006)
HMCB	DMEM	10%	WT	NRAS	
SKMEL 23	DMEM	10%	WT	WT	
Na8	DMEM	10%	WT	WT	p53
Phoenix	DMEM	10%	WT	WT	
MGFP (MDA-MB-231)	DMEM	10%	G464V	WT	p53
M121 (MDA-MB-231)	DMEM	10%	G464V	WT	p53
M165 (MDA-MB-231)	DMEM	10%	G464V	WT	p53
LM-Mel-16	RPMI 1640	10%	V600E	WT	
LM-Mel-31	RPMI 1640	10%	V600E	WT	
LM-Mel-4	RPMI 1640	10%	V600E	WT	
LM-Mel-25	RPMI 1640	10%	WT	WT	
LM-Mel-39	RPMI 1640	10%	WT	WT	
LM-Mel-44	RPMI 1640	10%	WT	WT	
LM-Mel-19	RPMI 1640	10%	WT	NRAS	
LM-Mel-34	RPMI 1640	10%	WT	NRAS	
LM-Mel-5a	RPMI 1640	10%	WT	NRAS	

*Unless otherwise indicated, information about cell mutations was obtained from Sanger Cosmic database (https://cancer.sanger.ac.uk/cosmic).

2.2 Cell-based assays

2.2.1 Viability assay

Cells (1000 to 2000 cells per well depending on the proliferation rate of each cell line) were seeded in replicate wells of clear bottom 96-well microplates on day 1. Cells were treated with drugs or solvent control at 24 hours after seeding. Plates were incubated for another 72 hours at 37 ˚C in normoxia or 0.1% O_2 in the hypoxia chamber. Cell viability was measured in the wells using CellTiter-Glo® Luminescent Assay (Promega). Addition of this assay reagent resulted in cell lysis and generation of a luminescent signal proportional to the amount of ATP present. The amount of ATP was directly proportional to the number of cells present in the wells. The CellTiter-Glo reagent was added to the wells in a 1:1 ratio to the cell medium. Plates were then incubated the dark on a shaker for 5 minutes before the luminescent signal was measured using a microplate reader (POLARstar Omega).

2.2.2 3D Spheroid assay

Cells were kept on ice for 30 minutes and seeded in 6 replicate wells (5000 cells per well) in Costar® Ultra-low adherent round bottom 96-well plates (#7007) in medium containing 5% Corning® Matrigel® matrix (#354248). Plates were centrifuged at 2000 revolutions per minute (rpm) for 10 minutes at 4 ˚C and incubated at 37 ˚C/10% CO_2 for 48 hours. Once the spheroids were formed after 48 hours, the size of each spheroid was measured using GELCOUNT™, before drug or dimethyl sulfoxide (DMSO) was added to the wells. Growth of the spheroids was measured before each medium change at every 2 days.

2.2.3 Wound healing assay

Cells were seeded in quadruplicate in 6-well cell culture plates on day 1. Then on day 2, bevacizumab (150 µg/ml; Avastin®) was added to the wells. Avastin® was purchased from the Churchill Hospital Pharmacy of Oxford University Hospitals NHS Foundation Trust. A straight scratch was created with a 200 µl pipette tip across each well when cells reached 80 ~ 90 confluence on day 3 or 4 depending on their proliferation rates. Wells were washed twice with phosphate-buffered saline (PBS, #SLBZ3711, Sigma), and medium containing 150 µg/ml bevacizumab was added. Plates were incubated in a 37 ˚C/10% CO_2 incubator, and cell growth was monitored using Live Cell Imaging Analyser IncuCyte ZOOM®. Images were taken every 3 hours for 24 hours, and the relative wound density was calculated using the IncuCyte 2011A analysis software.

2.2.4 Determining cell population doubling time

Cells were seeded in duplicate dishes on day 1. On day 2, Cells were washed with PBS twice before they were trypsinised and harvested. Cell number from each dish was then counted and recorded using the Countess™ automated cell counter. The same procedure was repeated daily on day 3 to 5 for the remaining dishes. Doubling time for each cell line was then calculated based on the cell numbers on GraphPad Prism v5.

2.3 Protein analysis

2.3.1 Western blotting

Cells were harvested at 70-80% confluence after treatments required by the experiments. Cells were washed with ice-cold PBS twice before they were collected by scraping into 1ml

PBS, followed by centrifugation at 1200 rpm for 5 minutes at 4 °C. After removing the supernatant, 100 µl of radioimmunoprecipitation assay buffer (RIPA buffer, Thermo Scientific, #89900) containing protease and phosphatase inhibitors (Thermo Scientific, #78444) was added. After incubating on ice for 30 minutes, the cell lysate was centrifuged at 14,000 rpm for 15 minutes at 4 °C to remove cell debris. Soluble protein was quantified using the Pierce Bicinchoninic Acid (BCA) protein assay (Thermo Fisher Scientific, UK) and equal amounts of protein were denatured in 3 x Laemmli Buffer (70 mM Tris pH 6.8, 5% (v/v) β-mercaptoethanol, 40% (v/v) glycerol, 3% (w/v) SDS, 0.05 (w/v) Bromophenol Blue) at 95 °C for 5 minutes. Proteins were separated by molecular weight by SDS polyacrylamide gel electrophoresis on 5 – 15% gels. Proteins were transferred to Hybond C extra nitrocellulose membrane (Amersham Pharmacia Biotech) in semi-dry transfer buffer (48 mM Tris, 39 mM glycine, 20% methanol, 1.3 mM SDS, final pH 9.2) using a semi-dry transfer apparatus (Hoefer SemiPhor Transfer Unit, Amersham Biosciences) at a constant current of 35 milliamps per 80 cm^2 gel for 3 hours, or the Trans-Blot® Turbo™ Transfer System for 10 minutes. Membranes were blocked to reduce nonspecific protein binding, with either 5% (w/v) skimmed milk (Sigma) or bovine serum albumin (BSA, Sigma) in TBS-T (Tris-buffered saline with 0.1% Tween 20 [Sigma]) at room temperature for 1 hour. Diluted primary antibodies (Table 2-2) were added to the membranes and incubated at 4 °C overnight on a shaker. After washing with TBS-T for 4 times with 5 minutes each time, membranes were incubated with goat anti-rabbit or goat anti-mouse secondary antibody conjugated to horse-radish peroxide (DAKO, Ely, UK) for one hour at room temperature. Membranes were then washed again and proteins were detected using Enhanced Chemiluminescence (ECLplus, Amersham Pharmacia Biotech).

Table 2-2: Primary antibodies for western blotting.

Antibody	Source	Blocking	Dilution	Molecular Weight (kDa)
pVEGFR2	Cell Signaling; #2478	5% BSA	1:1000	210/230
VEGFR2	Cell Signaling; #2479	5% milk	1:1000	230
VEGFA	Abcam #ab183100	5% milk	1:1000	37
BRAF V600E	Abcam #ab200535	5% milk	1:1000	84
pAKT	Cell Signaling; #4058	5% BSA	1:1000	60
Total AKT	Cell Signaling; #9272	5% milk	1:1000	60
HIF-1α	BD Transduction Laboratory	5% milk	1:1000	120
pERK	Cell Signaling; #4370	5% BSA	1:1000	42/44
Total ERK	Cell Signaling; #4695	5% milk	1:1000	42/44
pMEK	Cell Signaling; #9121	5% BSA	1:1000	45
Total MEK	Cell Signaling; #4694	5% milk	1:1000	45
β-tubulin	Cell Signaling; #2146	5% milk	1:5000	55

2.3.2 VEGF enzyme-linked immunosorbent assay (ELISA)

2.3.2.1 Sample preparation for cell lines

Cells were seeded in triplicate 60 mm cell culture dishes in 10% FCS medium on day 1. Cells for hypoxic investigations were placed in a 0.1% O_2 hypoxic chamber. Medium was changed to 2% FCS on day 2, and again on day 3. Medium samples were collected on day 4 (24 hr samples) and day 5 (48 hr samples). Medium was centrifuged at 12,000 rpm for 10 minutes to remove cell debris, before it was stored at -20 °C. The corresponding cells in each dish were harvested and their total protein was quantified with BCA protein assay. For the intracellular VEGF assay, cells were seeded in 100 mm culture dishes and harvested at 60~70 confluence. Cells were washed with ice-cold PBS twice before they were collected by scraping into 1ml PBS, followed by centrifugation at 1200 rpm for 5 minutes at 4 °C. After removing the supernatant, 200 µl of RIPA buffer (containing protease and phosphatase inhibitors) was added. Two more independent sets of samples for each cell line were collected at 24 hr and 48 hr following the same procedure, and stored at -20 °C. VEGF in

medium samples and in the cell lysate was measured with the R&D system VEGF ELISA kit (R&D system, #DVE00). Total protein in the lysate samples was also quantified (BCA protein assay). VEGF assays were performed as described below and were presented VEGF pg/µg total protein).

2.3.2.2 VEGF Enzyme-linked immunosorbent assay

The R&D system Quantikine Human VEGF ELISA contains Sf21 (baculovirus)-expressed recombinant human $VEGF_{165}$ and antibodies raised against the recombinant protein. Data provided by the manufacturer showed that in specificity testing, 100% cross-reactivity was observed with recombinant human $VEGF_{121}$, therefore, results generated from this assay reflected the combined VEGF levels of both isoforms. The results of VEGF assay were presented as pg of VEGF per µg of total protein.

Wash buffer and standard dilutions were prepared according to the manufacturer's protocol, and 50 µl of assay diluent was added to each well of the microplate that has been pre-coated with VEGF-specific monoclonal antibody. Standard or samples (200 µl) was added to the well, and the plate was covered with a plate sealer, before it was left to incubate at room temptation for 2 hours. The plate was then washed with wash buffer for 3 times, before 200 µl conjugate solution was added to each well. The plate was covered and was left to incubate for another 2 hours. The plate was washed with wash buffer for 3 times again, before 200 µl of substrate solution was added. The plate was sealed again and placed in the dark for 20 minutes to protect from light. After the incubation, 50 µl of stop solution containing 0.2M sulfuric acid was added to each well. The plate was then read at 450 nm using the POLARstar Omega (BMG labtech) plate reader with a wavelength correction at 540 nm.

2.3.3 Flow cytometry

Cells were serum starved overnight in 2% FCS containing media, before being stimulated with 50ng/ml VEGFA for 30 min. All cells were harvested using enzyme free dissociation buffer (Millipore; #P59226) and kept on ice. Cells were washed three times with ice-cold PBS, before they were incubated with primary antibody against VEGFR2 (Cell Signalling, #9698) in 1:400 dilution in incubation buffer (PBS containing 0.5% BSA) for 60 minutes at room temperature (RT). Cells were washed three times before incubating in Alexa Fluor® 488-labelled secondary antibodies at 1:1000 in incubation buffer for 30 minutes at RT. Cells were washed three times with PBS before analysed by flow cytometry using a FACSCalibur flow cytometer (BD Biosciences) and CellQuest software (BD Biosciences).

2.4 Generating a BRAF WT/V600E Isogenic model using retroviral system

2.4.1 Preparation of plasmids

Plasmids were received as transformed bacteria in stab culture. The bacterial stab was streaked on to ampicillin Luria Broth (LB)-agar plates and incubated at 37 ˚C overnight. Single colonies from the streaked LB agar plate were picked and transferred into Falcon tubes containing 5 ml LB medium with 5 µl of 100 mg/ml ampicillin. The liquid culture was then incubated in a shaker at 37 ˚C overnight. Plasmid DNA were extracted using the QIAprep spin miniprep kit (QIAGEN, #27104).

In brief, to isolate the plasmid DNA, bacterial cells were collected by centrifugation at 2000 rpm for 5 minutes, before 250 µl of P1 buffer containing RNase was added to resuspend the

cells. Cells were lysed with 250 µl P2 buffer and incubated for 3 minutes at room temperature. After the incubation, neutralising solution N3 buffer was added, and the tube was inverted for 10-12 times until the solution became clear. The tubes were centrifuged for 10 minutes, before the supernatant was transferred to a QIApre spin column for plasmid binding. The spin column was then washed with 500 µl Buffer PB and then Buffer PE before the plasmid DNA was eluted in 50 µl of Milli-Q water. The concentration of DNA samples was determined using the NanoDrop 2000c Spectrophotometer.

2.4.2 Site-directed mutagenesis

2.4.2.1 Mutant strand synthesis reaction

A *BRAF* V600E expression vector pBabe-Puro-*BRAF*-V600E was obtained from Addgene ((Boehm et al., 2007; Plasmid #15269), and a corresponding *BRAF* WT vector was created based on pBabe-Puro-*BRAF*-V600E using the QuikChange II XL Site-Directed Mutagenesis Kit (Agilent, #210515). Forward and reverse primers (#AN2003048) containing the *BRAF* WT sequence were generated using the Quikchange Primer Design tool and synthesised by Life Technologies Ltd. The sequence information of primer pair AN2003048 can be found in Table 2-6. Sample reaction was then set up as indicated in Table 2-3.

Table 2-3: Setup of the sample reaction for QuikChange site-directed mutagenesis.

Reagents	Volume (µl)
10x reaction buffer	5
Plasmid #15269 (10 ng)	3.2
Forward primer (125 ng)	9.7
Reverse primer (125 ng)	9.2
dNTP mix	1
Quiksolution	3
Molecular grade water	18.9
Total	50

After mixing these components above, 1 µl of 2.5 U/ul *pfuUltra* HF DNA polymerase was added to the mixture. The tube was then placed in the Thermo Cycler (MJ research, USA) and cycling parameters were set up as in Table 2-4.

Table 2-4: Cycling parameters for Quikchange site-directed mutagenesis.

Segment	Cycles	Temperature	Time
1	1	95 °C	60s
2	18	95 °C	50s
		60 °C	50s
		68 °C	8 min
3	1	68 °C	7 min

2.4.2.2 *Dpn* I Digestion of the amplification products

The *Dpn* I endonuclease, specific for methylated DNA, was used to digest the parental template containing *BRAF* V600E. One µl of the *Dpn* I restriction enzyme (10U/µl) was added to the reaction mix, and the contents were gently mixed before centrifugation for 1 minute. The mixture was then immediately incubated at 37 ˚C for 1 hour.

2.4.2.3 Transformation of XL10-Gold Ultracompetent cells

XL10-Gold Ultracompetent cells were gently thawed on ice. For each reaction, 45 µl of competent cells was added to a prechilled 15 ml Falcon tube. Two µl of β-mercaptoethanol was added to the tube on ice, and it was mixed gently every 2 minutes for 10 minutes. Two µl of *Dpn* I-treated DNA was then added to the competent cells. The mixture was then incubated on ice for 30 minutes, heat-shocked at 42 ˚C for 30 seconds, then immediately placed on ice for 2 minutes. NZY$^+$ broth was pre-heated at 42 ˚C, and 0.5 ml of the pre-heated broth was added the competent cells, before the mixture was incubated at 37 ˚C for 1 hour with shaking at 250 rpm. After the incubation, 250 µl of the transformation mix was spread on each LB-ampicillin agar plate. The plate was then incubated at 37 ˚C overnight. After overnight incubation, single colonies from the LB agar plate were picked and transferred into

Falcon tubes containing 5 ml autoclaved LB medium with 5 µl of 100 mg/ml ampicillin. The liquid culture was then incubated in a shaker at 37 ˚C overnight. Plasmids were isolated using the QIAprep spin miniprep kit (QIAGEN, #27104).

2.4.3 Preparation of plasmids for DNA sequencing

Sequencing primers (Seq-braf-1 to Seq-braf-5) were designed and synthesised by Life Technologies Ltd. The sequences of these primers is given in Table 2-6. Both primers and plasmids were quantified using the NanoDrop 2000c Spectrophotometer, before they were diluted to a suitable concentration (100ng/µl for plasmids, 3.2pmol/µl for primers) and sent for sequencing by Source BioScience Oxford.

2.4.4 Polyethylenimine transfection

To make the transfection mix, 7.5 µl of 20% glucose was added to 18 µg of plasmid DNA in 22.5 µl of H_2O, then 9.0 µl of 5.6 mg/ml polyethylenimine (Sigma Aldrich, #408727) was added to the mixture, mixed gently, and then added to 6 ml fresh DMEM for transfection. Phoenix Retrovirus production cells were seeded into T75 tissue flasks (6 x 10^6 per flask), and used for transfection at 70-80% conflence. Growth medium was removed, and the transfection medium was added to the cells. After overnight incubation at 37 ˚C/10% CO_2, the transfection medium was removed and 7 ml of fresh DMEM was added to the cells. After 48 hours incubation, the medium containing retrovirus was harvested and centrifuged at 2000 rpm for 10 minutes. The supernatant was aliquoted and stored at -80 ˚C.

2.4.5 Retroviral infection

Melanoma cells were seeded in a 6 well plate (2 x 10^5 per well) on day 1. On day 2, 1 ml of viral medium supplemented with 8 µg/ml polybrene (Sigma Aldrich, #H9268) was incubated at 37 ˚C for 30 minutes before adding to the cells. On day 3, the conditioned medium was replaced with fresh DMEM, and the 5th day, infected cells were selected with 2 µg/ml of puromycin (Sigma-Aldrich, #P8833).

2.5 Generating a *BRAF* WT/V600E Isogenic model using CRISPR-Cas9 system

To generate a *BRAF* WT/V600E Isogenic model using Clustered Regularly Interspaced Short Palindromic Repeats (CRISPR), *BRAF* WT cell lines were screened first for suitability by fluorescence *in situ* hybridisation (FISH) for the copy number of the *BRAF* gene.

2.5.1 Fluorescence *In Situ* Hybridisation (FISH)

2.5.1.1 Chromosome harvesting

One T25 flask per cell line was seeded at approximately 60% confluence on day 1. On day 2, 30 ng/ml of Colcemid (ThermoFisher) was added to the culture and the flask was incubated at 37 ˚C for 3 hours. Cells were harvested with trypsinisation and the cell pellet was resuspended in 10 ml of 75mM KCl in water. After an incubation at 37 ˚C for 20 minutes, cells were centrifuged and pelleted before they were resuspended in cold Carnoy's fixative (3:1 methanol:glacial acetic acid) and incubated at RT for 30 minutes. Cells were pelleted, resuspended in cold fixative again, and incubated at RT for 10 minutes. Cells were pelleted

and resuspended again in 200 µl of fixative, before they were placed onto a slide. The slide was then left to dry overnight before hybridisation.

2.5.1.2 Probe preparation

BRAF-specific probes PAC RP5-839B19 (AC006347.2, chr7:140811304-140880878, hg38) and BAC RP11-60D5 (chr7;155229982-155394379, hg19) were obtained from SourceBioscience, and harvested using the QIAprep spin miniprep kit (QIAGEN, #27104). The purified DNA was labelled by incorporating digoxigenin-11-dUTP (Sigma) in RP5-839B19, and biotin-16-dUTP (Sigma) in RP11-60D5, by nick translation (Abbott Molecular Nick translation kit). The labelled probes were purified by ethanol precipitation, and resuspended in hybridization mix (50% formamide, 10% Dextran sulphate, 1x Denhart's, 0.1% SDS, 2xSSC) at 10 ng/ul, with the addition of 100 ng/ul of unlabelled human repetitive C0t1 DNA (Thermo Fisher).

2.5.1.3 FISH

FISH experiment was carried out by Dr Daniela Morlli in the Wellcome Trust Centre for Human Genetics in Oxford. To denature the cells, the slides were incubated in 2x Saline Sodium Citrate (SSC) buffer (Sigma, #S6639) at 70 ˚C for 30 minutes, followed by 1 minute in 0.1x SSC buffer and then 1 minute in NaOH 0.07M. Cells were washed in 0.1x SSC buffer at 4 ˚C for 1 min, and 2x SSC buffer at 4 ˚C, for 1 minute, and finally dehydrated through alcohol series 2 minutes each in 70%, 90%, and 100% ethanol. The slides were left to air-dry.

The labelled DNA probes (RP5-839B19 + RP11-60D5) were mixed in 1:1 ratio and denatured for 8 minutes at 80 ˚C on a PCR plate. Repetitive sequence was removed to avoid cross-

hybridisation by allowing the probes to pre-anneal at 37 ˚C for 30 minutes. On each slide, 10-20 µl of probe were added before covering with a coverslip and sealing with Weldtite. The slides were incubated at 37 ˚C in a humidifying chamber.

The following day, the coverslip was gently removed, and the slides were washed 3 times in 0.1xSSC at 60 ˚C for 5 minutes. The probes were detected by applying to the cells, under a coverslip, 50 µl of a solution containing anti-digoxigenin antibody, conjugated with rhodamine (Sigma), plus avidin FITC (Thermo Fisher), both at 5 µg/ml in 4x SSC, 0. 1% Tween20 and 4% BSA. The slides were incubated at 37 ˚C in a humidifying chamber for 30 minutes. The slides were then washed 3 times in 4x SSC, 0.1% Tween20 at 42 ˚C. Following final wash in 4x SSC without Tween20 at RT for 3 seconds, the slides were mounted in DAPI/Vectashield mounting medium (Oncor). The slides were visualised on an Olympus BX60 microscope for epifluorescence equipped with a Sensys CCD camera (Photometrics, USA). Images were captured using Genus Cytovision software (Leica).

2.5.2 Lipofectamine® 2000 transfection

For the transfection, cells were seeded in antibiotic-free medium in a 6-well plate at a density resulting in 70% confluence the next day. Both plasmids, Knock-out plasmid GRP582 and the BRAF V600E donor plasmid pAAV0990 with green fluorescent protein (GFP) tag were used for the transfection on day 2. The knock-out plasmid GRP582 and the donor plasmid pAAV0990 were co-designed with Dr Daniele Gaudiosi, Horizon Discovery, and produced by Horizon Discovery Group PLC. For the details of plasmid design, see Table 2-6 and Figure 4-3. For the transfection, tube A of 250 µl Opti-MEM® (Thermo Fisher, #31985062) containing 1 µg of each plasmid, and tube B of 250 µl Opti-MEM® containing 8 µl of Lipofectamine® 2000 (Invitrogen, # 11668027) were prepared and incubated separately for

5 minutes at room temperature. The contents of the tubes were then mixed and incubated for 20 minutes at room temperature before adding to the cells in 2 ml antibiotic-free medium. Cells were cultured at 37 ˚C, with their GFP expression monitored under a microscope every 2-3 days, before GFP-positive cells were sorted by flow cytometry.

2.5.3 Cell sorting for GFP-positive cells

After Lipofectamine® 2000 transfection, cells were cultured for ten days and then sorted for GFP positivity. On the day of cell sorting, cells were trypsinised and resuspended at 5 x 10^6/ml in DMEM containing 5% serum and placed on ice. Untransfected cells were also provided as negative control for auto-fluorescence. The cell suspension was analysed on the Beckman Coulter Legacy MoFlo MLS High Speed Cell Sorter, and GFP-positive cells were single-cell sorted into 96 well plates. The single-cell sorting was performed by Mr Andrew Worth, Flow Cytometry facility, Jenner Institute, Oxford. Cells in the 96 well plates were then placed back in the 37 ˚C incubator for culture of single cell colonies.

2.5.4 Genetic analysis for the CRISPR clones

2.5.4.1 Releasing DNA for polymerase chain reaction (PCR) amplification

CRISPR clones in 96-well plates were passaged to duplicate 96-well plates. Medium was removed after the plates were centrifuged at 1200 rpm for 5 minutes. Cells were washed with PBS and centrifuged again (1200 rpm for 5 minutes) and the PBS was removed. Then 10 µl of microLYSIS® DNA release buffer (Microzone, #2ML-250) was added to each well. The

plates were then placed in a PCR Thermo Cycler (MJ research, USA) and cycling parameters were set up as in Table 2-5.

Table 2-5: Cycling parameters for DNA release.

Steps	Temperature	Time
1	65 °C	5 min
2	96 °C	2 min
3	65 °C	4 min
4	96 °C	1 min
5	65 °C	1 min
6	96 °C	30s
7	20 °C	5 min

2.5.4.2 PCR amplification

PCR reactions were then set up using the *Taq* PCR Master Mix kit (QIAGEN, #201443) using per reaction a mix containing 12.5 µl of QIAGEN Master mix, 1 µl of each primer (10 µM), 2 µl of the cell lysate, and 8.5 µl of molecular grade water for each reaction. Primers used for this experiment were CET0366 and CET0367 for the left arm, and CET0370 and CET2482 for the right arm selection. Two pairs of confirmation primers (6F and 6R; 12F and 12R) were also used on positive clones screened by the screening primer pairs. For the location and sequences of these primers, see Table 2-6 and Figure 4-3C. The PCR plates were then placed in the Thermo Cycler with the programme set as below:

Step 1: 94 °C for 3 mins
Step 2:
    3 cycles: 94 °C for 15s, 64 °C for 30s, 70 °C for 120s
    3 cycles: 94 °C for 15s, 61 °C for 30s, 70 °C for 120s
    3 cycles: 94 °C for 15s, 58 °C for 30s, 70 °C for 120s
    35 cycles: 94 °C for 15s, 57 °C for 30s, 70 °C for 120s
Step 3: 70 °C for 5 mins
Step 4: 4 °C ready to use

PCR products were then ready to be analysed by gel electrophoresis or purified for DNA sequencing.

2.5.4.3 Gel electrophoresis

To analyse the PCR products, 1% agarose gels were made by melting 1 g of agarose (Gibco-BRL) in 100 ml Tris-acetate-EDTA (TAE) buffer (Thermo Scientific, #28354). The melted gel mix was then left to cool down to 55 °C, before 50 µg of ethidium bromide (Pierce, #61734) was added to the gel. The gel was then poured into a gel tank to set. TAE buffer was then added to the tank to submerge the gel and PCR products were mixed with 6x DNA loading dye and loaded into the wells, in parallel with a DNA ladder (Thermo Scientific, #R0611). Electrophoresis was performed at 125 volts for 45 minutes, before the gel was visualised using BIO-RAD Gel Doc™ XR+.

2.5.4.4 PCR purification and sequencing

PCR products were purified using the QIAquick PCR purification kit (QIAGEN, #28104) according to the manufacturing instruction. To purify the DNA products, 5x volume of PB buffer containing ethanol was added to the PCR reaction and mixed. The mixture was then transferred to a QIAquick column for the DNA to bind to the membrane in the column. The column was then washed with Buffer PE and DNA was eluted in 50 µl of molecular grade water. DNA was quantified using the NanoDrop 2000c Spectrophotometer, and samples were diluted to a suitable concentration (100ng/µl for plasmids, 3.2pmol/µl for primers) and sequenced by Source BioScience Oxford. Confirmation primer pairs (6F and 6R; 12F and 12R) were used in this experiment. For information about these primers, see Table 2-6 and Figure 4-3. DNA sequences were analysed using SnapGene® Viewer 3.1.2.

2.6 RNA analysis

2.6.1 RNA extraction

RNA was extracted from cell lysates obtained from cultured cells or homogenised tumour tissue using the RNeasy kit (QIAGEN, #75144) according to the manufacturer's protocol. Cells were lysed in 700 µl of RTL buffer with 0.1 M β-mercaptoethanol added. Lysates were passed through a 19 gauge needle 10 times, before they were transferred to a extraction column for the RNA to bind to the membrane. DNase I (QIAGEN, 15200-50) diluted in RDD buffer was then added to the membrane to digest the genomic DNA. The column was incubated at room temperature for 15 minutes and washed with 350 µl RW1 buffer. After one more wash of 700 µl of RW1, the column was washed twice with buffer RPE, before the RNA was eluted in 30 µl of DEPC-treated RNase-free Water, and then quantified using the NanoDrop 2000c Spectrophotometer.

2.6.2 Reverse transcription (RT)

Complementary DNA (cDNA) was reverse transcribed from RNA samples using the SuperScript® III First-Strand Synthesis SuperMix (Invitrogen, #11752-050) according to the manufacturer's protocol. To make the reaction mix, 2 µl of the enzyme mix containing reverse transcriptase, 1 µg of total RNA and 10 µl of 2x RT reaction buffer (containing random primers and dNTPs) were added to a PCR tube, before RNase-free water was added to make the final volume of 20 µl. The contents were gently mixed and placed in a Thermo Cycler to incubate for 10 minutes at 25 °C, then 30 minutes at 50 °C, then 5 minutes at 85 °C. After the incubation, the PCR tubes were placed on ice to chill, before 1 µl (2 U) of *E. coli* RNase

H was added. Tubes were incubated at 37 °C for 20 minutes. The cDNA samples were used immediately or stored at -20 °C.

2.6.3 Quantitative real-time PCR (qRT-PCR)

SYBR Select master mix (Applied Biosystems, #4472908) was used for qRT-PCR reactions according to the manufacturer's protocol. For each reaction, 20 ng of cDNA and 10 pmol of forward and reverse primers were added to 10 µl of 2x SYBR Select Master Mix containing SYBR GreenER Dye, AmpliTaq DNA polymerase Ultra Pure with hot start and dNTPs. RNase-free water was added to make the final volume of 20 µl. The reaction mix was then placed on the Applied Biosystems® 7500 Real-Time PCR System to quantify the expression with respect to a housekeeping gene, *B2M* (β-2-microglobulin). For this project, qRT-PCR primers were used to quantify expression of the following genes: *BRAF* WT, *BRAF* V600E, *VEGFR2*, *VEGFA*, *HIF1α*, *B2M*. The sequences of these primers is given in Table 2-6.

2.6.4 Human HT12v4.0 Illumina microarray analysis

Cultures of isogenic BRAF WT and V600E clones were harvested at 60-70% confluence from 10 cm dishes and pelleted by centrifugation. To lyse the cells, 700 µl of RTL lysis buffer with 0.1 M β-mercaptoethanol was added to the cell pellet. The cell lysates were then passed through a 19-gauge needle 10 times to be further homogenised. Total RNA was extracted using the QIAGEN RNeasy kit, as described in section 2.6.1. RNAs were quantified using the NanoDrop 2000c and sent to the Wellcome Trust Centre for Human Genetics (WTCHG) in Oxford for gene expression array analysis. Samples were submitted in 2 x 96-well plates, with one plate containing 500ng total RNA in 12µl of RNAse free water for sample processing,

and 500ng in 5µl for quality control (QC). RNA samples were processed using the Illumina TotalPrep-96 RNA Amplification Kit followed by the Illumina Whole-Genome Gene Expresssion Direct Hybridisation Assay. The labelled cRNA was then hybridised to HumanHT-12_V4_BeadChip for gene expression analysis.

Triplicate independently-collected RNAs were characterised for gene expression from 8 cultures: the parental CHL1 cell line, three *BRAF* WT and four *BRAF* V600E clones. This gave twenty-four RNAs in total, with 12 samples being wild-type samples, and the other 12 samples having induced *BRAF* V600E mutation. The signal for control probes of biotin and hybridisation were checked as quality control (QC). Variability in sample-dependent plots of average signal intensity and signal from housekeeping genes, caused by sample quality, labelling efficiency, amount of material loaded, were corrected by normalisation. Overall signal, housekeeping gene signal and the number of detected genes were checked to be high and no QC concerns were raised.

The raw beadchip data were pre-processed by WTCHG in Illumina Inc. GenomeStudio (version 1.9.0). and the resulting signals for each probe were further processed for quantile normalisation, log2 transformation, and gene filtering, by Dr Ruud Van Stiphout (Dr Francesca Buffa's group, University of Oxford). The quantile normalisation was to make two distributions identical in statistical properties by ranked mean values, as previously described by Bolstad et al (Bolstad et al, 2003). Genes not expressed were filtered out by only including probes that had detection p-values ≤ 0.05 for at least one sample. Subsequent analysis was as described in section 2.7.2 below.

2.6.5 Sample preparation for RNA Sequencing from fresh frozen patient tumours

Fresh frozen melanoma tumour samples were cryosectioned on a Cryostat (Cryostar™, ThermoScientific) and slides were stained with Hematoxylin and Eosin (H & E). Tumour content was examined under a microscope with Dr Ruth Asher, Dermatopathologist at the John Radcliffe hospital, to identify areas of melanoma. Tumour samples were macro-dissected, placed in pre-chilled RNAlater® (Ambion, #76104) solution overnight, and homogenised in 600 µl RLT buffer from the RNeasy Mini Kit (QIAGEN, #74104) with 1% β-mercaptoethanol added. RNA was then extracted from the cell lysate using the QIAGEN RNeasy kit as described in section 2.6.1.

RNA samples were quantified using the NanoDrop 2000c and their quality was checked by measuring the RNA Integrity Number (RIN), determined using the Agilent RNA 6000 Nano Kit (Agilent, #5067-1511) on the Agilent 2100 Bioanalyser. Samples of RNA ladder were prepared by heat denaturing for 2 minutes at 70 °C, then immediately cooling on ice. Gel-dye mix was prepared by adding 1 µl RNA dye into 65 µl gel matrix. For each RNA sample, 9 µl of gel-dye mix was pipetted in the well in a RNA chip, after it was primed at the chip priming station. Next, 5 µl of RNA marker, 1 µl of RNA ladder, and 1 µl of each RNA sample were pipetted in the wells in the chip. The chip was then vortexed for 1 minutes and loaded in the Agilent 2100 bioanalyser instrument before an Electrophoretic Chip Run was started. Results were analysed using the 2100 Expert software and the RIN (between 1 to 10) for each sample was calculated to present their degradation state, with 1 for a completely degraded sample, and 10 for a perfect RNA sample without any degradation products. Samples with a RNA Integrity Number (RIN) greater than 7 were sent to Oxford Gene Technology for RNA sequencing.

2.6.6 Primer design

Primers used for site-directed mutagenesis were generated using the QuikChange Primer Design tool (http://www.genomics.agilent.com/primerDesignProgram.jsp). Other primers used in this project were generated using Primer-BLAST (https://www.ncbi.nlm.nih.gov/tools/primer-blast/). All the primers were synthesised by Life Technologies Ltd and are listed in table 2-6.

Table 2-6: Details of primers used in this project.

Name	Assay	Forward sequence (5' to 3')	Reverse sequence (5' to 3')
AN2003048	QuikChange Site-directed mutagenesis	CCACTCCATCGAGATTTCACTGTAGCTAGACCAAAAT	ATTTTGGTCTAGCTACAGTGAAATCTCGATGGAGTGG
Seq-braf-1	Sequencing BRAF gene-region 1	TGTTCAACGGGGACATGGAG	CCTCTGTTTGTTGGGCAGGA
Seq-braf-2	Sequencing BRAF gene-region 2	AGTGGTACCTGCAAGGTGTG	-
Seq-braf-3	Sequencing BRAF gene-region 3	TCCAATTCCACAGCCCTTCC	-
Seq-braf-4	Sequencing BRAF gene-region 4	GCACCTACACCTCAGCAGTT	-
Seq-braf-5	Sequencing BRAF gene-region 5	GTGGATGGCACCAGAAGTCA	AACCAGCCCGATTCAAGGAG
CET0366; CET0367	CRISPR screening (left arm)	GTGTAGGAGGGGAGCATTGA	CTTCCAGCTGCCCCCATAAT
CET0370; CET2482	CRISPR screening (right arm)	CTGCAGCATCTTCATCCAA	AAAAAGGGGCATTGGAATC
6F; 6R	CRISPR- confirmation6	AGAGCCTTTACTGCTCGCC	CCCGTGAGTCAAACCGCTAT
12F; 12R	CRISPR- confirmation12	TGAAGAGCCTTTACTGCTCGC	CACGCCCATTGATGTACTGC
BRAFWT-q	qRT-PCR for BRAF WT	GCTACAGTGAAATCTCGATGGA	GCATTCTGATGACTTCTGGTGC
BRAFmut-q	qRT-PCR for BRAF V600E	GCTACAGAGAAGTCACGTTGGA	GCATTCTGATGACTTCTGGTGC
VEGFR2-q	qRT-PCR for VEGFR2	GGCCCAATAATCAGAGTGGCA	CCAGTGTCATTTCCGATCACTTT
VEGFA-q	qRT-PCR for VEGFA	AGGGCAGAATCATCACGAAGT	AGGGTCTCGATTGGATGGCA
HIF1α-q	qRT-PCR for HIF1α	GCCAGACGATCATGCAGCTA	ATCCATTGATTGCCCCAGCA
HK-β2-q	qRT-PCR for β-2-microglobulin	TGCTGTCTCCATGTTTGATGTATCT	TCTCTGCTCCCCACCTCTAAGT

2.7 Analysis of gene expression

These analyses were performed by Dr Ruud van Stiphout, Post-doctoral Bioinformatician in the group of Dr Francesca Buffa, Principal Investigator, Head of the Bioinformatics Hub, Department of Oncology Oxford.

2.7.1 Melanoma cell line panel from Ludwig Institute for Cancer Research Melbourne

Publicly available data on the Melbourne LM cell line panel (Behren et al 2013) were used to compare gene expression in cell lines harbouring *BRAF* mutations V600E and V600K (discarding G469E and K601E) vs the rest (WT/*NRAS*), treating *NRAS* Q61Q mutation as wild-type since this is a silent mutation. This gave 30 cell lines with *BRAF* mutation, 5 *NRAS* mutant, 22 *BRAF/NRAS* WT, total 52. The raw expression data were available at (http://www.ebi.ac.uk/arrayexpress/experiments/E-MTAB-1496/) and were pre-processed by quantile normalisation, making all the distributions identical by forcing each quantile to be the same across samples (Bolstad et al., 2003). Values were then logged base 2. To enable analysis of gene expression by mutation status, the cell lines were divided into 2 groups: mutant *BRAF* vs WT BRAS/NRAS. To gain power in the analysis, genes were pre-filtered using expression and variability. Only genes that were commonly expressed among all cell lines were included; threshold for expression was based on the median expression for all genes across all cell lines, this simple rule is based on the assumption that roughly half of the genome is expressed at any given time and it has been shown by the Buffa group and other labs to achieve similar results with respect to more complex algorithms that estimate presence/absence of a gene. Variable genes which had standard deviation >1 (in log2 scale this represent 1-fold change in expression) were also selected. Three methods were then

applied to find differentially expressed genes, firstly by LIMMA in which for each gene a linear model was fitted and the estimated parameters were compared between the BRAF and non-BRAF groups. SAMR was also used to measure the strength of the association between gene expression and BRAF status. This method uses repeated permutations of the data to determine if the expression of any genes is significantly related to the response, using 1000 permutations and a cut-off for significance determined by a tuning parameter delta (Δ=0 in this case). Finally, Rank product is a simple non-parametric statistical method based on ranks of fold changes, using 1000 as the number of permutations. The genes were then ranked based on p-values from the three methods and the 3 rankings merged using rank product. A table was generated in which the genes were sorted on average rank. This was used to produce a heat map with hierarchical clustering of gene expression, including the top 50 differentially expressed genes. From this analysis, a Venn diagram was generated using an adjusted p-value threshold of 0.1 to identify the overlap of genes found to be differentially expressed using the three methods.

2.7.2 Illumina microarray analysis of gene expression in isogenic melanoma clones

RNAs extracted as described in section 2.6.4 were analysed by Human HT12v4.0 Illumina microarray analysis at WTCHG. There were triplicate independently collected samples from the parental CHL1 cell line, three *BRAF* WT clones and four *BRAF* V600E clones. QC metrics indicated that the control probes for biotin and hybridization were sample-independent and gave consistently high signal, indicating that the experimental steps were successful. All the samples gave good overall signal, and housekeeping gene signal was very high as expected. The raw beadchip data were first pre-processed by Oxford Genomics Centre at the WTCHG

using Illumina Inc. GenomeStudio version 1.9.0. The resulting signals for each probe were further processed by Dr van Stiphout by quantile normalisation and log2 transformation. Genes that were not expressed were filtered out by only including probes with detection p-values $\leqslant$ 0.05 for at least one sample. The normalised and filtered data were subject to hierarchical clustering, differently expressed genes were identified by LIMMA, and an expression heatmap was used to present the top 50 genes. The significant differentially expressed genes were assessed for pathway ontology using PANTHER analysis from GeneCodis http://genecodis.cnb.csic.es/ (Carmona-Saez et al., 2007; Nogales-Cadenas et al., 2009; Tabas-Madrid et al., 2012).

2.7.3 RNA-seq on fresh frozen melanoma samples

This analysis was performed on RNAs extracted from fresh frozen melanoma tissues as described in section 2.6.5. RNA sequencing was carried out using the Illumina HiSeq 2000 platform from the Oxford WTCHG via Oxford Gene Technology. For all samples for which data were presented, Quality Control showed good alignment metrics and read quality metrics. Differentially expressed genes were identified by Dr van Stiphout using a pipeline based on the Tuxedo suite tools TopHat (Langmead et al., 2009) and CuffDiff (Langmead et al., 2009) from: https://support.illumina.com/help/BS_App_RNASeq_Alignment_OLH_1000000006112/Content/Source/Informatics/Apps/TuxedoSuite_RNASeqTools.htm), as used previously by Dr Buffa's group (Ledaki et al., 2015).

2.8 *In vivo* studies

Mice used in this experiment were female CD1 immunodeficient (nude) mice from Charles River, housed at Biomedical Services at John Radcliffe Hospital. Mice welfare was closely monitored throughout the experiment. The melanoma cells used for this experiment were two

BRAF WT clones, WT3 and WT7, and two *BRAF* V600E clones, F10 and 3F2. Cells were harvested, washed in PBS twice to remove all traces of serum containing media, before resuspending at $7.5x10^6$ cells/100µl in serum free RPMI medium. Cells were stored on ice and mixed 1:2 with ice-cold matrigel (Corning, #356237) before injecting subcutaneously in the lower flank of 6 week old CD1 mice (weight ~20g) under anaesthesia ($7.5x10^6$ cells per mouse). When tumours had reached approximately 150 mm^3 in size (calculated from the formula 1/6 x π x L x W x H, length [L], width [W], and height [H] of each tumour), they were randomised into 5 mice per group, with one group injected with vehicle control (PBS) and the other group injected with bevacizumab on schedule of 100µl (10mg per kg of the mouse) intraperitoneally three times a week. Mice were sacrificed when tumours had reached licence limits of 1.44 cm^3. Mice were injected intravenously with 2 mg pimonidazole (Hypoxylprobe-1) in 0.9% saline, and 100 µg biotinylated tomato lectin (Vector Laboratories) and 0.6 mg Hoechst 33342 mixed solution in 100 µl PBS 90 min and 2 min before sacrifice, respectively. Blood was collected via cardiac puncture, and tumour and organs were collected for histological evaluation. All work was conducted in accordance with the UK Home Office guidelines, under project licence of Professor Adrian Harris (PPL 30 /3197). *In vivo* experiments were carried out by Dr Ester Bridges from Hypoxia and Angiogenesis Group in Department of Oncology of University of Oxford.

2.8.1 Quantifying human VEGF and mouse VEGF levels in blood samples

Mouse blood samples were collected via cardiac puncture. The serum component was separated by centrifugation and stored in -20 ˚C. Human and mouse VEGF levels in serum samples were quantified using R&D system human VEGF Quantikine ELISA kit (R&D

system, #DVE00) and mouse VEGF Quantikine ELISA kit (R&D system, #MMV00), respectively, according to the manufacturer's instructions.

2.8.2 Immunohistochemistry

Immunohistochemical analysis of mouse tissue samples from *in vivo* studies was carried out by Dr Esther Bridges from the Hypoxia and Angiogenesis Group, Department of Oncology, University of Oxford. Paraffin-embedded tissue sections were retrieved, dewaxed and rehydrated according to standard procedures. Slides were stained using the FLEX staining kit (Ailgent). To summarise, endogenous peroxidase activity was blocked before slides were stained using antibodies to Ki67 (M7240; Dako, 1:50), CA9 (M75; BD Biosciences, 1:1000) and CD31 (#550274; BD Biosciences, 1:50) for 1 hour at room temperature. Slides were incubated with anti-rabbit/anti-mouse secondary antibody for 30 minutes at room temperature and washed in Flex buffer. 3,3-Diaminobenzidine (Flex-DAB) was applied to the sections for 10 minutes. The slides were counterstained by immersing in hematoxylin solution (Sigma-Aldrich) for 20 seconds, air-dried and mounted with Aquamount (VWR). Secondary-antibody only control staining was performed routinely, and these were negative. One section from each xenograft was analysed for each immunohistochemical marker, and one section was also used for H&E staining, using Giles haematoxylin (Sigma-Aldrich) and counter-stained with eosin (Sigma-Aldrich).

Necrosis was quantified histologically on the H&E-stained sections where necrotic areas were selected using Image J and results presented as a percentage of necrosis in the total area. Expression of CA9 and Ki67 in the tumour cells was quantified as indices of arbitrary units using ImageJ software (US National Institutes of Health, Bethesda, MD, USA) using colour deconvolution as described previously (Ruifrok and Johnston, 2001). Expression of

CD31 by blood vessels was quantified in 20 random fields at ×20 magnification, and was expressed as average number of vessels per field. Data were graphed and analysed on GraphPad Prism 7 using Students *t*-test to compare 2 groups, and one-way ANOVA for multiple groups. Pearson's correlation test was used for the correlation coefficient. All tests were 2-sided and p value < 0.05 was considered statistically significant.

Chapter 3: VEGF expression and characterisation of bevacizumab response in melanoma cell lines

3.1 Investigation of the hypothesis that the inhibition of autocrine VEGF signalling suppresses growth in *BRAF* mutant melanomas

Although the important role of VEGF in tumour angiogenesis has been well described since its discovery in 1989 (Ferrara and Henzel, 1989), emerging evidence has shown that the function of VEGF is not limited to angiogenesis and vascular permeability. For example, VEGF was reported to affect the function of immune cells that are present in the tumour microenvironment via binding to neuropilin-1 (NRP1), regulating tumour growth (Yaqoob et al. 2012; Hansen et al. 2012). Another potential mechanism of VEGF action, that has been investigated in recent years, is the autocrine VEGF signalling in tumour cells themselves, promoting tumour growth, migration and survival. VEGF mediates cell survival in breast carcinoma cells *in vitro* and the inhibition of VEGF expression results in apoptosis in these cells (Bachelder et al., 2001). The expression of VEGFR2 is associated with tumour invasion in head and neck carcinomas (Neuchrist et al., 2001). In bladder cancers, VEGF expression correlated with disease stage and muscle invasion, and bladder cancer cell lines showed increased invasion in response to VEGF (Xia et al., 2006), these data indicate possible autocrine loop of VEGF in progression in these tumours. VEGF/VEGFR2 signalling increases cell proliferation with VEGF stimulation in gastric cancer *in vitro* (Zhang et al., 2002) and the

blockade of such signalling inhibits tumour growth and engraftment in leukaemia *in vivo* (Dias et al., 2001).

It is already known that many tumour types, including melanoma, express VEGF receptors (Straume and Akslen, 2003), suggesting the possibility of functional autocrine VEGF/VEGFR signalling in melanoma. While Adamcic et al showed that inhibiting this autocrine signalling in two melanoma cell lines did not induce direct anti-proliferative effects (Adamcic et al., 2012); a decrease in tumour growth, induced by VEGF inhibition using bevacizumab, was observed in some Uveal melanomas *in vitro* (el Filali et al., 2012; Koch et al., 2014) and *in vivo* (Yang et al., 2010). However, whether *BRAF* mutation contributed to or differentiated this effect in these cancer cells has not been investigated in these studies. Therefore, this part of the project aimed to investigate this possibility that the inhibition of VEGF by bevacizumab directly affects melanoma cell growth via autocrine VEGF/VEGFR signalling in BRAF V600E melanoma cells.

3.2 Results

3.2.1 Detection of expression of VEGF signalling proteins and testing for the effects of bevacizumab on the signalling in melanoma cell lines

To investigate the bevacizumab response in melanoma cells, a melanoma cell line panel comprised of 5 *BRAF* WT and 7 *BRAF* V600E cell lines was assembled. Out of these cell lines, CHL1, HMCB, SKMEL23, SKMEL2, NA8 were derived from *BRAF* WT melanomas, while A375M, SKMEL28, ME, 501MEL, contain the *BRAF* V600E mutation.

The initial experiment investigated the expression of VEGF and VEGFR (figure 3-1A). Genetically modified MDA-MB-231 breast cancer cells MGFP, M121 and M165, kindly provided by Dr Helen Sheldon (Professor Adrian Harris's Group, University of Oxford), were used as controls for VEGF expression. MGFP contains an empty GFP vector, while M121 and M165 stably overexpress VEGF121 and VEGF165 isoforms, respectively. Cells were collected from routine culture in normoxia, and cells for the hypoxia experiment were grown in 0.1% O_2 in the hypoxic chamber overnight. Cells were collected and lysates were analysed by western blotting. VEGF was detected faintly in most of the cell lines in normoxia. An increase in VEGF expression in hypoxia could be seen in A375M (*BRAF* V600E) and HMCB (*BRAF* WT), compared to that in normoxia. HIF1α, a VEGF regulator, could be detected in two of the mutant cell lines, A375M and SKMEL28, and the *BRAF* WT cell line SKMEL2 in normoxia as expected. Increased levels of HIF1α in hypoxia were seen in all of the cell lines, except in HMCB (*BRAF* WT). It was also noted that, more phosphorylation of MEK was seen in hypoxia than in normoxia, especially in SKMEL28 (*BRAF* V600E) and SKMEL23 (*BRAF* WT) and SKMEL2 (*BRAF* WT). VEGFR2 could only be detected in normoxia for A375M, CHL1 and SKMEL28, but were elevated in hypoxia for all of the cell lines except HMCB. Thus, this experiment showed that VEGF and VEGFR2 were expressed in some of the melanoma cell lines, however, the levels of such expression varied, and did not appear to be related to their BRAF status.

The cell line panel was expanded with 11 more cell lines, as shown in figure 3-1B, including the newly established LM cell lines (Behren et al., 2013) obtained from the Ludwig Institute in Melbourne. These cell lines have had their mutational status determined and their transcriptomes profiled (Behren et al., 2013), making them excellent candidates for analysing the relationship between *BRAF* mutations and their downstream gene expression and

signalling. These cell lines were established from treatment-naïve patients, and the information of their tumour origins was summarised in table 3-1. Human Umbilical Vein Endothelial Cells (HUVECs) were used as a control for VEGFR2. VEGFR2 was detected in 3 of the WT cell lines (CHL1, LM69, and LM5a) and 3 mutant cell lines (LM4, LM16 and LM31). High levels of VEGFR2 were detected in HUVEC cells as expected(Meissner et al., 2011).

Table 3-1: tumour origins or the 9 LM melanoma cell lines.

LM-melanoma	Genotype	Site of primary tumour	Site of tumour for cell line
25	BRAF WT	Trunk	Lung
44	BRAF WT	Rectum	Lymph node rectum
39	BRAF WT	Upper limb	Small bowel
19	NRAS Q61K	Lower limb	Lymph node thigh
34	NRAS Q61K	Upper arm	Lymph node axilla
5a	NRAS Q61K	Unknown	Lymph node axilla
31	BRAF V600E	Lower limb	Lymph node inguinal
4	BRAF V600E	Upper limb	Lymph node inguinal
16	BRAF V600E	Trunk	Lymph node axilla

To test whether there was a differential effect of bevacizumab on VEGF/VEGFR2 signalling between *BRAF* WT and *BRAF* V600E melanoma cells, two VEGFR2-expressing cell lines LM5a (*BRAF* WT) and LM31 (*BRAF* V600E) were selected for further investigation. Cells were serum starved and treated with VEGF, bevacizumab or the combination as shown in figure 3-1C. Binding of VEGFA to VEGFR2 activates PI3K signalling pathway and its downstream effector AKT (Ruan and Kazlauskas, 2012). Bevacizumab did not inhibit phosphorylation of AKT in LM5a cells, but a suppression of AKT activation could be observed in serum-starved mutant LM31 cells when treated with the combination of VEGF and

Bevacizumab. Since the suppression of phospho-VEGFR2 could not be observed, this change of AKT activation was likely caused by activation of an alternative signalling pathway rather than VEGF/VEGFR2 pathway.

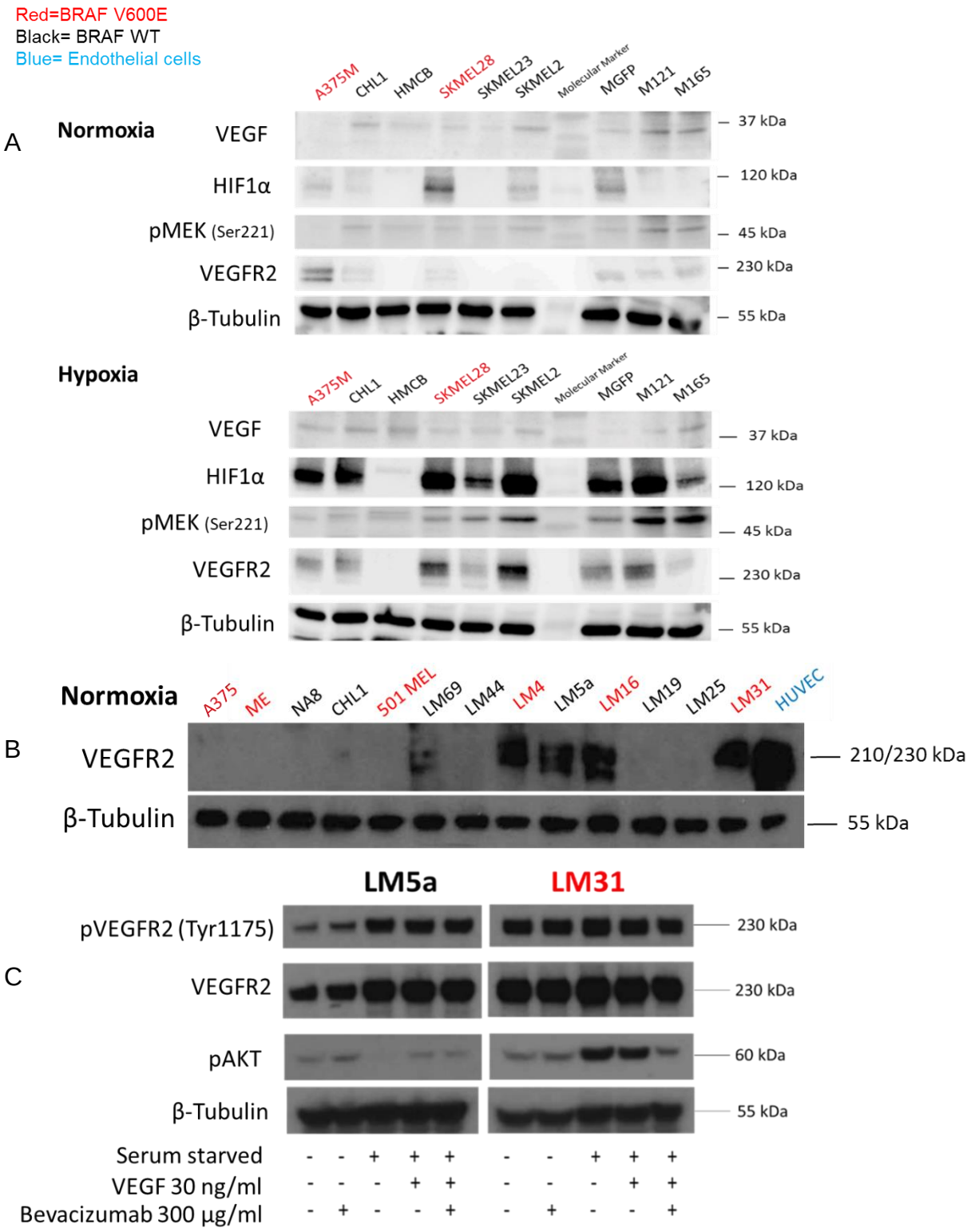


Figure 3-1: Expression of VEGF signalling proteins and effects of bevacizumab on cell signalling in melanoma cell lines.

A, Expressions of VEGF and VEGFR in the melanoma cell line panel. Genetically modified breast cancer cells MGFP, M121 and M165 were used as controls for VEGF. *BRAF* status was labelled as black for WT and red for V600E. **B,** Variable levels of VEGFR2 expression in normoxia detected in expanded melanoma cell line panel. HUVEC cells were used as the positive control for VEGFR2. **C,** Effects of bevacizumab on VEGFR2 phosphorylation in melanoma cell lines LM31 (*BRAF* V600E) and LM5a (*BRAF* WT). Bevacizumab (300 µg/ml) was added to cells for 24 hours, while VEGF (30 ng/ml) and VEGF + bevacizumab combination was added to overnight serum starved cells for 30 minutes before harvesting. VEGF and bevacizumab were mixed and left at room temperature to incubate for 1 hour before adding to the combination dishes. All experiments were repeated twice, and similar results were obtained.

3.2.2 Testing for direct effects of bevacizumab on two-dimensional (2D) growth of melanoma cells

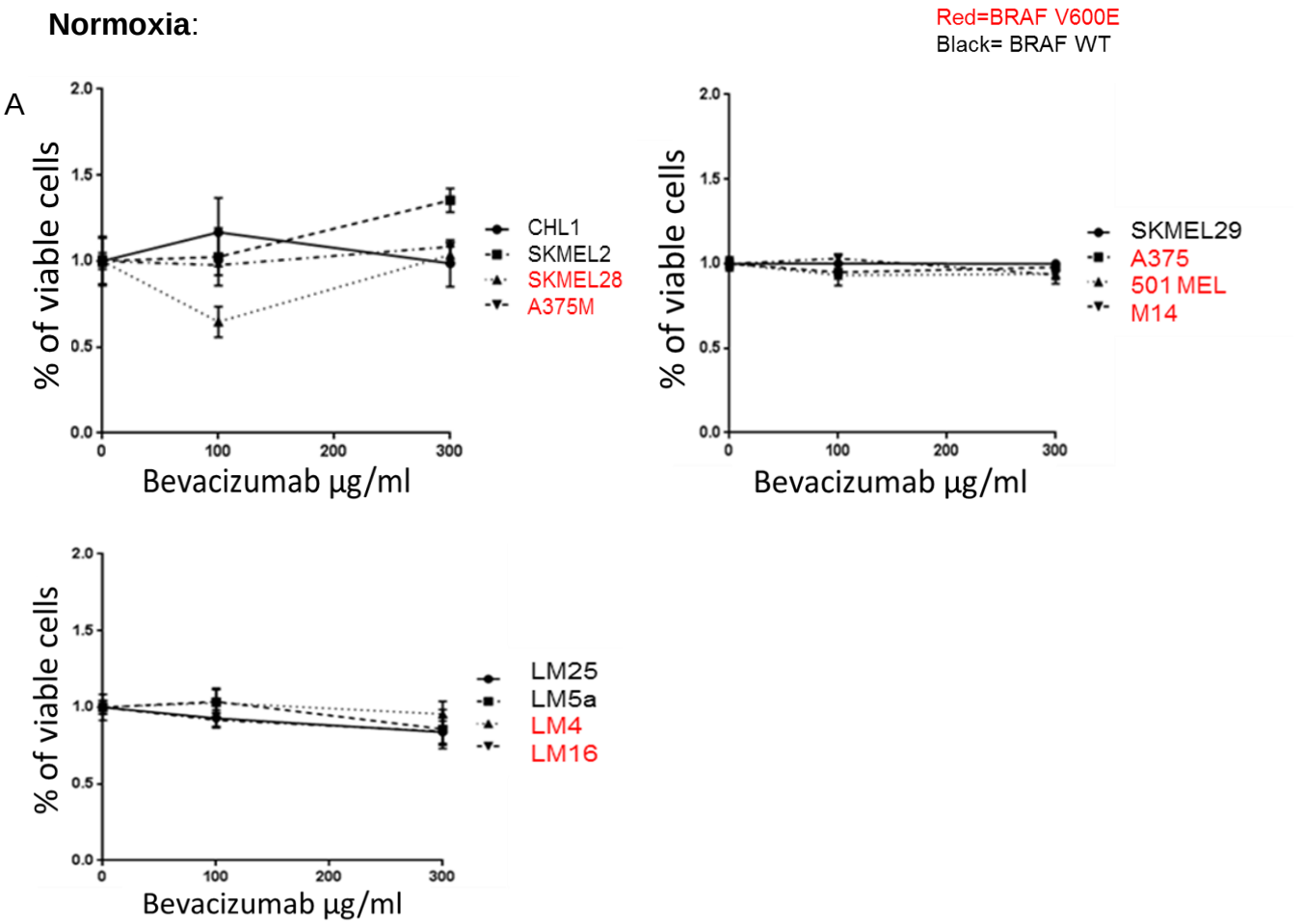
Results in figure 3-1 showed that variable levels of VEGFR2 expression were detected in the melanoma cell lines. Although the levels of protein expression detected in the initial experiment did not appear to be related to *BRAF* status of the cell lines, and the inhibition of VEGF by bevacizumab did not affect the phosphorylation of VEGFR2 in LM5a (*BRAF* WT) or in LM31 (*BRAF* V600E), it was still unclear whether bevacizumab could affect the proliferation or migration of the tumour cells, and whether such effects, if detected, would correlate with *BRAF* status. Therefore, further investigations were carried out to assess effects of bevacizumab on cell growth and migration.

Experiments in this section focused on the growth of the melanoma cell lines. Cells were treated with bevacizumab and their viability was measured with CellTiter-Glo Luminescent assay. Results in figure 3-2 showed that the treatment of bevacizumab did not appear to have affected the cell growth of melanoma cells in normoxia (figure 3-2A) or in hypoxia (figure 3-2B).

Bevacizumab is specific to human VEGF (Presta et al., 1997). To assess the possibility of activation of VEGF signalling in melanoma cells by bovine VEGF, contained in foetal calf serum, a separate experiment was performed, inhibiting VEGF signalling using the VEGFR inhibitor cediranib. Cediranib is a highly potent VEGFR inhibitor, inhibiting VEGFR2, as well as VEGFR1 and VEGFR3 in HUVEC cells (Wedge et al., 2005). Results in figure 3-3 showed that inhibiting VEGFR with increasing concentrations of cediranib did not influence the viability of CHL1 (*BRAF* WT) or A375M (*BRAF* V600E) cells in normoxia. In these

experiments, HUVEC cells were used as a positive control and inhibition in growth by cediranib was observed as expected (Beebe et al., 2003).

Normoxia:



Hypoxia:

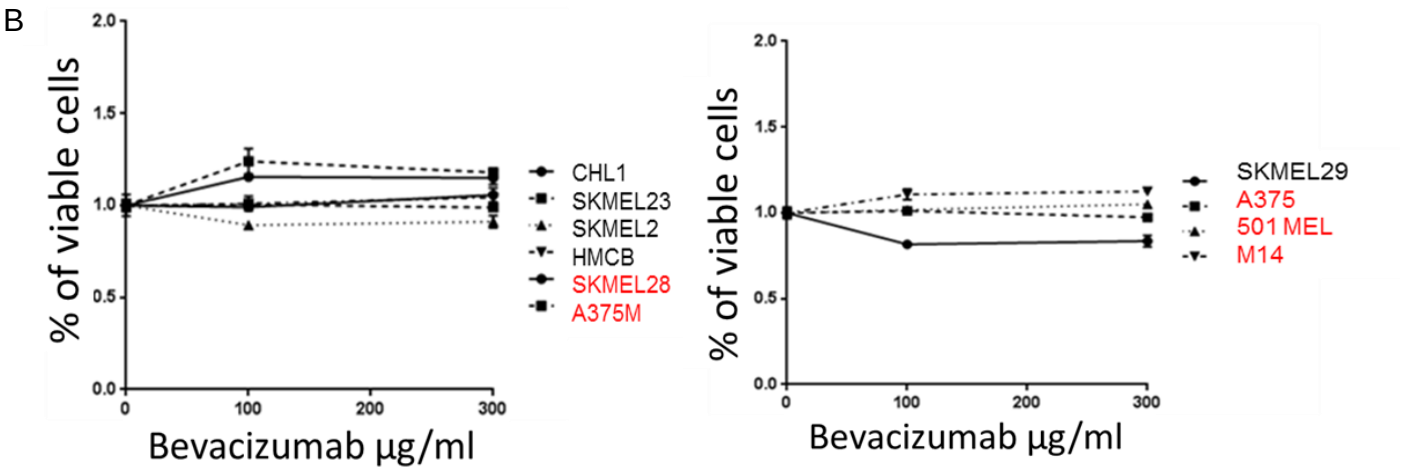


Figure 3-2: effects of inhibiting VEGF signalling by bevacizumab in 2D growth in melanoma cell lines.

A, Viability of *BRAF* WT cell lines (black) and *BRAF* V600E cell lines (red) treated with bevacizumab. Cells were treated with 100 or 300 µg/ml bevacizumab at 24 hours after seeding in 96-well plates. Plates were incubated for another 72 hours at 37 ˚C in normoxia or hypoxia (0.1% O_2). Cell viability was measured using the CellTiter-Glo Luminescent Assay kit (Promega). **B**, Viability of 5 *BRAF* WT cell lines and 5 *BRAF* V600E cell lines (red) treated with 300 µg/ml bevacizumab in hypoxia (0.1% O_2). Graphs are presented with mean ± SEM of 2 repeated experiments, each with 4 replicate wells.

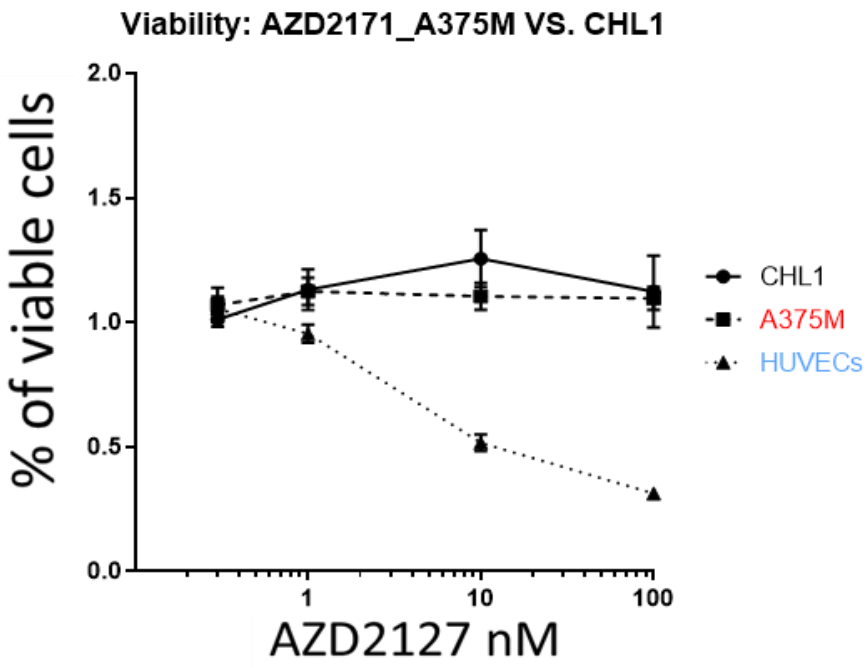


Figure 3-3: effects of inhibiting VEGF signalling with cediranib (AZD2127) in 2D growth in melanoma cell lines in normoxia.

Effect of VEGFR inhibitor cediranib (AZD2171) in 2D growth in CHL1 (*BRAF* WT) and A375M (*BRAF* V600E). HUVEC cells were used as a positive control. Cells were treated with increasing concentrations of cediranib (AZD2171, Selleck Chemicals, #S1017) at 24 hours after seeding in 96-well plates. Plates were incubated for another 72 hours at 37 ˚C in normoxia before the cell viability was measured. Graphs are presented with mean ± SEM of 2 repeated experiments, each with 4 replicate wells.

3.2.3 Testing for direct effects of bevacizumab on three-dimensional (3D) growth of melanoma cells

Although the results in figure 3-2 showed that bevacizumab did not influence 2D growth of melanoma cells, viability assays based on monolayer cell culture did have its limitations. Compared to 3D culture, 2D cell culture is less able to mimic the complexity and heterogeneity of tumours *in vivo*, and numerous cell signals could be lost when cells are grown in 2D (Lee et al., 2007). To further examine the direct effects of bevacizumab in melanoma cell growth, experiments using the 3D spheroid model were then carried out.

Cell spheroids were established as described in Materials and Methods. Representative spheroids for the CHL1, A375M and SKMEL28 cell lines are shown in Figure 3-4A. Additional *BRAF* WT and V600E melanoma cell lines were tested for their ability to form spheroids before the experiment was carried out. Unfortunately, a number of cell lines were found to be unable to form measurable, reproducible spheroids and were not used further in this experiment (figure 3-4B). Five days after seeding, spheroids formed by these cell lines had lost their spherical shape (SKMEL23) or structure (SKMEL29), or detached from the well surface and produced excess cell debris (SKMEL2), making it difficult for accurate volume measurements. Results in figure 3-4A showed that 3D spheroids were successfully established using two *BRAF* WT (CHL1, LM5a) and four *BRAF* V600E cell lines (A375M, SKMEL28, LM4, LM31). Once the spheroids had formed after 48 hours, the size of each spheroid was measured using the GELCOUNT™, before bevacizumab was added to the wells. Growth of the spheroids was then measured every 2 days, before each medium change with replacement of bevacizumab for appropriate wells. Results in figure 3-4C showed that bevacizumab did not affect 3D spheroid growth.

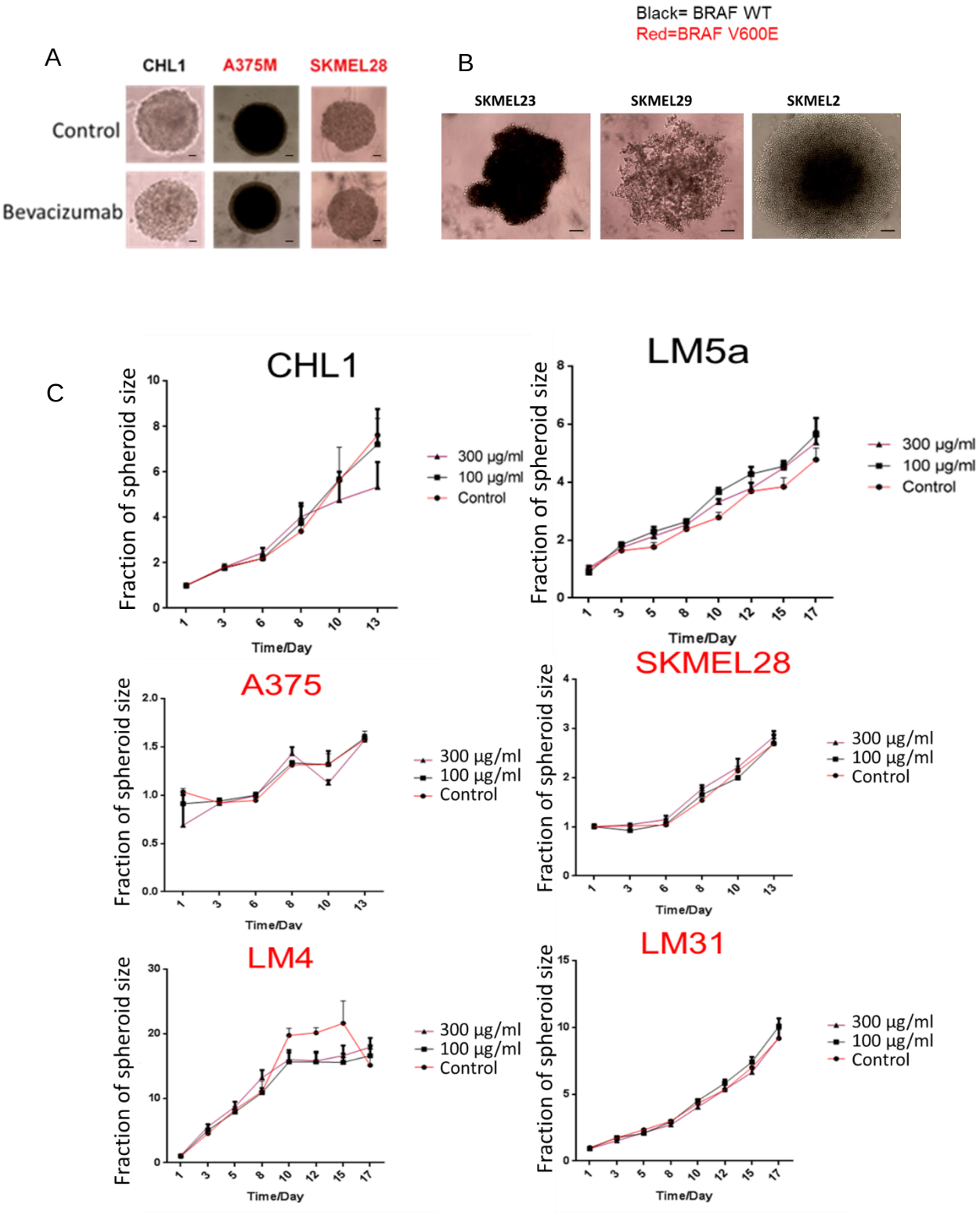


Figure 3-4: Effects bevacizumab on 3D spheroid growth of melanoma cell lines.

A, Representative images of spheroids 48 hours after seeding. Scale bar, 100 µm. **B**, Representative images of cell lines that failed to form measurable spheroids, therefore unsuitable for the experiment. Images were taken at 5 days after seeding. Scale bar, 100 µm. **C**, Effects of bevacizumab on 3D spheroid growth of two *BRAF* WT and four *BRAF* V600E cell lines. Graphs were presented with mean ± SEM of 6 replicate wells, showing spheroid size relative to size on day 1, immediately prior to addition of bevacizumab. Experiment was repeated two more times and similar results were produced.

3.2.4 Testing for direct effects of bevacizumab in cell migration of melanoma cell lines

It has been well established that VEGF increases endothelial cell permeability and stimulates cell migration (Olsson et al., 2006). Studies in recent years on VEGF signalling in tumours have found that VEGF could also promote the migration and invasion of cancer cells, independent of VEGF-mediated angiogenesis and vascular permeability. For example, a study of VEGF signalling in colorectal cancer showed that VEGF can promote the migration and invasion of colorectal carcinoma cells, by activating ERK1 or ERK2 via VEGFR1 (Fan et al., 2005). In breast cancer cells, higher levels of VEGF and NRP1 expression enhanced chemotactic activity, by competitive binding of VEGF to NRP1, displacing semaphorin 3A, a cell migration suppressor (Bachelder et al., 2003). Autocrine VEGF signalling via NRP1 could also induce the expression of chemokine receptor CXCR4 in breast cancer, mediating cell migration (Bachelder et al., 2002). In prostate cancer, autocrine VEGF signalling was shown to induce cell migration, by activating ERK1/2 via VEGFR2 (Darrington et al., 2012).

Although the studies mentioned above demonstrated that autocrine VEGF signalling can induce cell migration in various tumour types, the possibility of such an effect in melanoma cells has not been explored. Therefore, the effects of bevacizumab on cell migration of melanoma cell lines were investigated using wound healing assays.

Confluent melanoma monolayers were scratched and treated with bevacizumab as described in Materials and Methods. Healing of the wound was monitored using Live Cell Imaging Analyser IncuCyte ZOOM®. Figure 3-5A showed representative images of wound healing at different time points for two cell lines with or without bevacizumab treatment. Results in figure 3-5B showed no decrease in wound healing with bevacizumab treatment in either BRAF WT

cell line HMCB or *BRAF* V600E cell line SKMEL28. However, it was noted that compared to the *BRAF* WT cell line HMCB, the mutant SKMEL28 cells migrated faster than HMCB cells, suggesting a more aggressive phenotype in these *BRAF* mutant cells. If time had permitted, more cell lines could be used to further test whether there is a faster migration phenotype in *BRAF* V600E cells.

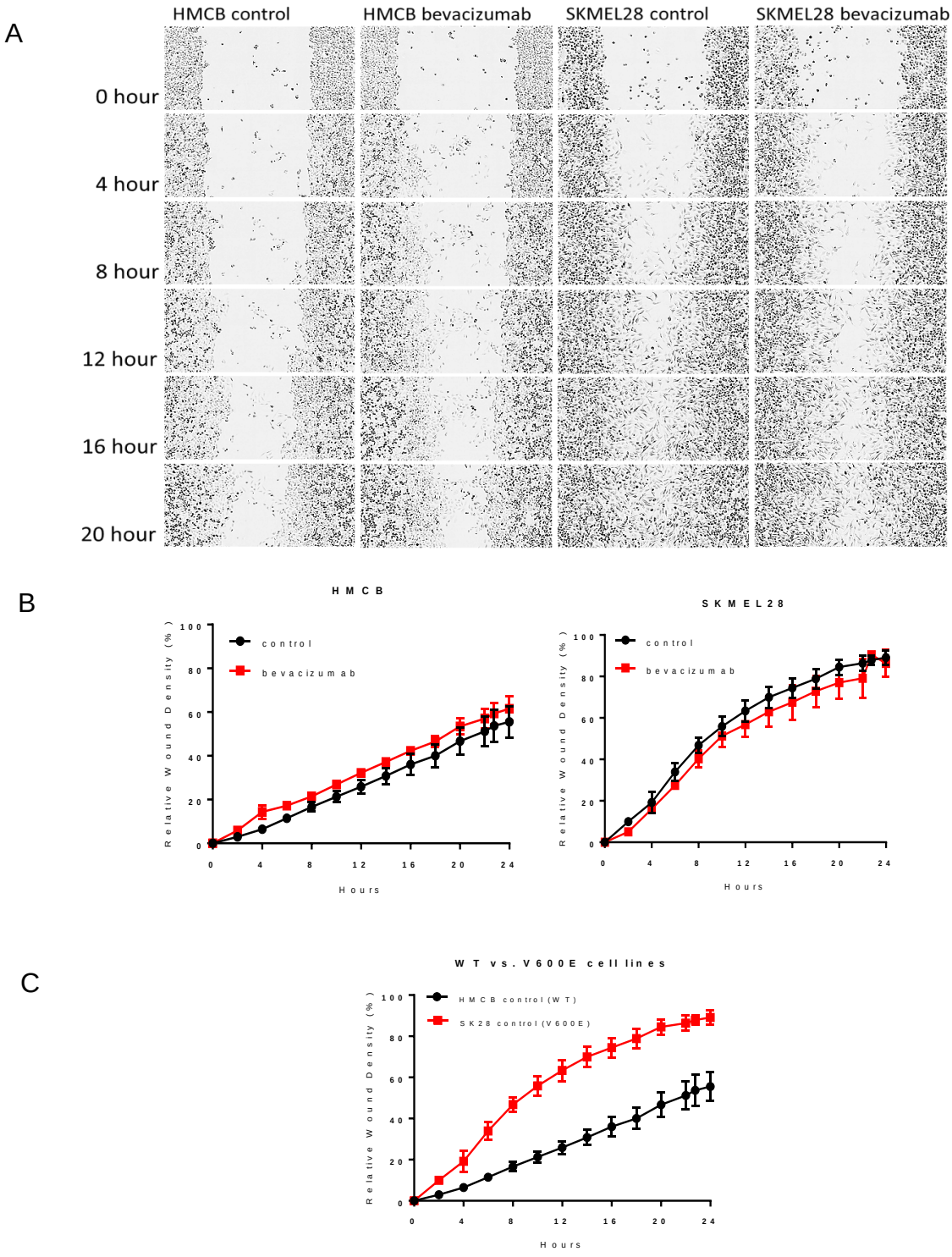


Figure 3-5: Effect of bevacizumab on cell migration in melanoma cell lines.

A, images showing wound healing at different time points for both cell lines treated with 300µg/ml bevacizumab. Images were taken by the cell Imaging Analyser IncuCyte ZOOM®. **B,** graphs show the addition of 300µg/ml bevacizumab did not influence cell migration over 24 hrs in HMCB (*BRAF* WT) or in SKMEL 28 (*BRAF* V600E). **C**, Faster migration could be observed in the mutant cell line SKMEL28, compared to the *BRAF* WT HMCB cell line. Graphs in B and C were presented with mean ± SEM of 4 replicate wells. The experiment was repeated twice, and similar results were produced.

3.3 VEGF expression in melanoma cell line panel

Although it has been shown that variable levels of VEGF and VEGFR2 were expressed in different melanoma cell lines (figure 3-1A), bevacizumab did not affect the cell growth or migration in these cells, as demonstrated in figure 3-2 to 3-4. These results suggest that autocrine VEGF signalling was unlikely to have been the main contributing factor to the differential response to bevacizumab in *BRAF* V600E vs. WT melanomas, as observed in the AVAST-M trial (Corrie et al., 2014).

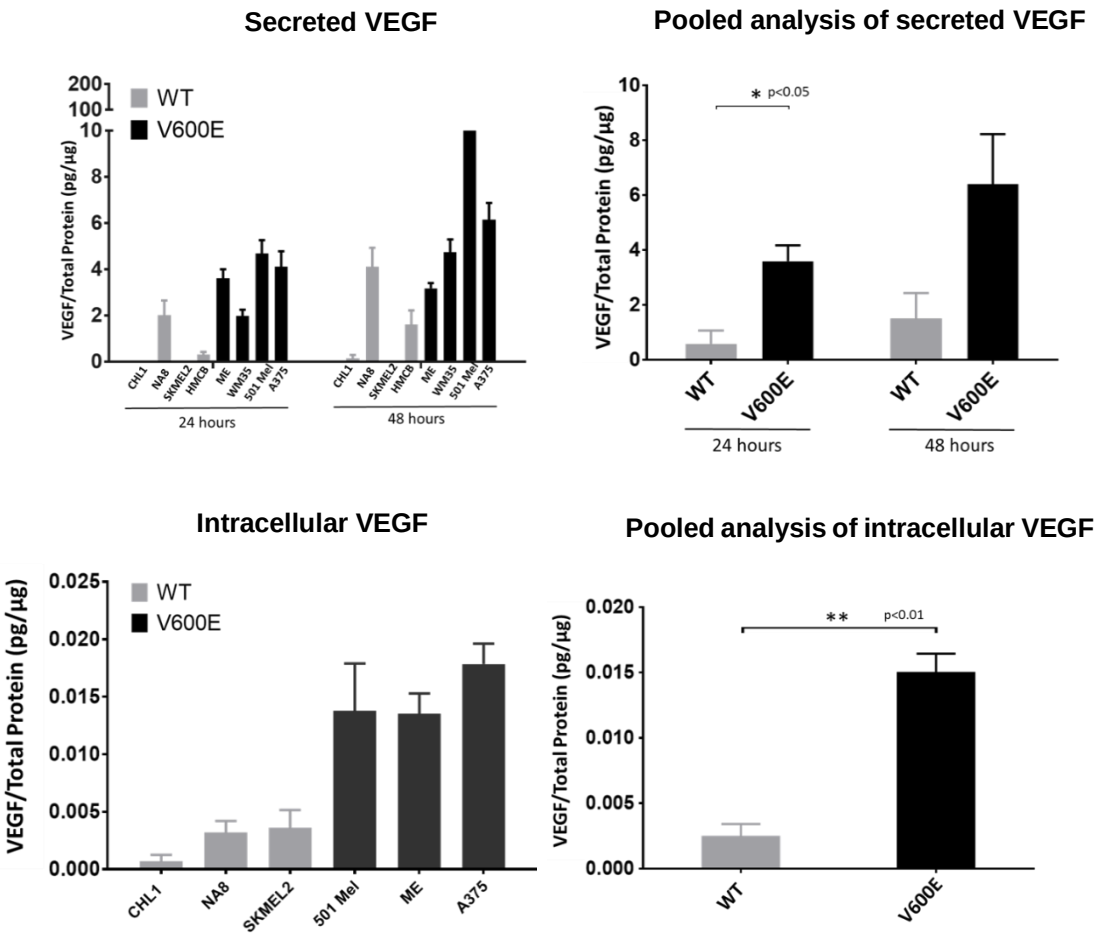
The next possibility proposed in the second hypothesis was that the inhibitory effects of bevacizumab in *BRAF* V600E melanomas could be mediated indirectly via effects on angiogenesis or other components of the tumour microenvironment. Therefore, experiments were carried out to test whether the *BRAF* V600E mutation is associated with increased VEGF expression.

To evaluate VEGF expression in the melanoma cells, both intracellular VEGF and secreted VEGF were quantified with the human VEGF enzyme-linked immunosorbent assay (ELISA). To measure secreted VEGF, cells were seeded in duplicate culture dishes in 10% foetal calf serum (FCS) medium on day 1 in normoxia, or in the 0.1% O_2 hypoxic chamber. The medium was changed to 2% FCS on day 2, and again on day 3, before all medium samples were collected on day 4 (24 hr samples) and day 5 (48 hr samples). Two more independent sets of samples for each condition were collected following the same procedure, and stored at -20 °C. Media were prepared and assayed using the R&D system quantikine human VEGF ELISA kit. The corresponding cell monolayers were harvested and total protein and

intracellular VEGF quantified as described in Materials and Methods, again using the R&D system human VEGF ELISA. Total protein in the lysate samples was also quantified.

Initial results of VEGF ELISA in the melanoma cell line panel showed that in normoxia, secreted VEGF levels and intracellular VEGF levels were significantly higher at 24 hours in cell lines with *BRAF* V600E status (figure 3-6A). Although not statistically significant, compared to the *BRAF* WT cell lines, a trend to increase in secreted VEGF levels could be observed in the *BRAF* V600E cell lines at 48 hours in normoxia (figure 3-6A), and in hypoxia (figure 3-6B).

A **Normoxia**



B **Hypoxia**

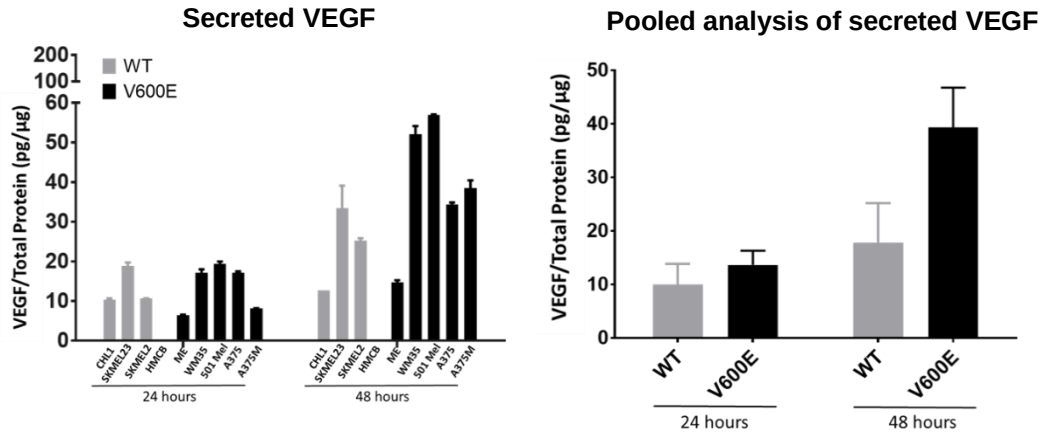


Figure 3-6: Secreted and intracellular VEGF levels of melanoma cell lines.

A, secreted and intracellular VEGF levels in melanoma cell lines measured using ELISA (n=3 independent samples). Conditioned media were collected at 24 and 48 hr and cell lysates collected at 48 hr were assayed and the levels of VEGF were presented as mean ± SEM pg/µg total protein. Secreted VEGF at 24 hr and intracellular VEGF levels were significantly higher in cell lines with *BRAF* V600E status (*p < 0.05 for 24 hr secreted and **p < 0.01 for intracellular results, by unpaired t-test). **B,** secreted VEGF levels of melanoma cell lines in hypoxia (0.1% O_2) measured with ELISA, presented as mean ± SEM pg/µg total protein. (n=3 independent samples).

3.4 VEGF expression in newly established LM-MEL melanoma cell lines

Results in figure 3-6 suggested that secreted VEGF as well as intracellular VEGF levels were higher in *BRAF* V600E cell lines, compared to the *BRAF* WT melanoma cells, indicating a link between *BRAF* V600E and increased VEGF expression. In an attempt to further confirm this phenotype, 9 newly established Ludwig-Melbourne-Melanoma (LM-Mel) cell lines were obtained from the Ludwig Institute in Melbourne. Three cell lines for each genotype, (*BRAF* WT, *NRAS* Q61K and *BRAF* V600E) were selected.

Both the intracellular VEGF and secreted VEGF in these LM cell lines were quantified as before using the human VEGF ELISA. Results in figure 3-7A showed that secreted VEGF levels were higher in two of the WT cell lines (LM25 and LM44), and two of the V600E cell lines (LM31 and LM16), compared to the rest of the cell line panel. The same pattern was found when assaying intracellular levels of VEGF (3-7B), and VEGF levels did not appear to be related to their mutation status. Pooled data suggested that the *NRAS* mutant cell lines showed lower VEGF expression than the WT group, but the differences were not significant. Levels of intracellular VEGF were significantly higher in V600E cell lines, compared to the NRAS group, in pooled results (3-7B). The link between *BRAF* mutation and increased VEGF expression found in the previously-tested cell line panel (figure 3-6) was not observed here in the LM cell lines.

To further probe the relationship between *BRAF* status and VEGF, we investigated the differential gene expression between *BRAF* WT and BRAF V600E cells from the publicly

available microarray data obtained from Illumina HumanHT-12 V4.0 expression beadchip arrays in the LM cell lines (ArrayExpress: http://www.ebi.ac.uk/arrayexpress/experiments/E-MTAB-1496/). The data were analysed by Dr Ruud Van Stiphout (Dr Francesca Buffa's group, University of Oxford), using averaged significance from three methods (linear models for microarray data, LIMMA; R Significance Analysis of Microarrays, SAMR; Rank Product, RP) to test the significance of differential gene expression. From Dr Van Stiphout's analysis, there was no difference between the levels of *VEGF* mRNA in *BRAF* WT vs. V600E (figure 3-8A). However, there was a strong correlation between the levels of *VEGF* mRNA and levels of secreted (figure 3-8B) or intracellular VEGF protein (figure 3-8C). Further analysis of gene expression in the LM cell lines will be presented in chapter 5.

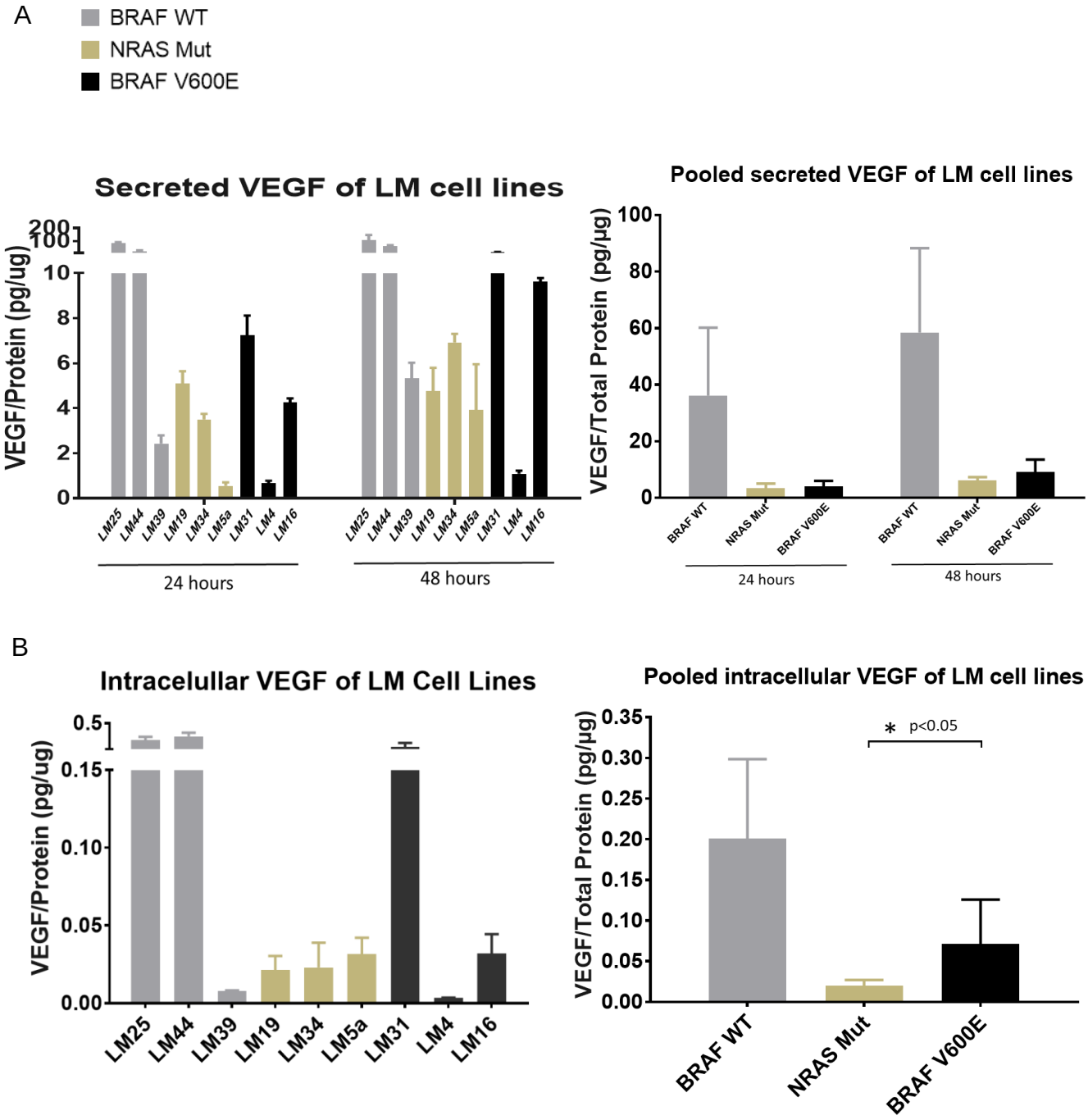


Figure 3-7: Secreted and intracellular VEGF levels of LM cell lines.

A, secreted VEGF levels in melanoma cell lines measured using ELISA (n=3 independent samples). Conditioned media (24 and 48 hr) were assayed and the levels of VEGF were presented as mean ± SEM pg/µg total protein. The secreted VEGF levels were much higher in two of the WT cell lines (LM25 and LM44), and two of the V600E cell lines (LM 31 and LM16), compared to the rest of the cell line panel. **B,** intracellular VEGF levels of melanoma cell lines were measured with ELISA, presented as mean ± SEM pg/µg total protein. Compared to the secreted VEGF results, a similar pattern was shown in the intracellular VEGF levels: higher levels of intracellular VEGF were found in two of the WT cell lines, and two of the V600E cell lines.

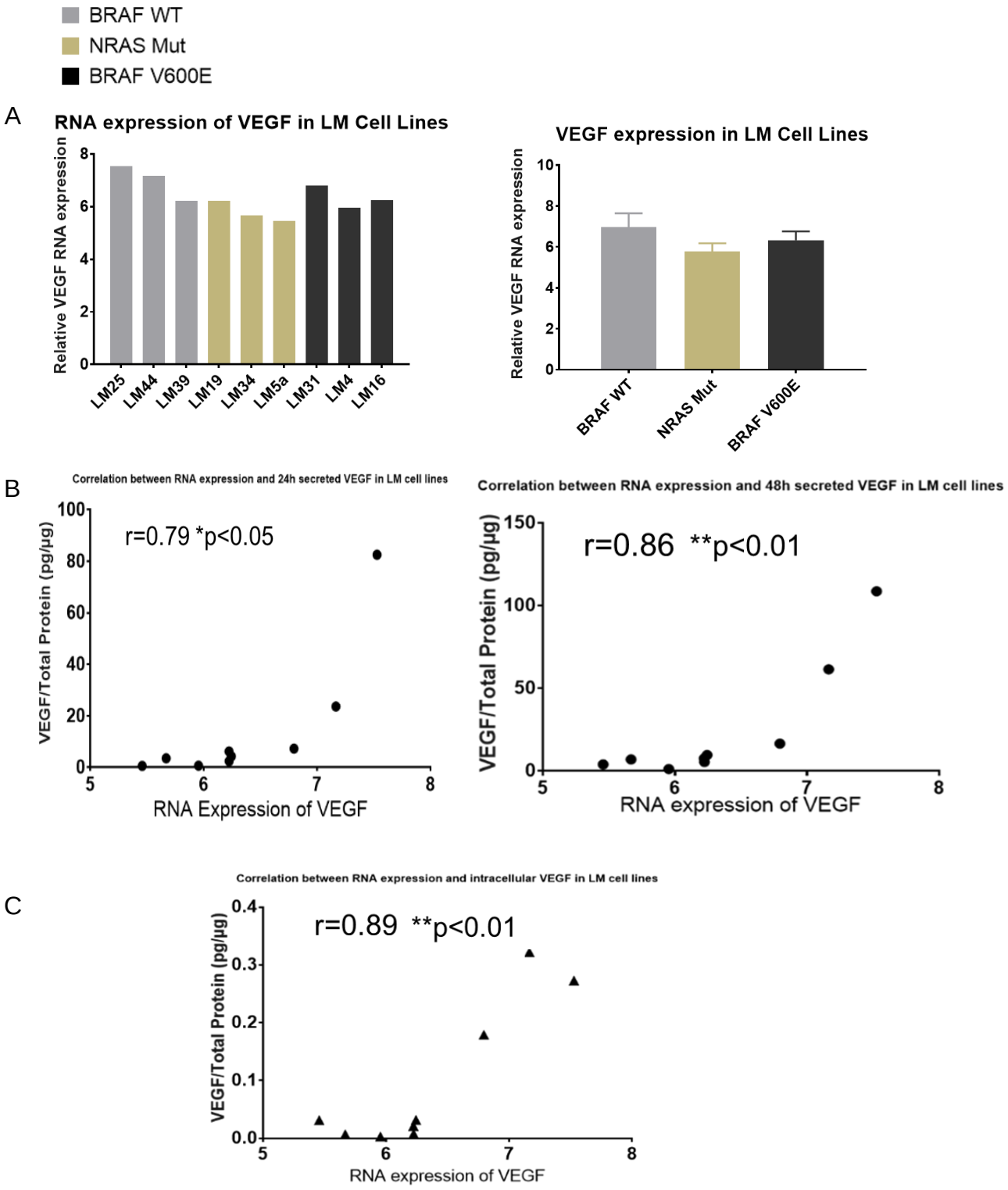


Figure 3-8: Levels of RNA expression of VEGF in LM cell lines.

A, RNA expression of VEGF in 9 LM melanoma cell lines. Y-axis represents the relative express of VEGF, normalised by the expression of the housekeeping gene. B, strong correlations could also be observed between the levels of RNA expression and the secreted VEGF levels at 24 hours (Pearson's correlation coefficient r=0.79, *p<0.05) and 48 hours (r=0.86, **p<0.01). **C**, the levels of RNA expression of VEGF correlate with the levels of intracellular VEGF protein in the LM cell lines. r=0.89, **p<0.01.

3.5 Discussion

The AVAST-M trial assessing bevacizumab as adjuvant therapy for high risk melanoma has shown that patients with *BRAF* V600E melanomas had improved disease-free interval, while those with *BRAF* WT melanomas did not benefit(Corrie et al., 2014). To investigate the molecular basis for this differential sensitivity of *BRAF* V600E melanomas to VEGF inhibition, two possibilities have been explored. The first was that the inhibition of VEGF by bevacizumab directly suppresses tumour progression via autocrine VEGF signalling in *BRAF* V600E tumour cells. Although expression of VEGFR2 and VEGF could be detected in some of the melanoma cell lines, experiments testing effects in 2D and 3D growth, and wound healing showed no significant effects on cell proliferation or migration, upon VEGF inhibition with bevacizumab.

This suggested that the direct anti-melanoma effects of bevacizumab via a possible autocrine VEGF signalling loop were unlikely. A high dose of 300µg/ml bevacizumab was selected for the experiments based on previous *in vitro* studies (Adamcic et al., 2012; Mahfouz et al., 2017; Hein and Graver, 2013). It would have been beneficial to have included HUVECs and VEGFR2 inhibitor cediranib (AZD2127) as positive controls in some of the bevacizumab experiments.

The second possibility considered was that the sensitivity of *BRAF* V600E melanomas to bevacizumab was mediated indirectly via effects on angiogenesis or other components of the tumour microenvironment. The results of VEGF ELISA in the melanoma cell line panel suggested that secreted and intracellular VEGF levels were significantly higher in cell lines with *BRAF* V600E status, indicating a possible association between *BRAF* V600E and

increased VEGF expression. This is consistent with the reported ability of *BRAF* V600E to promote HIF-1α expression (Kumar et al., 2007). However, the same phenotype was not observed in the newly established LM-Mel cell lines obtained from the Ludwig Institute in Melbourne. Due to this discrepancy in VEGF expression, and potentially confounding effects of other gene mutations that occur in melanoma cell lines (table 2-1), it was decided to generate an isogenic WT/V600E model from a *BRAF* WT melanoma cell line for further *in vitro* and *in vivo* investigations.

Chapter 4: Generating an isogenic WT/V600E melanoma cell line model and identifying differentially expressed genes between *BRAF* WT and V600E melanomas

4.1 Introduction

Cancers are the results of mutations in the genome that can fundamentally alter the function of the products of key cancer genes (Stratton et al., 2009). There have been more than 500 genes identified so far to be implicated in cancer (http://cancer.sanger.ac.uk/census). While some of these mutations are drivers that are responsible for initiating tumorigenesis, others are responsible for maintaining proliferation or other hallmarks of cancer, inducing angiogenesis, invasion and metastasis (Hanahan and Weinberg, 2011). To understand the cell intrinsic processes resulting from these mutations, and to test possible therapeutic strategies, cancer cell lines have been widely used since the establishment of the HeLa cell line more than 50 years ago (Scherer et al., 1953), and have been proven to be invaluable models in preclinical investigations. However, studies in cancer genomics in recent years have shown an enormous degree of genomic heterogeneity across the cancer patient population in many tumour types (Stratton et al., 2009) including melanoma (Akbani et al., 2015; Hayward et al., 2017), and therefore across the cancer cell lines derived from these patients. Molecularly defined subgroups within the same tumour type may exhibit different biological characteristics including responses to treatments (Weinstein, 2012), therefore,

studies that use cancer cell line panels might need a large scale to be able to accurately model the effects of gene mutations.

In the initial investigations for this project, cell line panels consisting of *BRAF* WT and V600E melanomas were assembled to test the effect of *BRAF* status in response to VEGF inhibition using bevacizumab. Results of these experiments suggested that it might be a possibility that the clinical sensitivity of *BRAF* V600E melanoma to bevacizumab (Corrie et al., 2014) was not mediated via direct effects on the tumour cells themselves. The results of the VEGF ELISA in the first panel of melanoma cell lines suggested a link between *BRAF* V600E mutation and increased VEGF expression (figure 3-6), raising the possibility of an effect on the tumour microenvironment, but the same finding could not be replicated in the subsequently acquired LM cell lines (figure 3-7). Due to this discrepancy and the potentially confounding effects of other gene mutations in cell lines, it was decided to generate an isogenic WT/V600E model from a *BRAF* WT melanoma cell line. In addition to the advantage of eliminating any differences due to other mutations, an isogenic cell model could also be more informative for *in vivo* investigations into the influence of tumour-stroma interactions, invasion and angiogenesis.

The aim was to perform gene expression array analysis on the isogenic model. The differentially expressed genes generated from this model would then be compared to the analysis from RNA sequencing of patient tumours, and publicly available array data on the LM cell lines from Melbourne (Behren et al., 2013).

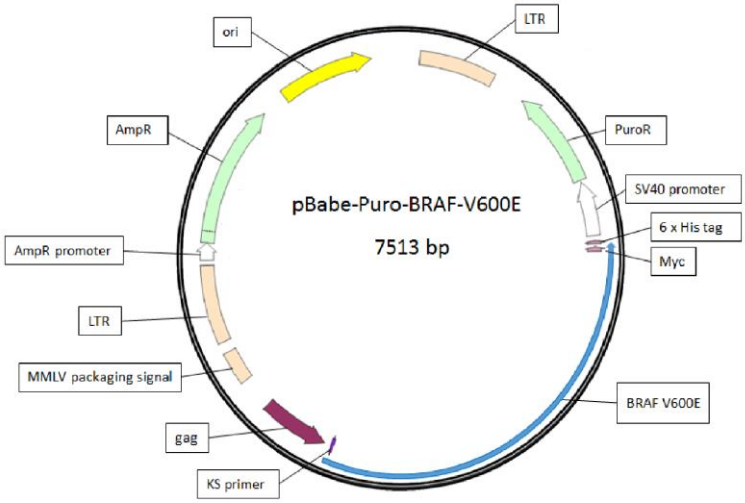
4.2 Retroviral expression of pBabe-Puro-*BRAF*-V600E in *BRAF* WT cell lines

The first attempt to generate an isogenic model was made using a retroviral system. A retroviral system can deliver genes of interest which become integrated into the host cell genome, offering an effective method to induce the expression required. To establish this system, a *BRAF* V600E expression vector pBabe-Puro-*BRAF*-V600E was obtained from Addgene (Boehm et al. 2007, figure 4-1A), and Phoenix packaging cells were kindly provided by Dr Judith Cossins from the Nuffield Department of Clinical Neurosciences, Oxford. A corresponding *BRAF* WT vector was created based on pBabe-Puro-BRAF-V600E using the QuikChange Multi Site-Directed Mutagenesis kit. All the plasmids were sequenced and the sequencing results confirmed the correct sequence of *BRAF* V600E (figure 4-1B) and WT (figure 4-1C) plasmids to be transfected.

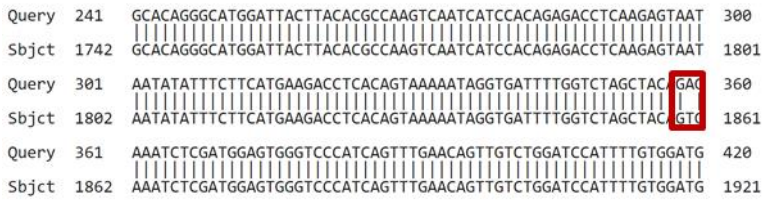
Phoenix cells were transfected and the viral medium was used to infect *BRAF* WT cell lines. Positive cells were then selected using puromycin. Results in figure 4-1D showed that overexpression of *BRAF* V600E and *BRAF* WT could be observed at 96 hours, compared to cells with infected empty vector (EV). An increase in phosphorylation of MEK and ERK were also found in the overexpressed cells, compared the EV control. However, this overexpression of *BRAF* could not be maintained after 96 hours. Repeated attempts on another *BRAF* WT cell line CHL1 encountered the same difficulty. This could due to *BRAF* V600E-induced senescence, as previously described in *BRAF* V600E expressing melanocytes (Michaloglou et al., 2005; Wajapeyee et al., 2008) and thyroid carcinoma cell lines (Vizioli et al., 2011).

Since the proposed investigations using the isogenic model might include co-culturing with HUVEC cells for experiments on angiogenesis and possible *in vivo* testing, a more stable model that can sustain the induced *BRAF* expression was required. After exploring other gene targeting methods including the 'PiggyBac (PB) Transposon Inducible System', it was decided to use CRISPR/Cas9, due to the potential advantage of using the endogenous promoter for the induced expression.

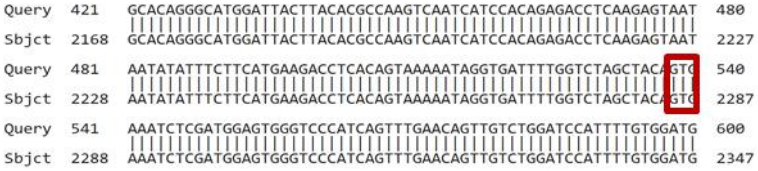
A



B



C



D

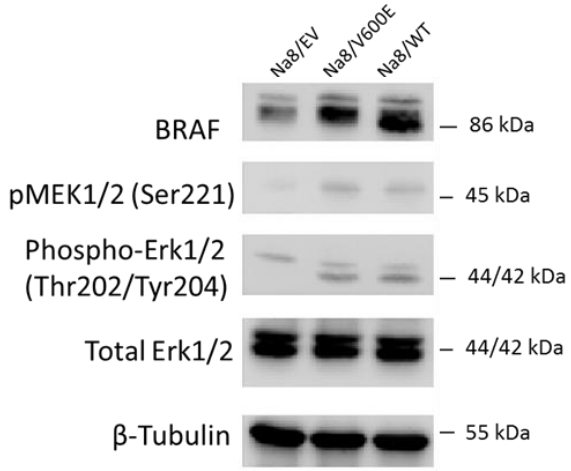


Figure 4-1: Retroviral expression of WT and V600E *BRAF* in *BRAF* WT cell line.

A, Sequence map for pBabe-Puro-*BRAF*-V600E, created with SnapGene®. **B**, Sequencing results confirmed the *BRAF* V600E mutation, highlighted in the red box. **C,** *BRAF* WT plasmid was created using site-directed mutagenesis, as shown in the sequencing results. **D**, upon successful transfection and infection, overexpression of *BRAF* V600E and *BRAF* WT could be observed in Na8 cells at 96 hours, compared to cells infected with an empty vector (EV). An increase in phosphorylation of MEK and ERK were also found in the *BRAF* overexpressing cells, compared with the EV control.

4.3 Generating an isogenic WT/V600E model using CRISPR/Cas9 system

4.3.1 Pre-transfection screening for suitable host cell lines

In preparation to generate the isogenic *BRAF* WT/V600E model using the CRISPR/Cas9 system, a range of *BRAF* WT cell lines were screened for their suitability, based on their transfection efficiency and their copy number of the *BRAF* gene.

To generate the isogenic WT/V600E model using CRISPR, a suitable host cell line was to be transfected with WT Cas9 to disrupt the *BRAF* WT gene, and donor plasmids to knock in the *BRAF* V600E mutation. Therefore, a high transfection efficiency (>50%) of the host cell line is essential for this gene editing process to be successful. Six *BRAF* WT cell lines were then tested for transfection efficiency, including CHL1, SKMEL2, NA8, LM5a, LM25 and LM44, using a GFP expression plasmid with Lipofectamine 2000 (Invitrogen). Five days after the transfection, GFP expression could be observed only in three cell lines, CHL1, SKMEL2 and LM44 (figure 4-2B). No GFP expression was seen in NA8, LM5a and LM44 cell lines. Results in figure 4-2B showed that out of the three GFP-positive cell lines, only CHL1 cells had achieved a transfection efficiency of more than 50%. SKMEL 2 and LM 25 cell lines were poorly transfectable, with the transfection efficiency being only 15% and 5% respectively.

BRAF gene copy numbers were also determined by cytogenetic analysis using fluorescence *in situ* hybridisation (FISH), carried out by Dr Daniela Moralli in the Wellcome Trust Centre for Human Genetics in Oxford. The FISH results on the cell lines revealed high heterogeneity in *BRAF* gene copy number in all three transfectable cell lines tested (Table 4.1). For

example, 57.4% of the CHL1 cells tested had 4 copies of *BRAF* gene, as shown in figure 4-2A. This heterogeneity in *BRAF* gene copy number in all of the transfectable cell lines was one of the factors taken into account in suitability for further study. There were two additional important considerations. Firstly, SKMEL2 cells harbour mutations in *NRAS*, which is usually mutually exclusive with *BRAF* mutation, and *KIT*, more typical of mucosal melanoma, while CHL1 is *NRAS* wild-type (Ranzani et al., 2015; Akbani et al., 2015; Hayward et al., 2017). LM 25 cells are *NRAS* wild-type (Behren et al., 2013) but had an extremely slow pattern of growth, both for this project and as found in a previous project in our group (Gupta, 2017). This together with their very poor transfectability made LM25 unsuitable for this study. Taking into account all of these considerations, CHL1 cells were selected to be the host cell line for generating the isogenic WT/V600E model.

Table 4-1: Copy number of BRAF gene in cell lines.

C	1 signal /cell	2 signals /cell	3 signals /cell	4 signals /cell	5 signals /cell	6 signals /cell	More than 6 signals /cell
CHL1	-	-	20.4%	57.4%	16.7%	3.7%	1.8% (8 signals/cell)
SK2	3.7%	25.9%	66.7%	3.7%	-	-	-
LM25	-	-	16.7%	24.1%	37%	22.2%	-

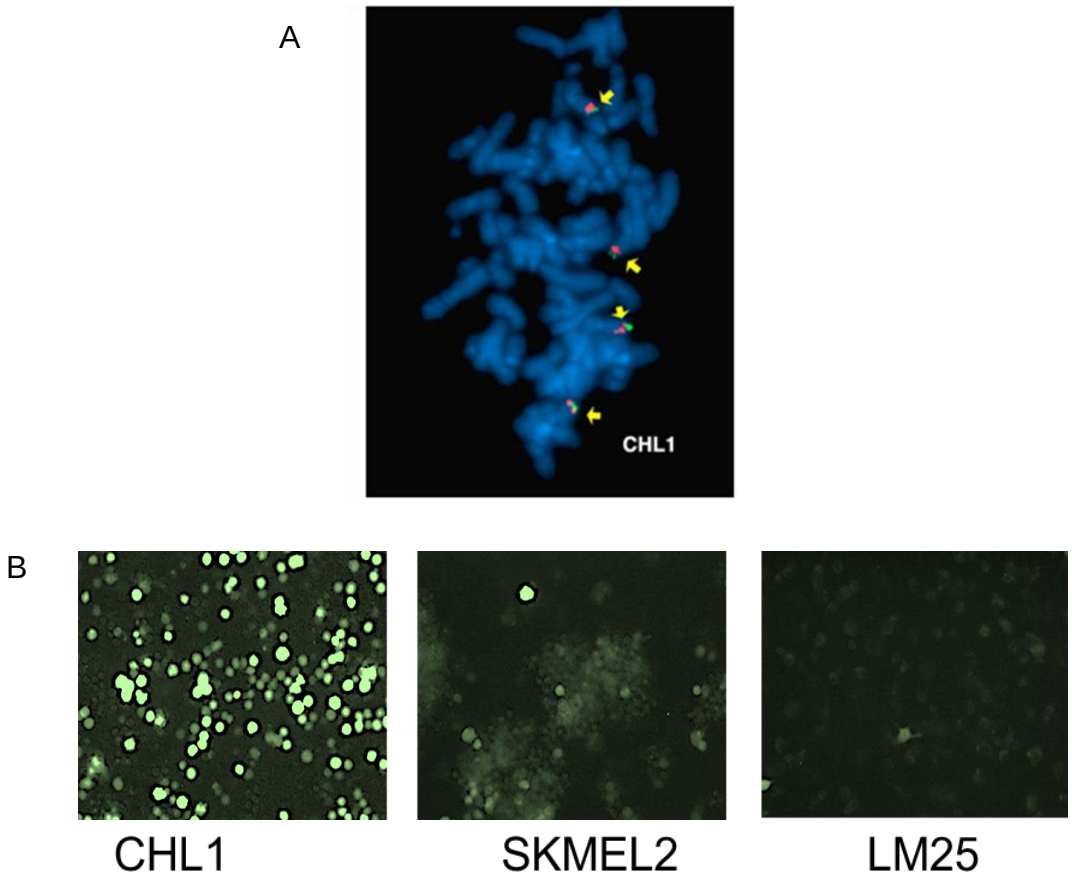


Figure 4-2: Copy number of *BRAF* gene and transfection efficiency for different *BRAF* WT cell lines were determined.

A, Multiple copies of *BRAF* gene in CHL1 cells were detected by FISH using two *BRAF* specific detecting probes (red=probe RP5-839B19; green=probe RP11-60D5). **B,** Three *BRAF* WT cell lines were transfected with GFP plasmid to test their transfection efficiency. The CHL1 cells achieved >50% transfection efficiency. The transfection efficiency was much lower in SKMEL 2 (15%) and LM 25 (5%) cell lines.

4.3.2 Transfection and selection for positive clones

The strategy for the gene editing using CRISPR to replace the *BRAF* WT with V600E is illustrated in figure 4-3A. A *BRAF* disrupting plasmid containing chimeric gRNA scaffold and WT Cas9 (Horizon Discovery Group), was used to introduce a double-stranded break in exon 15 of the *BRAF* gene. A donor plasmid containing the *BRAF* V600E mutation sequence (c. 1799T>A) was used to knock in the mutation by homologous recombination. A selection marker consisting of the CMV promotor and eGFP was integrated into intron 15. WT Cas9

was chosen for its higher efficiency compared to the nickase enzyme. To prevent re-cutting the donor by WT Cas9, three silent mutations were introduced in addition to the V600E, as shown in figure 4-3B.

CHL1 cells were co-transfected with the *BRAF* disrupting WT Cas9 plasmid and the donor plasmid containing an eGFP selection cassette. At 72 hours post-transfection, GFP expression in cells could be observed, and GFP-positive cells were sorted into 96 well plates (1 cell per well) by fluorescence-activated cell sorting (FACS), performed by Mr Andrew Worth, Flow Cytometry facility, Jenner Institute, Oxford. After cell sorting, growing colonies were tested by PCR using screening and confirmation primers (figure 4-3C). Two pairs of screening primers were used to select positive clones, and two pairs of confirmation primers were used to test for the *BRAF* V600E mutation in these clones.

The first attempt at CRISPR transfection generated only 4 positive clones out of 500 clones tested, and none of the positive clones showed homozygous V600E or a mutant *BRAF* phenotype. The transfection was repeated, and cells were sorted and left to grow for ten days before GFP-positive clones were selected for screening. Out of 2000 clones screened, 9 homozygous clones were identified, together with more than 20 heterozygous clones in which the V600E PCR product was stronger than the WT product. Results of PCR screening on some of these clones are shown in figure 4-4A. Sequencing results in figure 4-4B showed that the donor sequence (V600E plus three silent mutations) was successfully incorporated into the genome.

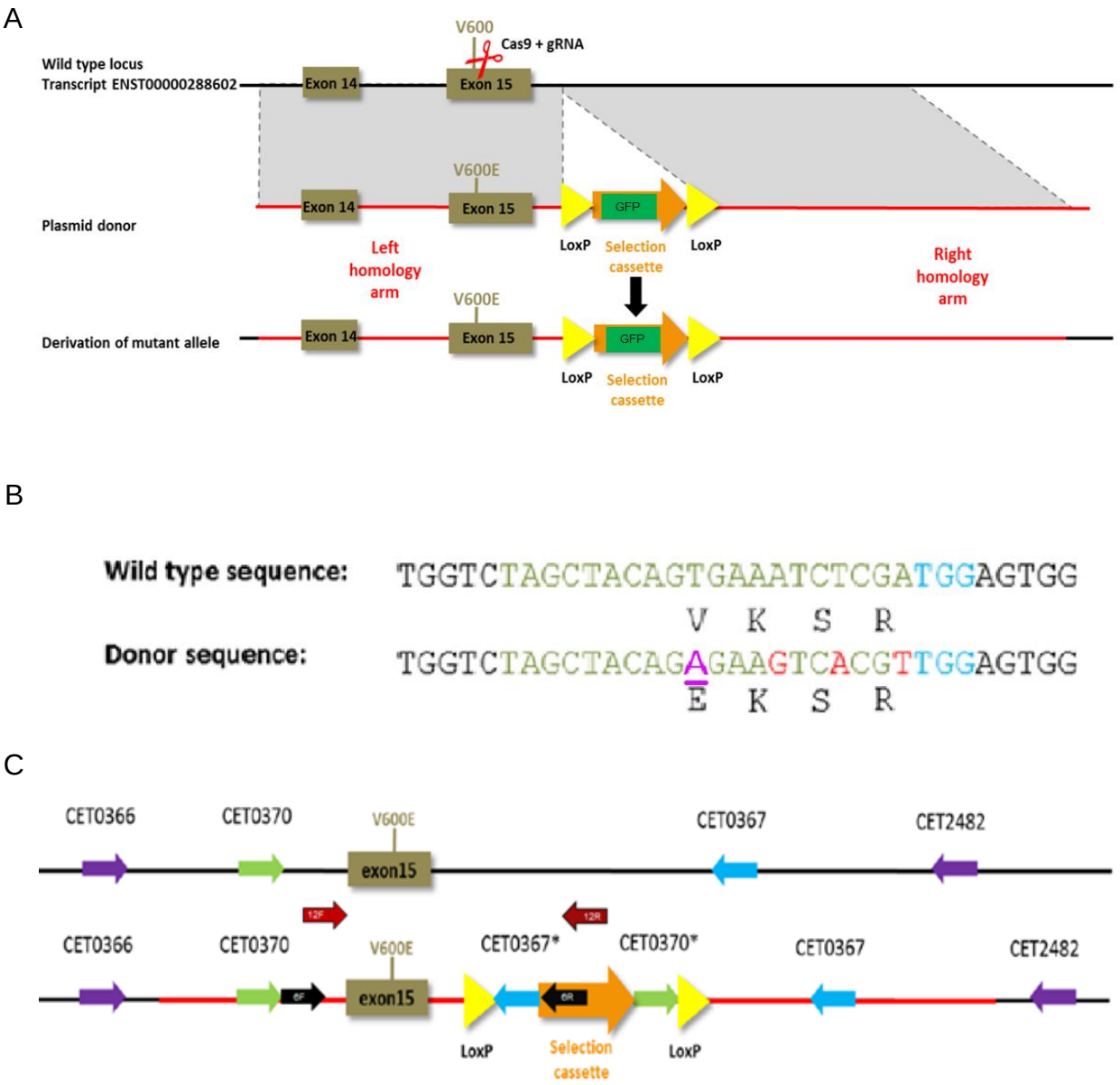
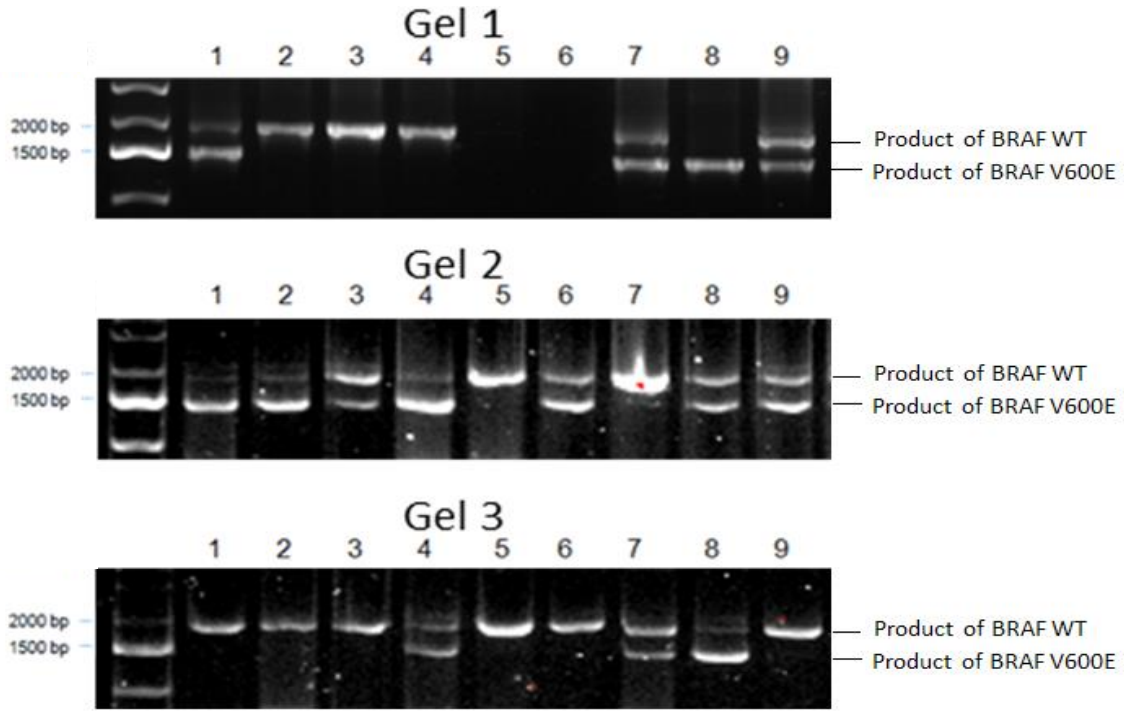


Figure 4-3: CRISPR plasmid design and targeting and screening strategy.

A, A knock-out plasmid (GRP582) containing wild type Cas9 was used to disrupt exon 15 and a plasmid donor (pAAV0990) to introduce *BRAF* V600E mutation. Within the donor plasmid pAAV0990, a selection cassette of eGFP was integrated in intron 15, and LoxP elements were placed at both ends of the selection cassette to provide an option to have the cassette removed with homologous recombination, if required. B, Mutations contained in the donor plasmid pAAV0990. In addition to the V600E mutation (purple), three silent mutations (red) were also introduced to prevent re-cutting the donor plasmid. The sequence bound by gRNA highlighted in green, and the PAM site is in blue. C, Primer binding sites within the donor plasmid pAAV0990, designed for efficient post-transfection screening. Donor contains sites for annealing of screening primers (purple, green and blue arrows). Positions for the two confirmation primers are indicated with black and red arrows, with the reverse primers of these two pairs being within the selection cassette and were specific to the donor sequence.

A



B



Figure 4-4: Selection and genetic confirmation of *BRAF* V600E positive clones.

A, selection of the positive clones using the screening primers. Representative images of PCR products using the left arm screening primer pair (CET0366 and CET0367; 1896 bp for WT and 1468 bp for V600E; see figure 4-3C) showed that some of clones contained homozygous (lane 8 on gel 1) or proportionally stronger V600E (lane 1 and 2 on gel 2; lane 8 on gel 3). B, Sequencing using primers specific for the mutant allele (indicated in black, 6F and 6R, and red, 12F and 12R, in figure 4-3C) showed that donor sequences were incorporated into the genome. Mutations including silent mutations boxed in red.

4.4 Validating the isogenic BRAF WT/V600E CRISPR model

4.4.1 *BRAF* expression in the CRISPR clones

Figure 4-4 showed that positive clones selected from screening had the *BRAF* V600E mutation incorporated into the genome, with results suggesting that 9 clones were homozygous and more than 20 clones were heterozygous. To test whether the knocked-in *BRAF* V600E was expressed at the mRNA level, qRT-PCR was then performed on the mRNAs extracted from these cells. Two WT clones (WT7 and WT9) and the parental CHL1 cell line were used as controls for the expression of WT *BRAF*. In addition to the 9 cell clones with homozygous *BRAF* V600E, 8 cell clones with a proportionally stronger V600E genotype (as shown in figure 4-4A) were also included in the cell panel.

While the primers used for *BRAF* WT were probing endogenous sequences, the primers for *BRAF* V600E were specifically designed for annealing the knocked in sequences with three additional silent mutations. This differentiates the expression induced by CRISPR from that of endogenous *BRAF* V600E.

The qRT-PCR results in figure 4-5A showed that that the *BRAF* WT expression was almost completely abolished in most of the CRISPR clones, compared to the levels in *BRAF* WT cells. For the CRISPR induced *BRAF* V600E expression, results in figure 4-5B showed that varied levels of *BRAF* V600E expression were detected in the CRISPR clones. The majority

of the homozygous CRISPR clones expressed much higher level than the cells with a heterozygous genotype. *BRAF* V600E was not expressed in *BRAF* WT cells as expected.

Since the qRT-PCR experiments on the CRISPR clones have shown that *BRAF* V600E was expressed at the mRNA level in these cells, experiments testing their protein levels with western blotting were then carried out. The result in figure 4-5C showed that the anti-BRAF V600E antibody (Abcam, #ab200535) was unable to distinguish the mutant form of the protein from its WT counterpart. This western blot did, however, confirm that the isogenic *BRAF* V600E clones F10 and B6 expressed BRAF protein at levels similar to the level in A375 cells that have an endogenous *BRAF* mutation, and similar to parental CHL1 cells and wild-type CHL1 clones WT7 and WT9, presumably because the expression in all clones was driven by the endogenous promoter. Therefore, functional studies on the BRAF protein in the MAPK pathway were then carried out next.

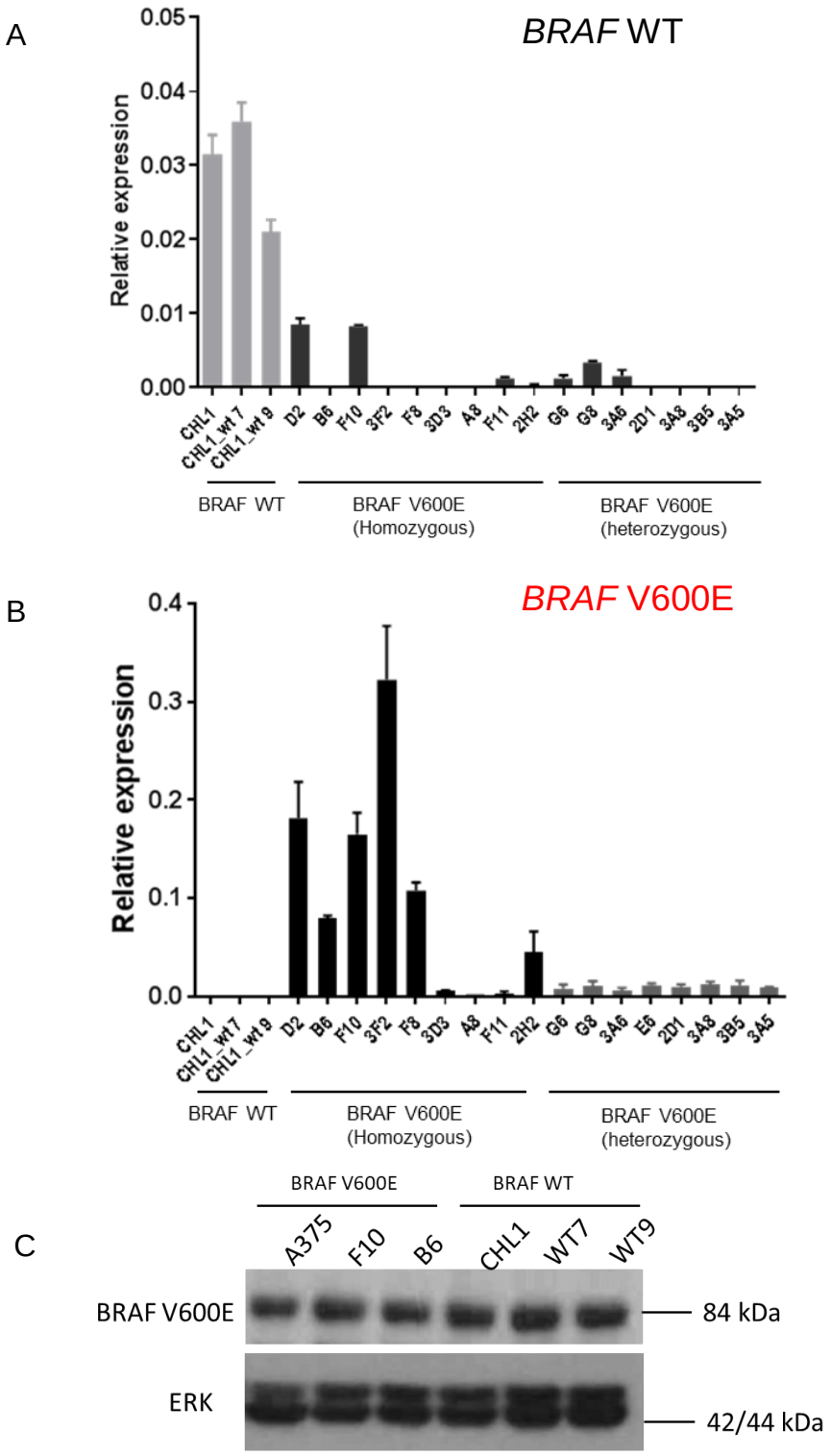


Figure 4-5: Expression of *BRAF* mRNA and BRAF protein in WT and knocked in V600E CRISPR clones.

A, Measuring expression of WT *BRAF* mRNA in the CRISPR clones. Compared to the levels in the *BRAF* WT cells (parental CHL1, WT clone 7 and 9), *BRAF* WT expression was almost completely abolished in most of the CRISPR clones. B, CRISPR induced *BRAF* V600E expression in the cell clones. Varied levels of *BRAF* V600E expression were detected in the CRISPR clones, but not in the *BRAF* WT cells. Levels of *BRAF* V600E mRNA were much higher in 6 out of 9 homozygous CRISPR clones, compared to the cells in the heterozygous group. Y-axis represents the relative expression, normalised by the expression of the housekeeping gene β-2-microglobulin. Error bars mean ± SEM. C, Western blotting using anti-BRAF V600E antibody did not show specificity for mutant BRAF. Similar levels of BRAF protein were detected in all of the WT melanoma cells (CHL1, WT7 and WT9), as well as in the mutant cells (A375, F10 and B6). Experiment was repeated twice and similar results were produced.

4.4.2 Sensitivity of the *BRAF* V600E clones to BRAF inhibitor PLX4720

BRAF mutations that lead to constitutive activation of the MAPK pathway occur in around 50% of melanomas, with 90% of such mutations being V600E (Davies et al., 2002). Vemurafenib (PLX4032) and its analogue PLX4720 are potent ATP-competitive small molecule drugs that selectively inhibit the kinase activity of BRAF V600E, while paradoxically in *BRAF* WT cancers are capable of increasing phosphorylation of downstream effectors MEK and ERK, inducing proliferation (Hatzivassiliou et al., 2010; Carnahan et al., 2010). Results in the previous experiments showed that the *BRAF* V600E mutation had been successfully edited into the genome using the CRISPR/Cas9 system and was expressed at the transcriptional level. However, its expression at the protein level and effects on cellular behaviour remained to be investigated. Since the BRAF inhibitor PLX4720 has selectivity in targeting BRAF V600E kinase vs. WT BRAF, functional studies testing effects of PLX4720 on the MAPK pathway and proliferation were then carried out.

Cells were treated with PLX4720 for 2 hours, collected and lysed for immunoblotting. Results in figure 4-6A showed that the phosphorylation of MEK and ERK was increased in the *BRAF* V600E clones, compared to the WT clones, indicating more activation of the MAPK pathway. Reduction in the phosphorylation of MEK and ERK was found in all the *BRAF* V600E clones treated with PLX4720. In contrast, no inhibition was observed in the PLX4720-treated WT clones. Indeed, an increase in ERK phosphorylation could be seen in two of the 4 WT clones (WT3 and WT9), after being treated with PLX4720. This is consistent with the effects on BRAF WT reported previously (Hatzivassiliou et al., 2010; Carnahan et al., 2010). It was also noted that in PLX4720-treated *BRAF* mutant cells, especially for B6 and F10, the

phosphorylation of MEK and ERK were reduced to the levels that were even lower than the basal levels in the WT cell lines. This finding was consistent with the results seen in figure 4-5A, suggesting that expression of WT *BRAF* in these mutant clones was almost completely abolished and replaced by mutant BRAF protein.

To test whether proliferation would be affected by PLX4720, viability assays were performed to assess 2D growth. Cells were seeded on day one and treated with increasing concentrations of PLX4720 on day 2. Cells were incubated for another 72 hours at 37 ˚C before viability was measured using the CellTiter-Glo Luminescent Assay. Results in figure 4-6B showed significantly greater inhibition of 2D growth in the *BRAF* V600E clones treated with PLX4720 at 3 µM, compared to the effect on the WT clones (experiment 1). Although not statistically significant, more inhibition could still be observed in the mutant group than in the WT cell clones at 1 and 5 µM for experiment 1. In parental CHL1 cells and WT clones, PLX4720 caused minor enhancement of viability at 1 and 3 µM, with a small inhibitory effect only at 5 µM. Results in experiment 2 showed that cell growth in the mutant group were significantly more inhibited by PLX4720, compared to WT cell clones at 3, 5 and 10 µM. This was consistent with the results obtained from experiment 1.

The effect of BRAF inhibition with PLX4720 on the 3D growth of the CRISPR clones was also assessed in spheroid assays. After the spheroids for each cell clone were formed and measured on the GELCOUNT™, increasing concentrations of PLX4720 were added to the wells. The growth of the spheroids was monitored every 2 days, and then the medium was changed, adding fresh PLX4720. Results in figure 4-7 showed that in the CRISPR V600E cell clones, 3D growth was inhibited by treatment with PLX4720 in a dose-dependent manner,

while only modest reduction in 3D growth was seen in treatment with the highest concentration (30 µM) in WT clones. Consistent with the results from the MAPK signalling study (figure 4-6A) and 2D growth experiments (figure 4-6B), 3D growth of *BRAF* WT cells was not inhibited but was rather stimulated after being treated with low concentrations (1-3 µM) of PLX4720.

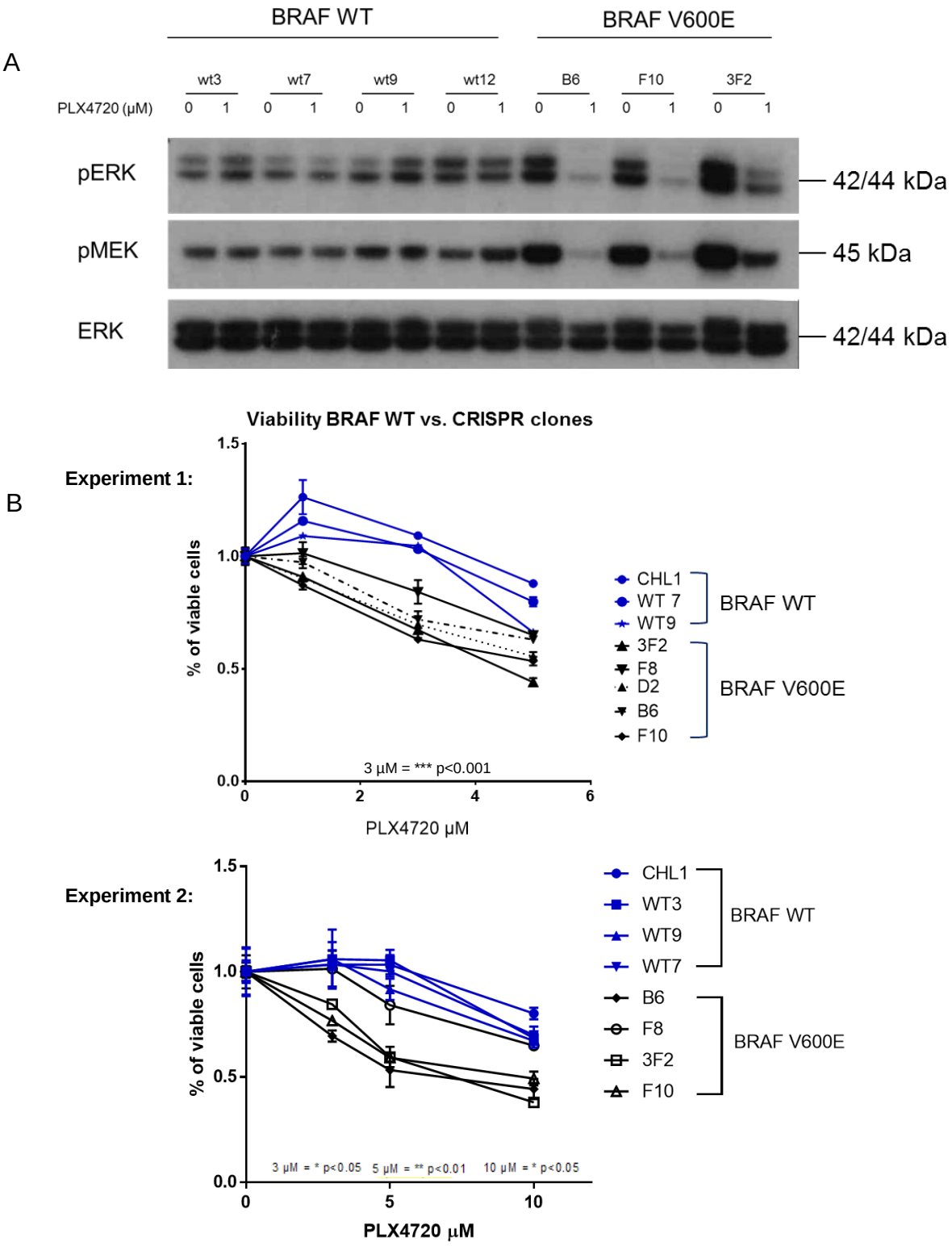


Figure 4-6: Response of *BRAF* WT and V600E clones to BRAFi (PLX4720) in the MAPK pathway and in 2D growth.

A, Response of *BRAF* clones to PLX4720 in the MAPK pathway. Four *BRAF* WT and three *BRAF* V600E clones were treated with solvent control (DMSO) or 1 μM PLX4720 for 2 hours before they were collected and lysed for western blotting. Experiment was repeated on a second set of independent lysates and similar results were produced. B, Cells were seeded on day one and treated with increasing concentrations (1, 3 and 5 μM) of PLX4720 on day 2 in experiment 1, and 3, 5 and 10 μM of PLX4720 in experiment 2. Viability was measured on day 5 using the CellTiter-Glo Luminescent Assay. Points represent mean ± SEM, n=3 independent technical replicates. In the first experiment, significantly greater inhibition was observed at 3 μM in *BRAF* V600E group, compared to WT cells (***p<0.001, by unpaired t-test). Significantly more inhibition was also observed at 3, 5 and 10 μM in *BRAF* V600E group, compared to WT cells for experiment 2 (*p<0.05, **p<0.01, *p<0.05 for 3, 5 and 10 μM respectively, by unpaired t-test).

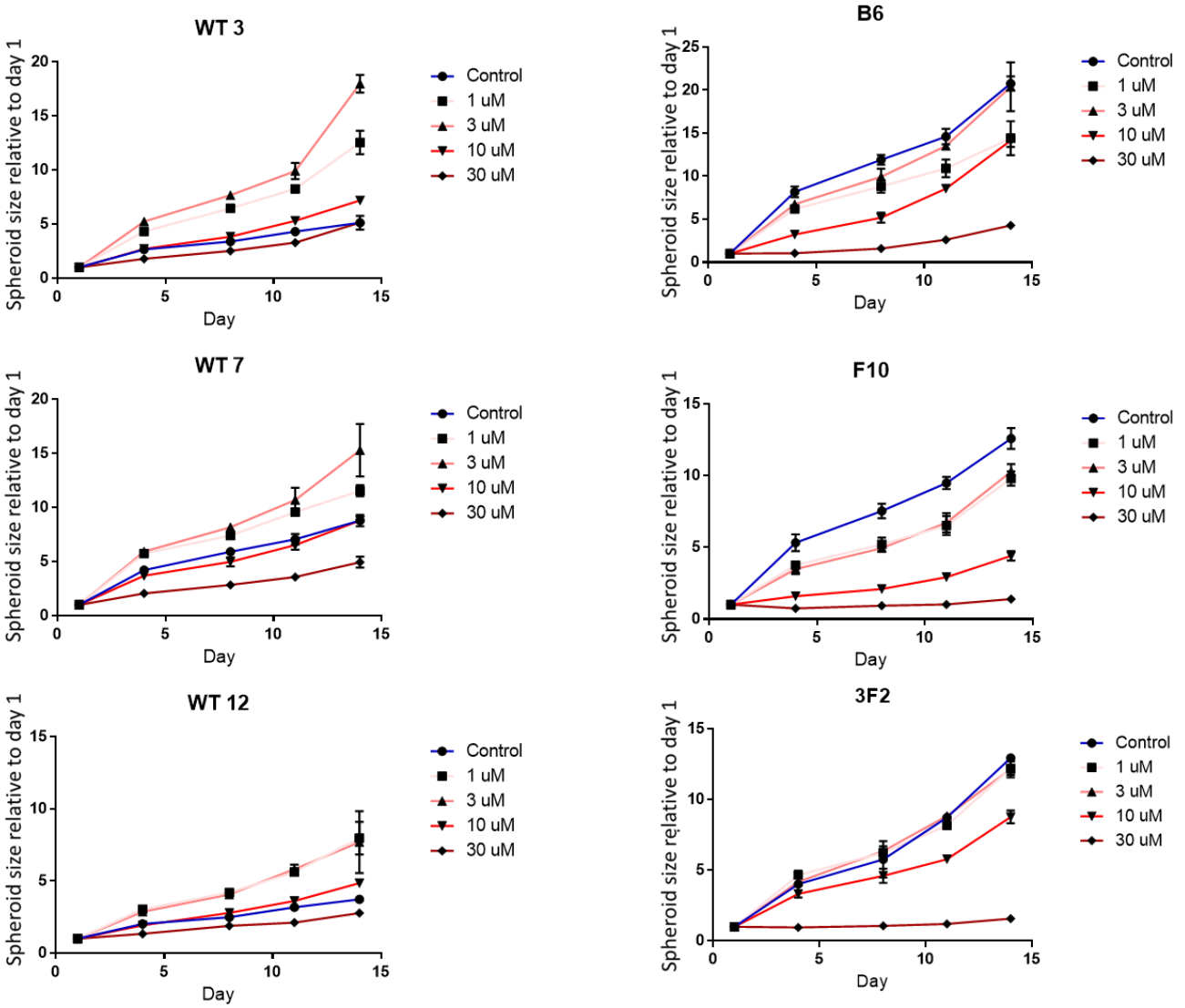


Figure 4-7: Testing response of *BRAF* WT or V600E clones to BRAFi (PLX4720) in 3D growth.

Sensitivity of the *BRAF* V600E clones to PLX4720 was assessed in spheroid assays. Spheroids for each cell clone were treated with increasing concentrations (1, 3, 10 and 30 µM) of PLX4720, and the growth of the spheroids was measured every 2-3 days. Graphs show mean ± SEM spheroid size (n=6) relative to day 1, immediately before PLX4720 treatment. Experiment was repeated and similar results were produced.

4.4.3 2D and 3D growth of CRISPR clones

Previous experiments have shown that mutant *BRAF* was expressed in the *BRAF* V600E clones, and the cells were sensitive to selective BRAF V600E inhibitor PLX4720, indicating that these CRISPR clones did exhibit a *BRAF* V600E phenotype. To further characterise these cells, the growth in 2D and 3D of the CRISPR cell clones was also assessed.

First, the doubling time for each clone was determined in 2D growth by counting the cell population each day for 5 days, and calculating the doubling time based on cell counts using GraphPad Prism v5. Figure 4-8A showed that the doubling times were similar between the *BRAF* WT and V600E groups. However, when 3D spheroid growth was monitored by comparing the rate of increase in control spheroids from the experiments shown in figure 4-7, the *BRAF* mutant cells appeared to be expanding faster compared to the WT cells (figure 4-8B), suggesting a more aggressive phenotype of these cells in anchorage-independent conditions.

To further understand the molecular basis for this differential growth between *BRAF* WT and V600E cells, and to identify other differentially expressed genes that could account for the sensitivity of *BRAF* V600E melanomas to anti-angiogenic therapy, Human Illumina gene expression array analysis was then performed.

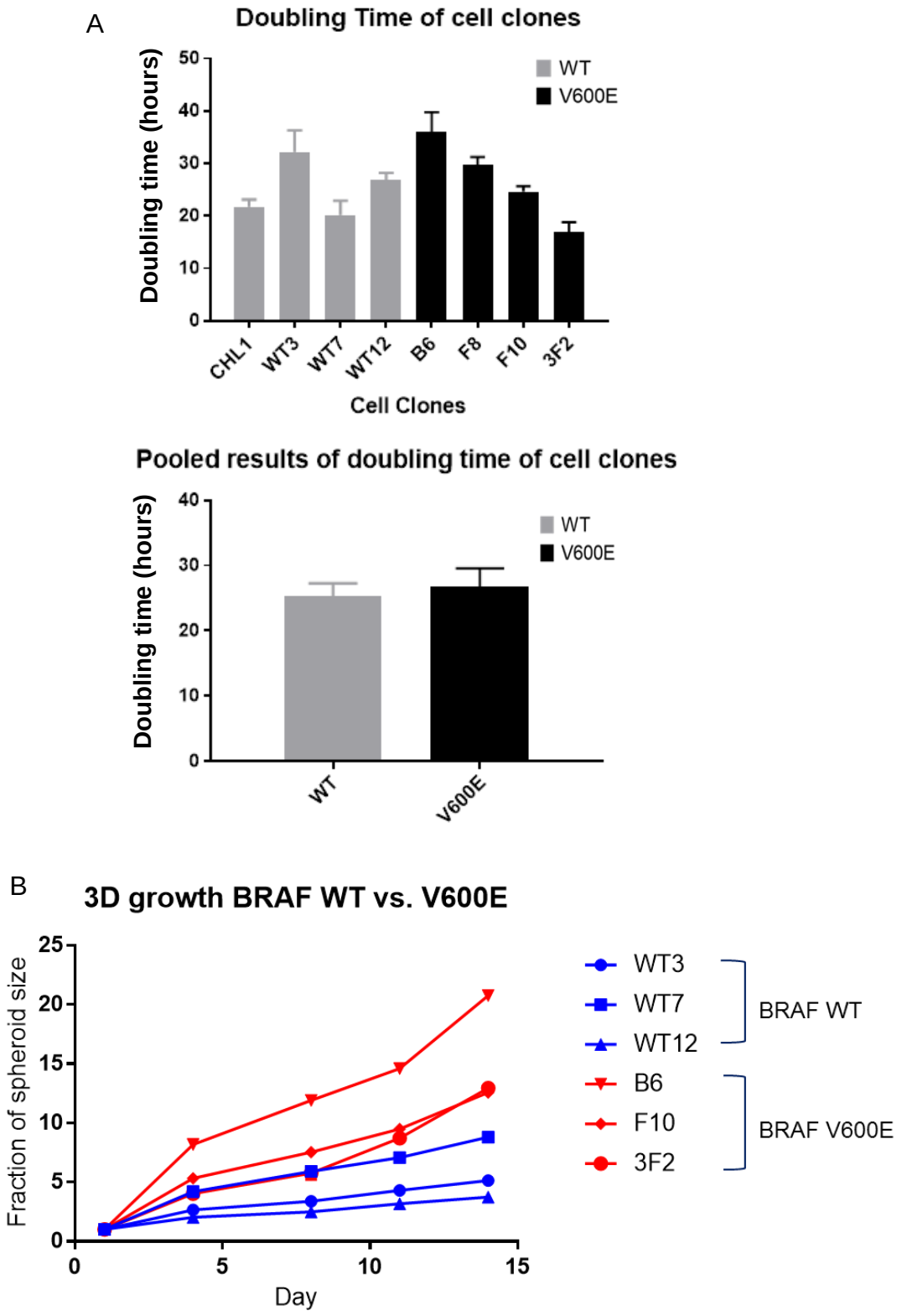


Figure 4-8: 2D and 3D growth comparison between the *BRAF* WT and V600E cell clones.

A, doubling time for each cell line was determined. Cells were seeded in triplicate plates for harvesting on each day for 5 days. Cells were counted every 24 hours and their doubling time was calculated using GraphPad Prism v5. Similar doubling time was observed between the cell groups. B, spheroids for each cell clone were formed (n=6) after 48 hours and their growth was monitored with GELCOUNT™ every 2 days. Points represent mean ± SEM (n=6) expressed as a fraction of size on day 1. Spheroids in the *BRAF* mutant group increased in size more rapidly, compared to the WT clones.

4.5 Differential gene expression between BRAF WT and V600E melanomas

4.5.1 Human HT12v4.0 Illumina array analysis on the CRISPR *BRAF* WT/V600E isogenic model

RNA was extracted from 4 of the *BRAF* V600E clones, 3 of the *BRAF* WT clones, and CHL1 parental cells. Quality of RNA samples was checked and samples were sent to the Wellcome Trust Centre for Human Genetics in Oxford for gene expression array analysis. RNA samples were processed using the Illumina TotalPrep-96 RNA Amplification Kit followed by the Illumina Whole-Genome Gene Expression Direct Hybridisation Assay. The labelled cRNA was then hybridised to HumanHT-12_V4_BeadChip for gene expression. The raw beadchip data were first pre-processed by Wellcome Trust Centre for Human Genetics in Oxford, and the resulting signals for each probe were further processed by Dr Ruud Van Stiphout (Dr Francesca Buffa's group, University of Oxford).

QC metrics in figure 4-9A showed that the control probes for biotin and hybridisation were sample-independent and consistently high signal was obtained in all samples, indicating that the experimental steps were successful. Variability in sample-dependent plots of average signal intensity and signal from housekeeping genes can be attributed to several different factors such as sample quality, labelling efficiency, and the amount of sample loaded. This variability was corrected with quantile normalisation by making two distributions identical in statistical properties by ranked mean values. The housekeeping gene signal was of high intensity and the number of detected genes was consistently high, raising no concerns about the quality of the data based on the technical metrics.

Figure 4-9B shows the hierarchical clustering of the normalised and filtered data, that can be used to identify outlier samples and assess the main factors influencing the expression profile, including experimental conditions or technical factors such as batch or chip. The dendrogram in figure 4-9B shows that there was clustering of replicate samples, and the experimental groups were distinctively distributed. Of note, the parental CHL1 samples occupied an intermediate position between the mutant and WT groups. Compared with the WT clones, the hierarchical clustering suggested that the V600E mutation had significantly affected the global gene expression.

There were 814 significantly differentially expressed genes identified between the *BRA*F WT group and V600E group using the LIMMA method. The top 50 genes ranked by t value are displayed in table 4-2. The expression heatmap in figure 4-10 showed that these top 50 genes shared a distinctive pattern of differential expression between the *BRAF* WT and V600E groups in the dendrogram, indicating a significant effect of the *BRAF* V600E mutation on gene expression. Of these 50 genes, 17 are related to Angiogenesis and 8 to VEGF pathways by the PANTHER pathway analysis, and these are listed in table 4-3 and 4-4.

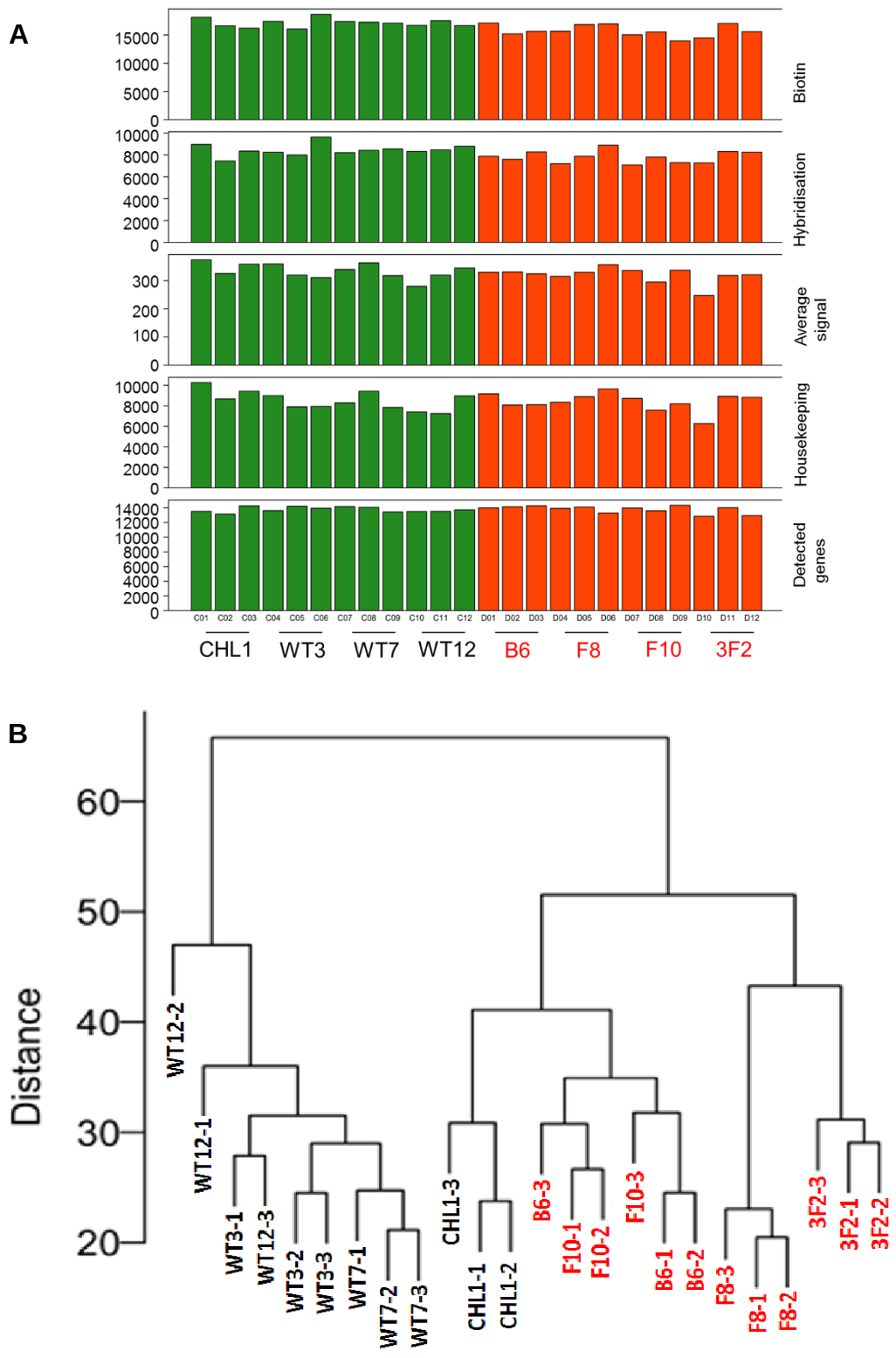


Figure 4-9: Technical and sample QC metrics and the hierarchical clustering.

Technical and sample QC metrics and the hierarchical clustering of the normalised filtered data of the 24 samples, comprising 3 independently collected RNAs for each cell line/clone; black=*BRAF* WT; red=*BRAF* V600E. A, Quality Control (QC) metrics. Sample-independent biotin and hybridisation were showing high signals in all samples. The housekeeping gene signal was high intensity and the number of detected genes was consistently high. B, Dendrogram showing hierarchical clustering of the normalised and filtered data of 24 samples. Sample groups could be distinguished by their clusters, and separation was observed between the *BRAF* WT and V600E groups.

Table 4-2: Top 50 differentially expressed genes ranked by t value.

Gene symbol	Definition	RANK	t	log2 Fold Change	P.Value	adj.P.Val
LYPD1	Homo sapiens LY6/PLAUR domain containing 1 (LYPD1), transcript variant 1, mRNA.	1	19.47	2.28	1.14E-17	2.11E-14
SLN	Homo sapiens sarcolipin (SLN), mRNA.	2	-18.60	-3.61	3.72E-17	3.44E-14
LOC100134073	PREDICTED: Homo sapiens similar to LYPDC1 protein (LOC100134073), mRNA.	3	16.97	1.99	3.84E-16	2.37E-13
COL9A1	Homo sapiens collagen, type IX, alpha 1 (COL9A1), transcript variant 1, mRNA.	4	-15.12	-1.82	6.89E-15	3.18E-12
PLAUR	Homo sapiens plasminogen activator, urokinase receptor (PLAUR), transcript variant 2, mRNA.	5	14.94	1.43	9.33E-15	3.45E-12
WSCD1	Homo sapiens WSC domain containing 1 (WSCD1), mRNA.	6	14.66	1.08	1.47E-14	4.54E-12
CD96	Homo sapiens CD96 molecule (CD96), transcript variant 1, mRNA.	7	-13.20	-2.35	1.89E-13	4.98E-11
BMP7	Homo sapiens bone morphogenetic protein 7 (osteogenic protein 1) (BMP7), mRNA.	8	13.10	2.31	2.27E-13	5.24E-11
NT5E	Homo sapiens 5'-nucleotidase, ecto (CD73) (NT5E), mRNA.	9	13.01	1.54	2.69E-13	5.52E-11
CARD10	Homo sapiens caspase recruitment domain family, member 10 (CARD10), mRNA.	11	-12.81	-1.29	3.90E-13	6.59E-11
PLAUR	Homo sapiens plasminogen activator, urokinase receptor (PLAUR), transcript variant 1, mRNA.	11	12.75	1.45	4.28E-13	6.59E-11
WFDC2	Homo sapiens WAP four-disulfide core domain 2 (WFDC2), mRNA.	11	12.79	1.06	4.02E-13	6.59E-11
TAGLN3	Homo sapiens transgelin 3 (TAGLN3), transcript variant 3, mRNA.	13	-12.39	-1.19	8.56E-13	1.22E-10
ROR2	Homo sapiens receptor tyrosine kinase-like orphan receptor 2 (ROR2), mRNA.	14	12.15	0.92	1.35E-12	1.78E-10
CD96	Homo sapiens CD96 molecule (CD96), transcript variant 2, mRNA.	15	-11.94	-2.27	2.04E-12	2.51E-10
BEX1	Homo sapiens brain expressed, X-linked 1 (BEX1), mRNA.	16	-11.88	-1.89	2.25E-12	2.60E-10
PLAUR	Homo sapiens plasminogen activator, urokinase receptor (PLAUR), transcript variant 2, mRNA.	17	11.85	1.40	2.41E-12	2.62E-10
BCAS1	Homo sapiens breast carcinoma amplified sequence 1 (BCAS1), mRNA.	18	-11.63	-2.06	3.73E-12	3.83E-10
MT2A	Homo sapiens metallothionein 2A (MT2A), mRNA.	19	11.53	1.14	4.54E-12	4.42E-10
BCAS1	Homo sapiens breast carcinoma amplified sequence 1 (BCAS1), mRNA.	20	-11.33	-1.91	6.82E-12	6.30E-10
MAG	Homo sapiens myelin associated glycoprotein (MAG), transcript variant 2, mRNA.	21	-11.27	-1.75	7.73E-12	6.80E-10
RXRG	Homo sapiens retinoid X receptor, gamma (RXRG), transcript variant 1, mRNA.	22	-11.18	-1.06	9.16E-12	7.69E-10
PPFIBP2	Homo sapiens PTPRF interacting protein, binding protein 2 (liprin beta 2) (PPFIBP2), mRNA.	23	-11.11	-1.23	1.07E-11	8.60E-10
VGF	Homo sapiens VGF nerve growth factor inducible (VGF), mRNA.	24	11.04	2.65	1.22E-11	9.38E-10
BCL6	Homo sapiens B-cell CLL/lymphoma 6 (zinc finger protein 51) (BCL6), transcript variant 1, mRNA.	25	11.00	1.30	1.34E-11	9.88E-10
KYNU	Homo sapiens kynureninase (L-kynurenine hydrolase) (KYNU), transcript variant 2, mRNA.	26.5	10.82	1.40	1.94E-11	1.32E-09
RHOU	Homo sapiens ras homolog gene family, member U (RHOU), mRNA.	26.5	-10.82	-1.43	1.92E-11	1.32E-09
PTGS1	Homo sapiens prostaglandin-endoperoxide synthase 1, transcript variant 2, mRNA.	28	-10.71	-1.78	2.42E-11	1.60E-09
MGC39900	PREDICTED: Homo sapiens hypothetical protein MGC39900 (MGC39900), mRNA.	29	10.50	1.99	3.82E-11	2.43E-09
SCARB1	Homo sapiens scavenger receptor class B, member 1 (SCARB1), mRNA.	30	-10.40	-1.07	4.66E-11	2.87E-09
PHLDA1	Homo sapiens pleckstrin homology-like domain, family A, member 1 (PHLDA1), mRNA.	31	10.33	1.65	5.47E-11	3.26E-09
DUSP23	Homo sapiens dual specificity phosphatase 23 (DUSP23), mRNA.	32	-10.24	-2.34	6.55E-11	3.78E-09
SEPT3	Homo sapiens septin 3 (SEPT3), transcript variant B, mRNA.	33	10.22	1.27	6.83E-11	3.82E-09
ACTL8	Homo sapiens actin-like 8 (ACTL8), mRNA.	34	-10.20	-0.97	7.22E-11	3.92E-09
LYPD1	Homo sapiens LY6/PLAUR domain containing 1 (LYPD1), transcript variant 2, mRNA.	35	10.17	0.92	7.62E-11	4.02E-09
SNRPN	Homo sapiens small nuclear ribonucleoprotein polypeptide N (SNRPN), transcript variant 2, mRNA.	36	-10.10	-1.05	8.87E-11	4.55E-09
CRABP1	Homo sapiens cellular retinoic acid binding protein 1 (CRABP1), mRNA.	37.5	-10.04	-1.21	1.01E-10	4.92E-09
MT1A	Homo sapiens metallothionein 1A (MT1A), mRNA.	37.5	10.04	0.95	1.01E-10	4.92E-09
STC1	Homo sapiens stanniocalcin 1 (STC1), mRNA.	39	9.89	2.70	1.40E-10	6.63E-09
KYNU	Homo sapiens kynureninase (L-kynurenine hydrolase) (KYNU), transcript variant 1, mRNA.	40.5	9.84	1.35	1.58E-10	7.13E-09
RHAG	Homo sapiens Rh-associated glycoprotein (RHAG), mRNA.	40.5	-9.84	-0.84	1.58E-10	7.13E-09
OLFML2B	Homo sapiens olfactomedin-like 2B (OLFML2B), mRNA.	42	-9.66	-1.33	2.38E-10	1.04E-08
FBXL21	Homo sapiens F-box and leucine-rich repeat protein 21 (FBXL21), mRNA.	43	9.55	1.23	3.03E-10	1.30E-08
PEG10	PREDICTED: Homo sapiens paternally expressed 10 (PEG10), mRNA.	44	-9.53	-1.38	3.16E-10	1.33E-08
TAGLN3	Homo sapiens transgelin 3 (TAGLN3), transcript variant 3, mRNA.	45	-9.51	-0.87	3.27E-10	1.34E-08
C12orf35	Homo sapiens chromosome 12 open reading frame 35 (C12orf35), mRNA.	46	9.46	0.67	3.70E-10	1.49E-08
PLP1	Homo sapiens proteolipid protein 1 (PLP1), transcript variant 2, mRNA.	47	-9.33	-0.96	4.93E-10	1.94E-08
TGFBI	Homo sapiens transforming growth factor, beta-induced, 68kDa (TGFBI), mRNA.	48	9.32	1.92	5.11E-10	1.97E-08
NOSTRIN	Homo sapiens nitric oxide synthase trafficker (NOSTRIN), transcript variant 1, mRNA.	49	-9.29	-1.02	5.38E-10	2.03E-08
RAB31	Homo sapiens RAB31, member RAS oncogene family (RAB31), mRNA.	50.5	9.25	1.46	5.95E-10	2.16E-08
XYLT1	Homo sapiens xylosyltransferase I (XYLT1), mRNA.	50.5	-9.26	-0.99	5.84E-10	2.16E-08

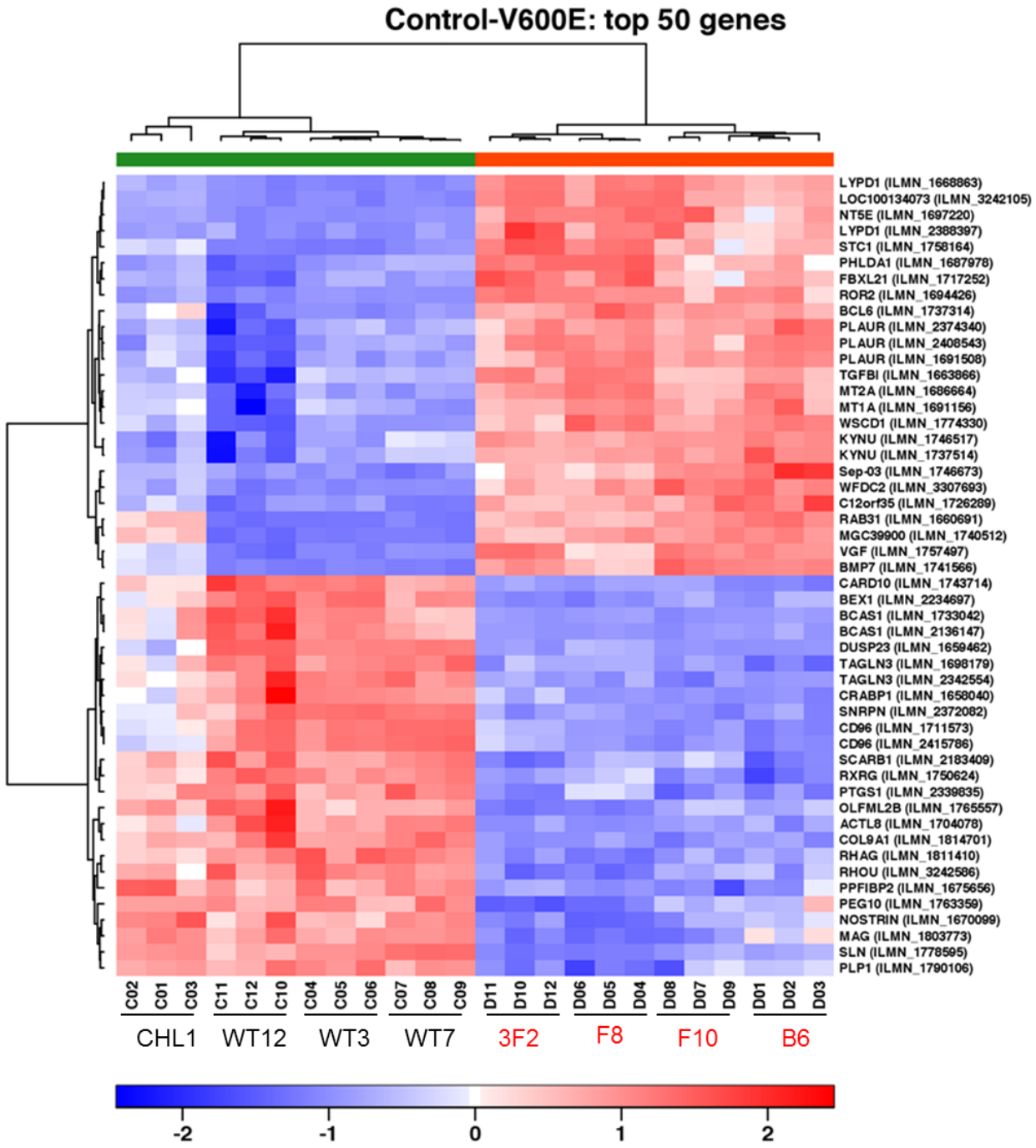


Figure 4-10: Expression heatmap of top 50 differentially expressed genes between *BRAF* WT and V600E melanoma cells.

Table 4-3: Significantly differentially expressed genes that are related to the angiogenesis pathway from PANTHER analysis.

Gene symbol	DEFINITION	RANK	t	logFC	AveExpr
NRG1	Homo sapiens neuregulin 1 (NRG1), transcript variant GGF2, mRNA.	82	-8.37	-0.91	7.89
FZD3	Homo sapiens frizzled homolog 3 (Drosophila) (FZD3), mRNA.	83	8.34	0.83	9.10
PRKCH	Homo sapiens protein kinase C, eta (PRKCH), mRNA.	117	7.93	1.15	8.95
GSK3B	Homo sapiens glycogen synthase kinase 3 beta (GSK3B), mRNA.	259	-6.64	-0.58	8.35
USP13	Homo sapiens ubiquitin specific peptidase 13 (isopeptidase T-3) (USP13), mRNA.	324	-6.18	-0.52	8.37
ARAF	Homo sapiens v-raf murine sarcoma 3611 viral oncogene homolog (ARAF), mRNA.	348	-6.00	-0.50	8.55
NCK2	Homo sapiens NCK adaptor protein 2 (NCK2), transcript variant 2, mRNA.	426.5	5.65	0.48	9.75
IRF7	Homo sapiens interferon regulatory factor 7 (IRF7), transcript variant b, mRNA.	442.5	5.58	0.47	7.53
SC4MOL	Homo sapiens sterol-C4-methyl oxidase-like (SC4MOL), transcript variant 2, mRNA.	671	-4.60	-0.59	9.05
CRYAB	Homo sapiens crystallin, alpha B (CRYAB), mRNA.	708	-4.44	-0.79	9.54
ETS1	Homo sapiens v-ets erythroblastosis virus E26 oncogene homolog 1 (avian) (ETS1), mRNA.	734.5	-4.35	-0.53	9.76
SFRP1	Homo sapiens secreted frizzled-related protein 1 (SFRP1), mRNA.	756	-4.26	-0.79	8.37
PRKCB	Homo sapiens protein kinase C, beta (PRKCB), transcript variant 1, mRNA.	759	-4.25	-0.58	7.84
ITGB1	Homo sapiens integrin, beta 1, transcript variant 1C-2, mRNA.	766	4.23	0.55	10.57
PRKCA	Homo sapiens protein kinase C, alpha (PRKCA), mRNA.	795	4.08	0.47	8.77
BBS2	Homo sapiens Bardet-Biedl syndrome 2 (BBS2), mRNA.	797	4.07	0.49	8.06
RHOC	Homo sapiens ras homolog gene family, member C (RHOC), transcript variant 2, mRNA.	799	-4.07	-0.41	10.37

Table 4-4: Significantly differentially expressed genes that are related to the VEGF pathway from PANTHER analysis.

Gene symbol	DEFINITION	RANK	t	logFC	AveExpr
PRKCH	Homo sapiens protein kinase C, eta (PRKCH), mRNA.	117	7.93	1.15	8.95
USP13	Homo sapiens ubiquitin specific peptidase 13 (isopeptidase T-3) (USP13), mRNA.	324	-6.18	-0.52	8.37
ARAF	Homo sapiens v-raf murine sarcoma 3611 viral oncogene homolog (ARAF), mRNA.	348	-6.00	-0.50	8.55
SC4MOL	Homo sapiens sterol-C4-methyl oxidase-like (SC4MOL), transcript variant 2, mRNA.	671	-4.60	-0.59	9.05
CRYAB	Homo sapiens crystallin, alpha B (CRYAB), mRNA.	708	-4.44	-0.79	9.54
ETS1	Homo sapiens v-ets erythroblastosis virus E26 oncogene homolog 1 (avian) (ETS1), mRNA.	734.5	-4.35	-0.53	9.76
PRKCB	Homo sapiens protein kinase C, beta (PRKCB), transcript variant 1, mRNA.	759	-4.25	-0.58	7.84
PRKCA	Homo sapiens protein kinase C, alpha (PRKCA), mRNA.	795	4.08	0.47	8.77

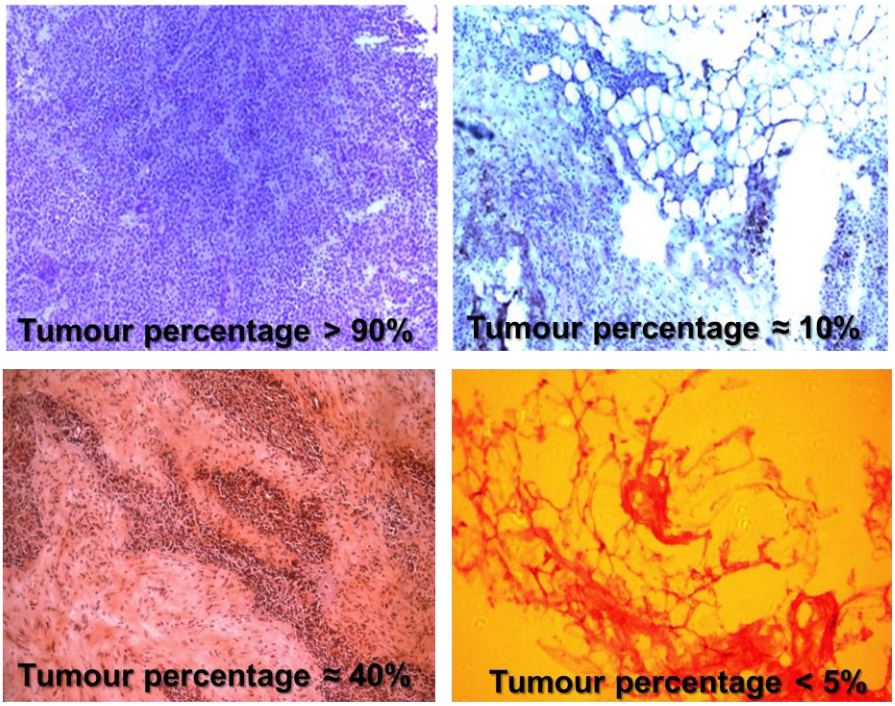
4.5.2 RNA sequencing analysis of 12 fresh frozen melanoma patient tumour samples

To investigate the clinical relevance of the genes found to be differentially expressed in CHL-1 clones, RNA sequencing analysis of clinical samples of melanoma was carried out. Fresh frozen melanoma tumour samples from treatment-naïve patients were obtained either from Oxford Biobank or the Sample Handling lab at the Oxford melanoma clinic with written patient consent and Research Ethics Committee approval (Study 07/H0606/120). Tumour samples were cryosectioned and the slides were stained with H & E to identify the tumour areas under a microscope with guidance from dermatopathologist Dr Ruth Asher (John Radcliffe Hospital, Oxford). Figure 4-11A showed variable percentages of tumour content in the patient biopsy samples. Tumour samples were macro-dissected to isolate the tumour areas before the RNA was extracted from the tumour using the QIAGEN RNeasy kit. Figure 4-11B showed that good quality RNA was extracted based on the RNA Integrity Number (RIN) using the Agilent 2100 Bioanalyser. Samples with RIN greater than 7 were sent to Oxford Gene Technology (OGT) for RNA sequencing (RNA-seq).

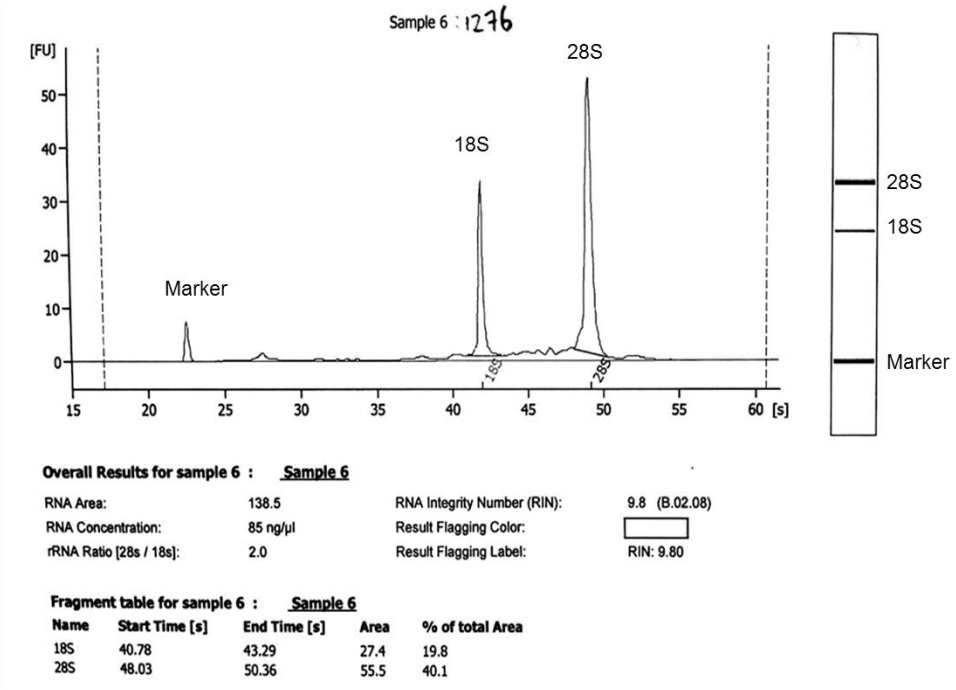
In total, 12 RNA samples from 6 *BRAF* WT and 6 *BRAF* V600E melanomas were analysed by RNA-seq. This included 4 primary skin melanomas and 8 node metastases. Of these, 3 skin samples were *BRAF* WT and one was *BRAF* V600E, and 3 node samples were *BRAF* WT and 5 were *BRAF* V600E as shown in table 4-5.

RNA-seq was carried out using the Illumina HiSeq 2000 platform from the Oxford Wellcome Trust Centre for Human Genetics via Oxford Gene Technology. For all samples Quality Control showed good alignment metrics and read quality metrics. The raw data were first pre-processed by OGT, and then further analysed by Dr Francesca Buffa and Dr Ruud Van Stiphout (Dr Francesca Buffa's group, University of Oxford). Significantly differentially expressed genes by LIMMA between the *BRAF* WT and V600E are presented in table 4-6 for skin samples and table 4-7 for the nodes.

A



B



Overall Results for sample 6 : Sample 6

RNA Area:	138.5	RNA Integrity Number (RIN):	9.8 (B.02.08)
RNA Concentration:	85 ng/µl	Result Flagging Color:	
rRNA Ratio [28s / 18s]:	2.0	Result Flagging Label:	RIN: 9.80

Fragment table for sample 6 : Sample 6

Name	Start Time [s]	End Time [s]	Area	% of total Area
18S	40.78	43.29	27.4	19.8
28S	48.03	50.36	55.5	40.1

Figure 4-11: Quality control for the tumour samples and extracted RNA.

A, H & E staining showing that the biopsies obtained contained different percentages of tumour. Tumour areas containing greater than 85% malignant cells were then macro-disected for RNA extraction. B, the electropherogram for one of the samples tested showing good quality RNA with RIN equal to 9.8. As RNA degradation proceeds, the decrease in the 18S to 28S ribosomal band ratio and the increase in the baseline signal between the two ribosomal peaks and the lower marker could then be used to detect the level of degradation in the sample. The bar presentation on the right shows no shorter fragments could be seen between the marker, 18S and 28S bands, indicating that almost no degradation could be detected in the sample.

Table 4-5: fresh frozen patient melanomas for RNA sequencing.

Genotype	SKIN	Nodes
BRAF WT	3	3
BRAF V600E	1	5

Table 4-6: Significantly differentially expressed genes between *BRAF* WT and V600E primary skin melanomas.

Gene Name(s)	Locus	Samples	Status	Value 1	Value 2	Test Stat	Log2 Fold Chang	P-Value	Q-Value	Significant	ProbeID
ABCB5	7:20654829-20816658	BrafWTSkin/BrafMutantS	OK	103.195	0.919149	-4.18205	-6.81086	0.00005	0.0305447	yes	ILMN_165825
ARPP21	3:35680436-35835988	BrafWTSkin/BrafMutantS	OK	3.40379	0		#NAME?	0.00005	0.0305447	yes	ILMN_228982
CADPS	3:62384021-62861221	BrafWTSkin/BrafMutantS	OK	12.4364	0.208692	-2.20441	-5.89705	0.00005	0.0305447	yes	ILMN_166554
CD74	5:149781162-149792492	BrafWTSkin/BrafMutantS	OK	94.4885	1434.3	4.56746	3.92406	0.00005	0.0305447	yes	ILMN_173656
CDH1	16:68769027-68869513	BrafWTSkin/BrafMutantS	OK	93.1934	0.163013	-3.5077	-9.1591	0.00005	0.0305447	yes	ILMN_177094
AC011754.1, AC096753.1, CTNNA2	2:79384131-80875996	BrafWTSkin/BrafMutantS	OK	3.2878	0		#NAME?	0.00005	0.0305447	yes	ILMN_219769
CYTL1	4:5016273-5021202	BrafWTSkin/BrafMutantS	OK	14.7313	0		#NAME?	0.00005	0.0305447	yes	ILMN_220159
FMN2	1:240177647-240643504	BrafWTSkin/BrafMutantS	OK	4.18592	0		#NAME?	0.00005	0.0305447	yes	ILMN_176479
FOXR2	X:55620471-55652980	BrafWTSkin/BrafMutantS	OK	0	2.49515		Infinity	0.00005	0.0305447	yes	ILMN_171175
HLA-DRB1, HLA-DRB5, HLA-DRB6	6:32485119-32557654	BrafWTSkin/BrafMutantS	OK	11.7633	454.043	5.52092	5.27047	0.00005	0.0305447	yes	ILMN_322868
RAPGEF4	2:173541868-173917704	BrafWTSkin/BrafMutantS	OK	27.0613	1.05428	-2.36441	-4.6819	0.00005	0.0305447	yes	ILMN_166180
KRT14	17:39738530-39743173	BrafWTSkin/BrafMutantS	OK	51.4762	0		#NAME?	0.00005	0.0305447	yes	-
NUDT10	X:51075082-51080377	BrafWTSkin/BrafMutantS	OK	3.4874	0		#NAME?	0.00005	0.0305447	yes	-

Table 4-7: Significantly differentially expressed genes between *BRAF* WT and V600E melanoma lymph node metastases.

Gene Name(s)	Locus	Samples	Status	Value 1	Value 2	Test Stat	Log2 Fold Chang	P-Value	Q-Value	Significant
ANXA1	9:75766672-75785309	BrafWTNode/BrafMutantN	OK	34.1863	215.316	2.30059	2.65496	0.00005	0.0128534	yes
ANXA3	4:79472672-79531597	BrafWTNode/BrafMutantN	OK	0.609133	19.7306	1.99246	5.01754	0.0002	0.0415982	yes
APOD	3:195295572-195311076	BrafWTNode/BrafMutantN	OK	50.9415	1545.69	3.8208	4.92327	0.00005	0.0128534	yes
CSGALNACT1	8:19260601-19615540	BrafWTNode/BrafMutantN	OK	4.91516	42.8839	1.78259	3.12512	0.00005	0.0128534	yes
DUSP5	10:112257595-11227585	BrafWTNode/BrafMutantN	OK	3.93302	33.4514	2.3149	3.08836	0.00005	0.0128534	yes
ELOVL2	6:10980991-11079351	BrafWTNode/BrafMutantN	OK	5.24124	30.8757	2.1116	2.55849	0.0002	0.0415982	yes
HAS2	8:122624355-122657651	BrafWTNode/BrafMutantN	OK	30.8338	0.908579	-3.02357	-5.08476	0.00005	0.0128534	yes
ITGA10, RP11-315I20.3	1:145524842-145544204	BrafWTNode/BrafMutantN	OK	1.22529	42.97	2.18849	5.13214	0.00005	0.0128534	yes
KCNN4	19:44270684-44287263	BrafWTNode/BrafMutantN	OK	2.86107	71.5166	2.13114	4.64365	0.0001	0.0233459	yes
MRGPRX3, MRGPRX4	11:18142501-18211168	BrafWTNode/BrafMutantN	OK	0.914727	109.219	2.86386	6.89967	0.00005	0.0128534	yes
MT2A	16:56642110-56643409	BrafWTNode/BrafMutantN	OK	144.725	674.434	2.70725	2.22036	0.00005	0.0128534	yes
OLFM1	9:137967267-138013028	BrafWTNode/BrafMutantN	OK	18.5898	1.33011	-2.00243	-3.8049	0.00025	0.0488868	yes
OR7A5, OR7C1	19:14899873-14946188	BrafWTNode/BrafMutantN	OK	0.0562322	8.84943	1.3417	7.29805	0.00005	0.0128534	yes
PLA1A	3:119316688-119348661	BrafWTNode/BrafMutantN	OK	3.35463	46.9323	2.21623	3.80636	0.0001	0.0233459	yes
PRDM7	16:90122973-90158620	BrafWTNode/BrafMutantN	OK	47.9688	1.29493	-2.43744	-5.21115	0.00005	0.0128534	yes
RNASE1	14:21269386-21271437	BrafWTNode/BrafMutantN	OK	35.8728	337.545	2.49927	3.23411	0.00005	0.0128534	yes
S100A16	1:153579361-153585644	BrafWTNode/BrafMutantN	OK	16.9804	108.202	2.11657	2.67179	0.0002	0.0415982	yes
S100A4	1:153516088-153525030	BrafWTNode/BrafMutantN	OK	55.8032	691.3	3.96617	3.63089	0.00005	0.0128534	yes
S100A6	1:153504331-153508720	BrafWTNode/BrafMutantN	OK	169.775	809.452	2.09137	2.25332	0.00025	0.0488868	yes
SEMA3B, U73166.2	3:50297734-50314977	BrafWTNode/BrafMutantN	OK	3.22403	45.6114	2.6212	3.82246	0.00005	0.0128534	yes
SEMA6B	19:4542530-4581855	BrafWTNode/BrafMutantN	OK	1.71616	45.8049	2.82257	4.73824	0.00005	0.0128534	yes
SERPINA3, SERPINA4, SERPIN	14:95027427-95090983	BrafWTNode/BrafMutantN	OK	23.099	410.796	2.43222	4.15252	0.00005	0.0128534	yes
SPP1	4:88896818-88904566	BrafWTNode/BrafMutantN	OK	50.4454	400.695	2.21695	2.98971	0.00005	0.0128534	yes
TESC	12:117476696-11753728	BrafWTNode/BrafMutantN	OK	1.15916	13.5913	1.89079	3.55153	0.0001	0.0233459	yes
AC010170.1, TMEM158	3:45265877-45267809	BrafWTNode/BrafMutantN	OK	3.8995	54.6853	3.72342	3.80979	0.00015	0.0323759	yes
TRPM8	2:234826042-234928167	BrafWTNode/BrafMutantN	OK	0.305586	32.0056	2.2028	6.7106	0.00005	0.0128534	yes
UCHL1	4:41222090-41270472	BrafWTNode/BrafMutantN	OK	43.4694	1.93916	-1.95001	-4.48649	0.00025	0.0488868	yes
C3orf67	3:58702137-59035810	BrafWTNode/BrafMutantN	OK	0.879906	15.0224	1.55749	4.09362	0.0001	0.0233459	yes
CDR1	X:139865424-139866723	BrafWTNode/BrafMutantN	OK	85.0732	7.75994	-2.27176	-3.45459	0.00015	0.0323759	yes
NPR1, RP11-354A16.2	1:153651112-153666636	BrafWTNode/BrafMutantN	OK	1.23751	42.8348	2.21422	5.11327	0.0001	0.0233459	yes
PCDH11X	X:91034259-91878229	BrafWTNode/BrafMutantN	OK	0.899763	0.025783	-1.56557	-5.12505	0.00005	0.0128534	yes
SOX1	13:112721912-11272602	BrafWTNode/BrafMutantN	OK	0	0.489553		Infinity	0.00005	0.0128534	yes
WNK2	9:95946478-96108696	BrafWTNode/BrafMutantN	OK	5.95324	0.17787	-1.31616	-5.06478	0.00015	0.0323759	yes

4.5.3 Differential gene expression analysis between *BRAF* WT and mutant LM-MELANOMA cell lines

To obtain a third dataset for comparison of gene expression in *BRAF* WT and mutant melanomas, analysis was carried out on the expression data of a new LM-MELANOMA cell line panel established by Behren et al in the Ludwig Institute in Melbourne (Behren et al., 2013). The LM cell lines have had their mutational status determined and their transcriptomes profiled, which can be publicly accessed at ArrayExpress (http://www.ebi.ac.uk/arrayexpress/experiments/E-MTAB-1496/). These public data were used to analyse differential gene expression between *BRAF* WT and *BRAF* V600 mutated melanomas in LM cell lines. The data were analysed by Dr Ruud Van Stiphout (Dr Francesca Buffa's group, University of Oxford), including 22 *BRAF* WT and 30 *BRAF* mutant cell lines, of which 23 were V600E and 7 V600K. Three statistical methods of LIMMA, SAMR and Rank Product (RP) were applied for the analysis. The top 50 probes identified by average ranking using all three methods are presented in table 4-8.

The list of differentially expressed genes between *BRAF* WT and mutant cell lines was then compared and combined with the results generated from the CRISPR isogenic model, and the gene list from RNA-seq of the fresh frozen patient melanomas. *In vitro* experiments to validate some of these differentially expressed genes were then carried out.

Table 4-8: Top 50 probes sorted on average ranking (AvgRank) for differential expression between *BRAF* WT versus mutant melanoma cell lines. P-values are reported for all three methods LIMMA, SAMR and RP**.**

Gene symbol	Definition	LIMMA	SAMR	RP	AvgRank	ProbeID
ENPP2	ectonucleotide pyrophosphatase/phosphodiesterase 2	0.011	0.001	0.001	3.3	**ILMN_1780799**
ENPP2	ectonucleotide pyrophosphatase/phosphodiesterase 2	0.011	0.001	0.001	5.03	**ILMN_2373791**
SPP1	Osteopontin	0.071	0.001	0.001	8.38	**ILMN_2374449**
SPP1	Osteopontin	0.071	0.001	0.001	9.11	**ILMN_1651354**
CTAG2	Autoimmunogenic Cancer/Testis Antigen 2	0.071	0.001	0.001	9.44	**ILMN_2336585**
FABP7	Fatty Acid Binding Protein 7	0.075	0.001	0.001	14.15	**ILMN_1745299**
OLIG2	Oligodendrocyte transcription factor	0.071	0.001	0.002	16.83	**ILMN_1727567**
RNASE1	Ribonuclease A Family Member 1	0.071	0.001	0.001	17.02	**ILMN_2333670**
APOD	Apolipoprotein D	0.098	0.001	0.001	17.29	**ILMN_1780170**
SHISA2	Shisa Family Member 2	0.075	0.001	0.001	17.93	**ILMN_1760412**
THBS2	Thrombospondin 2	0.125	0.001	0.001	19.63	**ILMN_1678842**
TFAP2C	Transcription factor AP-2 gamma	0.071	0.001	0.001	19.63	**ILMN_2096784**
FAM43A	family with sequence similarity 43, member A	0.071	0.001	0.029	20.05	**ILMN_1706015**
RXRG	Retinoic acid receptor gamma	0.071	0.001	0.001	21.82	**ILMN_1809730**
ACSS1	Acyl-CoA Synthetase Short-Chain Family Member 1	0.071	0.001	0.032	23.99	**ILMN_1752269**
SELENBP1	Selenium-binding protein 1	0.071	0.001	0.026	24.6	**ILMN_1680652**
LPAR6	Lysophosphatidic acid receptor 6	0.071	0.001	0.015	25.33	**ILMN_1786429**
LXN	Latexin	0.094	0.001	0.001	28.82	**ILMN_1723962**
PHGDH	Phosphoglycerate Dehydrogenase	0.198	0.001	0.001	30.11	**ILMN_1704537**
SERPINA3	Serpin Family A Member 3	0.198	0.001	0.001	30.49	**ILMN_1788874**
TPM2	Tropomyosin 2	0.198	0.001	0.001	31.05	**ILMN_1757604**
RFTN2	Raftlin Family Member 2	0.098	0.001	0.001	33.2	**ILMN_1801441**
TTYH1	Tweety Family Member 1	0.075	0.001	0.011	34.54	**ILMN_1758497**
CX3CL1	C-X3-C Motif Chemokine Ligand 1	0.094	0.001	0.012	41.58	**ILMN_1654072**
ST6GAL1	Beta-galactoside alpha-2,6-sialyltransferase 1	0.135	0.001	0.001	44	**ILMN_1756501**
DPYSL4	Dihydropyrimidinase Like 4	0.124	0.001	0.004	44.57	**ILMN_1792356**
PSAT1	Phosphoserine Aminotransferase 1	0.169	0.001	0.001	45.38	**ILMN_3305273**
CTSK	Cathepsin K	0.225	0.003	0.001	45.66	**ILMN_1758895**
HEY1	Hairy/enhancer-of-split related with YRPW motif protein 1	0.094	0.001	0.053	46.98	**ILMN_2407308**
TPM2	Tropomyosin 2	0.198	0.002	0.001	52.98	**ILMN_1789196**
PSAT1	Phosphoserine Aminotransferase 1	0.198	0.001	0.001	53.97	**ILMN_1692938**
RXRG	Retinoic acid receptor gamma	0.125	0.001	0.028	54.05	**ILMN_1750624**
CXCL16	Chemokine (C-X-C motif) ligand 16	0.125	0.001	0.025	54.23	**ILMN_1728478**
TAGLN	Transgelin	0.198	0.001	0.001	54.56	**ILMN_1778668**
LOXL4	Lysyl oxidase homolog 4	0.266	0.006	0.001	55.39	**ILMN_2179083**
COL1A1	Collagen, type I, alpha 1	0.198	0.002	0.001	57.04	**ILMN_1701308**
KRT81	Keratin, type II cuticular Hb1	0.198	0.002	0.001	59.52	**ILMN_1801442**
CELSR3	Cadherin EGF LAG seven-pass G-type receptor 3	0.169	0.001	0.027	60.12	**ILMN_1691290**
PGCP	carboxypeptidase Q	0.198	0.002	0.001	61.87	**ILMN_2058795**
TYMP	Thymidine Phosphorylase	0.171	0.001	0.027	63.54	**ILMN_2109708**
SPRY4	Sprouty RTK Signaling Antagonist 4	0.185	0.001	0.011	64.89	**ILMN_2086105**
APCDD1L	Adenomatosis Polyposis Coli Down-Regulated 1 Protein-Like	0.198	0.001	0.001	65.89	**ILMN_1689431**
HEY1	Hairy/enhancer-of-split related with YRPW motif protein 1	0.198	0.001	0.002	66.49	**ILMN_1788203**
CTAG1B	Cancer/Testis Antigen 1B	0.183	0.001	0.026	67.35	**ILMN_2206413**
PAWR	Pro-Apoptotic WT1 Regulator	0.171	0.001	0.045	67.39	**ILMN_1806907**
SPANXB2	Human SPANX family member B2	0.201	0.002	0.001	69.33	**ILMN_3244876**
CTAG1B	Cancer/Testis Antigen 1B	0.198	0.001	0.003	69.41	**ILMN_1652196**
UBE2E2	Ubiquitin-conjugating enzyme E2 E2	0.198	0.001	0.002	69.45	**ILMN_1707475**
STK32B	Serine/Threonine Kinase 32B	0.182	0.001	0.031	69.81	**ILMN_2216637**
ALDH1A1	Aldehyde Dehydrogenase 1 Family Member A1	0.198	0.001	0.003	70.84	**ILMN_1709348**

4.5.4 Validating the differentially expressed genes between *BRAF* WT and V600E melanoma cells

The differentially expressed genes between *BRAF* WT and V600E melanoma cells and tumours from the three data sets were compared. Initial analyses examined the overlap between significantly differentially expressed genes obtained from the isogenic model (680), the fresh frozen tumours (58) and the LM cell lines (80). A Venn diagram was generated to identify the genes that were common between the three data sets (figure 4-12). Out of these 818 differentially expressed genes, only one gene, S100A4 coding for S100 Calcium Binding Protein A4, was present in all three. S100A4 is a small Ca^{2+} binding protein that has previously been shown to have pro-angiogenic properties (Ambartsumian et al., 2001; Semov et al., 2005), and inhibition of S100A4 led to a decrease in tumour growth and angiogenesis in mice (Hernández et al., 2013).

Other genes in common between 2 out of the 3 datasets are shown in the Venn diagram in figure 4-12. There are 20 genes in common between the 2 cell line datasets (isogenic model and LM cell lines), and 6 in common between LM cell lines and fresh tumours. Only one gene, MT2A, coding for protein Metallothionein-2, was found in common between the isogenic model and fresh tumours. Metallothionein-2 (MT2A) is one of the isoforms of the metalloionein protein family that has an important role in zinc and copper homeostasis and in cellular defences against metals and free radicals (Si and Lang, 2018). It has been shown that down regulating MT2A inhibits cell growth by inducing cell cycle arrest (Lim et al., 2009), and the overexpression of MT2A increases the expression of MMP9 and invasion of breast cancer cells (Kim et al., 2011).

Selected genes have been validated and interrogated by DPhil student Dr Nick Coupe in our group, and this approach has become the main focus of his project. Dr Coupe's validation with qRT-PCR showed that S100A4 was not differentially expressed at mRNA level between *BRAF* WT and V600E in melanoma cell lines.

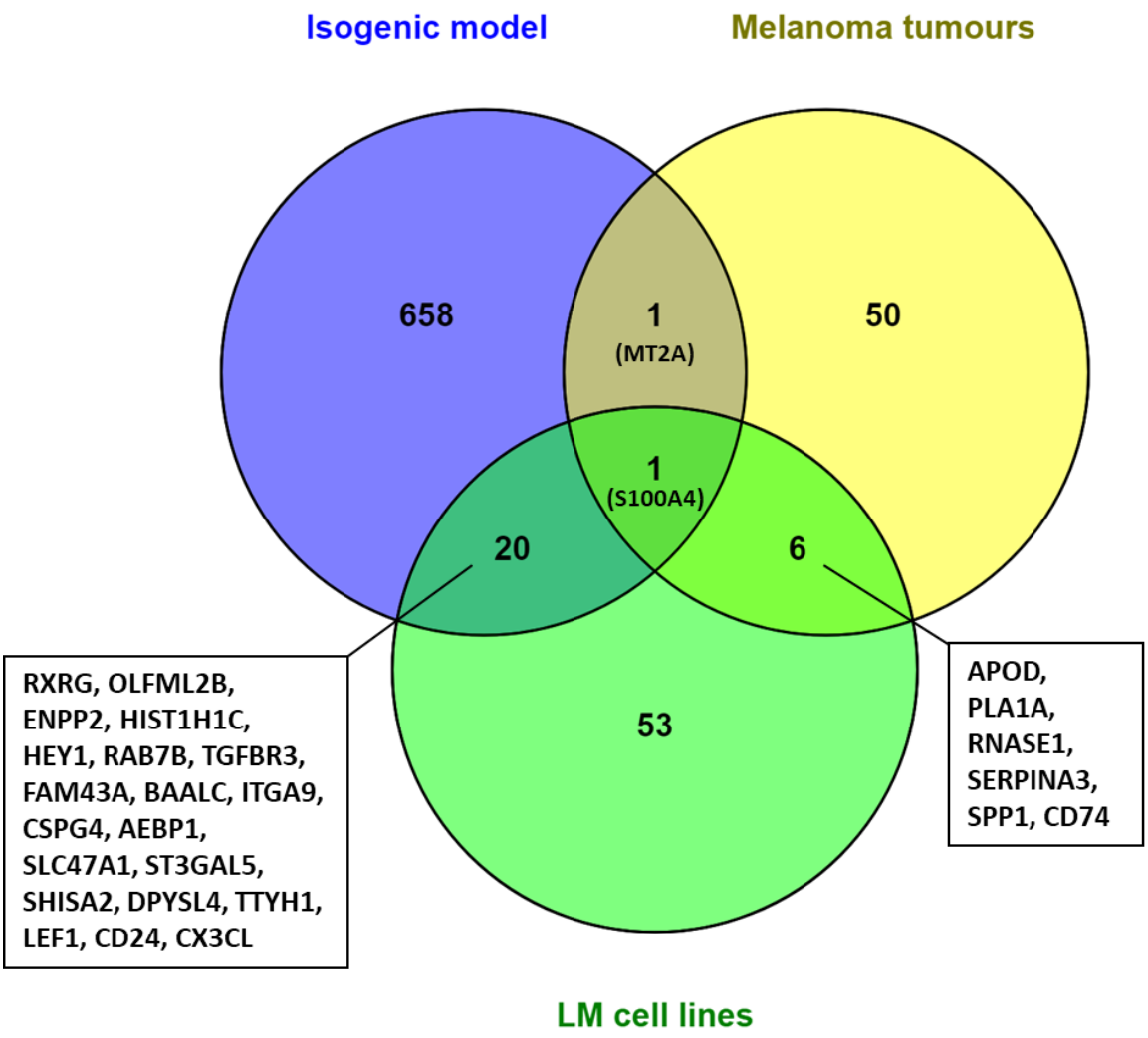


Figure 4-12: a Venn diagram of the significantly differentially expressed genes between *BRAF* WT and V600E melanomas in three data sets.

Three data sets were generated from analysis of the isogenic model (purple), 12 fresh frozen patient tumours (yellow) and the LM cell line panel established in Melbourne. The only common gene presented in all three sets is S100A4, coding for S100 calcium-binding protein A4.

Three further gene expression data sets were interrogated by Dr Coupe to refine the identification of differentially expressed genes between *BRAF* WT and V600E melanomas, with the assistance of the Oncology Department's Computational Biology and Integrative Genomics group (Dr Francesca Buffa and Ruud van Stiphout):

1. Gene expression on RNAs extracted from tumour samples taken from patients recruited to the AVAST-M trial, using the NanoString nCounter platform (performed by Genetech and analysed by Dr Francesca Buffa);
2. Gene expression of 56 Melanoma cell lines from the Cancer Cell Line Encyclopedia (CCLE; https://portals.broadinstitute.org/ccle);
3. Gene expression on patient derived melanomas from The Cancer Genome Atlas (TCGA) (Cerami et al., 2012; Gao et al., 2013).

Data were merged and SPP1 (Osteopontin) was identified as differentially expressed between *BRAF* WT and V600E melanomas in three sets (CCLE, LM-MEL cell lines from Ludwig Melbourne, and RNAseq from 12 patient tumours). Osteopontin (OPN) is a multifunctional secreted phosphoglycoprotein playing an important role in tumour progression (Rittling and Chambers, 2004). In breast cancer cell lines, OPN regulates tumor growth and angiogenesis by induction of VEGF expression through activation of Brk/NF-κB/ATF-4 pathways (Chakraborty et al., 2008). VEGF induces OPN expression in endothelial cells (Senger et al., 1996), and OPN binding to endothelial cells, through activation of PI3K/AKT and ERK1/2 pathways, further upregulates VEGF, initiating a VEGF positive feedback loop driving angiogenesis (Dai et al., 2009). Therefore, this gene was of interest in interrogating the response of *BRAF* WT vs. mutant melanomas to anti-VEGF therapy. However, Dr Coupe's validation results did not show differential expression of *OPN* at mRNA level in

melanoma cell lines, and *OPN* knockdown with siRNA did not affect transcription of either *VEGFA* or *HIF1A* in two *BRAF* V600E mutant cell lines, A375 and LM31. Validation at the protein level was not successful due to lack of a specific antibody.

Analysis of TCGA, AVAST-M and the isogenic cell line data sets identified a second gene of interest, *ROR2* (Receptor Tyrosine Kinase Like Orphan Receptor 2), which functions in Wnt signalling. ROR2 is signalling receptor that binds several of the Wnt ligands, including Wnt5a and Wnt3a to activate a combination of noncanonical and canonical Wnt signalling pathways (Green et al., 2008). ROR2 is upregulated in a number of tumour types including renal cell carcinoma (Wright et al., 2009), prostate carcinoma (Yamamoto et al., 2010), colorectal cancer (Mei et al., 2014), and melanoma (O'Connell et al., 2010). ROR2 mediates Wnt5A-induced invasion and is upregulated predominatly in metastatic melanoma (O'Connell et al., 2010). Dr Coupe's validation using the isogenic model showed that ROR2 is upregulated in the V600E clones compared with *BRAF* WT clones at the mRNA and protein level (figure 4-13A and B). ROR2 knockdown with siRNA significantly inhibited the cell growth (figure 4-13D), and also reduced VEGFA secretion in BRAF V600E melanoma cells (figure 4-13E), although there was no effect on *VEGFA* expression at mRNA level in melanoma cells (data not shown).

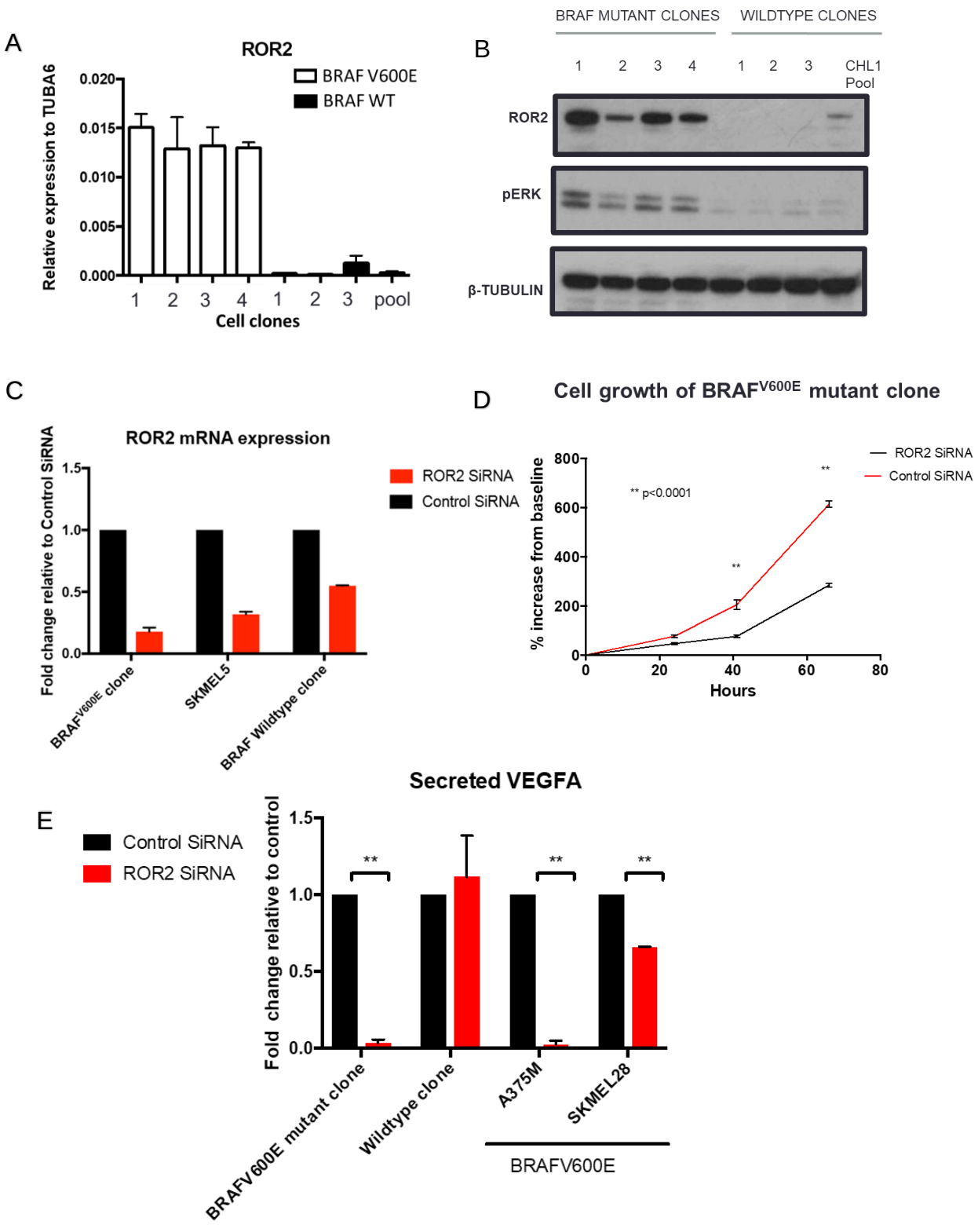


Figure 4-13: ROR2 is upregulated in *BRAF* V600E mutant melanoma cells and influences cell growth and VEGF secretion.

A, ROR2 expression at mRNA level was higher in *BRAF* V600E clones, compared to the WT group. B, levels of ROR2 protein were higher in *BRAF* V600E clones, compared to the WT group. C, *ROR2* expression at mRNA level showing ROR2 knockdown using siRNA in two *BRAF* V600E cell lines. D, Cell growth was significantly inhibited in ROR2 depleted cells, compared to the control siRNA transfectants. **E**, Levels of secreted VEGFA protein were significantly reduced with ROR2 depletion in *BRAF* V600E cells, compared to the WT clones. These experiments were performed on isogenic *BRAF* WT vs. V600E clones by Dr Nick Coupe.

4.6 Discussion

The clinical question that was the basis for this project focused on understanding the sensitivity of *BRAF* V600E melanoma in response to VEGF inhibition. Initial experiments using melanoma cell line panels to investigate the underlying molecular basis generated conflicting results. Therefore, an isogenic *BRAF* WT/V600E cell model was produced, aiming to identify mutation-specific mechanisms in melanoma relevant to angiogenesis. The traditional expression method using a retroviral system pBabe-Puro was tested first. Although ectopic expression was created with successful infection, the viral promoter induced constitutive high-level overexpression, which did not recapitulate what occurs in human cancers. This was the probable explanation for the *BRAF* V600E-induced senescence observed in the virally transduced cells (Damsky and Bosenberg, 2017).

In addition to over-expressing *BRAF* V600E using a viral system, another gene manipulating technique that has been widely used is gene silencing or knockdown using short interfering RNA (siRNA). As its name suggests, siRNA interferes with the expression of targeted genes using complementary nucleotide sequences to degrade mRNA after transcription (Hamilton and Baulcombe, 1999). siRNA has been used to silence the *BRAF* V600E gene for studies in melanoma (Tran et al., 2008; Kumar et al., 2007), as well as in other cancer types, such as papillary thyroid cancer (Liu et al., 2007). In these studies, the level of *BRAF* V600E gene expression was reduced using siRNA, and its downstream signalling related to this change of level of expression was investigated. However, siRNA was not thought to be a suitable technique to use in this project due to several limitations. First of all, the effect of gene silencing using siRNA is transient, especially in rapid dividing cancer cells. Therefore, it is not suitable for longer term experiments such as spheroid growth or *in vivo* investigations. This

limitation may be overcome by using expression of a short hairpin RNA (shRNA) in an expression vector to target the *BRAF* V600E gene, establishing a stable gene silencing (Paddison et al., 2002). However, a second limitation of gene silencing is that it does not abolish target gene expression but only reduces it, and so can assess the changes in cells that are related to the reduction in the level of mutant *BRAF* expression, but would be a less effective way to differentiate between *BRAF* WT and V600E. Thirdly, several studies have raised concerns that the efficiency of siRNA knockdown is reduced but not completely abolished by a single nucleotide difference in sequence, as reported for WT vs mutant *KRAS* by (Acunzo et al., 2017), and by our group for human vs murine *IGF1R* (Bohula et al., 2003).

To overcome these limitations, a CRISPR/Cas9 system was then used to introduce the *BRAF* V600E mutation, which would then be expressed using the endogenous promoter. Two approaches were considered for this genetic technique. The first approach considered was to replace the *BRAF* V600E gene with WT *BRAF* in *BRAF* mutant melanoma cells. The second approach would involve knocking out the WT gene in *BRAF* WT melanoma cells and replace it with the mutant *BRAF* V600E gene to create an isogenic pair.

The first approach considered for isogenic model generation was to correct the V600E alleles to WT in *BRAF* V600E melanoma cells. Since mutant *BRAF* is a dominant driver of tumour growth and maintenance (Flemming, 2010), in order to make this approach to work, it would be necessary to totally remove all copies of the mutant gene. However, it could be very challenging to eliminate oncogenic mutant *BRAF*, considering the high heterogeneity of *BRAF* copy numbers in the melanoma cells, as demonstrated in table 4-1. For example, approximately 80% of the CHL1 cells contain 4 or more copies of the *BRAF* gene (table 4-1). Another challenge this approach could encounter involves the fact that *BRAF* mutant

melanoma cells have already transformed and developed dependency on *BRAF* V600E. Therefore, eliminating *BRAF* V600E in these cells could severely impair their viability and growth, to an extent that they might no longer survive and be suitable for experiments. However, if time had permitted, this approach of replacing *BRAF* V600E with WT could have been attempted on mutant melanoma cells to test its validity, possibly providing another valuable tool for investigating *BRAF* V600E-specific functions in these cells.

Because of these considerations, it was decided to adopt the second approach, replacing WT with V600E *BRAF*. Given that *BRAF* V600E is a dominant oncogene (Flemming, 2010), it would in theory be necessary to replace only one WT *BRAF* allele with V600E *BRAF* to induce a mutant *BRAF* phenotype. Six *BRAF* WT cell lines were tested for suitability for this approach, including *NRAS* WT cell lines CHL1, NA8, LM25 and LM44, as well as *NRAS* mutant cell lines SKMEL 2 and LM5a. *NRAS* is an important oncogene that is mutated in less than 30% of all cutaneous melanomas (Hodis et al., 2012), and the major *NRAS* and *BRAF* mutations have been found to be mutually exclusive, suggesting that either can be sufficient for constitutive activation of the MAPK pathway (Ranzani et al., 2015). Therefore, it was thought preferable not to use either of the *NRAS* mutant cell lines, despite them being *BRAF* WT. Of the WT *BRAF*/WT *NRAS* cell lines tested, LM25 and LM44 grew extremely slowly in culture, and LM25 and NA8 were refractory to transfection. Taking these considerations into account, only CHL1 showed required properties to be a host cell line for use in generating an isogenic model. It is acknowledged that it is not ideal to base all the findings on an isogenic model generated from only one *BRAF* WT cell line. Therefore, if time and resources had permitted, more *BRAF/NRAS* WT cell lines could have been tested to find additional candidates in which to generate the isogenic model.

An important concern arising from this second approach was that since the WT *BRAF* CHL1 cell line had already transformed into malignant melanoma independently of *BRAF* mutation, introduction of *BRAF* V600E might not be able to reactivate MAPK signalling, inducing pathway dependence in these cells. Therefore, it was important to check not only that the mutation had been introduced, but that it had the predicted effect. Results in figure 4-6A showed that after successfully introducing the V600E mutation, greater activation of the MAPK pathway could be observed in the mutant clones compared to the WT clones. Sensitivity to the selective BRAF inhibitor PLX4720 was shown, with inhibition of MEK-ERK and 2D (figure 4-6) and 3D growth (figure 4-7), further confirming that the CRISPR clones exhibited a *BRAF* V600E phenotype.

Although there was no significant difference between the *BRAF* WT and V600E clones in 2D growth and doubling time, the spheroid assay showed that the V600E clones increased in size more rapidly in 3D growth compared to the WT, indicating a more aggressive phenotype that might be related to the microenvironment in the spheroids. To our knowledge, this differential effect on 3D growth has not been shown previously.

To investigate the molecular basis of this differential growth between *BRAF* WT and V600E cells, and to identify other differentially expressed genes that might have led to the sensitivity of *BRAF* V600E melanomas to anti-angiogenic therapy, gene expression array analysis on the CRISPR isogenic clones was then performed. In addition to the expression microarray on the isogenic model, 4 additional sets of differentially expressed genes were also identified between the *BRAF* WT and V600E melanoma cells. These include the analyses from 12 fresh frozen patient tumours samples, 52 LM melanoma cell lines in Ludwig Melbourne,

patient derived samples from TCGA and tumour samples from the AVAST-M trial. Although genes related to angiogenesis were identified in these comparisons, VEGF itself was not identified as differentially expressed. If time had permitted, validation experiments would have been carried out to investigate the significance of some of these genes. However, Dr Coupe's subsequent validation of the differentially expressed genes has identified ROR2 in the Wnt pathway as a gene of particular interest. The results of his ROR2 knockdown experiments suggested that ROR2 regulates VEGFA expression at post-transcriptional level, indicating a possible mechanism for the link between *BRAF* V600E mutation and higher VEGF protein level in *BRAF* V600E melanomas.

Chapter 5: Testing effect of the introduced *BRAF* V600E mutation to anti-angiogenic therapy *in vitro* and *in vivo*

5.1 Introduction

The finding of the AVAST-M trial that led to this project indicated sensitivity of melanoma patients with *BRAF* V600E mutated melanomas to VEGF inhibition by bevacizumab. To understand the molecular basis behind this sensitivity, an isogenic *BRAF* WT/V600E melanoma model was generated. Results in chapter 4 have shown that the CRISPR *BRAF* V600E clones expressed the mutant form of *BRAF*, were sensitive to the selective BRAF inhibitor and grew faster in 3D than *BRAF* WT cells, recapitulating an oncogenic *BRAF* phenotype. Therefore, experiments in this chapter aimed to further characterise this isogenic model and test their responses to anti-angiogenic therapy.

After the isogenic clones had been characterised *in vitro*, these melanoma cells would then be implanted subcutaneously into immunosuppressed mice to form xenografts. This would allow human melanoma cells to directly establish interactions with stromal components including lymphatic and blood vessels to study tumour growth, microenvironment and bevacizumab response *in vivo*.

5.2 Effects of inhibiting VEGF on growth of *BRAF* V600E clones

To test the effects of inhibiting VEGF signalling on the CRISPR clones, the levels of VEGFR expression were first quantified by qRT-PCR and Flow Cytometry (FACS). Results of qRT-PCR showed that VEGFR2 was expressed at the transcriptional level at much higher levels in two of the 4 mutant clones compared to the WT clones (figure 5-1A). To further investigate VEGFR expression at the protein level in these cells, FACS was then performed by Dr Esther Bridges (Professor Adrian Harris's Group, University of Oxford). Results in figure 5-1B showed the proportion of cells expressing VEGFR2 was higher in *BRAF* V600E clones, compared to the *BRAF* WT cells. This difference in levels of VEGFR2 expression between the *BRAF* WT and V600E clones suggests a possibility of differential activation in the VEGF signalling pathway associated with *BRAF* status in these cells.

To further explore this possibility, viability assays testing the direct effect of inhibiting autocrine VEGF signalling was then performed. Results in figure 5-2A showed that VEGF inhibition by bevacizumab did not affect 2D cell growth in either *BRAF* WT or V600E melanoma cells tested. Results of experiments using the VEGFR inhibitor cediranib (AZD2171) to block VEGF signalling also failed to show growth inhibition (figure 5-2B), although it did inhibit growth of HUVECs, used as a control to check that the cediranib was active. These results are consistent with the findings from similar experiments performed on non-isogenic cell lines in chapter 3 (figure 3-2).

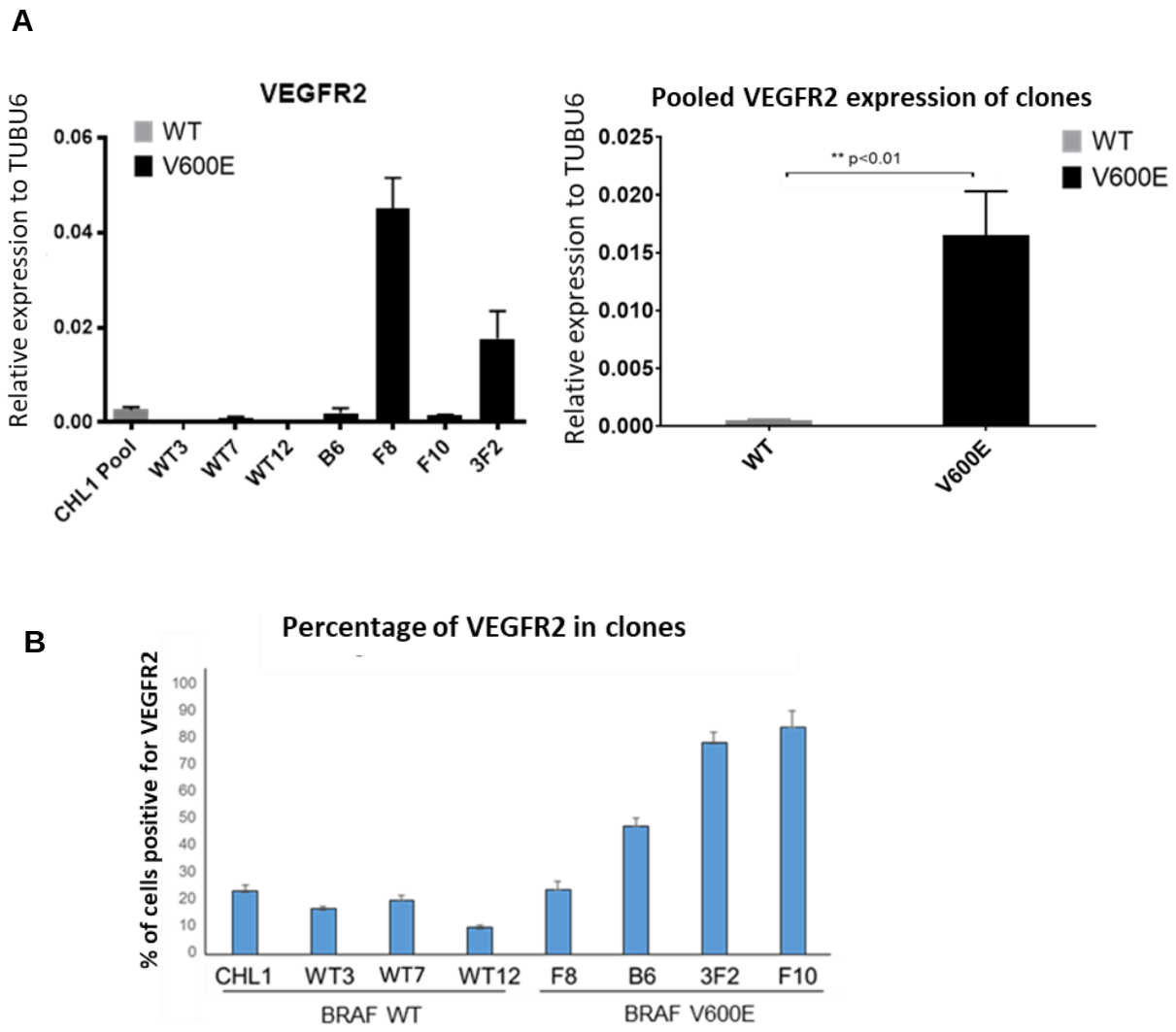
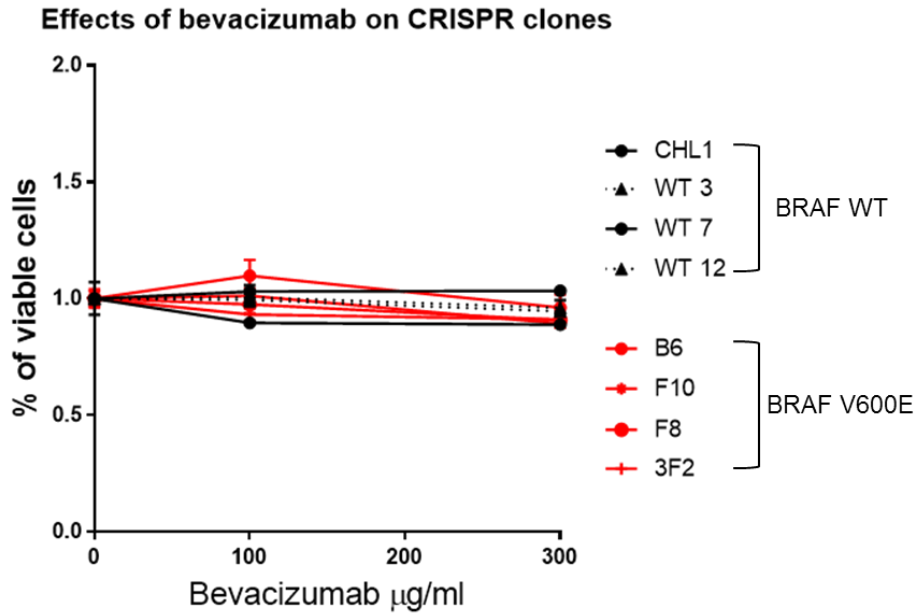


Figure 5-1: VEGFR expression in *BRAF* WT and V600E clones.

A, VEGFR2 mRNA expression in cell clones. Y-axis represents the relative expression, normalised by the expression of the housekeeping gene β-2-microglobulin. Significantly higher levels of VEGFR2 were expressed in the mutant cell clones, however, variation could be seen in the V600E clones. (n=6, **p<0.01 by unpaired t-test). B, Proportion of cells positive for total VEGFR2 expression. Higher levels of VEGFR2 expression could be observed in the mutant group, compared to the levels in the WT cell clones. n=3 independent samples; error bars are mean ± SEM.

A



B

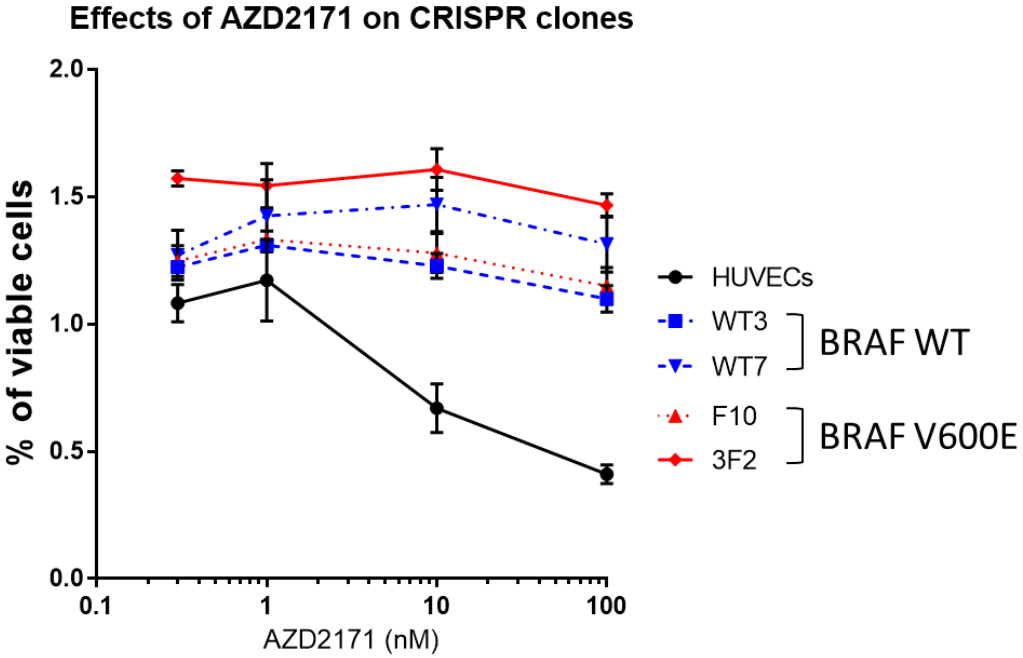


Figure 5-2: the effects of VEGF inhibition on the growth of clones.

A, effects of bevacizumab on 2D growth in viability assay. No inhibition of growth was observed with treatment of bevacizumab (100 or 300 µg/ml) n=3 technical replicates. Repeated experiment produced similar results. B, effects of VEGFR inhibitor AZD2171 on the growth in viability assay. Cells were treated with increasing concentrations of AZD2171 (0.1, 1, 10 or 100 nM) and no inhibition of growth was observed (n=3). Experiment was repeated twice and similar results were produced. HUVEC cells were used as a positive control for growth inhibition by AZD2171. Error bars are mean ± SEM.

5.3 VEGF expression in CRISPR *BRAF* V600E and WT clones

The initial experiments using the first panel of melanoma cell lines had shown that the levels of intracellular and secreted VEGF were higher in the *BRAF* V600E cell lines, compared to *BRAF* WT cells (figure 3-5). However, when the cell panel was expanded with newly established LM melanoma cell lines, the same phenotype could not be observed. This discrepancy was one of the factors that prompted the generation of the isogenic model.

To investigate whether differential VEGF expression between *BRAF* WT and V600E cells could be seen in the isogenic clones, the expression of VEGF and its regulator HIF1α at mRNA level was assessed first with qRT-PCR. Results in figure 5-3A showed that while the expression of HIF1α was significantly higher in V600E clones compared to the WT cells, there was no difference in VEGF expression at the transcriptional level between these two groups (figure 5-3B).

Human VEGF ELISA was then performed on the clones to quantify the VEGF expression at the protein level. Results in figure 5-4 showed that at the intracellular as well as the secreted level, VEGF protein was present at significantly higher levels in the *BRAF* V600E clones (although with marked variation in secreted levels) than in the WT cells.

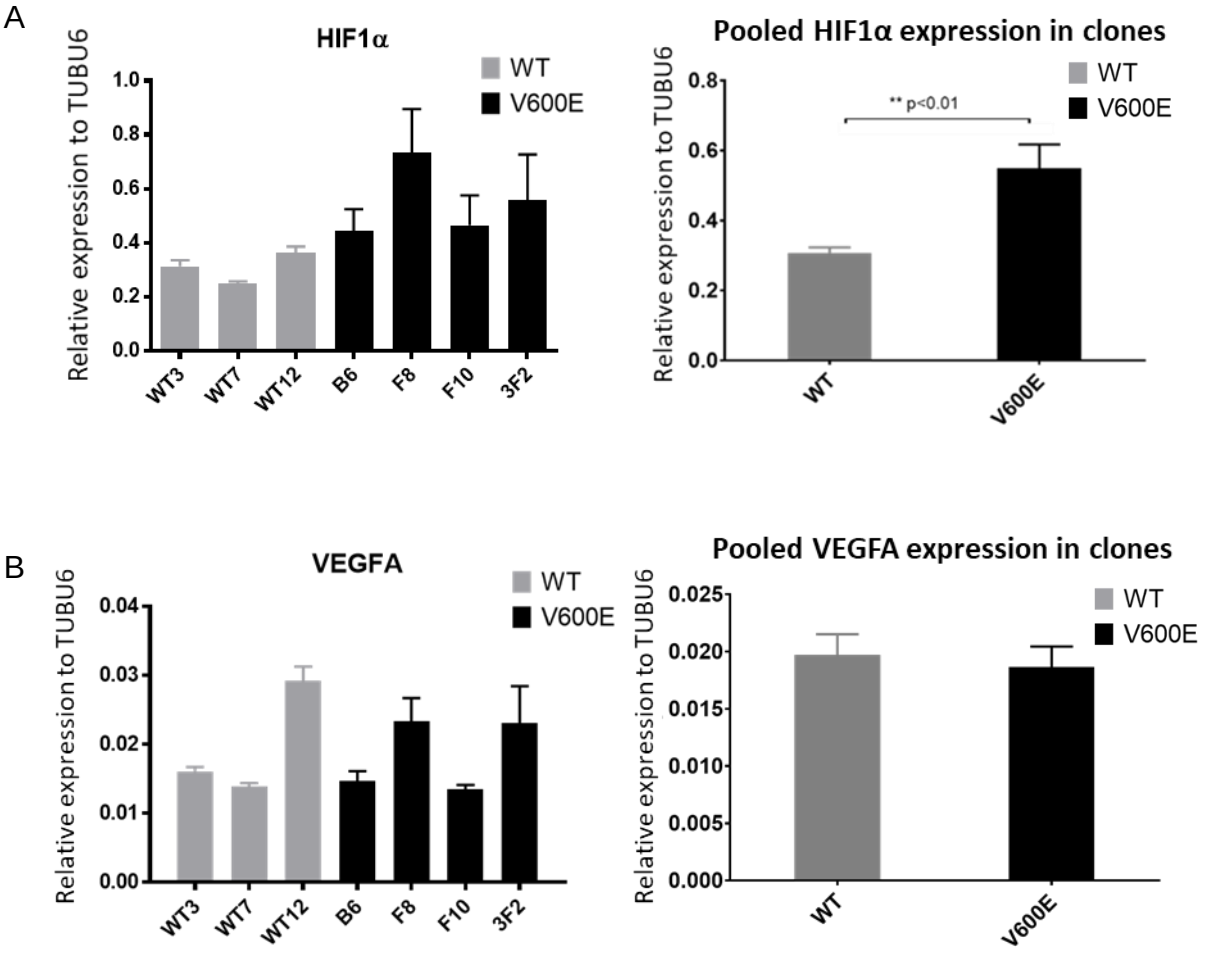


Figure 5-3: RNA expression of HIF1α and VEGF in the CRISPR cell clones.

A, HIF1α mRNA expression in clones. Significantly higher levels of HIF1α were expressed in the mutant cell clones. (n=3 independent samples, **p<0.01 by unpaired t-test). B, VEGF mRNA expression in clones. No difference in VEGF expression was observed between the WT and V600E cells. n=3 independent samples. Y-axis represents the relative expression, normalised by the expression of the housekeeping gene β-2-microglobulin. Error bars are mean ± SEM.

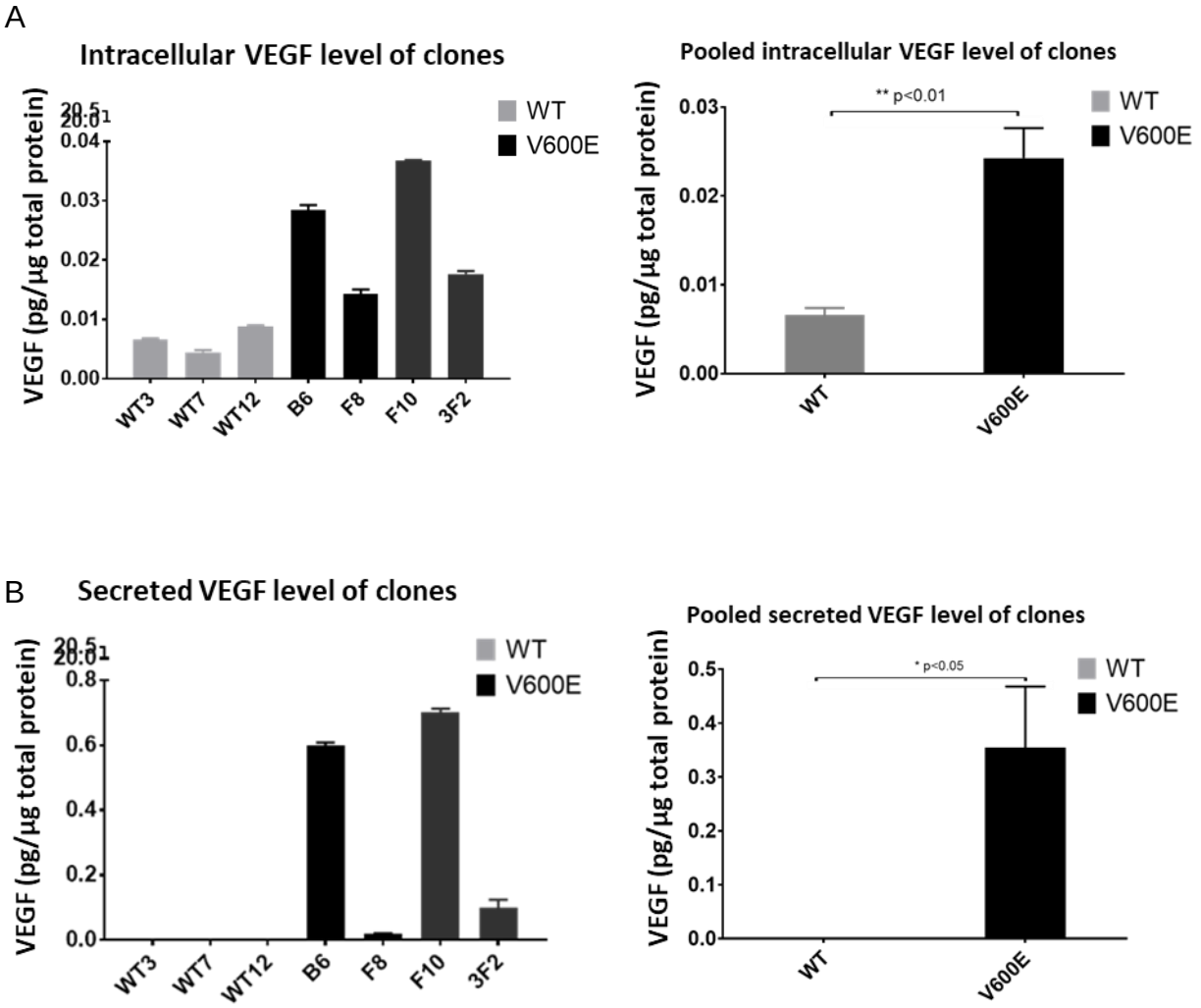


Figure 5-4: Human VEGF ELISA in CRISPR clones.

A, levels of intracellular VEGF quantified by human VEGF ELISA. VEGF ELISA was performed on cell lysates and levels of VEGF were presented as mean ± SEM pg/µg total protein. At the intracellular level, VEGF protein was significantly higher in the V600E cells, compared to the levels in the WT group. (n=3 independent samples, **p<0.01 by unpaired t-test) B,Secreted VEGF in conditioned medium collected at 48 hours. The corresponding cells were lysed and their total protein was quantified with BCA protein assay. The levels of VEGF for each cell clone were then presented as mean ± SEM pg/µg total protein. Similar to the intracellular results, the levels of secreted VEGF protein were significantly higher in the V600E group, compared to the levels in the WT cells. Within the BRAF V600E group, B6 and F10 cells secreted much higher level of VEGF than the other two V600E clones F8 and 3F2. (n=3 independent samples, *p<0.05 by unpaired t-test).

5.4 Testing response of isogenic *BRAF* WT/V600E xenografts to anti-angiogenic therapy *in vivo*

5.4.1 Growth of isogenic *BRAF* WT and V600E melanoma clones as xenografts treated with bevacizumab

Four clones, *BRAF* WT clones WT3 and WT7, and *BRAF* V600E clones F10 and 3F2 were used for *in vivo* study. Animal experiments were conducted under the project licence PPL 30 /3197, by Dr Esther Bridges from Hypoxia and Angiogenesis Group in Department of Oncology of University of Oxford. Cells were harvested, washed in PBS, mixed 1:2 with matrigel before they were injected subcutaneously into CD1 nude mice. These mice were developed from the transfer of the nude gene from Crl:NU-Foxn1nu to CD-1® mice through a series of crosses and backcrosses beginning in 1979 at Charles River Laboratories (Charles River, Strain code#: 086). Since they lack a thymus and are unable to produce T-cells, they are immunodeficient, and therefore are less prone to reject human cancer cell xenografts (Szadvari et al., 2016).

When WT7 and 3F2 tumours in mice had reached approximately 150 mm^3 in size (calculated from the formula 1/6 x π x L x W x H, length [L], width [W], and height [H] of each tumour), they were randomised into 5 mice per group and one group injected with vehicle control (PBS) and the other group injected with bevacizumab intraperitoneally three times a week. When tumours had reached endpoint (1.44 cm^3) permitted by the Home Office license, pimonidazole and Hoechst 33342/tomato lectin mixed solution, were injected intravenously

90 minutes and 2 minutes before sacrifice of mice. Blood, tumour and organs were collected for histological evaluation.

This experiment started by inoculating 10 mice each with cells from the 4 clones (WT clones WT3 and WT7, and V600E clones F10 and 3F2), however, the mice bearing F10 (BRAF V600E) xenografts had to be sacrificed before the scheduled bevacizumab treatment could be introduced, due to rapid tumour growth. These tumours appeared to be highly vascular when harvested. Mice in one of the *BRAF* WT control groups (WT3) were also culled at the same time for comparison purposes. Results of analysis of these tumours is shown in section 5.4.2.

Results in figure 5-5A showed that in *BRAF* V600E xenografts, the tumour growth rate was significantly lower with the bevacizumab treatment, compared to the untreated group, after day 27 until the endpoint for the untreated group on day 36. However, this inhibition in tumour growth with bevacizumab treatment could not be observed in *BRAF* WT xenografts (figure 5-5B), indicating a differential sensitivity of BRAF V600E melanoma cells to human VEGF inhibition, compared to *BRAF* WT.

Results in figure 5-5C showed a trend to more rapid tumour growth rate in *BRAF* V600E (3F2), compared to *BRAF* WT (WT7). However, this difference in growth was not statistically significant. Survival data in figure 5-5D showed that bevacizumab prolonged survival for both *BRAF* WT and V600E groups, however, the separation between treated and untreated groups was greater for *BRAF* V600E, compared to *BRAF* WT.

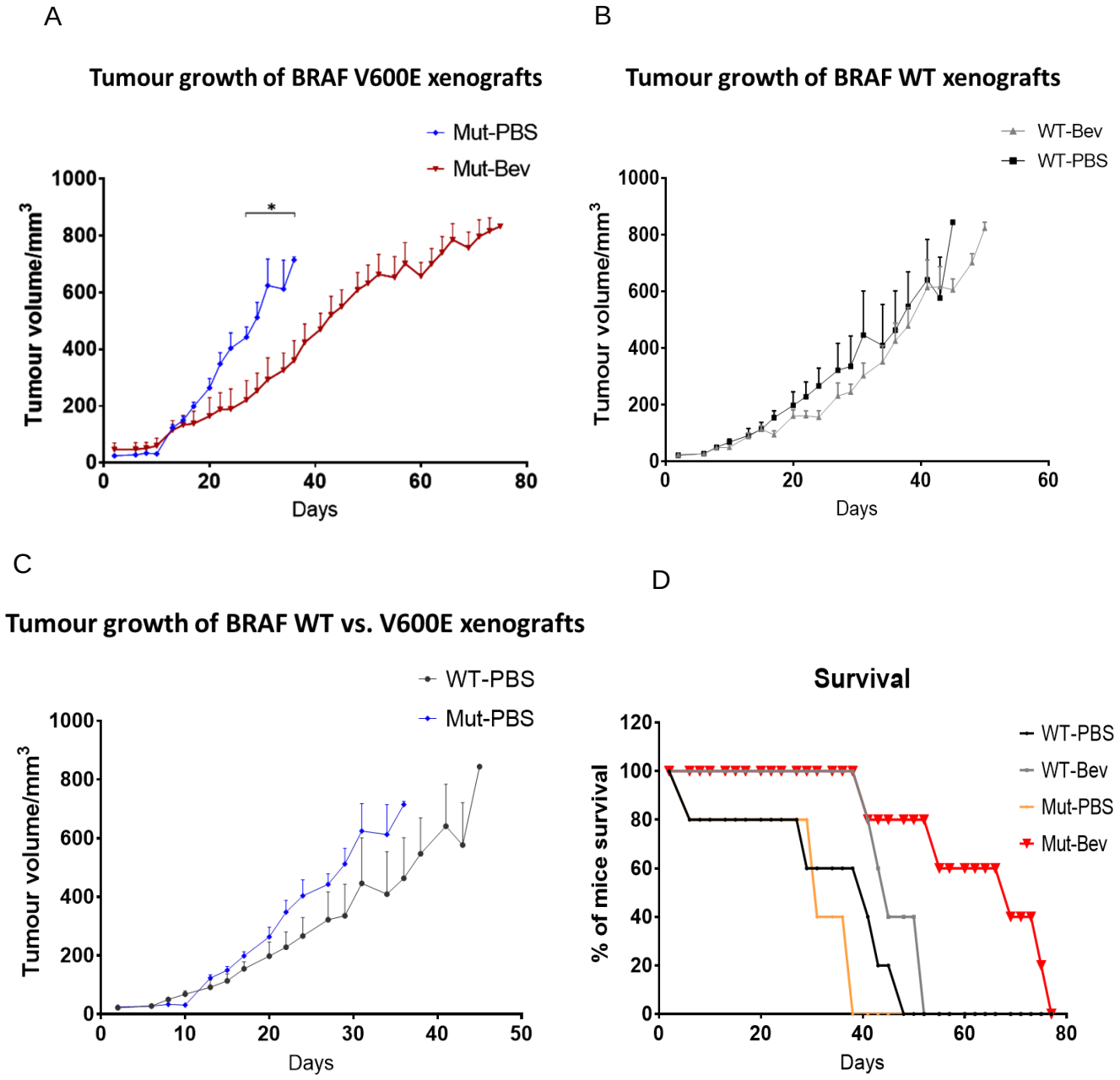


Figure 5-5: Tumour growth response to bevacizumab and survival of CD1 nude mice bearing *BRAF* WT (WT7) and V600E (3F2) xenografts.

A, tumour growth was significantly inhibited with bevacizumab treatment in *BRAF* V600E mice from day 27 (from day 27 to 36: *p<0.05). Bevacizumab was given (10mg/kg) intraperitoneally three times a week. Bevacizumab treatment group=red; untreated group=blue. B, No inhibition could be observed in *BRAF* WT xenografts with bevacizumab treatment. Treatment group=grey; untreated=black. C, No significant difference in tumour growth between *BRAF* WT and V600E untreated groups. Points in A, B and C represent mean ± SEM tumour size. n=5 mice per group. D, Bevacizumab prolonged survival in *BRAF* V600E mice, but not BRAF WT mice.

5.4.2 Immunohistochemical analysis of WT3 vs. F10 xenografts without bevacizumab treatment

Mice bearing F10 *BRAF* V600E xenografts were sacrificed 12 days after tumour cell inoculation due to aggressive growth in these tumours. The WT3 group were sacrificed at the same time for comparison. Immunohistochemical staining was performed by Dr Esther Bridges from Hypoxia and Angiogenesis Group in Department of Oncology of University of Oxford.

Carbonic Anhydrase 9 (CA9) is a hypoxia marker that catalyses the reversible hydration of carbon dioxide to carbonic acid (Wykoff et al., 2000). Transcription of this gene is known to be regulated by the Von Hippel-Lindau (*VHL*) gene (Olive et al., 2001), and high expression of CA9 has been found in regions of tumour hypoxia in a broad range of tumour types, including melanoma (Ivanov et al., 2001). Immunohistochemical analysis showed that CA9 expression was significantly higher in the *BRAF* WT (WT3) group than *BRAF* V600E group (F10), indicating a more hypoxic condition in WT tumours (figure 5-6C). CD31 staining showed that a significantly higher blood vessel number and less necrosis in the *BRAF* V600E group than in *BRAF* WT (figure 5-6F and 5-6G). Ki67 staining (figure 5-6H and 5-6I) showed that F10 tumours had a significantly higher proliferation rate than WT3 tumours.

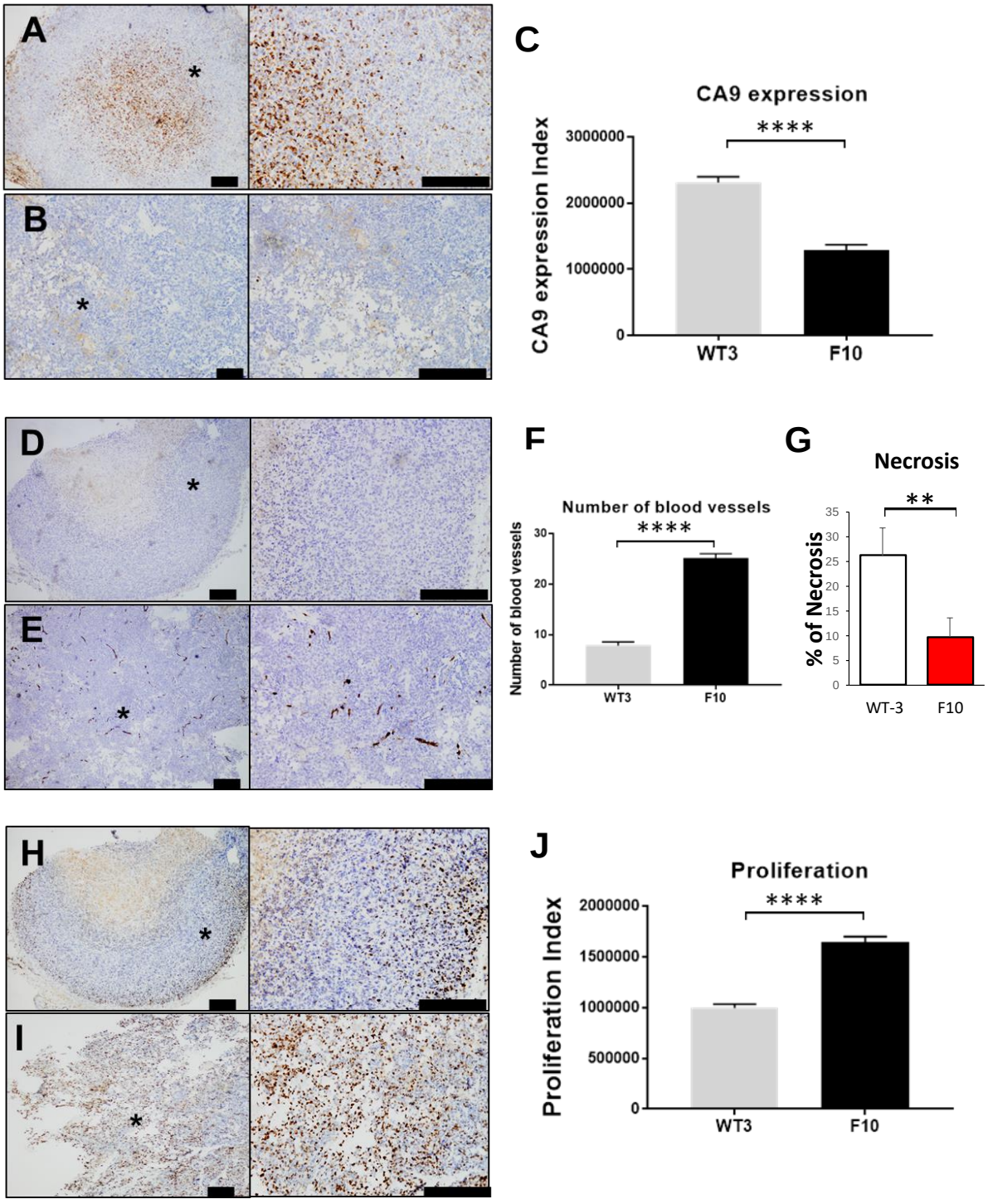


Figure 5-6: Immunohistochemical analysis of WT3 (*BRAF* WT) and F10 (*BRAF* V600E) xenografts.

Sections were stained for CA9, Ki67 and CD31. Expression of CA9, Ki67 was quantified on whole sections by ImageJ software using colour deconvolution. Scale bars represent 100 µm. Asterisks indicate the areas shown in higher magnification on the right. A and B, representative images of CA9 staining in WT3 and F10 xenografts respectively. C, CA9 expression could be seen significantly higher in WT3 than F10. **** p<0.0001 n=5. Error bars are mean ± SEM. D and E, representative images of CD31 staining in WT3 and F10 xenografts respectively. F, significantly higher number of blood vessels in WT3 tumours than in F10. **** P < 0.0001. n=5. Error bars are mean ± SEM. G, less necrosis was found in WT3 than F10 xenografts. Necrosis was quantified histologically on H&E sections, and quantified as a percentage of the necrotic area over the total area. **, P < 0.01. n=5. H and I, representative images of Ki67 staining for WT3 and F10. J, Ki67 staining showed significantly higher proliferation rate in F10 tumours than WT3. ****, P < 0.0001. n=5. Error bars are mean ± SEM.

5.4.3 Immunohistochemical analysis of WT7 vs. 3F2 xenografts treated with bevacizumab

Mice in the remaining two groups (WT7 and 3F2) were treated with PBS or bevacizumab after tumours reached approximately 150 mm^3. Figure 5-7E showed that CA9 expression was significantly higher in *BRAF* WT (WT7) than *BRAF* V600E (3F2) treatment naïve xenografts, indicating more hypoxia in WT tumours compared to V600. This is consistent with the findings in the comparison between WT3 and F10 xenografts in figure 5-6C. However, upon bevacizumab treatment, CA9 expression was reduced in WT tumours, while in V600E CA9 increased significantly.

CD31 staining of blood vessels showed that the number of blood vessels was significantly higher in the control-treated 3F2 V600E tumours than control-treated WT7 (figure5-8E). Bevacizumab treatment increased the vessel numbers in WT7 tumours, while in the mutant 3F2 tumours the number of vessels were reduced by the drug treatment (figure5-8E). Necrosis was quantified histologically on the hematoxylin-stained sections where necrotic areas were selected using image J and results presented as a percentage of necrosis in the total tumour area. Figure 5-8F showed that the percentage of necrotic areas was significantly higher in the control-treated WT7 group than control-treated 3F2 tumours. Necrosis was reduced by bevacizumab in the WT7 tumours, however, in the mutant 3F2 tumours, bevacizumab increased necrosis.

Expression of Ki67 was quantified on whole sections using ImageJ software and colour deconvolution method. There was a trend to higher Ki67 expression in control-treated 3F2 tumours than WT7 controls, suggesting greater proliferation in these tumours (figure 5-9E). The proliferation index was not affected by bevacizumab in WT7 tumours, while there was a

trend to reduced proliferation in the mutant 3F2 group after bevacizumab treatment (figure 5-9E). However, the difference in proliferation with bevacizumab treatment was not significant in either the WT or mutant group (figure 5-9E).

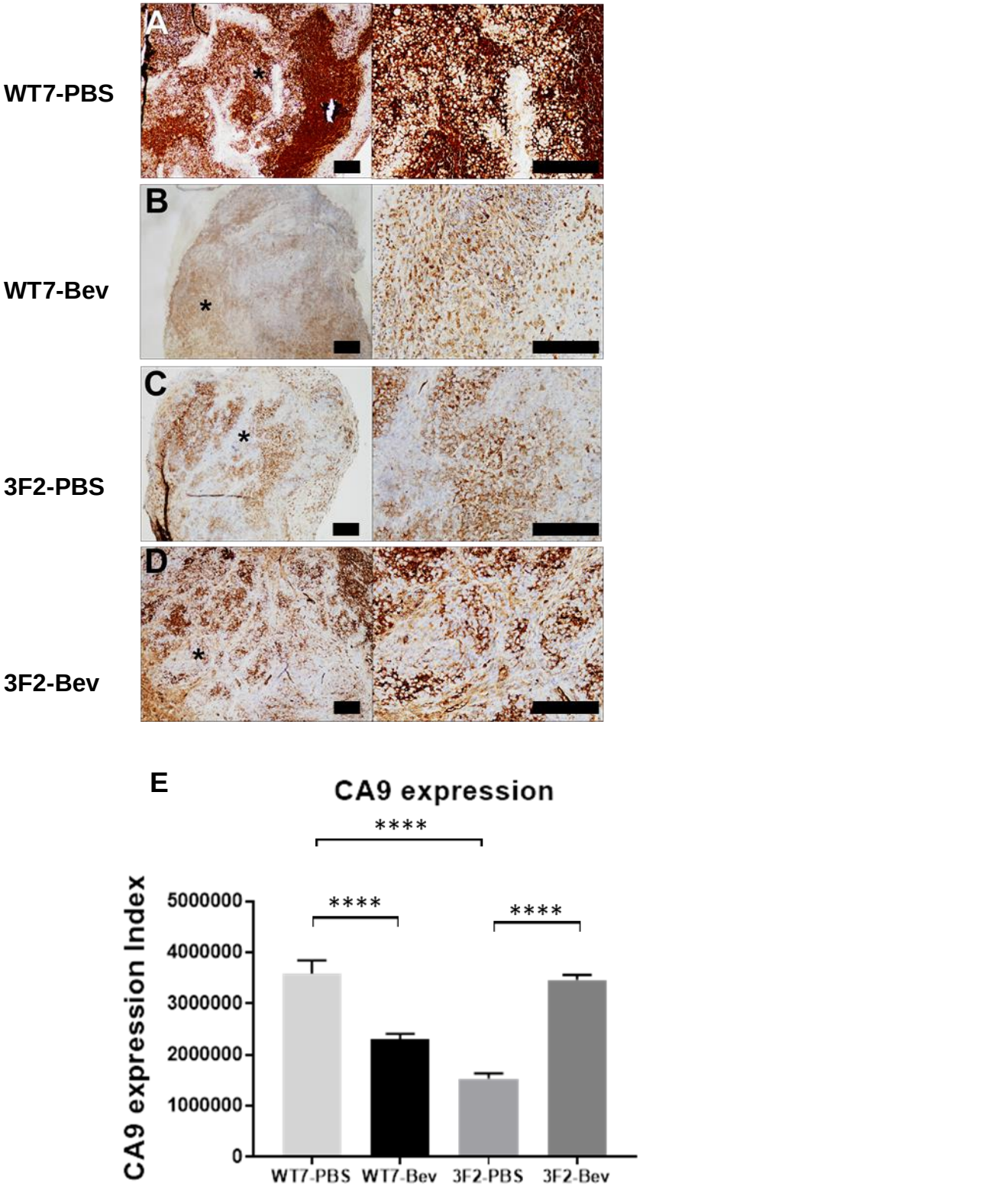


Figure 5-7: CA9 expression in WT7 (*BRAF* WT) and 3F2 (*BRAF* V600E) xenografts.

A to D, representative images of CA9 staining in WT7 and 3F2 xenografts with or without bevacizumab treatment. Asterisks indicate the areas shown in higher magnification on the right. Scale bars represent 100 µm. E, Quantification of CA9 expression. Mean ± SEM. n=5 tumours in each group. CA9 expression was significantly higher in WT7-PBS group than 3F2-PBS. **** p<0.0001 by unpaired t-test. Bevacizumab treatment reduced CA9 expression in WT7 tumours, while in the mutant 3F2 group CA9 was increased by the drug treatment. **** P < 0.0001.

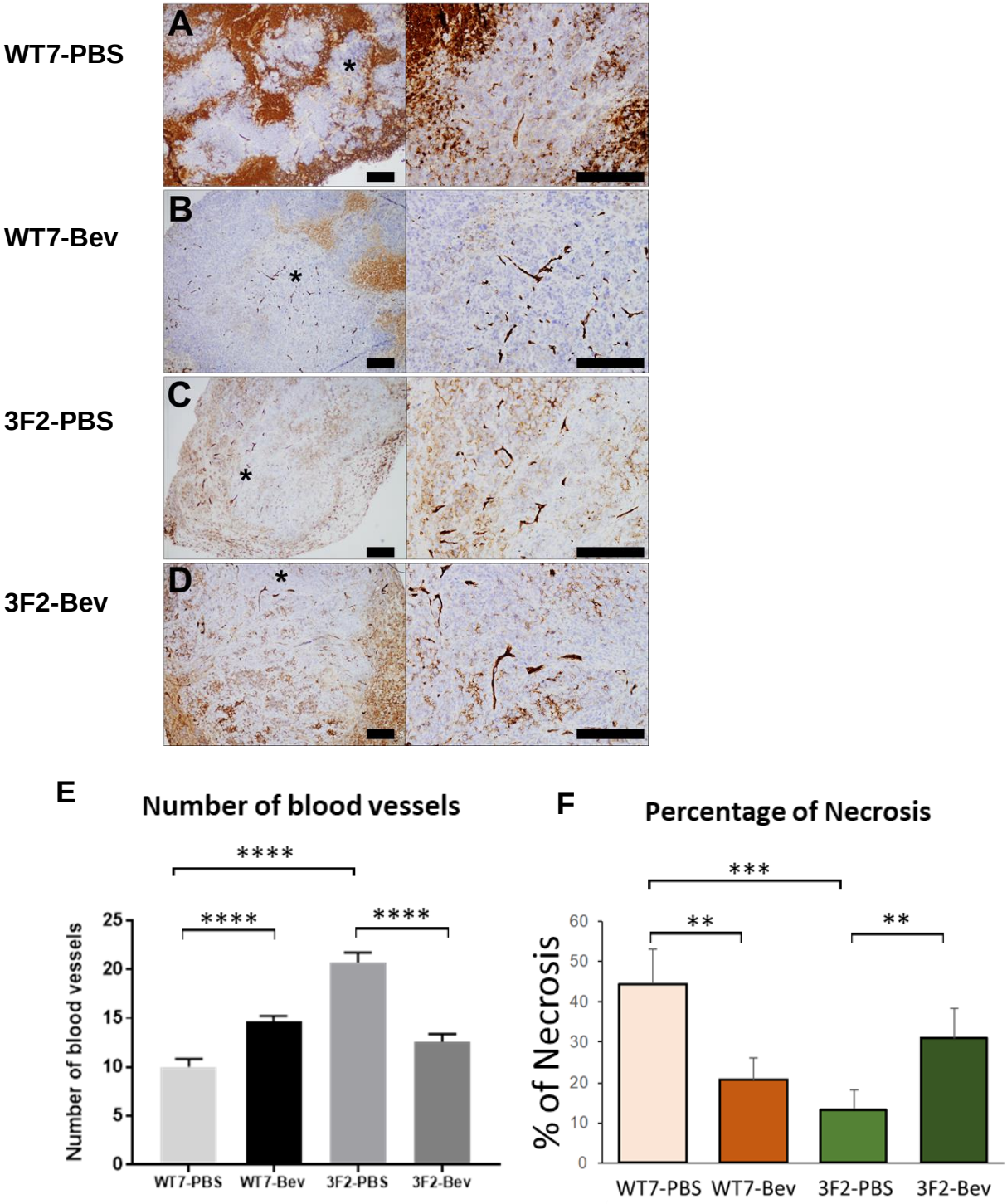
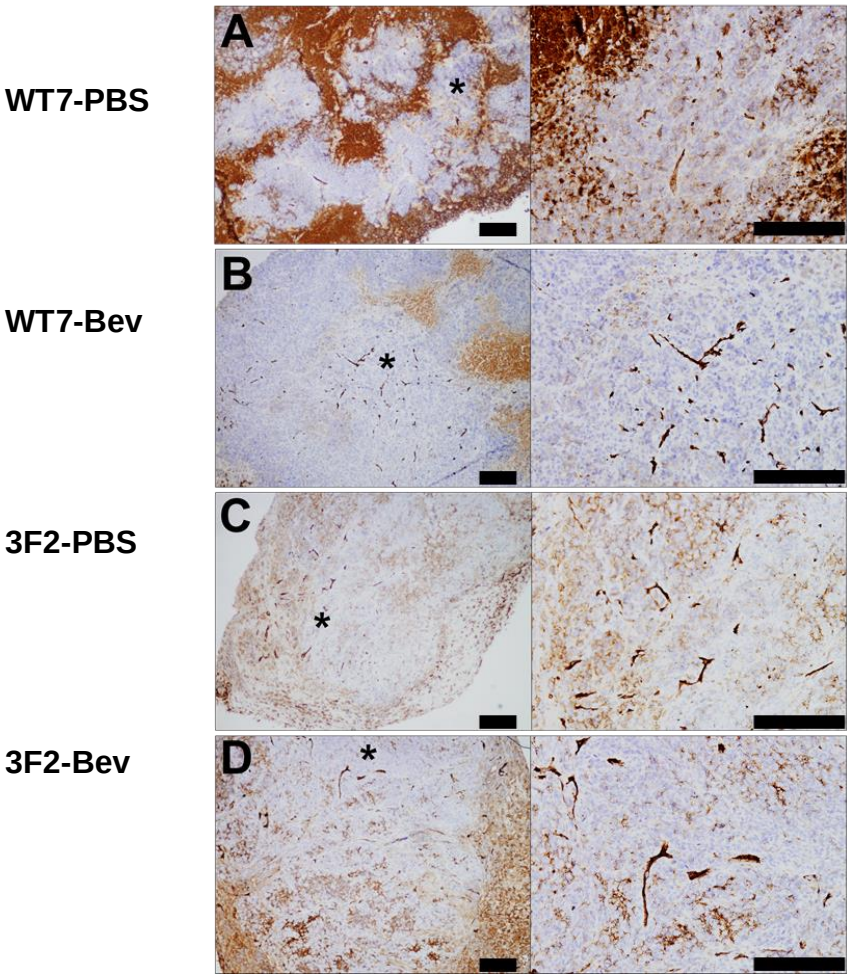


Figure 5-8: Number of blood vessels and percentage of necrosis in WT7 (*BRAF* WT) and 3F2 (*BRAF* V600E) xenografts.

A to D, representative images of CD31 staining in WT7 and 3F2 xenografts with or without bevacizumab treatment. Asterisks indicate the areas shown in higher magnification on the right. Scale bars represent 100 µm. E, Number of blood vessels. Mean ± SEM. n=5 tumours in each group. Number of blood vessels was significantly higher in 3F2-PBS group than WT7-PBS. **** p<0.0001 by unpaired t-test. Bevacizumab treatment increased the vessel numbers in WT7 tumours, while in the mutant 3F2 tumours the number of vessels were reduced by the drug treatment. **** P < 0.0001. n=5. F, Percentage of necrotic areas. Mean ± SEM. n=5 tumours in each group. The percentage of necrotic areas was significantly higher in WT7-PBS group than 3F2-PBS. *** p<0.001 by unpaired t-test. Necrosis was reduced by bevacizumab in WT7 tumours, however, in the mutant 3F2 tumours, treatment of bevacizumab increased necrosis. ** p<0.01.



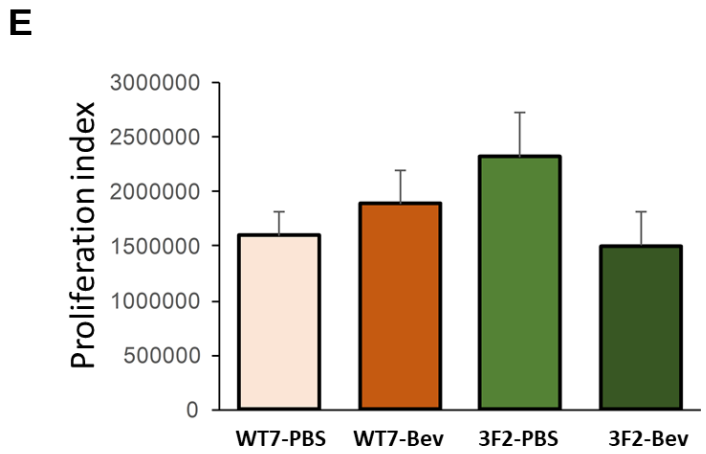


Figure 5-9: Proliferation quantified by Ki67 staining in WT7 (*BRAF* WT) and 3F2 (*BRAF* V600E) xenografts.

A to D, representative images of Ki67 staining in WT7 and 3F2 xenografts with or without bevacizumab treatment. Asterisks indicate the areas shown in higher magnification on the right. Scale bars represent 100 µm. E, Expression of Ki67 was quantified on whole sections quantitatively using ImageJ software and colour deconvolution method. n=5 tumours in each group. Graph shows mean ± SEM Ki67 index. Ki67 index was increased by bevacizumab treatment in WT7 tumours, while the drug treatment reduced Ki67 positivity in mutant 3F2 group. However, difference in proliferation with bevacizumab treatment was not significant in either the WT or mutant groups.

5.4.4 Serum VEGF protein in mice bearing BRAF WT or V600E xenografts

Blood samples were collected from mice via cardiac puncture at the time of sacrifice. Levels of human VEGF and mouse VEGF in serum were quantified using Human and mouse VEGF Quantikine ELISA Kits. The assay for human VEGF aimed to detect VEGF production by the tumours, but human VEGF was not detectable in mouse serum samples. Mouse VEGF was detected, but there were no significant differences in levels of mouse VEGF between BRAF WT and V600E treatment naïve groups (figure 5-9A and 5-9B). Bevacizumab treatment significantly increased the concentration of mouse VEGF in mice bearing 3F2 tumours, but not in the WT7 group (figure 5-9B).

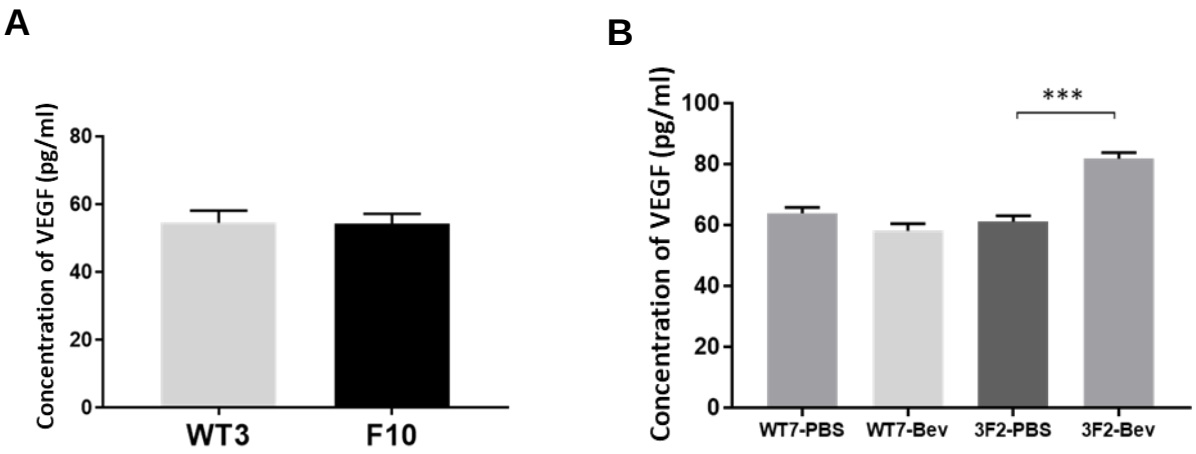


Figure 5-10: Mouse VEGF concentrations in mice bearing *BRAF* WT and V600E xenografts.

A, In treatment naïve animals, there was no difference in mouse VEGF levels between WT3 and F10 groups. Serum levels were assayed in n=5 mice per group. B, Mouse VEGF concentration in control and bevacizumab-treated mice. n=5 mice per group. Graph shows mean ± SEM VEGF concentration. No difference in VEGF levels between WT7-PBS and 3F2-PBS groups. Bevacizumab treatment significantly increased the mouse VEGF level in mutant 3F2 tumours, but not in the WT7 group. *** $p<0.001$ by unpaired t-test.

5.5 Discussion

Results of experiments on the CRISPR isogenic clones in chapter 4 have shown that the *BRAF* V600E clones expressed mutant BRAF, and were sensitive to BRAF inhibition. In this chapter, the clones were further characterised and their responses to anti-angiogenic therapy were tested *in vitro* and *in vivo*.

Although VEGF or VEGFR were not highlighted in the analysis of differential gene expression in chapter 4, they were tested in this chapter due to their important roles in angiogenesis (Fan et al., 2005). The angiogenesis response to VEGF is predominantly mediated through the activation of VEGFR2 on endothelial cells (Ferrara et al., 2003), however, many tumour types including melanoma express VEGF receptors (Straume and Akslen, 2003), suggesting the possibility of functional autocrine VEGF/VEGFR signalling in melanoma. Figure 5-1 showed that although V600E clones expressed more VEGFR2 at the mRNA level and on the cell surface, inhibiting VEGF signalling did not inhibit the growth in any of the clones tested (figure 5-2). This is consistent with the results obtained from experiments on cell line panels (figure 3-2), suggesting that the effect of bevacizumab on tumour growth was unlikely to be a direct effect via autocrine VEGF signalling

The qRT-PCR results in figure 5-3A showed that the VEGF regulator HIF1α was expressed more in the *BRAF* V600E clones than in the WT cells at the transcriptional level. Surprisingly, given that HIF1α is an important regulator of VEGF expression (Kaelin and Ratcliffe, 2008), the results of testing VEGF mRNA expression (figure 5-3B) did not follow this pattern. However, the levels of intracellular and secreted VEGF protein were significantly higher in the mutant cells (figure 5-4). This presents the same observation found in the first melanoma

cell line panel (figure 3-6A), suggesting a strong association between the *BRAF* V600E mutation and increased VEGF expression at the protein level. One interesting finding in this experiment was that in the mutant cell clones, the levels of intracellular and secreted VEGF protein (figure 5-4) were the inverse of *VEGFR2* expression at the transcriptional level (figure 5-1). *VEGFR2* was highly expressed in clones F8 and 3F2 at the transcriptional level as shown in figure 5-1, but not in B6 and F10, while for the VEGF protein it was the opposite (figure 5-4).

It is reported that in endothelial cells, treatment with exogenous recombinant VEGF upregulates VEGFR2 expression at the transcriptional and protein level (Shen et al., 1998). However, a study led by Guangqi et al in 2012 has found that endogenous VEGF functions differently from exogenous VEGF (Guangqi et al., 2012). It has been shown that knockdown of endogenous VEGF down-regulates VEGFR2 consistent with the findings of (Shen et al., 1998), however, this down-regulation could not be rescued by exogenous VEGF, and furthermore overexpression of a non-secreted form of VEGF strongly upregulates VEGFR2 mRNA, whereas WT VEGF does not (Guangqi et al., 2012). A previous study in endothelial cells reported that exogenous VEGF could induce VEGFR2 protein degradation through the lysosomal pathway (Ewan et al., 2006). Considering that B6 and F10 cells produced much higher levels of secreted VEGF than F8 and 3F2 (Figure 5.4B), it is possible that this overproduction of VEGF may trigger VEGFR2 internalisation and degradation, consistent with reports of (Dougher and Terman, 1999; Ewan et al., 2006). However, given that differential *VEGFR2* expression was detected here by RT-qPCR (Figure 5.1A), it appears that *VEGFR2* was downregulated at the transcriptional level. More cell clones could be tested to assess the relationship between VEGF and VEGFR2 expression.

To test the response of isogenic clones to anti-angiogenic therapy *in vivo*, BRAF WT and V600E clones were injected into CD1 nude mice to form xenografts. The selection of clones WT3 and WT7 (*BRAF* WT), and F10 and 3F2 (*BRAF* V600E) was based on the results of the functional studies and the microarray analysis. Figure 4-9 shows close hierarchical clustering for the selected clones, and also indicated that the transcriptional profile of the 3F2 clone was most different from the *BRAF* WT phenotype. On testing functional response to the selective BRAF V600E inhibitor PLX4720 (Figure 4-6), clones F10 and 3F2 had both shown inhibition of MAPK pathway activity and cell viability that differed from the response of *BRAF* WT clones. It was decided to make this choice based on this general phenotypic response, rather than on the specific results of VEGF and VEGFR2 assays presented here, in order to avoid biasing the outcome by selecting eg clones with high VEGF expression. It was noted that of the two selected *BRAF* V600E clones, 3F2 secreted high levels of VEGF and F10 relatively low VEGF levels, although still higher than the *BRAF* WT clones (Figure 5.4B).

Results of the *in vivo* experiments showed that bevacizumab significantly reduced tumour size and prolonged survival for the mice bearing *BRAF* V600E melanomas, but not for mice bearing *BRAF* WT xenografts. Immunohistochemical analysis of xenografts showed that *BRAF* V600E tumours were less hypoxic, proliferated more, and contained more blood vessels, compared to the *BRAF* WT group. These changes suggest functional response of mouse vascular endothelial cells to VEGF produced by *BRAF* V600E xenografts. Overall, these findings demonstrated the sensitivity of *BRAF* V600E tumours to bevacizumab, consistent with the hypothesis that *BRAF* V600E melanomas are more dependent on VEGF, and also consistent with the findings from the AVAST-M trial (Corrie et al., 2014).

Bevacizumab induced significantly more hypoxia and reduced the vascularity of *BRAF* V600E tumours, but not in the WT group. Indeed, vessel counts were increased and necrosis

reduced by bevacizumab treatment of *BRAF* WT melanomas (Figure 5.8E-F). This opposing effect on vascular markers in *BRAF* WT versus V600E tumours after bevacizumab treatment appears paradoxical. As bevacizumab can only inhibit human VEGF produced by xenografts, the lack of an inhibitory response to bevacizumab indicates that *BRAF* WT tumours are less dependent on tumour derived VEGF than V600E tumours. This is consistent with the results shown in figure 5-4 that *BRAF* V600E cells have higher VEGF production than WT. Compared to the control (treatment-naïve) group of *BRAF* V600E tumours, tumours in the WT control group were more hypoxic, with less vasculature and lower proliferation index (figure 5-6 to 5-9), likely reflecting lower levels of pro-angiogenic factors, including human VEGF, present in these WT tumours. However, the apparent pro-vascular response to bevacizumab is more difficult to explain. It is possible that, due to very low levels of human VEGF, the WT tumours might be more dependent on other pro-angiogenic mechanisms, such as the recruitment of stromal pro-angiogenic cells including pro-angiogenic bone-marrow-derived cells (BMDCs), macrophages or activated cancer-associated fibroblasts (CAFs)(Grunewald et al., 2006; Du et al., 2008; Pollard, 2004; Yang et al., 2004; Bergers and Hanahan, 2008). Inhibition of human VEGF in these WT tumours might then have promoted production of other pro-angiogenic factors from the stroma, leading to the increase in vasculature and proliferation upon bevacizumab treatment in WT tumours. This hypothesis could be tested by repeating the xenograft experiment, replacing bevacizumab with an inhibitor of the actions of other pro-angiogenic factors such as FGF.

Finally, levels of human VEGF and mouse VEGF in the mouse serum samples were quantified with ELISA. Only mouse VEGF, not human VEGF, could be detected in the serum samples. Assays for mouse VEGF showed that inhibiting human VEGF with bevacizumab increased the concentration of mouse VEGF in the serum of mice bearing 3F2 tumours (figure 5-10B). This could be due to compensatory production of VEGF and other pro-angiogenic

factors from recruited BMDCs or macrophages, upon treatment with antiangiogenic therapy (Grunewald et al., 2006; Du et al., 2008; Pollard, 2004). However, despite this increase in serum levels of mouse VEGF, there was still evidence of an anti-angiogenic effect in 3F2 xenografts in response to bevacizumab.

Two factors probably contributed to inability to detect human VEGF in mouse serum. Firstly, it is possible that the amount of xenograft-derived human VEGF that reached the circulation was too dilute to be above the detectable level of 9 pg/ml (sensitivity value of Human VEGF Quantikine ELISA Kit; R&D system) in the samples assayed. Secondly, only around 200 to 300 µl of serum was obtained from each mouse, and this had to be diluted two to three fold with assay diluent to meet the minimal volume requirement for triplicate wells for both the human VEGF and mouse VEGF ELISAs. This very probably further contributed to the finding that human VEGF levels were below the detection limit of the assay. Although it was not possible to measure the levels of human VEGF in the serum, the concentration in the tumours could be high enough for its functional effects. In support of this suggestion, a study investigating photodynamic therapy in nasopharyngeal carcinomas found that levels of human VEGF were 30 - 60 times higher in tumour tissue than in serum of mice bearing human nasopharyngeal xenografts (Bhuvaneswari et al., 2007).

Chapter 6: Conclusions and Future Directions

The AVAST-M trial that led to this project assessed bevacizumab as adjuvant therapy after surgery for high risk melanomas (Corrie et al., 2014). The initial results showed that patients with *BRAF* V600E melanomas had significant improvement in disease-free interval, while those with *BRAF* WT melanomas did not benefit. More recent analysis after 6.4-year median follow up has shown a trend towards poorer overall survival in patients with *BRAF* mutant vs WT tumours on the observation arm (P=0.06) (Corrie et al., 2018). However, the prognostic role of *BRAF* V600E in disease progression is still a controversial one. While one study found an approximate 3-fold increased risk of death in high risk melanomas harbouring *BRAF* mutation (Thomas et al., 2015), mutant *BRAF* was not shown to be prognostic for overall survival. In this recent AVAST-M clinical trial update, there was still evidence of benefit from bevacizumab in patients with *BRAF* mutant melanomas, with a trend for improved overall survival with bevacizumab (hazard ratio 0.8, CI 0.57–1.13, P=0.21) but no benefit in patients with *BRAF* WT melanomas (HR = 1.17; CI 0.82–1.61; P = 0.34) (Corrie et al., 2018).

The work presented here focused on investigating the molecular basis for this differential sensitivity of *BRAF* V600E melanomas to VEGF inhibition. The first possibility that was explored was that the inhibition of VEGF by bevacizumab directly suppresses growth via autocrine VEGF signalling in *BRAF* V600E tumour cells. Although it has been established that many tumour types, including melanoma, express VEGF receptors (Straume and Akslen, 2003; Molhoek et al., 2011), and studies in other tumour types suggested a possibility of VEGF/VEGFR2 signalling promoting cell proliferation or tumour progression (Zhang et al.,

2002; Dias et al., 2001; Xia et al., 2006), the function of this autocrine signalling pathway in melanoma remains unclear. Results in chapter 3 have shown that, although expression of VEGFR2 and VEGF could be detected in melanoma cell lines, there were no significant effects on cell proliferation or migration. This is consistent with previous findings where autocrine VEGF/VEGFR2 signalling was identified in BRAF mutant melanoma cells, but bevacizumab did not inhibit proliferation (Adamcic et al., 2012).

The second possibility considered was that the sensitivity of *BRAF* V600E melanomas to bevacizumab was mediated indirectly via effects on angiogenesis or other components of the tumour microenvironment. As a first step to test this hypothesis, VEGF expression was quantified in cell line panels consisting of *BRAF* WT and V600E melanoma cells. The results in the first panel of cell lines (figure 3-6) showed that secreted and intracellular VEGF levels were significantly higher in *BRAF* V600E cells compared to the WT cell lines, indicating a possible association between *BRAF* V600E and increased VEGF expression. However, this same phenotype was not observed in the newly established LM cell lines. The cause of this discrepancy in VEGF expression is unclear. Because of this, and also because of potentially confounding effects of other gene mutations that occur in melanoma cell lines (Akbani et al., 2015), an isogenic WT/V600E model was generated from a BRAF WT melanoma cell line for further *in vitro* and *in vivo* investigations. The isogenic model used in the experiments had its limitations, since the clones were generated from one *BRAF* WT cell line CHL1. Although other WT cell lines were tested for their suitability, only CHL1 was shown to be suitable for CRISPR transfection (figure 4-2). Other *BRAF* WT cell lines tested for this purpose included SKMEL2, which harbours *NRAS* mutation, and LM 25 cells (Behren et al 2013) which grow extremely slowly. If time had permitted, more *BRAF* WT melanoma cell lines could have been

obtained to screen more candidates that could be used to generate additional isogenic pairs. This would enable testing of the consequences of *BRAF* mutation status in different genetic backgrounds.

Results in chapter 4 showed that the *BRAF* WT codon V600 was replaced with V600E, and as a result, greater activation was observed in the MAPK pathway in the CRISPR mutant cell clones. Their sensitivity to the selective BRAF inhibitor PLX4720 confirmed that the mutant CRISPR clones exhibit a *BRAF* V600E phenotype. The *BRAF* V600E melanoma cells were shown to grow more rapidly in 3D (figure 4-8), with a trend to more rapid *in vivo* growth (figure 5-5C), which paralleled the trend to worse overall survival in patients with *BRAF* mutant tumours on the observation arm of the AVAST-M trial (Corrie et al., 2018). Further characterisation of the isogenic model has shown that levels of intracellular and secreted VEGF protein were significantly higher in the mutant clones compared to the WT group. This is consistent with the findings in the first panel of melanoma cell panel in chapter 3. It has been reported previously that in papillary thyroid cancer, *BRAF* V600E was associated with higher VEGF expression in tumour tissue (Jo et al., 2006). In Bottos et al's study, knocked-in *BRAF* V600E in human mammary epithelial cells increased level of secreted VEGFA and enhanced angiogenesis, although inhibiting BRAF V600E with PLX4720 did not show significant reduction in VEGF production (Bottos et al., 2012). My experiment found similar lack of reduction in VEGF at the mRNA and protein levels when treating *BRAF* V600E melanoma cell line A375 with PLX4720 (data not shown). The qRT-PCR results in chapter 5 showed that the VEGF regulator HIF1α was expressed at a higher level in the *BRAF* V600E clones than in the WT cells at the transcriptional level. This is consistent with the previous findings of *BRAF* V600E increasing HIF-1α expression (Kumar et al., 2007). However, this increase in HIF1α expression did not appear to upregulate VEGF expression at the

transcriptional level in the mutant cells, suggesting that the upregulation of VEGF protein in these cells was unlikely through HIF1α. If time had permitted, further experiments would have explored the contribution of other pathways reported to regulate VEGF secretion, including Matrix Metalloproteinase-2 (MMP2) and MMP9 in heparin-bound VEGF cleavage (Belotti et al., 2003; Hawinkels et al., 2008), and Wnt5A in exosome-mediated VEGF secretion (Ekström et al., 2014).

To test effects of bevacizumab *in vivo*, isogenic cell lines were injected into nude mice to form xenografts. The results (figure 5-5) showed that bevacizumab significantly reduced tumour size and prolonged survival in nude mice bearing BRAF V600E xenografts, compared to the WT group. This is consistent with the clinical observation that patients with *BRAF* V600E mutation appeared to benefit from bevacizumab in the AVAST-M trial (Corrie et al., 2018). The subsequent immunohistochemical analysis of the xenografts showed that bevacizumab significantly reduced vascularity of *BRAF* V600E tumours, but not of the WT tumours, further supporting the selective anti-angiogenic effect of bevacizumab on *BRAF* V600E tumours. It is known that bevacizumab, a humanised monoclonal antibody, does not interact with mouse VEGF (Yu et al., 2008), therefore, this anti-angiogenic effect was likely due to inhibition of human VEGF produced by melanoma cells in the xenografts. It did not prove possible to detect human VEGF in mouse blood samples, and as a secreted protein, it could not be quantified accurately with immunohistochemical analysis. However, results of the mouse serum VEGF showed an increase in mouse VEGF levels in the *BRAF* V600E group treated with bevacizumab. This could suggest a compensatory up-regulation of murine VEGF upon human VEGF inhibition in these mice, as observed previously in mouse models of rhabdomyosarcoma, pancreatic and colorectal cancer and Ewing sarcoma (Gerber et al., 2000; Liang et al., 2006).

Melanoma patients treated surgically are still at risk of recurrence, since fewer than 50% of patients with resected high risk melanoma survive to 5 years (Balch et al., 2009). Effective systemic adjuvant therapy after surgery might offer improved outcomes. The AVAST-M trial was based on the concept that since proangiogenic factors play a key role in neovascularisation of invading and metastasising cancer (Folkman, 2004), VEGF blockade with bevacizumab after surgery might prevent spread of disease. Therefore, the *in vivo* experiment in this project aimed to test effects of *BRAF* status on response to bevacizumab in human melanoma xenografts. A simple design was used in which mice bearing subcutaneous xenografts were treated with control (PBS) or bevacizumab. The experiment could with benefit have included an antibody IgG control group, in addition to or instead of the PBS control group. In testing responses in measurable subcutaneous tumours, the *in vivo* experiment differed from the context of the clinical trial, which treated patients with micrometastatic disease. To more closely mimic the trial design, bevacizumab treatment could have been started soon after tumour cell injection, when the tumour burden was smaller.

If time and resources had permitted, it would also have been interesting to test effects of bevacizimab on metastasis *in vivo* in *BRAF* mutant vs WT melanoma, using models similar to those described previously to test treatments for brain, liver, lung and bone metastases (Cruz-Munoz et al., 2008; Céspedes et al., 2007; Kuperwasser et al., 2005). However, many xenograft models used highly metastatic cell line variants that were derived through *in vivo* selection, which casts doubt on their physiological relevance. It is also possible that cells with limited metastatic potential, possibly including the WT *BRAF* melanoma clones generated in this project, might not be suitable for studies on metastatic capacity *in vivo*. In models of metastasis from subcutaneous xenografts, it is worth mentioning that there may be a long

latency for metastasis, and the primary tumour may need to be resected to allow development of metastases. This has been done for example in models of melanoma and breast cancer (Cruz-Munoz et al., 2008; Coffelt et al., 2015). Therefore, if the CHL1 cell line has intrinsic metastatic potential, this approach could be tested using the isogenic clones generated in this project, to assess the potential benefit of adjuvant bevacizumab therapy in metastasis. A different experimental model using tail vein injection in mice could also be used to evaluate the capacity of melanoma cells to form lung metastases (Fidler and Nicolson, 1976, 1977; Poste et al., 1980). The limitation of this approach is that it does not recapitulate the initial steps of metastasis before cells reach the bloodstream. To evaluate both the tumour cell autonomous and stromal effects on metastasis, genetically engineered mouse models (GEMMs) could be generated by activating oncogenic *BRAF*, combined with inactivation of the tumour suppressor *PTEN* in somatic cells, shown to induce melanomas that metastasise to lymph nodes and lungs (Dankort et al., 2009). However, since tumorigenesis and metastasis were dependent on mutation of *BRAF* and *PTEN* in this model, this approach could not be used to compare effects of treatment in *BRAF* mutant vs WT melanomas.

Previous studies have explored the relationship between *BRAF* status and angiogenic markers in other models, with mixed results. Knock-in of BRAF V600E in human mammary epithelial cells triggered an angiogenic response that was blocked by PLX4720 (Bottos et al., 2012). In contrast, a study in papillary thyroid cancer finding that *BRAF* mutation was associated with reduced expression of proangiogenic markers including VEGFA, in contrast to findings here in melanoma (Durante et al., 2011). Data from this study and the AVAST-M trial in melanoma suggest that *BRAF* mutation does associate with response to bevacizumab. However, the effect is probably not strong enough for *BRAF* status to be used as a predictive biomarker to select patients for bevacizumab treatment. Therefore, to investigate the molecular basis for differential growth of *BRAF* WT and V600E melanoma cells, and to

identify other differentially expressed genes that may contribute to the sensitivity of *BRAF* V600E melanomas to anti-angiogenic therapy, microarray analysis on the CRISPR isogenic clones was performed and differentially expressed genes were identified. Combined with 4 additional data sets, more differentially expressed genes were identified between the *BRAF* WT and V600E melanomas. These datasets include the analyses from 12 fresh frozen patient tumours, 52 LM melanoma cell lines from Ludwig Institute Melbourne, patient derived melanomas from TCGA and tumour samples from the AVAST-M trial. Genes differentially expressed in all datasets were identified and some have been validated and interrogated by Dr Nick Coupe. Out of the genes validated, *ROR2* in the Wnt pathway has become of particular interest, being one of only 5 genes found in multiple datasets to be upregulated in *BRAF* mutant melanoma. *ROR2* has been found to be exclusively expressed in the *BRAF* V600E isogenic clones, and results of ROR2 knockdown experiments in mutant melanoma cells suggested that ROR2 upregulates VEGF expression at the post-transcriptional level, indicating a possible mechanism for the link between *BRAF* V600E mutation and higher VEGF protein level in *BRAF* V600E melanoma cells. Future investigations could include testing effects of ROR2 overexpression or knock-down, testing effects on angiogenesis *in vivo* using the Chick Chorioallantoic Membrane (CAM) assay. It may be informative to determine whether ROR2 is differentially expressed by BRAF WT and V600E xenografts using immunohistochemistry analysis. This analysis of ROR2 expression could also be performed on patient tumour samples from the AVAST-M trial.

Many trials have tested bevacizumab in combination with other agents in various cancer types including melanoma. There are currently ~40 bevacizumab trials in melanoma listed on https://clinicaltrials.gov, including trials in combination with chemotherapy, immunotherapy and/or targeted agents. Adjuvant bevacizumab has been evaluated in a study by Miller et al,

who reported no benefit of adding bevacizumab to adjuvant chemotherapy in patients with HER2-negative, node-positive or high-risk node-negative breast cancer (Miller et al., 2018). Adding bevacizumab to adjuvant chemotherapy did not improve survival for patients with surgically resected early-stage, non-small-cell lung cancer (NSCLC) either (Wakelee et al., 2017). Bevacizumab as an adjuvant therapy for glioblastoma in elderly patients has shown increased OS (Nghiemphu et al., 2009; Babu et al., 2016). In addition to improved PFS, bevacizumab was found to improve quality of life in glioblastoma patients due to its steroid-sparing effect in blood brain barrier and blood tumour barrier restoration (Reyes - Botero et al., 2018). Bevacizumab is also reported to reduce the amount of radiation necrosis in glioblastomas of elderly patients (Matsuda et al., 2018), and in melanoma brain metastases (Glitza et al., 2017), providing additional benefit for these patients receiving radiotherapy. Combination of bevacizumab with ipilimumab in patients with metastatic melanoma has shown improved efficacy (Hodi et al., 2014), however, whether combining bevacizumab with immune checkpoint inhibitors could benefit high risk *BRAF* mutant melanoma patients remains to be evaluated.

In summary, evidence provided in this thesis supports the hypothesis that *BRAF* V600E melanomas are more sensitive to bevacizumab by a mechanism that involves *BRAF* V600E upregulating VEGF at the post-transcriptional level, enhancing dependence on angiogenesis. Future investigations that could further our understanding of the relationship between *BRAF* V600E and VEGF include exploring the mechanisms by which BRAF V600E upregulates VEGF protein, possibly via ROR2. Data generated here may also help to test whether expression of ROR2 or other differentially expressed gene can be used to select patients with BRAF mutant melanoma likely to respond to anti-angiogenic therapy. Finally, it is possible

that ROR2 or other newly identified differentially expressed genes could prove to be new targets for treatment of BRAF V600E melanoma.

Bibliography

Abe, H. et al. (2011) Discovery of a Highly Potent and Selective MEK Inhibitor: GSK1120212 (JTP-74057 DMSO Solvate). *ACS Medicinal Chemistry Letters*. [Online] 2 (4), 320–324.

Acunzo, M. et al. (2017) Selective targeting of point-mutated KRAS through artificial microRNAs. *Proceedings of the National Academy of Sciences*. [Online] 114 (21), E4203–E4212.

Adamcic, U. et al. (2012) The Effect of Bevacizumab on Human Malignant Melanoma Cells with Functional VEGF/VEGFR2 Autocrine and Intracrine Signaling Loops. *Neoplasia*. [Online] 14 (7), 612-IN16.

Ahonen, M. et al. (1998) Adenovirus-mediated gene delivery of tissue inhibitor of metalloproteinases-3 inhibits invasion and induces apoptosis in melanoma cells. *Cancer Research*. 58 (11), 2310–2315.

Aitken, J. F. et al. (1996) The Queensland Familial Melanoma Project: study design and characteristics of participants. *Melanoma Research*. 6 (2), 155–165.

Akbani, R. et al. (2015) Genomic Classification of Cutaneous Melanoma. *Cell*. [Online] 161 (7), 1681–1696.

Ambartsumian, N. et al. (2001) The metastasis-associated Mts1(S100A4) protein could act as an angiogenic factor. *Oncogene*. [Online] 20 (34), 4685–4695.

Angelo, L. S. & Kurzrock, R. (2007) Vascular endothelial growth factor and its relationship to inflammatory mediators. *Clinical Cancer Research.* [Online] 13 (10), 2825–2830.

Anon (2017) WHO | Skin cancers.

Azuma, M. et al. (1993) B70 antigen is a second ligand for CTLA-4 and CD28. *Nature*. [Online] 366 (6450), 76–79.

Babu, R. et al. (2016) Glioblastoma in the elderly: the effect of aggressive and modern therapies on survival. *Journal of Neurosurgery*. [Online] 124 (4), 998–1007.

Bachelder, R. E. et al. (2003) Competing autocrine pathways involving alternative neuropilin-1 ligands regulate chemotaxis of carcinoma cells. *Cancer Research*. 63 (17), 5230–5233.

Bachelder, R. E. et al. (2001) Vascular Endothelial Growth Factor Is an Autocrine Survival Factor for Neuropilin-expressing Breast Carcinoma Cells. *Cancer Research.* 61 (15), 5736–5740.

Bachelder, R. E. et al. (2002) Vascular endothelial growth factor promotes breast carcinoma invasion in an autocrine manner by regulating the chemokine receptor CXCR4. *Cancer Research*. 62 (24), 7203–7206.

Balch, C. M. et al. (2009) Final version of 2009 AJCC melanoma staging and classification. *Journal of Clinical Oncology.* [Online] 27 (36), 6199–6206.

Bates, D. O. et al. (2002) VEGF165b, an inhibitory splice variant of vascular endothelial growth factor, is down-regulated in renal cell carcinoma. *Cancer Research.* 60 (17), 4819–4824.

Bates, S. et al. (1998) p14ARF links the tumour suppressors RB and p53. *Nature*. [Online] 395 (6698), 124–125.

Batistatou, A. et al. (2007) A new concept of melanocytic neoplasia pathogenesis based on the phenotype of

common acquired nevi. *Medical Hypotheses*. [Online] 69 (6), 1334–1339.

Baudino, T. A. et al. (2002) c-Myc is essential for vasculogenesis and angiogenesis during development and tumor progression. *Genes & Development*. [Online] 16 (19), 2530–2543.

Beebe, J. S. et al. (2003) Pharmacological characterization of CP-547,632, a novel vascular endothelial growth factor receptor-2 tyrosine kinase inhibitor for cancer therapy. *Cancer Research*. [Online] 63 (21), 7301–7309.

Behren, A. et al. (2013) The Ludwig institute for cancer Research Melbourne melanoma cell line panel. *Pigment Cell & Melanoma Research*. [Online] 26 (4), 597–600.

Bell, R. E. et al. (2014) Transcription Factor/microRNA Axis Blocks Melanoma Invasion Program by miR-211 Targeting NUAK1. *Journal of Investigative Dermatology*. [Online] 134 (2), 441–451.

Belotti, D. et al. (2003) Matrix metalloproteinases (MMP9 and MMP2) induce the release of vascular endothelial growth factor (VEGF) by ovarian carcinoma cells: implications for ascites formation. *Cancer Research*. 63 (17), 5224–5229.

Bergers, G. & Hanahan, D. (2008) Modes of resistance to anti-angiogenic therapy. *Nature reviews. Cancer*. [Online] 8 (8), 592–603.

Bertolotto, C. et al. (2011) A SUMOylation-defective MITF germline mutation predisposes to melanoma and renal carcinoma. *Nature*. [Online] 480 (7375), 94–98.

Bhatia, S. et al. (2009) Treatment of metastatic melanoma: an overview. *Oncology (Williston Park, N.Y.)*. 23 (6), 488–496.

Bhuvaneswari, R. et al. (2007) Effect of hypericin-mediated photodynamic therapy on the expression of vascular endothelial growth factor in human nasopharyngeal carcinoma. *International Journal of Molecular Medicine*. [Online]

Blanco, R. & Gerhardt, H. (2013) VEGF and Notch in tip and stalk cell selection. *Cold Spring Harbor Perspectives in Medicine*. [Online] 3 (1), a006569.

Blank, C. et al. (2006) Blockade of PD-L1 (B7-H1) augments human tumor-specific T cell responses *in vitro*. *International Journal of Cancer*. [Online] 119 (2), 317–327.

Boehm, J. S. et al. (2007) Integrative Genomic Approaches Identify IKBKE as a Breast Cancer Oncogene. *Cell*. [Online] 129 (6), 1065–1079.

Bohula, E. A. et al. (2003) The Efficacy of Small Interfering RNAs Targeted to the Type 1 Insulin-like Growth Factor Receptor (IGF1R) Is Influenced by Secondary Structure in the IGF1R Transcript. *Journal of Biological Chemistry*. [Online] 278 (18), 15991–15997.

Bolstad, B. M. et al. (2003) A comparison of normalization methods for high density oligonucleotide array data based on variance and bias. *Bioinformatics*. [Online] 19 (2), 185–193.

Bottos, a. et al. (2012) PNAS Plus: Targeting oncogenic serine/threonine-protein kinase BRAF in cancer cells inhibits angiogenesis and abrogates hypoxia. *Proceedings of the National Academy of Sciences*. [Online] 109 (6), E353–E359.

Brooks, P. C., Montgomery, A. M., et al. (1994) Integrin alpha v beta 3 antagonists promote tumor regression

by inducing apoptosis of angiogenic blood vessels. *Cell*. 79 (7), 1157–1164.

Brooks, P. C., Clark, R. A., et al. (1994) Requirement of vascular integrin alpha v beta 3 for angiogenesis. *Science (New York, N.Y.)*. 264 (5158), 569–571.

Bruick, R. K. & McKnight, S. L. (2001) A Conserved Family of Prolyl-4-Hydroxylases That Modify HIF. *Science*. [Online] 294 (5545), 1337–1340.

Callahan, M. K. et al. (2010) Anti-CTLA-4 antibody therapy: immune monitoring during clinical development of a novel immunotherapy. *Seminars in Oncology*. [Online] 37 (5), 473–484.

Cancer Research UK (2018) *Skin cancer statistics | Cancer Research UK* [online]. Available from: http://www.cancerresearchuk.org/health-professional/cancer-statistics/statistics-by-cancer-type/skin-cancer#heading-Zero (Accessed 31 March 2018).

Carmeliet, P. & Jain, R. K. (2000) Angiogenesis in cancer and other diseases. *Nature*. [Online] 407 (6801), 249–257.

Carmeliet, P. & Jain, R. K. (2011) Molecular mechanisms and clinical applications of angiogenesis. *Nature*. [Online] 473 (7347), 298–307.

Carmona-Saez, P. et al. (2007) GENECODIS: a web-based tool for finding significant concurrent annotations in gene lists. *Genome Biology*. [Online] 8 (1), R3.

Carnahan, J. et al. (2010) Selective and potent Raf inhibitors paradoxically stimulate normal cell proliferation and tumor growth. *Molecular Cancer Therapeutics*. [Online] 9 (8), 2399–2410.

Carracedo, A. & Pandolfi, P. P. (2008) The PTEN–PI3K pathway: of feedbacks and cross-talks. *Oncogene*. [Online] 27 (41), 5527–5541.

Carreira, S. et al. (2005) Mitf cooperates with Rb1 and activates p21 Cip1 expression to regulate cell cycle progression. *Nature*. [Online] 433 (7027), 764–769.

Carvajal, R. D. et al. (2011) KIT as a Therapeutic Target in Metastatic Melanoma. *JAMA*. [Online] 305 (22), 2327.

Cascio, S. et al. (2009) Expression of angiogenic regulators, VEGF and leptin, is regulated by the EGF/PI3K/STAT3 pathway in colorectal cancer cells. *Journal of Cellular Physiology*. [Online] 221 (1), 189–194.

Cébe Suarez, S. et al. (2006) A VEGF-A splice variant defective for heparan sulfate and neuropilin-1 binding shows attenuated signaling through VEGFR-2. *Cellular and Molecular Life Sciences*. [Online] 63 (17), 2067–2077.

Celebi, J. T. et al. (2000) Identification of PTEN mutations in metastatic melanoma specimens. *Journal of Medical Genetics*. 37 (9), 653–657.

Cerami, E. et al. (2012) The cBio cancer genomics portal: an open platform for exploring multidimensional cancer genomics data. *Cancer Discovery*. [Online] 2 (5), 401–404.

Ceresa, B. P. et al. (1997) Signal Transducer and Activator of Transcription-3 Serine Phosphorylation by Insulin Is Mediated by a Ras/Raf/MEK-Dependent Pathway. *Endocrinology*. [Online] 138 (10), 4131–4137.

Céspedes, M. V. et al. (2007) Orthotopic Microinjection of Human Colon Cancer Cells in Nude Mice Induces

Tumor Foci in All Clinically Relevant Metastatic Sites. *The American Journal of Pathology*. [Online] 170 (3), 1077–1085.

Chakraborty, G. et al. (2008) Cancer Research. *Cancer Res.* [Online] 53 (21), 5300–5307.

Chapman, P. B. et al. (2011) Improved Survival with Vemurafenib in Melanoma with BRAF V600E Mutation. *New England Journal of Medicine*. [Online] 364 (26), 2507–2516.

Cheli, Y. et al. (2012) Hypoxia and MITF control metastatic behaviour in mouse and human melanoma cells. *Oncogene*. [Online] 31 (19), 2461–2470.

Claffey, K. P. et al. (1996) Expression of vascular permeability factor/vascular endothelial growth factor by melanoma cells increases tumor growth, angiogenesis, and experimental metastasis. *Cancer Research*. 56 (1), 172–181.

Coffelt, S. B. et al. (2015) IL-17-producing γδ T cells and neutrophils conspire to promote breast cancer metastasis. *Nature*. [Online] 522 (7556), 345–348.

Corrie, P. G. et al. (2018) Adjuvant bevacizumab for melanoma patients at high risk of recurrence: survival analysis of the AVAST-M trial. *Annals of Oncology*. [Online] 29 (8), 1843–1852.

Corrie, Pippa G. et al. (2014) Adjuvant bevacizumab in patients with melanoma at high risk of recurrence (AVAST-M): Preplanned interim results from a multicentre, open-label, randomised controlled phase 3 study. *The Lancet Oncology*. [Online] 15 (6), 620–630.

Cruz-Munoz, W. et al. (2008) Development of a Preclinical Model of Spontaneous Human Melanoma Central Nervous System Metastasis. *Cancer Research*. [Online] 68 (12), 4500–4505.

Curtin, J. A. et al. (2005) Distinct Sets of Genetic Alterations in Melanoma. *New England Journal of Medicine*. [Online] 353 (20), 2135–2147.

Curtin, J. A. et al. (2006) Somatic Activation of KIT in Distinct Subtypes of Melanoma. *Journal of Clinical Oncology*. [Online] 24 (26), 4340–4346.

Dai, J. et al. (2009) Osteopontin induces angiogenesis through activation of PI3K/AKT and ERK1/2 in endothelial cells. *Oncogene*. [Online] 28 (38), 3412–3422.

Damsky, W. E. & Bosenberg, M. (2017) Melanocytic nevi and melanoma: unraveling a complex relationship. *Oncogene*. [Online] 36 (42), 5771–5792.

Dankort, D. et al. (2009) BrafV600E cooperates with Pten loss to induce metastatic melanoma. *Nature Genetics*. [Online] 41 (5), 544–552.

Darrington, E. et al. (2012) Vascular endothelial growth factor A, secreted in response to transforming growth factor-β1 under hypoxic conditions, induces autocrine effects on migration of prostate cancer cells. *Asian Journal of Andrology*. [Online] 14 (5), 745–751.

Davies, H. et al. (2002a) Bibliography. *Nature*. [Online] 417 (6892), 949–954.

Davies, H. et al. (2002b) Mutations of the BRAF gene in human cancer. *Nature*. [Online] 417 (6892), 949–954.

Denko, N. C. (2008) Hypoxia, HIF1 and glucose metabolism in the solid tumour. *Nature Reviews Cancer*. [Online] 8 (9), 705–713.

Deryugina, E. I. & Quigley, J. P. (2010) Pleiotropic roles of matrix metalloproteinases in tumor angiogenesis: Contrasting, overlapping and compensatory functions. *Biochimica et Biophysica Acta (BBA) - Molecular Cell Research*. [Online] 1803 (1), 103–120.

Desch, A. et al. (2012) Highly Invasive Melanoma Cells Activate the Vascular Endothelium via an MMP-2/Integrin αvβ5–Induced Secretion of VEGF-A. *The American Journal of Pathology*. [Online] 181 (2), 693–705.

Dias, S. et al. (2001) Inhibition of both paracrine and autocrine VEGF/ VEGFR-2 signaling pathways is essential to induce long-term remission of xenotransplanted human leukemias. *Proceedings of the National Academy of Sciences of the United States of America*. [Online] 98 (19), 10857–10862.

Donnem, T. et al. (2018) Non-angiogenic tumours and their influence on cancer biology. *Nature Reviews Cancer*. [Online] 18 (5), 323–336.

Du, H. et al. (2015) Cross-talk between endothelial and tumor cells via basic fibroblast growth factor and vascular endothelial growth factor signaling promotes lung cancer growth and angiogenesis. *Oncology Letters*. [Online] 9 (3), 1089–1094.

Du, J. et al. (2004) Critical role of CDK2 for melanoma growth linked to its melanocyte-specific transcriptional regulation by MITF. *Cancer Cell*. [Online] 6 (6), 565–576.

Du, R. et al. (2008) HIF1α Induces the Recruitment of Bone Marrow-Derived Vascular Modulatory Cells to Regulate Tumor Angiogenesis and Invasion. *Cancer Cell*. [Online]

Durante, C. et al. (2011) BRAFV600E mutation and expression of proangiogenic molecular markers in papillary thyroid carcinomas. *European Journal of Endocrinology*. [Online] 165 (3), 455–463.

Ekström, E. J. et al. (2014) WNT5A induces release of exosomes containing pro-angiogenic and immunosuppressive factors from malignant melanoma cells. *Molecular Cancer*. [Online] 1388.

Ellis, L. M. (2006) The role of neuropilins in cancer. *Molecular Cancer Therapeutics*. [Online] 5 (5), 1099–1107.

Ellis, L. M. & Hicklin, D. J. (2008) Pathways Mediating Resistance to Vascular Endothelial Growth Factor-Targeted Therapy. *Clinical Cancer Research*. [Online] 14 (20), 6371–6375.

Emery, C. M. et al. (2009) MEK1 mutations confer resistance to MEK and B-RAF inhibition. *Proceedings of the National Academy of Sciences*. [Online] 106 (48), 20411–20416.

Emmett, M. S. et al. (2011) Angiogenesis and melanoma - from basic science to clinical trials. *American Journal of Cancer Research*. 1 (7), 852–868.

Eng, C. (2003) PTEN: One Gene, Many Syndromes. *Human Mutation*. [Online] 22 (3), 183–198.

Erhard, H. et al. (1997) Transition of horizontal to vertical growth phase melanoma is accompanied by induction of vascular endothelial growth factor expression and angiogenesis. *Melanoma Research*. 7 Suppl 2S19-26.

Essner, R. (2003) Surgical treatment of malignant melanoma. *Surgical Clinics of North America*. [Online] 83 (1), 109–156.

Eswarakumar, V. P. et al. (2005) Cellular signaling by fibroblast growth factor receptors. *Cytokine & Growth Factor Reviews*. [Online] 16 (2), 139–149.

Fagiani, E. & Christofori, G. (2013) Angiopoietins in angiogenesis. *Cancer Letters*. [Online] 328 (1), 18–26.

Fallowfield, M. E. & Cook, M. G. (1991) The vascularity of primary cutaneous melanoma. *The Journal of Pathology*. [Online] 164 (3), 241–244.

Fan, F. et al. (2005) Expression and function of vascular endothelial growth factor receptor-1 on human colorectal cancer cells. *Oncogene*. [Online] 24 (16), 2647–2653.

Fedorenko, I. V et al. (2013) NRAS mutant melanoma: biological behavior and future strategies for therapeutic management. *Oncogene*. [Online] 32 (25), 3009–3018.

Ferrara, N. et al. (2005) Bevacizumab (Avastin), a humanized anti-VEGF monoclonal antibody for cancer therapy. *Biochemical and Biophysical Research Communications*. [Online] 333 (2), 328–335.

Ferrara, N. et al. (2003) The biology of VEGF and its receptors. *Nature Medicine*. [Online] 9 (6), 669–676.

Ferrara, N. (2009) VEGF-A: a critical regulator of blood vessel growth. *European Cytokine Network*. [Online] 20 (4), 158–163.

Ferrara, N. & Henzel, W. J. (1989) Pituitary follicular cells secrete a novel heparin-binding growth factor specific for vascular endothelial cells. *Biochemical and Biophysical Research Communications*. 161 (2), 851–858.

Fidler, I. J. & Nicolson, G. L. (1977) Fate of Recirculating B16 Melanoma Metastatic Variant Cells in Parabiotic Syngeneic Recipients: Brief Communication 2. *JNCI: Journal of the National Cancer Institute*. [Online] 58 (6), 1867–1872.

Fidler, I. J. & Nicolson, G. L. (1976) Organ Selectivity for Implantation Survival and Growth of B16 Melanoma Variant Tumor Lines 2. *JNCI: Journal of the National Cancer Institute*. [Online] 57 (5), 1199–1202.

el Filali, M. et al. (2012) Bevacizumab and intraocular tumors: an intriguing paradox. *Molecular Vision*. 182454–2467.

Fischer, C. et al. (2008) FLT1 and its ligands VEGFB and PlGF: drug targets for anti-angiogenic therapy? *Nature Reviews Cancer*. [Online] 8 (12), 942–956.

Flaherty, K. T. et al. (2012) Improved Survival with MEK Inhibition in BRAF-Mutated Melanoma. *New England Journal of Medicine*. [Online] 367 (2), 107–114.

Flemming, A. (2010) Targeting mutant BRAF in metastatic melanoma. *Nature Reviews Drug Discovery*. [Online] 9 (11), 841–841.

Folkman, J. (2004) Endogenous angiogenesis inhibitors. *APMIS*. [Online] 112 (7–8), 496–507.

Fong, G.-H. et al. (1995) Role of the Flt-1 receptor tyrosine kinase in regulating the assembly of vascular endothelium. *Nature*. [Online] 376 (6535), 66–70.

Forsythe, J. A. et al. (1996) Activation of vascular endothelial growth factor gene transcription by hypoxia-inducible factor 1. *Molecular and Cellular Biology*. 16 (9), 4604–4613.

Freeman, G. J. et al. (1993) Cloning of B7-2: a CTLA-4 counter-receptor that costimulates human T cell proliferation. *Science (New York, N.Y.)*. 262 (5135), 909–911.

Freeman, G. J. et al. (2000) Engagement of the PD-1 immunoinhibitory receptor by a novel B7 family member

leads to negative regulation of lymphocyte activation. *The Journal of Experimental Medicine*. 192 (7), 1027–1034.

Friedlander, M. et al. (1995) Definition of two angiogenic pathways by distinct alpha v integrins. *Science (New York, N.Y.)*. 270 (5241), 1500–1502.

Fruehauf, J. et al. (2011) Multicenter, Phase II Study of Axitinib, a Selective Second-Generation Inhibitor of Vascular Endothelial Growth Factor Receptors 1, 2, and 3, in Patients with Metastatic Melanoma. *Clinical Cancer Research*. [Online] 17 (23), 7462–7469.

Gao, J. et al. (2013) Integrative analysis of complex cancer genomics and clinical profiles using the cBioPortal. *Science Signaling*. [Online] 6 (269), pl1.

Garraway, L. A. et al. (2005) Integrative genomic analyses identify MITF as a lineage survival oncogene amplified in malignant melanoma. *Nature*. [Online] 436 (7047), 117–122.

Garrido, M. C. & Bastian, B. C. (2010) KIT as a Therapeutic Target in Melanoma. *Journal of Investigative Dermatology*. [Online] 130 (1), 20–27.

Gerber, H. P. et al. (2000) Complete inhibition of rhabdomyosarcoma xenograft growth and neovascularization requires blockade of both tumor and host vascular endothelial growth factor. *Cancer Research*. 60 (22), 6253–6258.

Gingras, A.-C. et al. (2001) Regulation of translation initiation by FRAP/mTOR. *Genes & Development*. [Online] 15 (7), 807–826.

Glitza, I. C. et al. (2017) Bevacizumab as an effective treatment for radiation necrosis after radiotherapy for melanoma brain metastases. *Melanoma Research*. [Online] 27 (6), 580–584.

Goel, H. L. & Mercurio, A. M. (2013) VEGF targets the tumour cell. *Nature reviews. Cancer*. [Online] 13 (12), 871–882.

Goel, S. et al. (2012a) Vascular Normalization as a Therapeutic Strategy for Malignant and Nonmalignant Disease. *Cold Spring Harbor Perspectives in Medicine*. [Online] 2 (3), a006486–a006486.

Goel, S. et al. (2012b) Normalization of the tumor vasculature through oncogenic inhibition: an emerging paradigm in tumor biology. *Proceedings of the National Academy of Sciences of the United States of America*. [Online] 109 (20), E1214.

Goldstein, A. M. et al. (2000) Genotype-phenotype relationships in U.S. melanoma-prone families with CDKN2A and CDK4 mutations. *Journal of the National Cancer Institute*. 92 (12), 1006–1010.

Gong, J. et al. (2018) Development of PD-1 and PD-L1 inhibitors as a form of cancer immunotherapy: a comprehensive review of registration trials and future considerations. *Journal for Immunotherapy of Cancer*. [Online] 6 (1), 8.

Gorski, D. H. et al. (2003) Differential expression of vascular endothelial growth factor–A isoforms at different stages of melanoma progression. *Journal of the American College of Surgeons*. [Online] 197 (3), 408–418.

Gossage, L. et al. (2015) VHL, the story of a tumour suppressor gene. *Nature Reviews Cancer*. [Online] 15 (1), 55–64.

Green, J. L. et al. (2008) Ror receptor tyrosine kinases: orphans no more. *Trends in Cell Biology*. [Online] 18

(11), 536–544.

Greider, C. W. & Blackburn, E. H. (1989) A telomeric sequence in the RNA of Tetrahymena telomerase required for telomere repeat synthesis. *Nature*. [Online] 337 (6205), 331–337.

Griewank, K. G. et al. (2014) TERT Promoter Mutation Status as an Independent Prognostic Factor in Cutaneous Melanoma. *JNCI: Journal of the National Cancer Institute*. [Online] 106 (9), .

Grignol, V. P. et al. (2011) A Phase 2 Trial of Bevacizumab and High-dose Interferon Alpha 2B in Metastatic Melanoma. *Journal of Immunotherapy*. [Online] 34 (6), 509–515.

Grunewald, M. et al. (2006) VEGF-induced adult neovascularization: recruitment, retention, and role of accessory cells. *Cell*. [Online] 124 (1), 175–189.

Guangqi, E. et al. (2012) Endogenous vascular endothelial growth factor-A (VEGF-A) maintains endothelial cell homeostasis by regulating VEGF receptor-2 transcription. *Journal of Biological Chemistry*. [Online] 287(5): 3029–3041.

Guo, J. et al. (2011) Phase II, Open-Label, Single-Arm Trial of Imatinib Mesylate in Patients With Metastatic Melanoma Harboring *c-Kit* Mutation or Amplification. *Journal of Clinical Oncology*. [Online] 29 (21), 2904–2909.

Gupta, A. (2017) *Potential drivers of melanoma growth in BRAF wild-type cutaneous melanoma and use of novel combination regimes in this patient population. MD Thesis, University of London 2017.*

Guzmán-Hernández, M. L. et al. (2014) Secretion of VEGF-165 has unique characteristics, including shedding from the plasma membrane. *Molecular Biology of the Cell*. [Online] 25 (7), 1061–1072.

Haanen, J. B. A. G. (2013) Immunotherapy of melanoma. *EJC supplements*. [Online] 11 (2), 97–105.

Halper, J. & Kjaer, M. (2014) Basic Components of Connective Tissues and Extracellular Matrix: Elastin, Fibrillin, Fibulins, Fibrinogen, Fibronectin, Laminin, Tenascins and Thrombospondins. *Advances in Experimental Medicine and Biology*. [Online]. pp. 31–47.

Hamilton, A. J. & Baulcombe, D. C. (1999) A species of small antisense RNA in posttranscriptional gene silencing in plants. *Science (New York, N.Y.)*. 286 (5441), 950–952.

Hanahan, D. & Folkman, J. (1996) Patterns and emerging mechanisms of the angiogenic switch during tumorigenesis. *Cell*. 86 (3), 353–364.

Hanahan, D. & Weinberg, R. a. (2011) Hallmarks of cancer: The next generation. *Cell*. [Online] 144 (5), 646–674.

Hansen, W. et al. (2012) Neuropilin 1 deficiency on CD4+Foxp3+ regulatory T cells impairs mouse melanoma growth. *Journal of Experimental Medicine*. [Online] 209 (11), 2001–2016.

Haq, R. et al. (2013) *BCL2A1* is a lineage-specific antiapoptotic melanoma oncogene that confers resistance to BRAF inhibition. *Proceedings of the National Academy of Sciences*. [Online] 110 (11), 4321–4326.

Harris, A. L. (2002) Hypoxia--a key regulatory factor in tumour growth. *Nature Reviews Cancer*. [Online] 2 (1), 38–47.

Hathcock, K. S. et al. (1993) Identification of an alternative CTLA-4 ligand costimulatory for T cell activation.

Science (New York, N.Y.). 262 (5135), 905–907.

Hatzivassiliou, G. et al. (2010) RAF inhibitors prime wild-type RAF to activate the MAPK pathway and enhance growth. *Nature*. [Online] 464 (7287), 431–435.

Hauschild, A. et al. (2012) Dabrafenib in BRAF-mutated metastatic melanoma: a multicentre, open-label, phase 3 randomised controlled trial. *The Lancet*. [Online] 380 (9839), 358–365.

Hauschild, A. et al. (2009) Results of a phase III, randomized, placebo-controlled study of sorafenib in combination with carboplatin and paclitaxel as second-line treatment in patients with unresectable stage III or stage IV melanoma. *Journal of Clinical Oncology*. [Online] 27 (17), 2823–2830.

Hawinkels, L. J. A. C. et al. (2008) VEGF release by MMP-9 mediated heparan sulphate cleavage induces colorectal cancer angiogenesis. *European Journal of Cancer*. [Online] 44 (13), 1904–1913.

Hayward, N. K. et al. (2017) Whole-genome landscapes of major melanoma subtypes. *Nature*. [Online] 545 (7653), 175–180.

Heasley, D. D. et al. (1996) Pathology of malignant melanoma. *The Surgical clinics of North America*. 76 (6), 1223–1255.

Hein, M. & Graver, S. (2013) Tumor cell response to bevacizumab single agent therapy in vitro. *Cancer Cell International*. [Online] 13 (1), 94.

Helfrich, I. et al. (2009) Angiopoietin-2 Levels Are Associated with Disease Progression in Metastatic Malignant Melanoma. *Clinical Cancer Research*. [Online] 15 (4), 1384–1392.

Helfrich, I. et al. (2010) Resistance to antiangiogenic therapy is directed by vascular phenotype, vessel stabilization, and maturation in malignant melanoma. *The Journal of Experimental Medicine*. [Online] 207 (3), 491–503.

Hernández, J. L. et al. (2013) Therapeutic Targeting of Tumor Growth and Angiogenesis with a Novel Anti-S100A4 Monoclonal Antibody Sujit Basu (ed.). *PLoS ONE*. [Online] 8 (9), e72480.

Hirano, F. et al. (2005) Blockade of B7-H1 and PD-1 by monoclonal antibodies potentiates cancer therapeutic immunity. *Cancer Research*. 65 (3), 1089–1096.

Hodi, F. S. et al. (2014) Bevacizumab plus Ipilimumab in Patients with Metastatic Melanoma. *Cancer Immunology Research*. [Online] 2 (7), 632–642.

Hodi, F. S. et al. (2016) Combined nivolumab and ipilimumab versus ipilimumab alone in patients with advanced melanoma: 2-year overall survival outcomes in a multicentre, randomised, controlled, phase 2 trial. *The Lancet Oncology*. [Online] 17 (11), 1558–1568.

Hodi, F. S. et al. (2013) Imatinib for Melanomas Harboring Mutationally Activated or Amplified *KIT* Arising on Mucosal, Acral, and Chronically Sun-Damaged Skin. *Journal of Clinical Oncology*. [Online] 31 (26), 3182–3190.

Hodi, F. S. et al. (2010) Improved Survival with Ipilimumab in Patients with Metastatic Melanoma. *New England Journal of Medicine*. [Online] 363 (8), 711–723.

Hodis, E. et al. (2012) A Landscape of Driver Mutations in Melanoma. *Cell*. [Online] 150 (2), 251–263.

Hoek, K. S. et al. (2008) Novel MITF targets identified using a two-step DNA microarray strategy. *Pigment Cell & Melanoma Research*. [Online] 21 (6), 665–676.

Hofmann, U. B. et al. (1999) Matrix metalloproteinases in human melanoma cell lines and xenografts: increased expression of activated matrix metalloproteinase-2 (MMP-2) correlates with melanoma progression. *British Journal of Cancer*. [Online] 81 (5), 774–782.

Holland, E. A. et al. (1995) Analysis of the p16 gene, CDKN2, in 17 Australian melanoma kindreds. *Oncogene*. 11 (11), 2289–2294.

Horn, S. et al. (2013) TERT Promoter Mutations in Familial and Sporadic Melanoma. *Science*. [Online] 339 (6122), 959–961.

Houben, R. et al. (2004) Constitutive activation of the Ras-Raf signaling pathway in metastatic melanoma is associated with poor prognosis. *Journal of Carcinogenesis*. [Online] 3 (1), 6.

Houck, K. A. et al. (1991) The Vascular Endothelial Growth Factor Family: Identification of a Fourth Molecular Species and Characterization of Alternative Splicing of RNA. *Molecular Endocrinology*. [Online] 5 (12), 1806–1814.

Huang, F. W. et al. (2013) Highly recurrent TERT promoter mutations in human melanoma. *Science (New York, N.Y.)*. [Online] 339 (6122), 957–959.

Huang, H. et al. (2010) Targeting the ANGPT–TIE2 pathway in malignancy. *Nature Reviews Cancer*. [Online] 10 (8), 575–585.

Hynes, R. O. (2002) Integrins: bidirectional, allosteric signaling machines. *Cell*. 110 (6), 673–687.

IERVOLINO, A. et al. (2002) Bcl-2 overexpression in human melanoma cells increases angiogenesis through VEGF mRNA stabilization and HIF-1-mediated transcriptional activity. *The FASEB Journal*. [Online] 16 (11), 1453–1455.

Iida, J. et al. (2004) Membrane Type-1 Matrix Metalloproteinase Promotes Human Melanoma Invasion and Growth. *Journal of Investigative Dermatology*. [Online] 122 (1), 167–176.

Ikediobi, O. N. et al. (2006) Mutation analysis of 24 known cancer genes in the NCI-60 cell line set. *Molecular Cancer Therapeutics*. [Online] 5 (11), 2606–2612.

Ishida, Y. et al. (1992) Induced expression of PD-1, a novel member of the immunoglobulin gene superfamily, upon programmed cell death. *The EMBO journal*. 11 (11), 3887–3895.

Itoh, T. et al. (1999) Experimental metastasis is suppressed in MMP-9-deficient mice. *Clinical & Experimental Metastasis*. [Online] 17 (2), 177–181.

Ivanov, S. et al. (2001) Expression of hypoxia-inducible cell-surface transmembrane carbonic anhydrases in human cancer. *The American Journal of Pathology*. [Online] 158 (3), 905–919.

Iwai, K. et al. (1999) Identification of the von Hippel-Lindau tumor-suppressor protein as part of an active E3 ubiquitin ligase complex. *Proceedings of the National Academy of Sciences*. [Online] 96 (22), 12436–12441.

Iwai, Y. et al. (2002) Involvement of PD-L1 on tumor cells in the escape from host immune system and tumor immunotherapy by PD-L1 blockade. *Proceedings of the National Academy of Sciences of the United States*

of America. [Online] 99 (19), 12293–12297.

Jain, R. K. (2001) Normalizing tumor vasculature with anti-angiogenic therapy: A new paradigm for combination therapy. *Nature Medicine*. [Online] 7 (9), 987–989.

Jeong, J.-W. et al. (2002) Regulation and Destabilization of HIF-1α by ARD1-Mediated Acetylation. *Cell*. [Online] 111 (5), 709–720.

Ji, Z. et al. (2012) Targeting the RAS pathway in melanoma. *Trends in Molecular Medicine*. [Online] 18 (1), 27–35.

Jiang, B. H. et al. (2001) Phosphatidylinositol 3-kinase signaling controls levels of hypoxia-inducible factor 1. *Cell growth & differentiation : the molecular biology journal of the American Association for Cancer Research*. 12 (7), 363–369.

Jiao, Y. et al. (2012) Matrix metalloproteinase-2 promotes αvβ3 integrin-mediated adhesion and migration of human melanoma cells by cleaving fibronectin. *PloS one*. [Online] 7 (7), e41591.

Jing, S.-W. et al. (2012) HIF-1α contributes to hypoxia-induced invasion and metastasis of esophageal carcinoma via inhibiting E-cadherin and promoting MMP-2 expression. *Acta Medica Okayama*. [Online] 66 (5), 399–407.

Jo, Y. S. et al. (2006) Influence of the BRAF V600E Mutation on Expression of Vascular Endothelial Growth Factor in Papillary Thyroid Cancer. *The Journal of Clinical Endocrinology & Metabolism*. [Online] 91 (9), 3667–3670.

Jour, G. et al. (2016) Angiogenesis in melanoma: an update with a focus on current targeted therapies. *Journal of Clinical Pathology*. [Online] 69 (6), 472–483.

Kaelin, W. G. & Ratcliffe, P. J. (2008) Oxygen Sensing by Metazoans: The Central Role of the HIF Hydroxylase Pathway. *Molecular Cell*. [Online] 30 (4), 393–402.

Kamb, A. et al. (1994) Analysis of the p16 gene (CDKN2) as a candidate for the chromosome 9p melanoma susceptibility locus. *Nature Genetics*. [Online] 8 (1), 22–26.

Kashani-Sabet, M. et al. (2002) Tumor Vascularity in the Prognostic Assessment of Primary Cutaneous Melanoma. *Journal of Clinical Oncology*. [Online] 20 (7), 1826–1831.

Kevil, C. G. et al. (1998) Vascular permeability factor/vascular endothelial cell growth factor-mediated permeability occurs through disorganization of endothelial junctional proteins. *The Journal of Biological Chemistry*. 273 (24), 15099–15103.

Khokha, R. (1994) Suppression of the tumorigenic and metastatic abilities of murine B16-F10 melanoma cells in vivo by the overexpression of the tissue inhibitor of the metalloproteinases-1. *Journal of the National Cancer Institute*. 86 (4), 299–304.

Kienast, Y. et al. (2010) Real-time imaging reveals the single steps of brain metastasis formation. *Nature Medicine*. [Online] 16 (1), 116–122.

Kim, H. G. et al. (2011) Metallothionein-2A overexpression increases the expression of matrix metalloproteinase-9 and invasion of breast cancer cells. *FEBS Letters*. [Online] 585 (2), 421–428.

Kim, K. B. et al. (2012) BEAM: a randomized phase II study evaluating the activity of bevacizumab in

combination with carboplatin plus paclitaxel in patients with previously untreated advanced melanoma. *Journal of clinical oncology : official journal of the American Society of Clinical Oncology*. [Online] 30 (1), 34–41.

Kim, M. P. et al. (2009) Src family kinases as mediators of endothelial permeability: effects on inflammation and metastasis. *Cell and Tissue Research*. [Online] 335 (1), 249–259.

Kitayama, H. et al. (1995) Constitutively activating mutations of c-kit receptor tyrosine kinase confer factor-independent growth and tumorigenicity of factor-dependent hematopoietic cell lines. *Blood*. 85 (3), 790–798.

Kiuru, M. & Busam, K. J. (2017) The NF1 gene in tumor syndromes and melanoma. *Laboratory Investigation*. 97 (2), 146–157.

Knudsen, E. S. & Wang, J. Y. J. (2010) Targeting the RB-pathway in cancer therapy. *Clinical cancer Research : an official journal of the American Association for Cancer Research*. [Online] 16 (4), 1094–1099.

Koch, A. E. et al. (1992) Interleukin-8 as a macrophage-derived mediator of angiogenesis. *Science (New York, N.Y.)*. 258 (5089), 1798–1801.

Koch, K. R. et al. (2014) Autocrine Impact of VEGF-A on Uveal Melanoma Cells. *Investigative Opthalmology & Visual Science*. [Online] 55 (4), 2697.

Kottschade, L. A. et al. (2013) A randomized phase 2 study of temozolomide and bevacizumab or *nab* -paclitaxel, carboplatin, and bevacizumab in patients with unresectable stage IV melanoma. *Cancer*. [Online] 119 (3), 586–592.

Kowanetz, M. & Ferrara, N. (2006) Vascular endothelial growth factor signaling pathways: therapeutic perspective. *Clinical cancer Research : an official journal of the American Association for Cancer Research*. [Online] 12 (17), 5018–5022.

Kudchadkar, R. (2010) Novel targeted therapies for the treatment of metastatic melanoma. *The Ochsner Journal*. 10 (2), 117–124.

Kumar, S. M. et al. (2007) Mutant V600E BRAF increases hypoxia inducible factor-1α expression in melanoma. *Cancer Research*. [Online] 67 (7), 3177–3184.

Kuperwasser, C. et al. (2005) A Mouse Model of Human Breast Cancer Metastasis to Human Bone. *Cancer Research*. [Online] 65 (14), 6130–6138.

Langmead, B. et al. (2009) Ultrafast and memory-efficient alignment of short DNA sequences to the human genome. *Genome Biology*. [Online] 10 (3), R25.

Larkin, J. et al. (2014) Combined Vemurafenib and Cobimetinib in *BRAF* -Mutated Melanoma. *New England Journal of Medicine*. [Online] 371 (20), 1867–1876.

Ledaki, I. et al. (2015) Carbonic anhydrase IX induction defines a heterogeneous cancer cell response to hypoxia and mediates stem cell-like properties and sensitivity to HDAC inhibition. *Oncotarget*. [Online] 6 (23), 19413–19427.

Lee, G. Y. et al. (2007) Three-dimensional culture models of normal and malignant breast epithelial cells. *Nature Methods*. [Online] 4 (4), 359–365.

Leenders, W. P. J. et al. (2004) Antiangiogenic Therapy of Cerebral Melanoma Metastases Results in Sustained Tumor Progression via Vessel Co-Option. *Clinical Cancer Research*. [Online] 10 (18), 6222–6230.

Leicht, D. T. et al. (2007) Raf kinases: Function, regulation and role in human cancer. *Biochimica et Biophysica Acta (BBA) - Molecular Cell Research*. [Online] 1773 (8), 1196–1212.

Li, A. et al. (2003) IL-8 directly enhanced endothelial cell survival, proliferation, and matrix metalloproteinases production and regulated angiogenesis. *Journal of Immunology (Baltimore, Md. : 1950)*. 170 (6), 3369–3376.

Liang, W.-C. et al. (2006) Cross-species vascular endothelial growth factor (VEGF)-blocking antibodies completely inhibit the growth of human tumor xenografts and measure the contribution of stromal VEGF. *The Journal of Biological Chemistry*. [Online] 281 (2), 951–961.

Lim, D. et al. (2009) Silencing the Metallothionein-2A gene inhibits cell cycle progression from G1- to S-phase involving ATM and cdc25A signaling in breast cancer cells. *Cancer Letters*. [Online] 276 (1), 109–117.

Lingner, J. & Cech, T. R. (1996) Purification of telomerase from Euplotes aediculatus: requirement of a primer 3’ overhang. *Proceedings of the National Academy of Sciences of the United States of America*. 93 (20), 10712–10717.

Liu, D. et al. (2007) BRAF V600E maintains proliferation, transformation, and tumorigenicity of BRAF-mutant papillary thyroid cancer cells. *The Journal of Clinical Endocrinology and Metabolism*. [Online] 92 (6), 2264–2271.

Liu, G. et al. (2005) Selective induction of interleukin-8 expression in metastatic melanoma cells by transforming growth factor-β1. *Cytokine*. [Online] 31 (3), 241–249.

Liu, L. et al. (1999) Mutation of the CDKN2A 5’ UTR creates an aberrant initiation codon and predisposes to melanoma. *Nature Genetics*. [Online] 21 (1), 128–132.

Loercher, A. E. et al. (2005) MITF links differentiation with cell cycle arrest in melanocytes by transcriptional activation of INK4A. *The Journal of Cell Biology*. [Online] 168 (1), 35–40.

Lu, P. et al. (2011) Extracellular matrix degradation and remodeling in development and disease. *Cold Spring Harbor Perspectives in Biology*. [Online] 3 (12), .

Maertens, O. et al. (2013) Elucidating Distinct Roles for *NF1* in Melanomagenesis. *Cancer Discovery*. [Online] 3 (3), 338–349.

Mahfouz, N. et al. (2017) Gastrointestinal cancer cells treatment with bevacizumab activates a VEGF autoregulatory mechanism involving telomerase catalytic subunit hTERT via PI3K-AKT, HIF-1α and VEGF receptors Rajesh Mohanraj (ed.). *PLOS ONE*. [Online] 12 (6), e0179202.

Maniotis, A. J. et al. (1999) Vascular Channel Formation by Human Melanoma Cells in Vivo and in Vitro: Vasculogenic Mimicry. *The American Journal of Pathology*. [Online] 155 (3), 739–752.

Manning, B. D. & Cantley, L. C. (2007) AKT/PKB Signaling: Navigating Downstream. *Cell*. [Online] 129 (7), 1261–1274.

Marcoval, J. et al. (1997) Angiogenesis and malignant melanoma. Angiogenesis is related to the development of vertical (tumorigenic) growth phase. *Journal of Cutaneous Pathology*. 24 (4), 212–218.

Martin, M. J. et al. (2012) Metformin accelerates the growth of BRAF V600E -driven melanoma by upregulating VEGF-A. *Cancer Discovery*. [Online] 2 (4), 344–355.

Matsuda, K. et al. (2018) Treatment outcomes of hypofractionated radiotherapy combined with temozolomide followed by bevacizumab salvage therapy in glioblastoma patients aged > 75 years. *International Journal of Clinical Oncology*. [Online] 23 (5), 820–825.

Mattia, G. et al. (2018) Cell death-based treatments of melanoma:conventional treatments and new therapeutic strategies. *Cell Death & Disease*. [Online] 9 (2), 112.

Maxwell, P. H. et al. (1999) The tumour suppressor protein VHL targets hypoxia-inducible factors for oxygen-dependent proteolysis. *Nature*. [Online] 399 (6733), 271–275.

Mayerhofer, M. et al. (2002) BCR/ABL induces expression of vascular endothelial growth factor and its transcriptional activator, hypoxia inducible factor-1alpha , through a pathway involving phosphoinositide 3-kinase and the mammalian target of rapamycin. *Blood*. [Online] 100 (10), 3767–3775.

McGill, G. G. et al. (2002) Bcl2 regulation by the melanocyte master regulator Mitf modulates lineage survival and melanoma cell viability. *Cell*. 109 (6), 707–718.

Mei, H. et al. (2014) High expression of ROR2 in cancer cell correlates with unfavorable prognosis in colorectal cancer. *Biochemical and Biophysical Research Communications*. [Online] 453 (4), 703–709.

Meissner, M. et al. (2011) Suppression of VEGFR2 Expression in Human Endothelial Cells by Dimethylfumarate Treatment: Evidence for Anti-Angiogenic Action. *Journal of Investigative Dermatology*. [Online] 131 (6), 1356–1364.

Melnikova, V. O. & Bar-Eli, M. (2006) Bioimmunotherapy for melanoma using fully human antibodies targeting MCAM/MUC18 and IL-8. *Pigment Cell Research*. [Online] 19 (5), 395–405.

Michaloglou, C. et al. (2005) BRAFE600-associated senescence-like cell cycle arrest of human naevi. *Nature*. [Online] 436 (7051), 720–724.

Middleton, M. R. et al. (2000) Randomized Phase III Study of Temozolomide Versus Dacarbazine in the Treatment of Patients With Advanced Metastatic Malignant Melanoma. *Journal of Clinical Oncology*. [Online] 18 (1), 158–158.

Miele, C. et al. (2000) Insulin and insulin-like growth factor-I induce vascular endothelial growth factor mRNA expression via different signaling pathways. *The Journal of Biological Chemistry*. [Online] 275 (28), 21695–21702.

Miller-Kasprzak, E. & Jagodziński, P. P. (2008) 5-Aza-2'-deoxycytidine increases the expression of anti-angiogenic vascular endothelial growth factor 189b variant in human lung microvascular endothelial cells. *Biomedicine & Pharmacotherapy*. [Online] 62 (3), 158–163.

Miller, K. D. et al. (2018) Double-Blind Phase III Trial of Adjuvant Chemotherapy With and Without Bevacizumab in Patients With Lymph Node-Positive and High-Risk Lymph Node-Negative Breast Cancer (E5103). *Journal of Clinical Oncology*. [Online] 36 (25), 2621–2629.

Moan, J. et al. (2008) 'Ultraviolet Radiation and Malignant Melanoma', in *Sunlight, Vitamin D and Skin Cancer*. [Online]. New York, NY: Springer New York. pp. 104–116.

Molhoek, K. R. et al. (2011) VEGFR-2 expression in human melanoma: Revised assessment. *International*

Journal of Cancer. [Online] 129 (12), 2807–2815.

Molven, A. et al. (2005) A large Norwegian family with inherited malignant melanoma, multiple atypical nevi, andCDK4 mutation. *Genes, Chromosomes and Cancer*. [Online] 44 (1), 10–18.

Muñoz-Couselo, E. et al. (2017) NRAS-mutant melanoma: current challenges and future prospect. *OncoTargets and Therapy*. [Online] 103941–3947.

Murakami, M. & Simons, M. (2008) Fibroblast growth factor regulation of neovascularization. *Current Opinion in Hematology*. [Online] 15 (3), 215–220.

Nagineni, C. N. et al. (2003) Transforming growth factor-? induces expression of vascular endothelial growth factor in human retinal pigment epithelial cells: Involvement of mitogen-activated protein kinases. *Journal of Cellular Physiology*. [Online] 197 (3), 453–462.

Nagore, E. et al. (2016) *TERT* promoter mutations in melanoma survival. *International Journal of Cancer*. [Online] 139 (1), 75–84.

Narita, K. et al. (2009) Keratinocyte growth factor induces vascular endothelial growth factor-A expression in colorectal cancer cells. *International Journal of Oncology*. 34 (2), 355–360.

Nasarre, P. et al. (2009) Host-Derived Angiopoietin-2 Affects Early Stages of Tumor Development and Vessel Maturation but Is Dispensable for Later Stages of Tumor Growth. *Cancer Research*. [Online] 69 (4), 1324–1333.

Nazarian, R. et al. (2010) Melanomas acquire resistance to B-RAF(V600E) inhibition by RTK or N-RAS upregulation. *Nature*. [Online] 468 (7326), 973–977.

Neuchrist, C. et al. (2001) Vascular endothelial growth factor receptor 2 (VEGFR2) expression in squamous cell carcinomas of the head and neck. *The Laryngoscope*. [Online] 111 (10), 1834–1841.

Nghiemphu, P. L. et al. (2009) Bevacizumab and chemotherapy for recurrent glioblastoma: A single-institution experience. *Neurology*. [Online] 72 (14), 1217–1222.

Niault, T. S. & Baccarini, M. (2010) Targets of Raf in tumorigenesis. *Carcinogenesis*. [Online] 31 (7), 1165–1174.

Nikkola, J. et al. (2005) High Serum Levels of Matrix Metalloproteinase-9 and Matrix Metalloproteinase-1 Are Associated with Rapid Progression in Patients with Metastatic Melanoma. *Clinical Cancer Research*. [Online] 11 (14), 5158–5166.

Nikolaev, S. I. et al. (2012) Exome sequencing identifies recurrent somatic MAP2K1 and MAP2K2 mutations in melanoma. *Nature Genetics*. [Online] 44 (2), 133–139.

Nishimura, H. et al. (2001) Autoimmune Dilated Cardiomyopathy in PD-1 Receptor-Deficient Mice. *Science*. [Online] 291 (5502), 319–322.

Niu, G. et al. (2002) Constitutive Stat3 activity up-regulates VEGF expression and tumor angiogenesis. *Oncogene*. [Online] 21 (13), 2000–2008.

Nogales-Cadenas, R. et al. (2009) GeneCodis: interpreting gene lists through enrichment analysis and integration of diverse biological information. *Nucleic Acids Research*. [Online] 37, W317–W322.

O'Connell, M. P. et al. (2010) The orphan tyrosine kinase receptor, ROR2, mediates Wnt5A signaling in

metastatic melanoma. *Oncogene*. [Online] 29 (1), 34–44.

O'Day, S. J. et al. (2009) Phase II Multicenter Trial of Maintenance Biotherapy After Induction Concurrent Biochemotherapy for Patients With Metastatic Melanoma. *Journal of Clinical Oncology*. [Online] 27 (36), 6207–6212.

Oku, T. et al. (1998) Tumor growth modulation by sense and antisense vascular endothelial growth factor gene expression: effects on angiogenesis, vascular permeability, blood volume, blood flow, fluorodeoxyglucose uptake, and proliferation of human melanoma intracerebral xenografts. *Cancer Research*. 58 (18), 4185–4192.

Olive, P. L. et al. (2001) Carbonic anhydrase 9 as an endogenous marker for hypoxic cells in cervical cancer. *Cancer Research*. 61 (24), 8924–8929.

Olsson, A.-K. et al. (2006) VEGF receptor signalling — in control of vascular function. *Nature Reviews Molecular Cell Biology*. [Online] 7 (5), 359–371.

Omholt, K. et al. (2006) Mutations of PIK3CA are rare in cutaneous melanoma. *Melanoma Research*. [Online] 16 (2), 197–200.

Ornitz, D. M. & Itoh, N. (2015) The Fibroblast Growth Factor signaling pathway. *Wiley interdisciplinary reviews. Developmental Biology*. [Online] 4 (3), 215–266.

Oyama, T. et al. (1998) Vascular Endothelial Growth Factor Affects Dendritic Cell Maturation Through the Inhibition of Nuclear Factor-κB Activation in Hemopoietic Progenitor Cells. *J. Immunol.* 156 (7), 2591–2598.

Paddison, P. J. et al. (2002) Short hairpin RNAs (shRNAs) induce sequence-specific silencing in mammalian cells. *Genes & Development*. [Online] 16 (8), 948–958.

Pardoll, D. M. (2012) The blockade of immune checkpoints in cancer immunotherapy. *Nature Reviews Cancer*. [Online] 12 (4), 252–264.

Park, J. E. et al. (1993) The vascular endothelial growth factor (VEGF) isoforms: differential deposition into the subepithelial extracellular matrix and bioactivity of extracellular matrix-bound VEGF. *Molecular Biology of the Cell*. 4 (12), 1317–1326.

Parsons, H. M. et al. (2015) Who Treats Adolescents and Young Adults with Cancer? A Report from the AYA HOPE Study. *Journal of Adolescent and YoungAadult Oncology*. [Online] 4 (3), 141–150.

PDQ Adult Treatment Editorial Board, P. A. T. E. (2018) *Melanoma Treatment (PDQ®): Health Professional Version*. National Cancer Institute (US).

Pelletier, F. et al. (2005) Circulating vascular endothelial growth factor in cutaneous malignant melanoma. *British Journal of Dermatology*. [Online] 152 (4), 685–689.

Pepper, M. S. et al. (1992) Potent synergism between vascular endothelial growth factor and basic fibroblast growth factor in the induction of angiogenesis in vitro. *Biochemical and Biophysical Research Communications*. 189 (2), 824–831.

Perez, D. G. et al. (2009) Phase 2 trial of carboplatin, weekly paclitaxel, and biweekly bevacizumab in patients with unresectable stage IV melanoma. *Cancer*. [Online] 115 (1), 119–127.

Perrin, R. M. et al. (2005) Diabetic retinopathy is associated with a switch in splicing from anti- to pro-angiogenic isoforms of vascular endothelial growth factor. *Diabetologia*. [Online] 48 (11), 2422–2427.

Plotnikov, A. et al. (2011) The MAPK cascades: Signaling components, nuclear roles and mechanisms of nuclear translocation. *Biochimica et Biophysica Acta (BBA) - Molecular Cell Research*. [Online] 1813 (9), 1619–1633.

Pollard, J. W. (2004) Tumour-educated macrophages promote tumour progression and metastasis. *Nature Reviews Cancer.* 4 (1), 71–78

Pollock, P. M. et al. (2002) PTEN inactivation is rare in melanoma tumours but occurs frequently in melanoma cell lines. *Melanoma Research*. 12 (6), 565–575.

Poste, G. et al. (1980) In vitro selection of murine B16 melanoma variants with enhanced tissue-invasive properties. *Cancer Research*. 40 (5), 1636–1644.

Pötgens, A. J. et al. (1996) Analysis of the tumor vasculature and metastatic behavior of xenografts of human melanoma cell lines transfected with vascular permeability factor. *The American Journal of Pathology*. 148 (4), 1203–1217.

Pötgens, A. J. et al. (1995) Vascular permeability factor expression influences tumor angiogenesis in human melanoma lines xenografted to nude mice. *The American Journal of Pathology*. 146 (1), 197–209.

Powis, G. & Kirkpatrick, L. (2004) Hypoxia inducible factor-1alpha as a cancer drug target. *Molecular Cancer Therapeutics*. 3 (5), 647–654.

Presta, L. G. et al. (1997) Humanization of an anti-vascular endothelial growth factor monoclonal antibody for the therapy of solid tumors and other disorders. *Cancer Research.* 57 (20), 4593–4599.

Qiao, L. et al. (2015) Advanced research on vasculogenic mimicry in cancer. *Journal of Cellular and Molecular Medicine*. [Online] 19 (2), 315–326.

Van Raamsdonk, C. D. et al. (2009) Frequent somatic mutations of GNAQ in uveal melanoma and blue naevi. *Nature*. [Online] 457 (7229), 599–602.

Van Raamsdonk, C. D. et al. (2010) Mutations in *GNA11* in Uveal Melanoma. *New England Journal of Medicine*. [Online] 363 (23), 2191–2199.

Rak, J. et al. (1995) Mutant ras oncogenes upregulate VEGF/VPF expression: implications for induction and inhibition of tumor angiogenesis. *Cancer Research*. 55 (20), 4575–4580.

Rane, S. G. et al. (2002) Germ line transmission of the Cdk4(R24C) mutation facilitates tumorigenesis and escape from cellular senescence. *Molecular and Cellular Biology*. [Online] 22 (2), 644–656.

Ranzani, M. et al. (2015) *BRAF* / *NRAS* wild-type melanoma, NF1 status and sensitivity to trametinib. *Pigment Cell & Melanoma Research*. [Online] 28 (1), 117–119.

Rastrelli, M. et al. (2014) Melanoma: epidemiology, risk factors, pathogenesis, diagnosis and classification. *In Vivo (Athens, Greece)*. 28 (6), 1005–1011.

Raza, A. et al. (2010) Pericytes and vessel maturation during tumor angiogenesis and metastasis. *American Journal of Hematology*. [Online] 85 (8), 593–598.

Reifenberger, J. et al. (2000) Allelic losses on chromosome arm 10q and mutation of the PTEN (MMAC1) tumour suppressor gene in primary and metastatic malignant melanomas. *Virchows Archiv*. 436 (5), 487–493.

Reyes-Botero, G. et al. (2018) Temozolomide Plus Bevacizumab in Elderly Patients with Newly Diagnosed Glioblastoma and Poor Performance Status: An ANOCEF Phase II Trial (ATAG). *The Oncologist*. [Online] 23 (5), 524-e44.

Rheault, T. R. et al. (2013) Discovery of Dabrafenib: A Selective Inhibitor of Raf Kinases with Antitumor Activity against B-Raf-Driven Tumors. *ACS Medicinal Chemistry Letters*. [Online] 4 (3), 358–362.

Rhodes, A. R. et al. (1987) Risk factors for cutaneous melanoma. A practical method of recognizing predisposed individuals. *JAMA*. 258 (21), 3146–3154.

Ribas, A. (2010) Clinical development of the anti-CTLA-4 antibody tremelimumab. *Seminars in Oncology*. [Online] 37 (5), 450–454.

Ribas, A. et al. (2015) Pembrolizumab versus investigator-choice chemotherapy for ipilimumab-refractory melanoma (KEYNOTE-002): a randomised, controlled, phase 2 trial. *The Lancet Oncology*. [Online] 16 (8), 908–918.

Ribas, A. et al. (2012) Safety profile and pharmacokinetic analyses of the anti-CTLA4 antibody tremelimumab administered as a one hour infusion. *Journal of Translational Medicine*. [Online] 10 (1), 236.

Ribatti, D. et al. (2005) Microvascular density, vascular endothelial growth factor immunoreactivity in tumor cells, vessel diameter and intussusceptive microvascular growth in primary melanoma. *Oncology Reports*. [Online] 14 (1), 81–84.

Ribatti, D. & Crivellato, E. (2012) “Sprouting angiogenesis”, a reappraisal. *Developmental Biology*. [Online] 372 (2), 157–165.

Rigel, D. S. (2010) Epidemiology of Melanoma. *Seminars in Cutaneous Medicine and Surgery*. [Online] 29 (4), 204–209.

Rittling, S. R. & Chambers, A. F. (2004) Role of osteopontin in tumour progression. *British Journal of Cancer*. [Online] 90 (10), 1877–1881.

Robert, C. et al. (2011) Ipilimumab plus Dacarbazine for Previously Untreated Metastatic Melanoma. *New England Journal of Medicine*. [Online] 364 (26), 2517–2526.

Robert, C. et al. (2015a) Improved Overall Survival in Melanoma with Combined Dabrafenib and Trametinib. *New England Journal of Medicine*. [Online] 372 (1), 30–39.

Robert, C. et al. (2015b) Nivolumab in Previously Untreated Melanoma without *BRAF* Mutation. *New England Journal of Medicine*. [Online] 372 (4), 320–330.

Robert, C. et al. (2015c) Pembrolizumab versus Ipilimumab in Advanced Melanoma. *New England Journal of Medicine*. [Online] 372 (26), 2521–2532.

Ruan, G.-X. & Kazlauskas, A. (2012) Axl is essential for VEGF-A-dependent activation of PI3K/Akt. *The EMBO Journal*. [Online] 31 (7), 1692–1703.

Rudd, C. E. et al. (2009) CD28 and CTLA-4 coreceptor expression and signal transduction. *Immunological*

Reviews. [Online] 229 (1), 12–26.

Ruifrok, A. C. & Johnston, D. A. (2001) Quantification of histochemical staining by color deconvolution. *Analytical and Quantitative Cytology and Histology*. 23 (4), 291–299.

Ryuto, M. et al. (1996) Induction of vascular endothelial growth factor by tumor necrosis factor alpha in human glioma cells. Possible roles of SP-1. *The Journal of Biological Chemistry*. [Online] 271 (45), 28220–28228.

Salmena, L. et al. (2008) Tenets of PTEN Tumor Suppression. *Cell*. [Online] 133 (3), 403–414.

Sanada, M. et al. (2004) Killing and mutagenic actions of dacarbazine, a chemotherapeutic alkylating agent, on human and mouse cells: effects of Mgmt and Mlh1 mutations. *DNA Repair*. [Online] 3 (4), 413–420.

Sang, N. et al. (2003) MAPK Signaling Up-regulates the Activity of Hypoxia-inducible Factors by Its Effects on p300. *Journal of Biological Chemistry*. [Online] 278 (16), 14013–14019.

Scherer, W. F. et al. (1953) Studies on the propagation in vitro of poliomyelitis viruses. IV. Viral multiplication in a stable strain of human malignant epithelial cells (strain HeLa) derived from an epidermoid carcinoma of the cervix. *The Journal of Experimental Medicine*. [Online] 97 (5), 695–710.

Scolyer, R. A. et al. (2011) Evolving concepts in melanoma classification and their relevance to multidisciplinary melanoma patient care. *Molecular Oncology*. [Online] 5 (2), 124–136.

Seftor, R. E. B. et al. (2012) Tumor Cell Vasculogenic Mimicry. *The American Journal of Pathology*. [Online] 181 (4), 1115–1125.

Semenza, G. L. (2012) Hypoxia-Inducible Factors in Physiology and Medicine. *Cell*. [Online] 148 (3), 399–408.

Semov, A. et al. (2005) Metastasis-associated protein S100A4 induces angiogenesis through interaction with Annexin II and accelerated plasmin formation. *The Journal of Biological Chemistry*. [Online] 280 (21), 20833–20841.

Senger, D. R. et al. (1996) Stimulation of endothelial cell migration by vascular permeability factor/vascular endothelial growth factor through cooperative mechanisms involving the alphavbeta3 integrin, osteopontin, and thrombin. *The American Journal of Pathology*. 149 (1), 293–305.

Sheppard, K. E. & McArthur, G. A. (2013) The cell-cycle regulator CDK4: an emerging therapeutic target in melanoma. *Clinical Cancer Research*. [Online] 19 (19), 5320–5328.

Sherwood, L. M. et al. (1971) Tumor Angiogenesis: Therapeutic Implications. *New England Journal of Medicine*. [Online] 285 (21), 1182–1186.

Shing, Y. et al. (1984) Heparin affinity: purification of a tumor-derived capillary endothelial cell growth factor. *Science (New York, N.Y.)*. 223 (4642), 1296–1299.

Si, M. & Lang, J. (2018) The roles of metallothioneins in carcinogenesis. *Journal of Hematology & Oncology*. [Online] 11 (1), 107.

Singh, R. K. & Varney, M. L. (2000) IL-8 expression in malignant melanoma: implications in growth and metastasis. *Histology and Histopathology*. [Online] 15 (3), 843–849.

Slingluff, C. L. et al. (2013) Clinical activity and safety of combination therapy with temsirolimus and bevacizumab for advanced melanoma: a phase II trial (CTEP 7190/Mel47). *Clinical Cancer Research*.

[Online] 19 (13), 3611–3620.

Smalley, K. S. M. et al. (2009) CRAF inhibition induces apoptosis in melanoma cells with non-V600E BRAF mutations. *Oncogene*. [Online] 28 (1), 85–94.

Soufir, N. et al. (1998) Prevalence of p16 and CDK4 germline mutations in 48 melanoma-prone families in France. The French Familial Melanoma Study Group. *Human Molecular Genetics*. 7 (2), 209–216.

Sounni, N. E. et al. (2002) Expression of membrane type 1 matrix metalloproteinase (MT1-MMP) in A2058 melanoma cells is associated with MMP-2 activation and increased tumor growth and vascularization. *International Journal of Cancer*. [Online] 98 (1), 23–28.

Spinella, F. et al. (2014) The interplay between hypoxia, endothelial and melanoma cells regulates vascularization and cell motility through endothelin-1 and vascular endothelial growth factor. *Carcinogenesis*. [Online] 35 (4), 840–848.

Srivastava, A. et al. (1988) The prognostic significance of tumor vascularity in intermediate-thickness (0.76-4.0 mm thick) skin melanoma. A quantitative histologic study. *The American Journal of Pathology*. 133 (2), 419–423.

Stratton, M. R. et al. (2009) The cancer genome. *Nature*. [Online] 458 (7239), 719–724.

Straume, O. & Akslen, L. A. (2003) Increased expression of VEGF-receptors (FLT-1, KDR, NRP-1) and thrombospondin-1 is associated with glomeruloid microvascular proliferation, an aggressive angiogenic phenotype, in malignant melanoma. *Angiogenesis*. [Online] 6 (4), 295–301.

Strömblad, S. et al. (1996) Suppression of p53 activity and p21WAF1/CIP1 expression by vascular cell integrin alphaVbeta3 during angiogenesis. *Journal of Clinical Investigation*. [Online] 98 (2), 426–433.

Stupack, D. G. et al. (2001) Apoptosis of adherent cells by recruitment of caspase-8 to unligated integrins. *The Journal of Cell Biology*. [Online] 155 (3), 459–470.

Sullivan, R. J. & Flaherty, K. (2013) MAP kinase signaling and inhibition in melanoma. *Oncogene*. [Online] 32 (19), 2373–2379.

Szadvari, I. et al. (2016) Athymic Nude Mice as an Experimental Model for Cancer Treatment Cancer diseases and their treatment. *Physiological Research*. 65441–453.

Tabas-Madrid, D. et al. (2012) GeneCodis3: a non-redundant and modular enrichment analysis tool for functional genomics. *Nucleic Acids Research*. [Online] 40 (W1), W478–W483.

Takahashi, T. et al. (1999) VEGF activates protein kinase C-dependent, but Ras-independent Raf-MEK-MAP kinase pathway for DNA synthesis in primary endothelial cells. *Oncogene*. [Online] 18 (13), 2221–2230.

Takakura, M. et al. (1999) Cloning of human telomerase catalytic subunit (hTERT) gene promoter and identification of proximal core promoter sequences essential for transcriptional activation in immortalized and cancer cells. *Cancer Research*. 59 (3), 551–557.

Tas, F. et al. (2011) Noncutaneous Melanoma Have Distinct Features from Each Other and Cutaneous Melanoma. *Oncology*. [Online] 81 (5–6), 353–358.

Thomas, N. E. et al. (2015) Association Between *NRAS* and *BRAF* Mutational Status and Melanoma-Specific Survival Among Patients With Higher-Risk Primary Melanoma. *JAMA Oncology*. [Online] 1 (3), 359.

Thurber, A. E. et al. (2011) Inverse expression states of the BRN2 and MITF transcription factors in melanoma spheres and tumour xenografts regulate the NOTCH pathway. *Oncogene*. [Online] 30 (27), 3036–3048.

Torres-Cabala, C. A. et al. (2009) Correlation between KIT expression and KIT mutation in melanoma: a study of 173 cases with emphasis on the acral-lentiginous/mucosal type. *Modern Pathology*. [Online] 22 (11), 1446–1456.

Tran, M. A. et al. (2008) Cancer Research. *Cancer Research.* [Online] 62 (23), 6997–7000.

Trisciuoglio, D. et al. (2010) Bcl-2 Regulates HIF-1α Protein Stabilization in Hypoxic Melanoma Cells via the Molecular Chaperone HSP90 Marc Vooijs (ed.). *PLoS ONE*. [Online] 5 (7), e11772.

Tsai, J. et al. (2008) Discovery of a selective inhibitor of oncogenic B-Raf kinase with potent antimelanoma activity. *Proceedings of the National Academy of Sciences of the United States of America*. [Online] 105 (8), 3041–3046.

Tsao, H. et al. (1998) Identification of PTEN/MMAC1 alterations in uncultured melanomas and melanoma cell lines. *Oncogene*. [Online] 16 (26), 3397–3402.

Tsao, H. et al. (2012) Melanoma: from mutations to medicine. *Genes & Development*. [Online] 26 (11), 1131–1155.

Ugurel, S. et al. (2001) Increased Serum Concentration of Angiogenic Factors in Malignant Melanoma Patients Correlates With Tumor Progression and Survival. *Journal of Clinical Oncology*. [Online] 19 (2), 577–583.

Valente, P. et al. (1998) TIMP-2 over-expression reduces invasion and angiogenesis and protects B16F10 melanoma cells from apoptosis. *International Journal of Cancer*. [Online] 75 (2), 246–253.

Varella, L. et al. (2017) Revisiting the Role of Bevacizumab in the Treatment of Breast Cancer. *Seminars in Oncology*. [Online] 44 (4), 273–285.

Varker, K. A. et al. (2007) A Randomized Phase 2 Trial of Bevacizumab with or without Daily Low-Dose Interferon Alfa-2b in Metastatic Malignant Melanoma. *Annals of Surgical Oncology*. [Online] 14 (8), 2367–2376.

Vihinen, P. P. et al. (2010) A phase II trial of bevacizumab with dacarbazine and daily low-dose interferon-α2a as first line treatment in metastatic melanoma. *Melanoma Research*. [Online] 20 (4), 318–325.

Viros, A. et al. (2008) Improving Melanoma Classification by Integrating Genetic and Morphologic Features Jonathan Rees (ed.). *PLoS Medicine*. [Online] 5 (6), e120.

Vizioli, M. G. et al. (2011) Evidence of oncogene-induced senescence in thyroid carcinogenesis. *Endocrine-Related Cancer*. [Online] 18 (6), 743–757.

Vousden, K. H. & Lu, X. (2002) Live or let die: the cell's response to p53. *Nature Reviews Cancer*. [Online] 2 (8), 594–604.

Vu, H. L. & Aplin, A. E. (2016) Targeting mutant NRAS signaling pathways in melanoma. *Pharmacological Research*. [Online] 107111–116.

Wajapeyee, N. et al. (2008) Oncogenic BRAF induces senescence and apoptosis through pathways mediated by the secreted protein IGFBP7. *Cell*. [Online] 132 (3), 363–374.

Wakelee, H. A. et al. (2017) Adjuvant chemotherapy with or without bevacizumab in patients with resected non-small-cell lung cancer (E1505): an open-label, multicentre, randomised, phase 3 trial. *The Lancet Oncology*. [Online] 18 (12), 1610–1623.

Wang, D. et al. (1999) Induction of vascular endothelial growth factor expression in endothelial cells by platelet-derived growth factor through the activation of phosphatidylinositol 3-kinase. *Cancer Research*. 59 (7), 1464–1472.

Wang, G. L. et al. (1995) Hypoxia-inducible factor 1 is a basic-helix-loop-helix-PAS heterodimer regulated by cellular O2 tension. *Proceedings of the National Academy of Sciences of the United States of America*. 92 (12), 5510–5514.

Weber, J. S. et al. (2015) Nivolumab versus chemotherapy in patients with advanced melanoma who progressed after anti-CTLA-4 treatment (CheckMate 037): a randomised, controlled, open-label, phase 3 trial. *The Lancet Oncology*. [Online] 16 (4), 375–384.

Wedge, S. R. et al. (2005) AZD2171: A Highly Potent, Orally Bioavailable, Vascular Endothelial Growth Factor Receptor-2 Tyrosine Kinase Inhibitor for the Treatment of Cancer. *Cancer Research*. [Online] 65 (10), 4389–4400.

Weinstein, J. N. (2012) Drug discovery: Cell lines battle cancer. *Nature*. [Online] 483 (7391), 544–545.

Weinstock, M. A. et al. (1989) Nonfamilial cutaneous melanoma incidence in women associated with sun exposure before 20 years of age. *Pediatrics*. 84 (2), 199–204.

Wellbrock, C. et al. (2004) *V599E B-RAF is an Oncogene in Melanocytes B-RAF is an Oncogene in Melanocytes*. [Online] 2338–2342.

Widmer, D. S. et al. (2012) Systematic classification of melanoma cells by phenotype-specific gene expression mapping. *Pigment Cell & Melanoma Research*. [Online] 25 (3), 343–353.

Wieder, T. et al. (2016) Immunotherapy of melanoma: efficacy and mode of action. *JDDG: Journal der Deutschen Dermatologischen Gesellschaft*. [Online] 14 (1), 28–36.

Willmore-Payne, C. et al. (2005) Human malignant melanoma: detection of BRAF- and c-kit–activating mutations by high-resolution amplicon melting analysis. *Human Pathology*. [Online] 36 (5), 486–493.

Wilson, M. A. & Schuchter, L. M. (2016) 'Chemotherapy for Melanoma', in *Cancer Treatment and Research*. [Online]. pp. 209–229.

Woolard, J. et al. (2004) VEGF $_{165}$ b, an Inhibitory Vascular Endothelial Growth Factor Splice Variant. *Cancer Research*. [Online] 64 (21), 7822–7835.

Wright, T. M. et al. (2009) Ror2, a developmentally regulated kinase, promotes tumor growth potential in renal cell carcinoma. *Oncogene*. [Online] 28 (27), 2513–2523.

Wykoff, C. C. et al. (2000) Hypoxia-inducible expression of tumor-associated carbonic anhydrases. *Cancer Research*. 60 (24), 7075–7083.

Xia, G. et al. (2006) Expression and significance of vascular endothelial growth factor receptor 2 in bladder cancer. *The Journal of Urology*. [Online] 175 (April), 1245–1252.

Yamamoto, H. et al. (2010) Wnt5a signaling is involved in the aggressiveness of prostate cancer and expression

of metalloproteinase. *Oncogene*. [Online] 29 (14), 2036–2046.

Yang, H. et al. (2010) Bevacizumab Suppression of Establishment of Micrometastases in Experimental Ocular Melanoma. *Investigative Opthalmology & Visual Science*. [Online] 51 (6), 2835.

Yang, L. et al. (2004) Expansion of myeloid immune suppressor Gr+CD11b+ cells in tumor-bearing host directly promotes tumor angiogenesis. *Cancer Cell*. [Online] 6 (4), 409–421.

Yaqoob, U. et al. (2012) Neuropilin-1 stimulates tumor growth by increasing fibronectin fibril assembly in the tumor microenvironment. *Cancer Research*. [Online] 72 (16), 4047–4059.

Yi, X. et al. (1999) Both transcriptional and posttranscriptional mechanisms regulate human telomerase template RNA levels. *Molecular and Cellular Biology*. 19 (6), 3989–3997.

Yin, M. et al. (2014) Osteopontin Promotes the Invasive Growth of Melanoma Cells by Activating Integrin αvβ3 and Down-Regulating Tetraspanin CD9. *The American Journal of Pathology*. [Online] 184 (3), 842–858.

Yokoyama, S. et al. (2011) A novel recurrent mutation in MITF predisposes to familial and sporadic melanoma. *Nature*. [Online] 480 (7375), 99–103.

Yonemura, Y. et al. (2005) Role of VEGF-C and VEGF-D in lymphangiogenesis in gastric cancer. *International Journal of Clinical Oncology*. [Online] 10 (5), 318–327.

Yu, J. L. et al. (2002) Vascular endothelial growth factor isoform expression as a determinant of blood vessel patterning in human melanoma xenografts. *Cancer Research*. 62 (6), 1838–1846.

Yu, L. et al. (2008) Interaction between Bevacizumab and Murine VEGF-A: A Reassessment. *Investigative Opthalmology & Visual Science*. [Online] 49 (2), 522.

Zbytek, B. et al. (2013) Putative role of HIF transcriptional activity in melanocytes and melanoma biology. *Dermato-Endocrinology*. [Online] 5 (2), 239–251.

Zelboraf (2014) *Genentech: Zelboraf® (vemurafenib) - Information for Patients* [online]. Available from: https://www.gene.com/patients/medicines/zelboraf (Accessed 9 July 2018).

Zetter, PhD, B. R. (1998) ANGIOGENESIS AND TUMOR METASTASIS. *Annual Review of Medicine*. [Online] 49 (1), 407–424.

Zhang, H. et al. (2002) Expression of vascular endothelial growth factor and its receptors KDR and Flt-1 in gastric cancer cells. *World Journal of Gastroenterology*. [Online] 8 (6), 994–998.